Doctoral Dissertation

Development of Unique Switching Systems Based on Multifunctional Hydrocarbons with Dibenzo-Fused Seven-Membered Rings

（ジベンゾ縮環型七員環骨格をもつ多機能性炭化水素
に基づく特異なスイッチングシステムの開拓）

Yuki HAYASHI

Laboratory of Organic Chemistry I
Graduate School of Chemical Sciences and Engineering
Hokkaido University

2023

Table of Contents

Chapter 1

General Introduction

1-1. Well-Designed π-Conjugated Hydrocarbon Scaffolds

Rigid π-conjugated carbon scaffolds are important components that can determine the fundamental characteristics of organic molecules, such as their geometries and physical properties. The arrangement of carbon atoms involving π-conjugation and the modification of substituents and fused-ring structures responsible for localization and/or delocalization of π-electrons can control properties such as color, luminescence behavior, electrochemical properties, magnetism, and reactivity of the molecules.

In particular, much attention has been focused on sterically congested and/or curved polycyclic aromatic hydrocarbons (PAHs)[1–14], cyclic π-conjugated molecules such as cycloparaphenylenes[15–22] and carbon nanobelts[23–27] and extraordinarily long C–C bond.[28-31] Some of them have been shown to have intriguing geometric and electronic features. For example, Kamikawa *et al*. reported the hexapole helicene,[9] in which the largest twisting angle on a benzene ring was observed (Figure 1-1a). Itami *et al*. synthesized a carbon nanobelt,[23,24,26] which is a partial structure of carbon nanotubes attracting as next-generation materials (Figure 1-1b). These molecules have unusual optical properties based on extended π-conjugated skeletons and are really attractive for their potential applications. Juríček *et al*. reported a reversible photochromic switch via conrotatory electrocyclization by attachment of two methyl groups into cethrene skeleton (Figure 1-1c).[32] With regard to redox-active hydrocarbons, Yamago *et al*. reported that cycloparaphenylenes[17] undergo one- and two-electron oxidation to generate corresponding cationic species, which were successfully isolated and characterized by X-ray analyses (Figure 1-1d). These well-designed hydrocarbons are potential candidates for making novel materials with special characteristic features that are not found in normal compounds.

(a) Hexapole helicene reported by Kamikawa *et al*.[9]

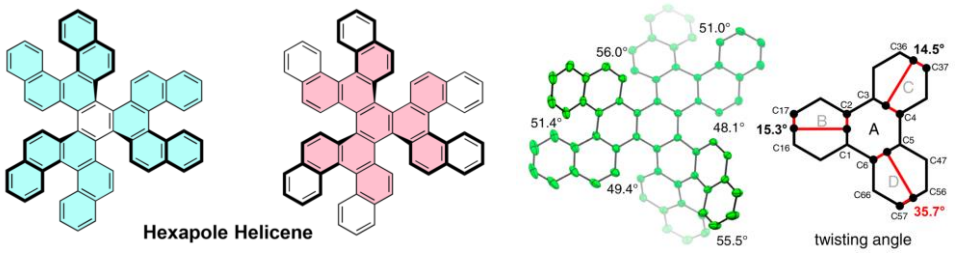

(b) Carbon nanobelt reported by Itami *et al*.[23]

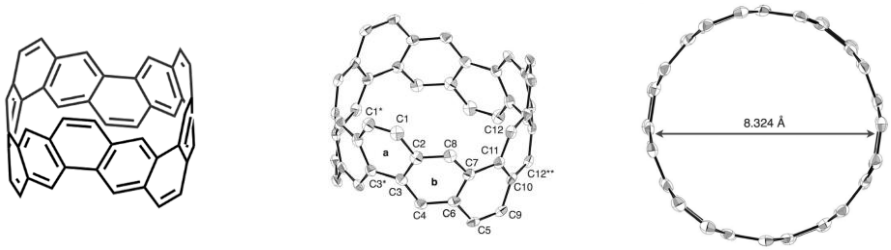

(c) Photochromic switching behavior of dimethylcethrene by Juríček *et al*.[32]

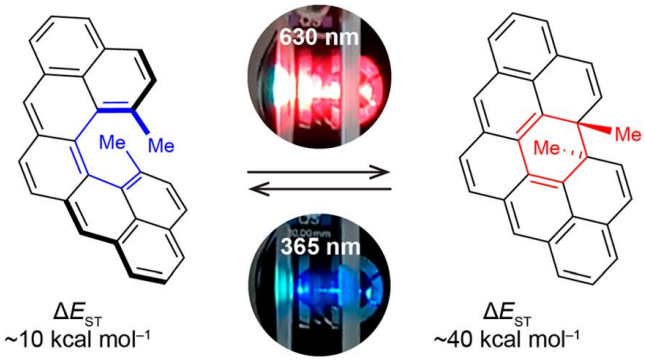

(d) Redox-active cycloparaphenylenes reported by Yamago *et al*.[17]

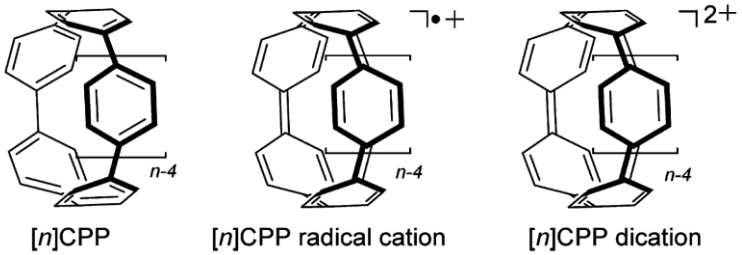

Figure 1-1. Examples of previously reported well-designed π-conjugated hydrocarbons.

1-2. Unique Properties Attained by the Seven-Membered Carbon Ring

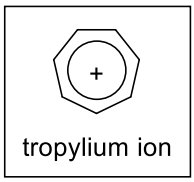

Non-benzenoid aromatic chemistry was pioneered by Nozoe since hinokitiol was discovered in 1936.[33,34] Starting with his study, many efforts for understanding non-benzenoid aromatic chemistry based on annulenes,[35] nonalternant hydrocarbons,[36] heterocyclic aromatic compounds,[37] and porphyrinoids,[38,39] have greatly contributed to the research fields such as pharmaceuticals and organic electronics. Particularly, tropylium ion, which is highly stabilized due to a 6π-electron system with a fully conjugated seven-membered carbon ring skeleton, is important and representative of non-benzenoid aromatic cation according to the Hückel's 4n+2 rule, despite the fact that carbocations are intrinsically unstable and usually known as an intermediate in reactions.[40] Since tropolones, including hinokitiol that Nozoe has studied on, have high stability against acids, bases and heat, their unique physical properties have been investigated by considering their aromaticity based on tropylium structure in their resonance formula (Scheme 1-1a).[33,34] In addition, azulene, in which seven- and five- membered rings fused to each other, is also stabilized by a polarized resonance structure with a contribution of aromatic tropylium structure(Scheme 1-1b).[41,42] Therefore, the energy gap between HOMO and LUMO of azulene is narrower than that of naphthalene which is a structural isomer of azulene, so that azulene and its derivatives have strong absorptions in the visible region whereas naphthalene exhibits absorptions only in the UV region.

Scheme 1-1. Resonance formulas of (a) tropolone and (b) azulene.

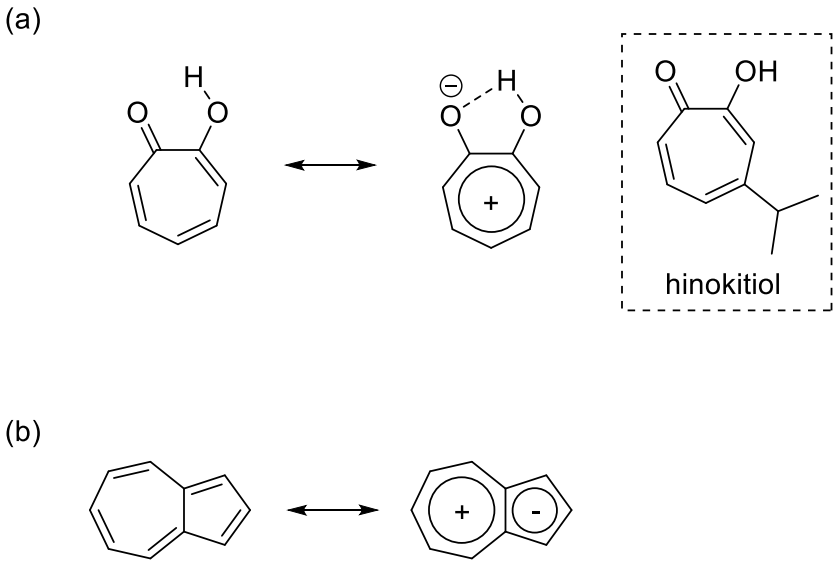

On the other hand, the cycloheptatriene skeleton, a reduced structure of the parent tropylium, also has recently attracted much attention due to its structural feature of seven-membered ring, which can impart a molecular strain and distortion into PAHs to induce a curved structure.[7,8,10,11,13] For example, Miao *et al*. synthesized a new type of saddle-shaped nanographene with a highly bent naphthalene moiety at the center of the polycyclic backbone by the introduction of seven-membered rings as a key structure, and successfully determined its structure by X-ray analysis (Figure 1-2).[10]

As mentioned above, the seven-membered carbon ring skeleton is highly attractive as an essential component not only for the elucidation of fundamental phenomena in organic chemistry but also for the development of advanced organic molecules.

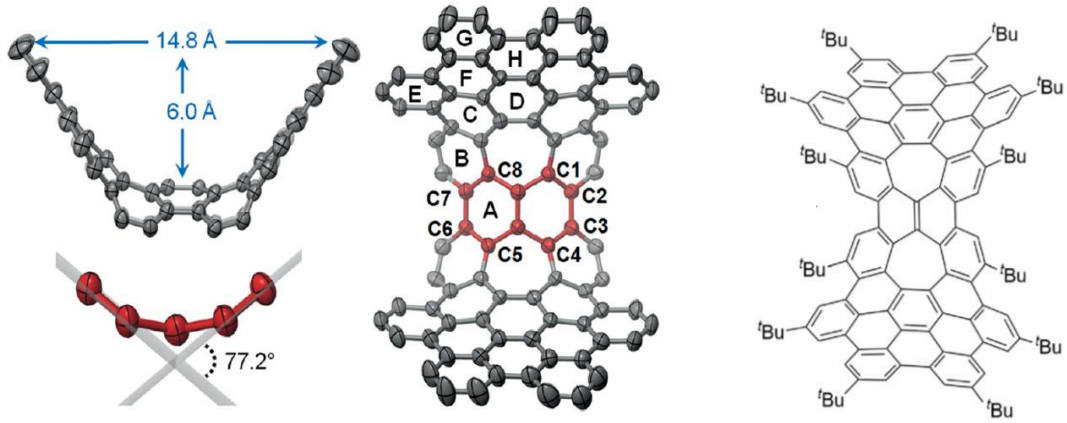

Figure 1-2. X-ray structures of previously reported saddle-shaped nanographene with seven-membered rings as a key structure.[10]

1-3. Dibenzo-Fused Seven-Membered Carbon Rings

5*H*-Dibenzo[*a*,*d*]cycloheptatriene (Figure 1-3a) and 5*H*-dibenzo[*a*,*d*]cycloheptatrienylidene (Figure 1-3b), reduced structures of dibenzo-fused tropylium, has been used as key building blocks for various functional organic materials such as molecular machines,[43-48] organic optoelectronics materials [11,49-53] and ligands of transition metal complexes,[54-56] due to its butterfly-shaped geometry based on the semi-rigid seven-membered carbon ring, which allows to obtain multiple conformations by a flapping motion of seven-membered ring core.

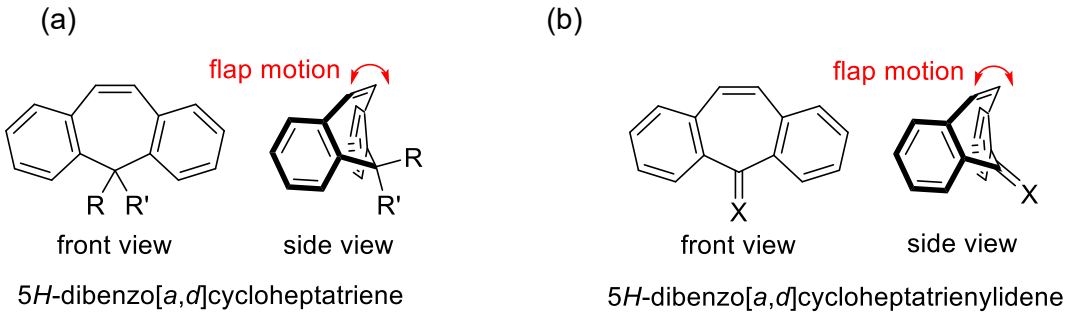

Figure 1-3. Reduced structures of dibenzo-fused tropylium with a butterfly-shaped geometry.

In several dibenzocycloheptatriene derivatives, the properties and the mechanism of interconversion between conformational isomers have been investigated. For example, Young *et al*. studied thermodynamical behavior of dibenzocycloheptatriene derivatives with two conformational isomers by NMR method (Scheme 1-2).[44] Jou *et al*. reported several spiro(dibenzocycloheptatriene) derivatives for their potential applications such as blue-fluorescent organic light emitting diodes (OLEDs), which can be furnished with high electroluminescence brightness and working efficiencies thanks to the geometrical feature of dibenzocycloheptatriene moieties (Figure 1-4).[51] On the other hand, dibenzocycloheptatrienylidene scaffold has been also used as functional molecules. Lehn *et al*. reported molecular motors composed of the combination of a dibenzocycloheptatrienylidene unit and a chiral *N*-alkyl imine (Scheme 1-3a). These molecular motors undergo unidirectional rotation induced by light and heat. In particular, there are two types of thermal isomerization, in-plane nitrogen inversion (NI) and ring inversion (RI), and it was revealed that NI-type isomerization selectively occurred when tribenzocycloheptatrienylidene unit was used in these molecular motors because of an increase in the activation energy barrier of RI-type isomerization(Scheme 1-3b).[48] Nguyen *et al*. reported that tetrabenzo[5.7]fulvalene exhibits aggregation-induced emission (AIE) properties based on a change in conformation (Figure 1-5).[52]

Scheme 1-2. Dibenzocycloheptatriene derivatives exhibiting ring inversion between two conformational isomers (X = H or Br).[44]

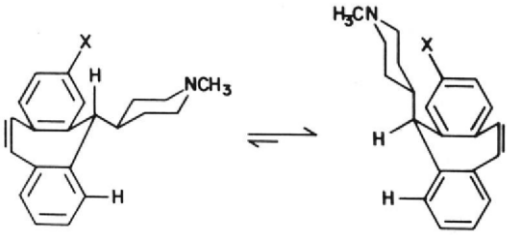

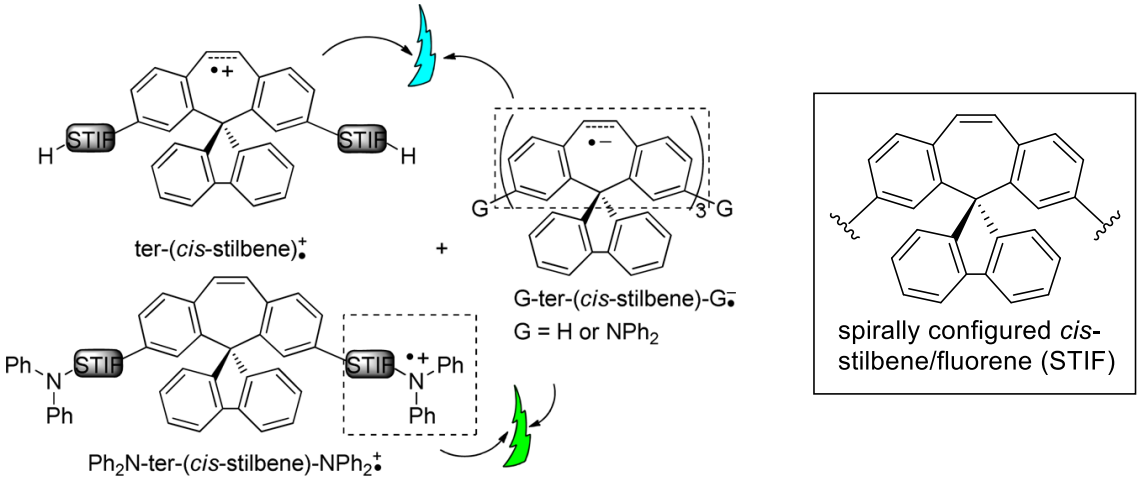

Figure 1-4. Spirally configured (*cis*-stilbene) trimers capable of applications in OLED.[51]

Scheme 1-3. Previously reported molecular motors, in which two types of thermal isomerization; in-plane nitrogen inversion (NI) and ring inversion (RI) of cycloheptatrienylidene unit.[48]

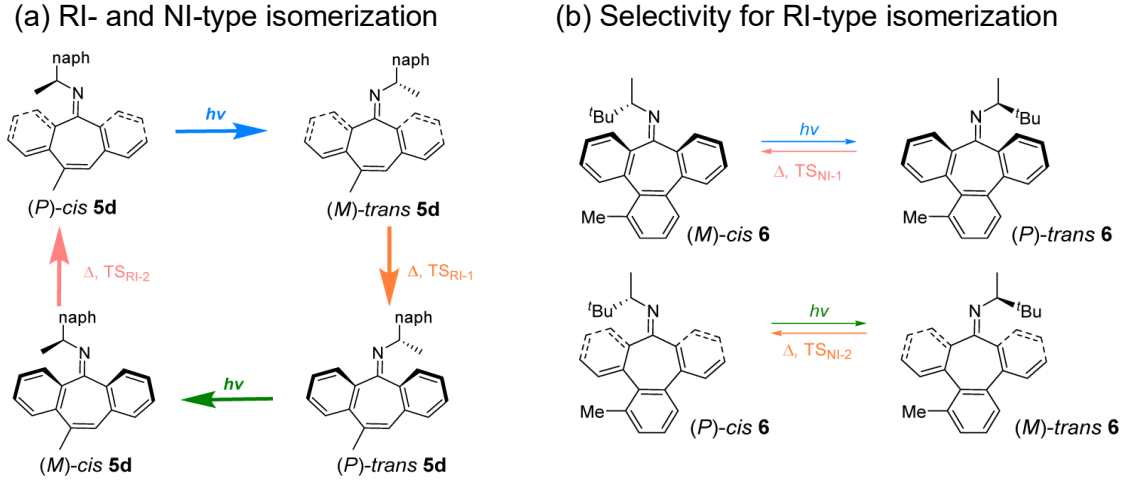

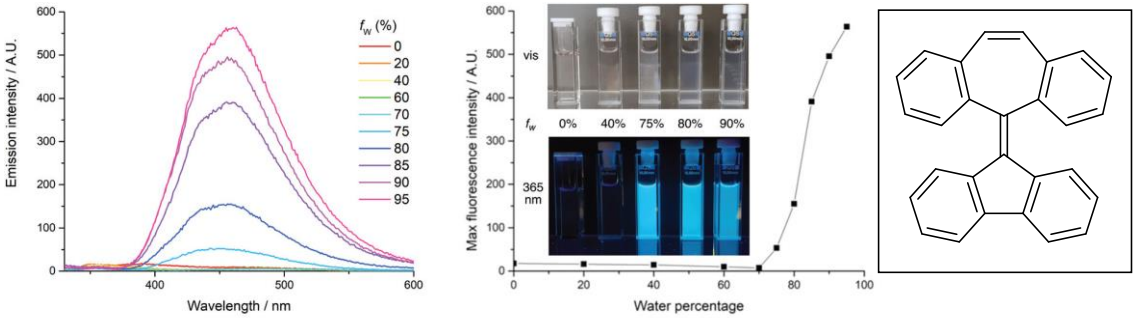

Figure 1-5. Emission spectra (λ_{ex} = 317 nm) and plot of maximum emission intensity of tetrabenzo[5.7]fulvalene in THF/H_2O.[52]

However, there are only a few examples of isolating cations composed of dibenzotropylium structures.[57-59] In addition, open-shell species with dibenzocycloheptatrienyl radical moieties has hardly been studied and almost all of them were reported after the author's work.[60-62] Besides, there were no reports for the reversible redox interconversion between dibenzotropylium-based cationic dye (**A**) and corresponding neutral species with various structures (**B**, **C**, and **D**). Thus, the author envisaged that more sophisticated molecular designs enabling the isolation and reversible switching of several conformations and redox states (**A**: dibenzotropylium, **B**: dibenzocycloheptatriene, **C**: dibenzocycloheptatrienylidene, and **D**: dibenzocycloheptatrienyl radical) would be necessary for the development of a new generation of advanced molecular response systems with multifunctions.

1-4. Contents of This Dissertation

Based on the above background, the author constructed the title unique switching systems based on multifunctional hydrocarbons with dibenzo-fused seven-membered rings, by focusing on redox interconversion between dibenzotropylium (**A**)-based dicationic dyes stabilized by non-benzenoid aromaticity and its corresponding neutral species with unique geometric features and various electronic structures such as **B**, **C** and **D** (Scheme 1-4). Notably, frontier orbital levels and distributions that can change oxidation potentials of neutral species were successfully controlled without the aid of heteroatoms by different approaches in three studies of this dissertation shown below (chapters 2-4). Such newly found functions of each derivative composed of pure hydrocarbons were realized by a proper molecular design, so that the modification of the skeletons such as the introduction of heteroatoms or extension of π-system would allow to fine-tune of their functions.

Scheme 1-4. The concept of this dissertation based on redox interconversion among various electronic structures of dibenzo-fused seven-membered ring skeleton.

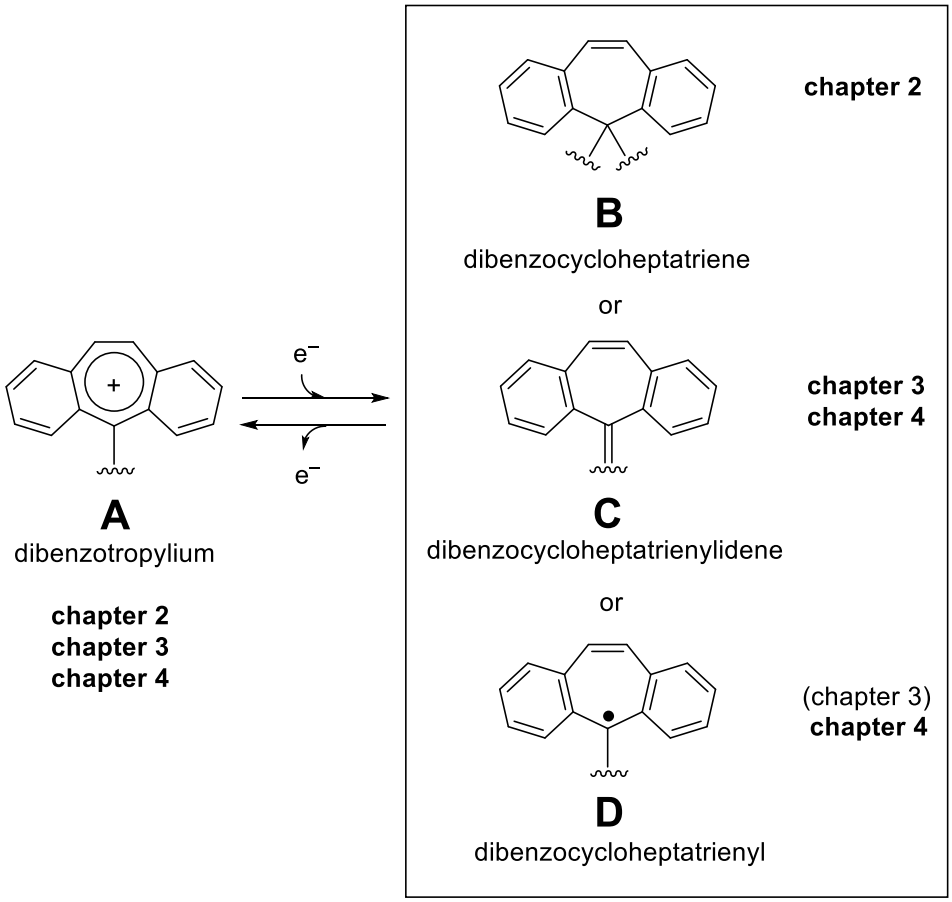

In chapter 2, the author designed and synthesized multiply clamped hexaphenylethane-type electron donor with two spiro rings as a new electrochromic hydrocarbon (Scheme 1-5).[63] X-ray analysis of the dispiro hydrocarbon revealed a highly strained structure as reflected by nearly eclipsed conformation with an elongated "ethane" bond [bond length: 1.6665(17) Å], which is greater than any C–C bonds ever reported for 9,9,10,10-tetraaryl-9,10-dihydrophenanthrene derivatives. The elongated and weakened bond was easily cleaved upon two-electron oxidation to generate the deeply colored dication, where the oxidation potential of dispiro hydrocarbon (+0.95 V vs. SCE in CH_2Cl_2) is far less positive than that of its analogue with four methoxyphenyl groups (+1.44 V), indicating the validity of a concept for raising the HOMO level by the effective through-bond interaction. The reversible interconversion between the dispiro hydrocarbon and the corresponding dication is accompanied not only by a drastic color change but also by C–C bond formation/cleavage. Thus, the voltammogram showed a pair of well-separated redox waves, which is characteristic of "dynamic redox (*dyrex*)" behavior. Moreover, the clean transformation from the dication to monocation with a spiro ring by Friedel–Crafts-type cyclization was also observed in a polar solvent such as acetonitrile.

Scheme 1-5. Clean dynamic redox interconversion between dication and dispiro hydrocarbon, the latter of which has lower oxidation potential despite being without heteroatoms, and clean transformation from the dication to monocation with a spiro ring in a polar solvent.

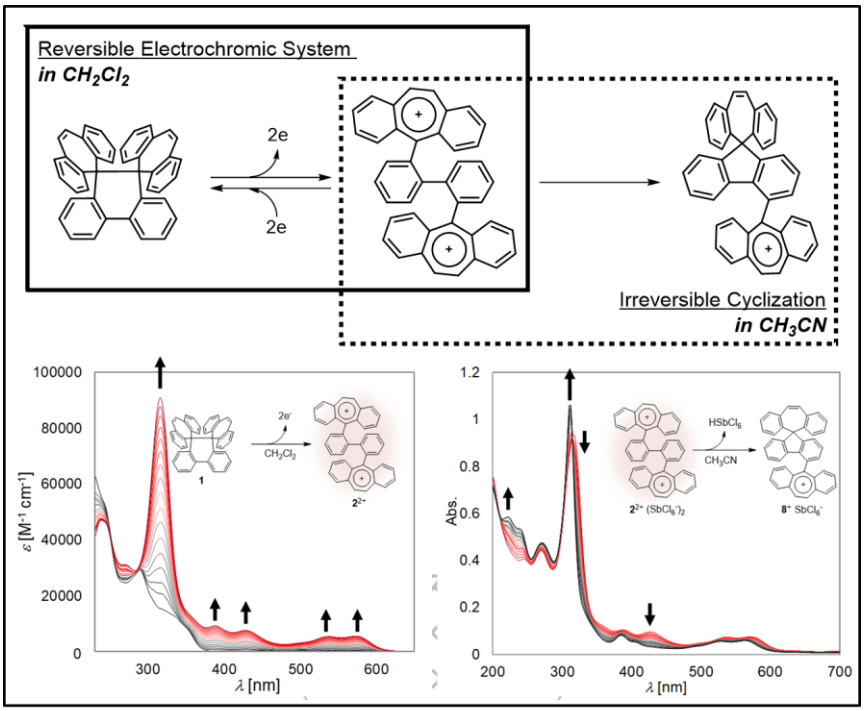

In chapter 3, the author realized to create highly strained hydrocarbons with two di-/tri-benzocycloheptatrienylidene units as electrochromic overcrowded ethylenes that undergo reversible interconversion with stable dicationic dyes upon two-electron transfer (Scheme 1-6).[64] Due to severe steric repulsion, two configurational isomers (*anti*,*anti*-folded and *syn*,*anti*-folded forms) were isolated as stable entities. Photo- and thermal interconversion of these isomers proceeded cleanly: one-way photoisomerization occurred from *anti*,*anti*- to *syn*,*anti*-form and one-way thermal isomerization proceeded from *syn*,*anti*- to *anti*,*anti*-form. Even though both isomers undergo two-electron oxidation into the same twisted dications, quite different oxidation potentials enable completely selective oxidation of *syn*,*anti*-isomers. Thus, the present multi-configurational strained hydrocarbons are capable of switching of activation/deactivation of their electrochromic properties by light/heat.

Scheme 1-6. Complete ON/OFF switching of oxidation properties triggered by light and heat based on reversible and quantitative interconversion between two configurational isomers, *anti*,*anti*- and *syn*,*anti*-forms.

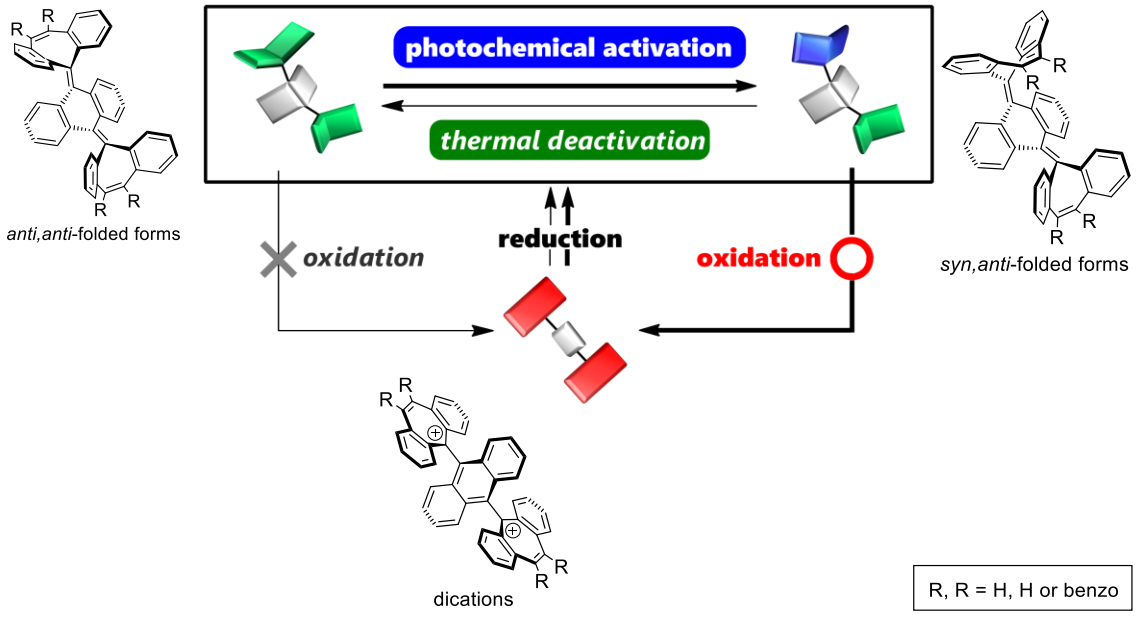

In chapter 4, the author constructed a series of six dications composed of pure hydrocarbons with one to six non-substituted 9,10-anthrylene units end-capped with two dibenzotropyliums to elucidate the electronic properties of huge oligo(9,10-anthrylene) backbones (Figure 1-6).[65] Their structures were successfully determined by X-ray analyses even in the case of eight planar 14π-electron units, revealing that all dications adopt almost orthogonally twisted structures between neighboring units. Spectroscopic and voltammetric analyses suggest that neither the significant overlap of orbitals nor the delocalization of electrons between 14π-electron units occur due to the orthogonally twisted geometry even in solution. As a result, sequential oxidation processes were observed with the reversible formation of multivalent cations with the release of the same number of electrons as the number of anthrylene units. Upon two-electron reduction, a closed-shell butterfly-shaped form was obtained from the dication containing one anthrylene unit whereas open-shell twisted biradicals were isolated as stable entities in the cases of derivatives containing three to six anthrylene units. Notably, from the derivative with two anthrylene units, a metastable open-shell isomer was obtained quantitatively and underwent slow thermal conversion to the most stable closed-shell isomer (E_a = 23.1 kcal mol^{-1}). There is a drastic change in oxidation potentials between two neutral species (ΔE = 1.32 V in CH_2Cl_2). Since the present dications were regenerated upon oxidation of the isolated reduction products, these systems may contribute to the development of advanced response systems capable of switching color, magnetic properties, and oxidative properties by using a "cation-capped orthogonal approach".

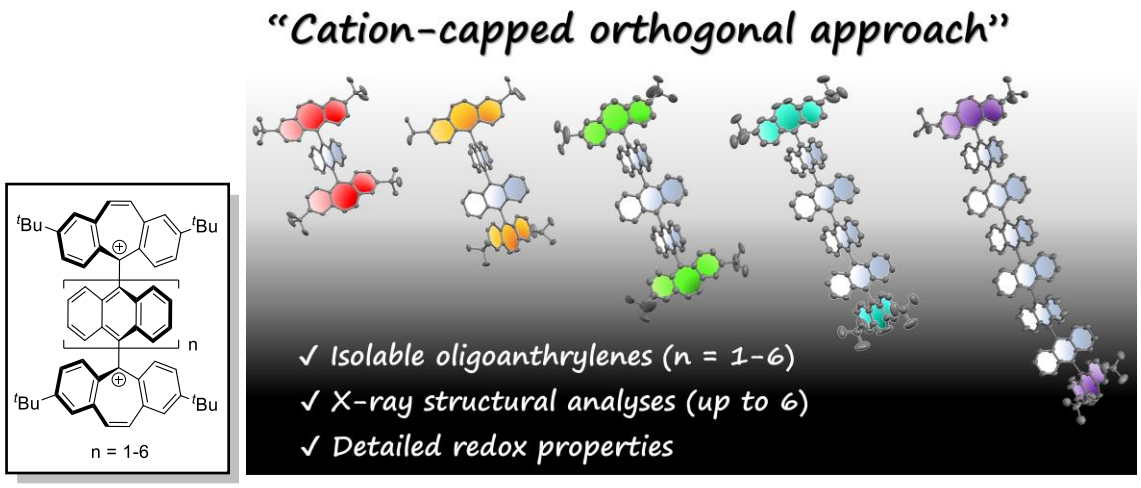

Figure 1-6. Dibenzotropylium-capped oligoanthrylenes (n = 1-6) enabling isolation of dications as stable entities and detailed investigation of their electronic and structural properties.

1-5. References

(1) Wu, Y.-T.; Siegel, J. S. Aromatic Molecular-Bowl Hydrocarbons: Synthetic Derivatives, Their Structures, and Physical Properties. *Chem. Rev*. **2006**, *106* (12), 4843–4867, DOI: 10.1021/cr050554q.

(2) Sygula, A.; Rabideau, P. W. Synthesis and Chemistry of Polycyclic Aromatic Hydrocarbons with Curved Surfaces: Buckybowls. In Carbon-Rich Compounds; Wiley-VCH Verlag: Weinheim, FRG, **2006**; pp 529–565, DOI: 10.1002/3527607994.ch12.

(3) Feng, C.-N.; Kuo, M.-Y.; Wu, Y.-T. Synthesis, Structural Analysis, and Properties of [8]Circulenes. *Angew. Chem. Int. Ed*. **2013**, *52* (30), 7791–7794, DOI: 10.1002/anie.201303875.

(4) Sakamoto, Y.; Suzuki, T. Tetrabenzo[8]Circulene: Aromatic Saddles from Negatively Curved Graphene. *J. Am. Chem. Soc*. **2013**, *135* (38), 14074–14077, DOI: 10.1021/ja407842z.

(5) Kashihara, H.; Asada, T.; Kamikawa, K. Synthesis of a Double Helicene by a Palladium-Catalyzed Cross-Coupling Reaction: Structure and Physical Properties. *Chem. Eur. J*. **2015**, *21* (17), 6523–6527, DOI: 10.1002/chem.201500074.

(6) Fujikawa, T.; Segawa, Y.; Itami, K. Synthesis, Structures, and Properties of π-Extended Double Helicene: A Combination of Planar and Nonplanar π-Systems. *J. Am. Chem. Soc*. **2015**, *137* (24), 7763–7768, DOI: 10.1021/jacs.5b03118.

(7) Gu, X.; Li, H.; Shan, B.; Liu, Z.; Miao, Q. Synthesis, Structure, and Properties of Tetrabenzo[7]Circulene. *Org. Lett*. **2017**, *19* (9), 2246–2249, DOI: 10.1021/acs.orglett.7b00714.

(8) Márquez, I. R.; Fuentes, N.; Cruz, C. M.; Puente-Muñoz, V.; Sotorrios, L.; Marcos, M. L.; Choquesillo-Lazarte, D.; Biel, B.; Crovetto, L.; Gómez-Bengoa, E.; González, M. T.; Martin, R.; Cuerva, J. M.; Campaña, A. G. Versatile Synthesis and Enlargement of Functionalized Distorted Heptagon-Containing Nanographenes. *Chem. Sci*. **2017**, *8* (2), 1068–1074, DOI: 10.1039/C6SC02895K.

(9) Hosokawa, T.; Takahashi, Y.; Matsushima, T.; Watanabe, S.; Kikkawa, S.; Azumaya, I.; Tsurusaki, A.; Kamikawa, K. Synthesis, Structures, and Properties of Hexapole Helicenes: Assembling Six [5]Helicene Substructures into Highly Twisted Aromatic Systems. *J. Am. Chem. Soc*. **2017**, *139* (51), 18512–18521, DOI: 10.1021/jacs.7b07113.

(10) Pun, S. H.; Chan, C. K.; Luo, J.; Liu, Z.; Miao, Q. A Dipleiadiene-Embedded Aromatic Saddle Consisting of 86 Carbon Atoms. *Angew. Chem. Int. Ed*. **2018**, *57*, 1581−1586, DOI: 10.1002/anie.201711437.

(11) Jiménez, V. G.; Tapia, R.; Medel, M. A.; Mariz, I. F. A.; Ribeiro, T.; Blanco, V.; Cuerva, J. M.; Maçôas, E.; Campaña, A. G. Aggregation-Induced Emission of [3]Cumulenes Functionalized with Heptagon-Containing Polyphenylenes. *Chem. Commun*. **2018**, *54*, 3359−3362, DOI: 10.1039/C8CC00386F.

(12) Clevenger, R. G.; Kumar, B.; Menuey, E. M.; Kilway, K. V. Synthesis and Structure of a Longitudinally Twisted Hexacene. *Chem. Eur. J*. **2018**, *24* (13), 3113–3116, DOI: 10.1002/chem.201705676.

(13) Pun, S. H.; Wang, Y.; Chu, M.; Chan, C. K.; Li, Y.; Liu, Z.; Miao, Q. Synthesis, Structures, and Properties of Heptabenzo[7]Circulene and Octabenzo[8]Circulene. *J. Am. Chem. Soc.* **2019**, *141* (24), 9680–9686, DOI: 10.1021/jacs.9b03910.

(14) Hu, Y.; Paternò, G. M.; Wang, X.-Y.; Wang, X.-C.; Guizzardi, M.; Chen, Q.; Schollmeyer, D.; Cao, X.-Y.; Cerullo, G.; Scotognella, F.; et al. π-Extended Pyrene-Fused Double [7]Carbohelicene as a Chiral Polycyclic Aromatic Hydrocarbon. *J. Am. Chem. Soc*. **2019**, *141* (32), 12797–12803, DOI: 10.1021/jacs.9b05610.

(15) Yamago, S.; Kayahara, E.; Iwamoto, T. Organoplatinum-Mediated Synthesis of Cyclic π-Conjugated Molecules: Towards a New Era of Three-Dimensional Aromatic Compounds. *Chem. Rec.* **2014**, *14* (1), 84–100, DOI: 10.1002/tcr.201300035.

(16) Iwamoto, T.; Kayahara, E.; Yasuda, N.; Suzuki, T.; Yamago, S. Synthesis, Characterization, and Properties of [4]Cyclo-2,7-Pyrenylene: Effects of Cyclic Structure on the Electronic Properties of Pyrene Oligomers. *Angew. Chem. Int. Ed*. **2014**,

53 (25), 6430–6434, DOI: 10.1002/anie.201403624.

(17) Kayahara, E; Kouyama, T; Kato, T; Yamago, S, Synthesis and Characterization of [n]CPP (n = 5, 6, 8, 10, and 12) Radical Cation and Dications: Size-Dependent Absorption, Spin, and Charge Delocalization. *J. Am. Chem. Soc*. **2016**, *138* (1), 338-344, DOI: 10.1021/jacs.5b10855.

(18) Darzi, E. R.; Jasti, R. The Dynamic, Size-Dependent Properties of [5]–[12]Cycloparaphenylenes. *Chem. Soc. Rev*. **2015**, *44* (18), 6401–6410, DOI: doi.org/10.1039/C5CS00143A.

(19) Li, P.; Zakharov, L. N.; Jasti, R. A Molecular Propeller with Three Nanohoop Blades: Synthesis, Characterization, and Solid-State Packing. *Angew. Chem. Int. Ed*. **2017**, *56* (19), 5237–5241, DOI: 10.1002/anie.201700935.

(20) Sun, Z.; Suenaga, T.; Sarkar, P.; Sato, S.; Kotani, M.; Isobe, H. Stereoisomerism, Crystal Structures, and Dynamics of Belt-Shaped Cyclonaphthylenes. *Proc. Natl. Acad. Sci*. **2016**, *113* (29), 8109–8114, DOI: 10.1073/pnas.1606530113.

(21) Hitosugi, S.; Sato, S.; Matsuno, T.; Koretsune, T.; Arita, R.; Isobe, H. Pentagon-Embedded Cycloarylenes with Cylindrical Shapes. *Angew. Chem. Int. Ed*. **2017**, *56* (31), 9106–9110, DOI: 10.1002/ange.201704676.

(22) Segawa, Y.; Yagi, A.; Matsui, K.; Itami, K. Design and Synthesis of Carbon Nanotube Segments. *Angew. Chem. Int. Ed*. **2016**, *55* (17), 5136–5158, DOI: 10.1002/anie.201508384.

(23) Povie, G.; Segawa, Y.; Nishihara, T.; Miyauchi, Y.; Itami, K. Synthesis of a Carbon Nanobelt. *Science* **2017**, *356* (6334), 172–175, DOI: 10.1126/science.aam8158.

(24) Povie, G.; Segawa, Y.; Nishihara, T.; Miyauchi, Y.; Itami, K. Synthesis and Size-Dependent Properties of [12], [16], and [24]Carbon Nanobelts. *J. Am. Chem. Soc*. **2018**, *140* (31), 10054–10059, DOI: 10.1021/jacs.8b06842.

(25) Lu, X.; Gopalakrishna, T. Y.; Han, Y.; Ni, Y.; Zou, Y.; Wu, J. Bowl-Shaped Carbon Nanobelts Showing Size-Dependent Properties and Selective Encapsulation of C70. *J. Am. Chem. Soc*. **2019**, *141* (14), 5934–5941, DOI: 10.1021/jacs.9b00683.

(26) Cheung, K. Y.; Watanabe, Ko.; Segawa Y.; Itami, K. Synthesis of a zigzag carbon nanobelt. *Nat. Chem.* **2021**, *13*, 255–259. DOI: 10.1038/s41557-020-00627-5.

(27) Han, Y.; Dong, S.; Shao, J.; Fan, W.; Chi, C. Synthesis of a Sidewall Fragment of a (12,0) Carbon Nanotube. *Angew. Chem. Int. Ed*. **2021**, *60*, 2658–2662, DOI: 10.1002/anie.202012651.

(28) Kammermeier, S.; Jones, P.G.; Herges, R. [2+2] Cycloaddition products of tetradehydrodianthracene: experimental and theoretical proof of extraordinary long C–C single bonds. *Angew. Chem. Int. Ed. Engl.* **1997**, *36*, 1757–1760, DOI:10.1002/anie.199717571.

(29) Takeda, T.; Uchimura, Y.; Kawai, H.; Katoono, R.; Fujiwara, K.; Suzuki, T. Hexaphenylethanes with an Ultralong C–C Bond: Expandability of the C–C Bond in Highly Strained Tetraarylpyracenes. *Chem. Lett.* **2013**, *42*, 954–962, DOI:10.1246/cl.130598.

(30) Nishiuchi, T.; Uno, S.; Hirao, Y.; Kubo, T. Intramolecular interaction, photoisomerization, and mechanical C–C bond dissociation of 1,2-di(9-anthryl)benzene and its photoisomer: A fundamental moiety of anthracene-based π-cluster molecules. *J. Org. Chem.* **2016**, *81*, 2106–2112, DOI: 10.1021/acs.joc.6b00134.

(31) Ishigaki, Y.; Shimajiri, T.; Takeda, T.; Katoono, R.; Suzuki, T. Longest C–C Single Bond among Neutral Hydrocarbons with a Bond Length beyond 1.8 Å. *Chem.* **2018**, *4*, 795–806, DOI: 10.1016/j.chempr.2018.01.011.

(32) Ravat, P.; Šolomek, T.; Häussinger, D.; Blacque, O.; Juríčk, M. Dimethylcethrene: A Chiroptical Diradicaloid Photoswitch. *J. Am. Chem. Soc.* **2018**, *140*, 10839–10847, DOI: 10.1021/jacs.8b05465.

(33) Nozoe, T. Substitution Products of Tropolone and Allied Compounds. *Nature,* **1951**, *167*, 1055– 1057. DOI: 10.1038/1671055a0.

(34) Nozoe, T. Toroponoidokagaku no Sodatsu Made (Until troponoid chemistry grow up).

kagakutoseibutsu, **1984**, *22*, 610– 616. DOI: 10.1271/kagakutoseibutsu1962.22.610.

(35) Spitler, E. L.; Johnson, C. A.; Haley, M. M. Renaissance of Annulene Chemistry. *Chem. Rev.* **2006**, *106*, 5344–5386, DOI: 10.1021/cr050541c.

(36) Konishi, A.; Yasuda, M. Breathing New Life into Nonalternant Hydrocarbon Chemistry: Syntheses and Properties of Polycyclic Hydrocarbons Containing Azulene, Pentalene, and Heptalene Frameworks. *Chem. Lett.* **2021**, *50*, 196–212, DOI: doi.org/10.1246/cl.200650.

(37) Balaban, A. T.; Oniciu, D. C.; Katritzky, A. R. Aromaticity as a Cornerstone of Heterocyclic Chemistry. *Chem. Rev.* **2004**, *104*, 2777-2812, DOI: 10.1021/cr0306790.

(38) Yoon, Z. S.; Osuka, A.; Kim, D. Möbius aromaticity and antiaromaticity in expanded porphyrins. *Nat. Chem.* **2009**, *1*, 113–122. DOI: 10.1038/nchem.172.

(39) Kim, J.; Oh, J.; Osuka, A.; Kim, D. Porphyrinoids, a unique platform for exploring excited-state aromaticity. *Chem. Soc. Rev.*, **2022**, *51*, 268-292, DOI: 10.1039/D1CS00742D.

(40) Komatsu, K. Professor Tetsuo Nozoe and My Tropylium Ion Chemistry. *Chem. Rec.*, **2015**, *15*, 160-174, DOI: 10.1002/tcr.201402048.

(41) Xin, H.; Gao, X. Application of Azulene in Constructing Organic Optoelectronic Materials: New Tricks for an Old Dog. *ChemPlusChem*, **2017**, *82*, 945-956, DOI: 10.1002/cplu.201700039.

(42) Xin, H.; Hou, B.; Gao, X. Azulene-Based π-Functional Materials: Design, Synthesis, and Applications. *Acc. Chem. Res.* **2021**, *54*, 1737–1753, DOI: 10.1021/acs.accounts.0c00893.

(43) Jensen, F. R.; Smith, L. A. The Structure and Interconversion of Cycloheptatriene. *J. Am. Chem. Soc*. **1964**, *86*, 956−957, DOI: 10.1021/ja01059a065

(44) Young, S. D.; Baldwin, J. J.; Cochran, D. W.; King, S. W.; Remy, D. C.; Springer, J. P. Conformational mobility of dibenzo[a,d]cycloheptene derivatives. Preparation and characterization of two intraconverting conformational isomers. *J. Org. Chem.* **1985**, *50*, 339–342, DOI: 10.1021/jo00203a010.

(45) Hjelmencrantz, A.; Friberg, A.; Berg, U. Conformational Analysis of Some 5-Substituted 5H-Dibenzo[a,d]Cycloheptenes. *J. Chem. Soc., Perkin Trans*. **2000**, *2*, 1293−1300, DOI: 10.1039/B001410I.

(46) Koumura, N.; Geertsema, E. M.; van Gelder, M. B.; Meetsma, A.; Feringa, B. L. Second generation light-driven molecular motors. Unidirectional rotation controlled by a single stereogenic center with near-perfect photoequilibria and acceleration of the speed of rotation by structural modification. *J. Am. Chem. Soc.* **2002**, *124*, 5037–5051, DOI: 10.1021/ja012499i.

(47) ter Wiel, M. K. J.; Vicario, J.; Davey, S. G.; Meetsma, A.; Feringa, B. L. New procedure for the preparation of highly sterically hindered alkenes using a hypervalent iodine reagent. *Org. Biomol. Chem*., **2005**, *3*, 28-30, DOI: 10.1039/b414959a.

(48) Greb, L.; Lehn, J.-M. Light-Driven Molecular Motors: Imines as Four-Step or Two-Step Unidirectional Rotors. *J. Am. Chem. Soc*. **2014**, *136*, 13114−13117, DOI: 10.1021/ja506034n.

(49) Wang, Z.; Shao, H.; Ye, J.; Tang, L.; Lu, P. Dibenzosuberenylidene-Ended Fluorophores: Rapid and Efficient Synthesis, Characterization, and Aggregation-Induced Emissions. *J. Phys. Chem. B* **2005**, *109*, 19627–19633, DOI: 10.1021/jp053113j.

(50) Wei, Y.; Chen, C.-T. Doubly Ortho-Linked cis-4,4′-Bis(diarylamino)stilbene/Fluorene Hybrids as Efficient Nondoped, Sky-Blue Fluorescent Materials for Optoelectronic Applications. *J. Am. Chem. Soc.* **2007**, *129*, 7478–7479, DOI: 10.1021/ja070822x.

(51) Hung, S.-F.; Fang, P. H.; Wei, Y.; Tsai, F.-Y.; Chen, C.-T.; Kimura, T.; Samori, S.; Fujitsuka, M.; Majima, T.; Lin, C.-H.; Peng, S.-H.; Jou. J.-H. Spirally Sonfigured (cis-Stilbene) Trimers: Steady-State and Time-Resolved Photophysical Studies and Organic Light-Emitting Diode Applications. *ACS Appl. Mater. Interfaces*, **2018**, *10*, 25561-25569, DOI: 10.1021/acsami.8b06137.

(52) Crocker, R. D.; Zhang, B.; Pace, D. P.; Wong, W. W. H.; Nguyen, T. V.

Tetrabenzo[5.7]fulvalene: a forgotten aggregation induced-emission luminogen. *Chem. Commun.,* **2019**, *55*, 11591–11594, DOI: 10.1039/C9CC06289K.

(53) Brouillac, C.; Shen, W.-S.; Rault-Berthelot, J.; Jeannin, O.; Quinton, C.; Jiang, Z.-Q.; Poriel, C. Spiro-configured dibenzosuberene compounds as deep-blue emitters for organic light-emitting diodes with a CIEy of 0.04. *Mater. Chem. Front.*, **2022**, *6*, 1803-1813, DOI: 10.1039/d2qm00287f.

(54) Rodríguez-Lugo, R. E.; Trincado, M.; Vogt, M.; Tewes, F.; Santiso-Quinones G.; Grützmacher, H. A homogeneous transition metal complex for clean hydrogen production from methanol–water mixtures. *Nat. Chem*. **2013**, *5*, 342–347, DOI: 10.1038/nchem.1595.

(55) Brusey, S. A.; Shen, W.; Müller-Bunz, H.; Ortin, Y.; Evans, P.; McGlinchey M. J. Alkynyldicobalt Derivatives of Dibenzosuberenol and Dibenzocyclooctatrien-5-ol: Ring Conformations, Ease of Carbonyl Elimination and Relevance to Pauson–Khand Cyclization. *Eur. J. Inorg. Chem*. **2017**, *13*, 2048–2057, DOI: 10.1002/ejic.201601538.

(56) Martin, J.; Langer, J.; Wiesinger, M.; Elsen, H.; Harder S. Dibenzotropylidene Substituted Ligands for Early Main Group Metal-Alkene Bonding. *Eur. J. Inorg. Chem*. **2020**, *27*, 2582–2595, DOI: 10.1002/ejic.202000524.

(57) Ito, S.; Kawakami, Jun.; Tajiri, A.; Ryuzaki, D.; Morita, N.; Asao T.; Watanabe, M.; Harada, N. Synthesis and Dynamic Stereochemistry of Azulene-Substituted 9-Fluorenyl, 9,10-Dihydro-10,10-dimethyl-9-anthryl, 10,11-Dihydro-5H-dibenzo[a,d]cyclohepten-5-yl, and 5H-Dibenzo[a,d]cyclohepten-5-yl Cations. Correlations of Stabilities of the Carbocations and Rotational Barrier of Azulene Ring. *Bull. Chem. Soc. Jpn*., **2005**, *78*, 2051–2065, DOI: 10.1246/bcsj.78.2051.

(58) Dyker, G.; Hagel, M.; Henkel, G.; Köckerling, M. Naphthyl-Substituted Carbocations: From peri Interaction to Cyclization. *Eur. J. Org. Chem.* **2008**, *18*, 3095–3101, DOI: 10.1002/ejoc.200800124.

(59) Barton, B.; Betz, R.; Caira, M. R.; Hosten, E. C.; McCleland, C. W.; Pohl, p. L.; Taljaard, B. Clathrates of novel ethylenediamine derivatives: thermal, X-ray crystallographic and conformational analysis of inclusion complexes of N,N′-bis(5-phenyl-5-dibenzo[a,d]cycloheptenyl)ethylenediamine and its 10,11-dihydro analogue. *Tetrahedron*, **2016**, *47*, 7536-7551, DOI: 10.1016/j.tet.2016.10.007.

(60) Nishiuchi, T.; Ito, R.; Takada, A.; Yasuda, Y.; Nagata, T.; Stratmann, E.; Kubo, T. Anthracene-Attached Persistent Tricyclic Aromatic Hydrocarbon Radicals. *Chem. Asian J*. **2019**, *14*, 1830–1836, DOI: 10.1002/asia.201801806

(61) Jiménez, V. G.; Mayorga-Burrezo, P.; Blanco, V.; Lloveras, V.; Gómez-García, C. J.; Šolomek, T.; Cuerva, J. M.; Veciana, J.; Campaña, A. G. Dibenzocycloheptatriene as End-Group of Thiele and Tetrabenzo-Chichibabin Hydrocarbons. *Chem. Commun*. **2020**, *56*, 12813–12816, DOI: 10.1039/D0CC04489J.

(62) Shimizu, A.; Morikoshi, T.; Sugisaki, K.; Shiomi, D.; Sato, K.; Takui, T.; Shintani R. Synthesis and Isolation of a Kekulé Hydrocarbon with a Triplet Ground State. *Angew. Chem. Int. Ed.* **2022**, *61*, e202205729 (pp1-5), DOI: 10.1002/anie.202205729.

(63) Ishigaki, Y.; Hayashi, Y.; Sugawara, K.; Shimajiri, T.; Nojo, W.; Katoono, R.; Suzuki, T. 9,10-Dihydrophenanthrene with Two Spiro(Dibenzocycloheptatriene) Units: A Highly Strained Caged Hydrocarbon Exhibiting Reversible Electrochromic Behavior. *Molecules* **2017**, *22*, 1900, DOI: 10.3390/molecules22111900.

(64) Ishigaki, Y.; Hayashi, Y.; Suzuki, T. Photo- and Thermal Interconversion of Multiconfigurational Strained Hydrocarbons Exhibiting Completely Switchable Oxidation to Stable Dicationic Dyes. *J. Am. Chem. Soc*. **2019**, *141*, 18293-18300, DOI: 10.1021/jacs.9b09646.

(65) Hayashi, Y.; Suzuki, S.; Suzuki, T.; Ishigaki, Y. Dibenzotropylium-Capped Orthogonal Geometry Enabling Isolation and Examination of a Series of Hydrocarbons with Multiple 14π-Aromatic Units. *J. Am. Chem. Soc*. **2023**, *145*, 2596-2608, DOI: 10.1021/jacs.2c12574.

Chapter 2

Strong Electron-Donating Abilities Attained by Through-Bond Interactions

" Compound numbers are independent in each Chapter."

2-1. Introduction

Redox-active molecules with an electrochromic property reversibly change their color by electrochemical stimulation, which can be applied to smart windows, sensors, and displays (Figure 2-1). Almost all of the redox-active molecules are constructed with the aid of the electronic-donating/withdrawing properties of heteroatoms, so that there are a few examples of reversible redox systems composed of pure hydrocarbons.[1]

A series of 9,10-dihydrophenanthrene (DHP) with four aryl groups at the 9,9,10,10-positions, tetraaryl-DHPs (Ar_4DHPs), are known as the electrochromic materials based on "dynamic redox (*dyrex*)" behavior with large structural change upon electron transfer.[2-7] Two-electron oxidation induces the formation of cationic chromophores accompanied by fission of the central C_9–C_{10} bond. Heterocyclic units (acridan/xanthene) or alkoxy/amino groups have often been incorporated into Ar_4DHP to raise the HOMO level and to stabilize the corresponding dicationic species. However, under an appropriate molecular design, the author envisaged that reversible electrochromic systems could be constructed without the aid of heteroatoms.

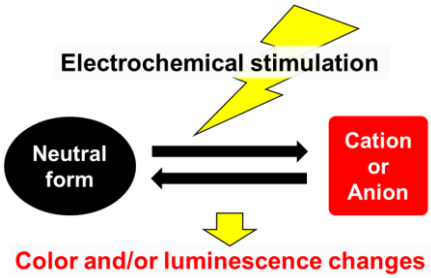

Figure 2-1. Redox-active molecules with an electrochromic property.

Another interesting point regarding Ar_4DHP is the unique geometric feature based on its highly strained structure. In contrast to the easy dissociation of unclamped hexaphenylethane (HPE) into two trityl radicals upon cleavage of the "ethane" bond,[8] Ar_4DHPs as clamped derivatives of HPE are considered to be thermally stable.[9] The C_9–C_{10} bond fission in Ar_4DHP is no longer entropically favored, so that even an elongated bond with a bond length far greater than the standard (1.54 Å) is intact when incorporated in the Ar_4DHP skeleton.[10] Thus, the DHP skeleton is one of the most useful scaffolds for examining highly strained structures and their special properties.

Hexabenzo[4.4.4]propellane **A**,[11] which was first reported in 1971, is a multiply clamped HPE in which the central Csp^3–Csp^3 bond [bond length: 1.563(2) Å] is not greatly expanded (Figure 2-2).[12] In this nonspiro-type clamped HPE, the steric repulsion among the six benzene rings is effectively reduced by adopting a twisted conformation with a torsion angle (α) of about 60° around the central C–C bond. On the other hand, dibenzodinaphtho[4.3.3]propellane **B**[13] has a longer bond [1.612(4) Å] because it has a less-skewed geometry due to the rigid naphthalene planes. This difference in bond length as well as its correlation with torsion/dihedral angles (α, θ) could be supported by density functional theory (DFT) calculations.[14] On the other hand, Ar_4DHPs were predicted to have much longer C–C bonds than that in **B** since the steric hindrance regarding the C_9–C_{10} bond is greater for two unfused benzene rings than for a naphthalene nucleus.

In the case of $(4\text{-}CH_3OC_6H_4)_4$DHP (**C**), accurate values for the bond length and torsion/twisting angles were not obtained by X-ray analysis due to the positional disorder of the ethane unit.[2] Such disorder has often been observed in globular ethanes (e.g., unclamped HPEs[15] or hexachloroethane[16]), but was not present in the spiro-type Ar_4DHPs (**D**[4] and **E**[5]). Their C_9–C_{10} bond lengths were able to be accurately determined to be 1.646(4) and 1.635(2) Å by X-ray analyses. These values are greater than those for other DHPs, and thus the spiro ring can be considered to be the key structure for observing a very long bond in Ar_4DHPs.

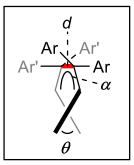

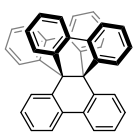

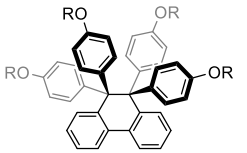

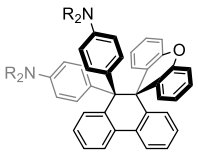

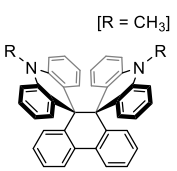

	A	B	C	D	E
α [°]	56.3(2)-56.7(2) (*57.97*)	24.8(4) (*28.85*)	60(2) (*58.82*)	40.4(3) (*45.38*)	47.1(1) (*43.95*)
θ [°]	16.3-17.8 (*23.0*)	16.6 (*13.6*)	5.9 (*24.4*)	16.6 (*17.9*)	19.7 (*18.9*)
d [Å]	1.563(2) (*1.579*)	1.612(4) (*1.611*)	1.50(3) (*1.652*)	1.646(4) (*1.652*)	1.635(2) (*1.665*)

Figure 2-2. Reported structural parameters of Ar_4DHPs determined by X-ray analyses. The values obtained by DFT calculations at the B3LYP/6-31G(d) level in this study are shown in brackets.

In this context, the author focused on the through-bond interaction (TBI)[17] that can effectively raise the HOMO level of Ar_4DHP and easily cleave the elongated C_9–C_{10} bond upon oxidation without the aid of heteroatoms. The TBI is an important factor which modifies the molecular orbital levels that determine their electron-donating properties. As postulated based on a simplified s-*cis* diphenylethane model (Figure 2-3), the σ–orbital of the ethane bond would be

lowered whereas the π^+–orbital should be raised through TBI. Greater perturbation is expected when the two energy levels are closer. The parallel arrangement of these orbitals is also important for realizing effective TBI.

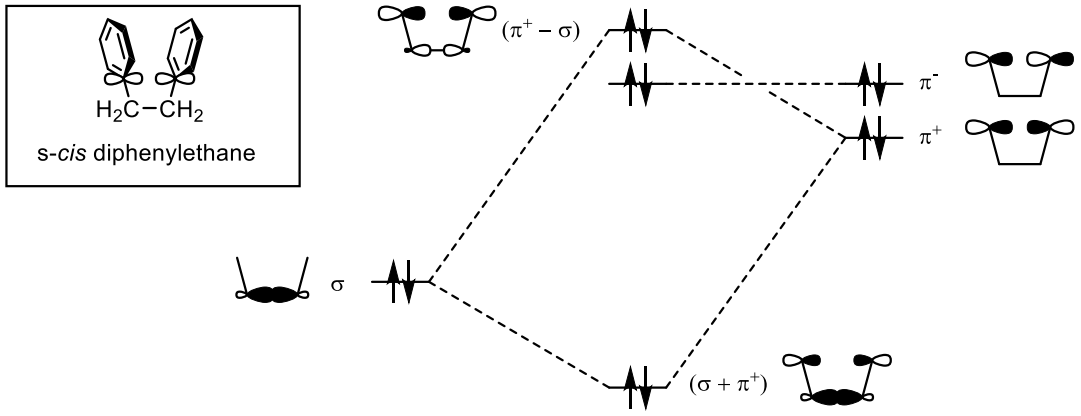

Figure 2-3. Schematic view of through-bond interaction in diphenylethane model.

For Ar_4DHPs, TBI would be maximized by elongation of the C_9–C_{10} bond, since a longer bond has a higher σ–orbital level to narrow the energy gap toward the π^+–orbital. At the same time, an eclipsed conformation is desirable to ensure that the orbitals are parallel. The spiro(dibenzocycloheptatriene) units are the ideal skeleton to be incorporated into Ar_4DHP (Figure 2-4). In general, Ar_4DHPs tend to adopt a skewed geometry to reduce the "front strain"[8] among the four aryl groups over the C_9–C_{10} bond. The spiro(xanthene or 10-methylacridane) with the central six-membered ring can force the DHP skeleton to adopt a less-skewed geometry.[4,5] Here, the author proposes that spiro(dibenzocycloheptatriene) derivative **1** with a central seven-membered ring is more favorable since it can make the DHP skeleton become nearly eclipsed by the greater steric hindrance between the inner protons on the benzo groups and the DHP plane. The nearly eclipsed conformation would also cause elongation of the C_9–C_{10} bond due to the greater steric repulsion than in the skewed conformation, and thus the HOMO level of Ar_4DHP derivative **1** with two spiro(dibenzocycloheptatriene) would be effectively raised through TBI.

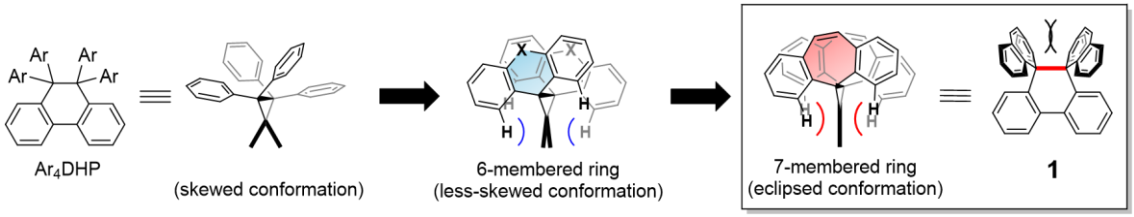

Figure 2-4. Design concept for Ar_4DHP **1** with two spiro(dibenzocycloheptatriene) units.

2-2. Results and Discussion

2-2-1. Theoretical study

DFT calculations at the B3LYP/6-31G(d) level predicted that the optimized structure of **1** adopts a nearly eclipsed conformation, as designed. The C_9–C_{10} bond length was estimated to be greater than 1.7 Å (Figure 2-5), which is much greater than the values previously reported for other Ar_4DHPs (Figure 2-2). The calculated HOMO level of **1** was raised to –5.25 eV, which is much higher than that of $(4\text{-}CH_3OC_6H_4)_4$DHP (–5.44 eV). Thus, the author designed a stronger electron-donating hydrocarbon than Ar_4DHP with four 4-methoxyphenyl groups.

As shown in Figure 2-6, the HOMO of **1** has the character of $(\pi^+ - \sigma)$, as evidenced by the large orbital coefficients on the ethane bond. Thus, the effective TBI between π^+ and σ causes the perturbation of both orbital levels, resulting in an increase in the energy of $(\pi^+ - \sigma)$ to become higher than that of π^- [HOMO-1, –5.39 eV].

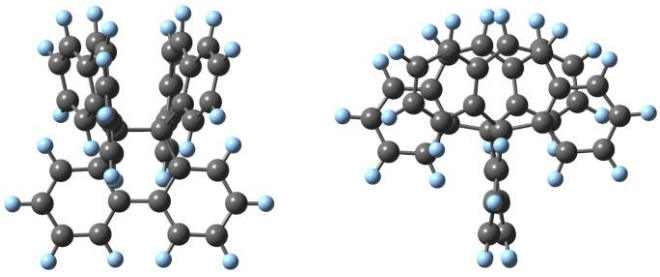

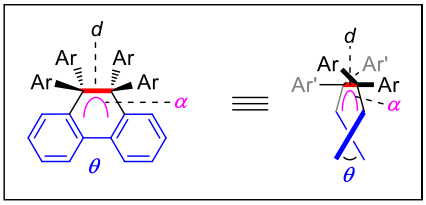

Calcd.	*α* [°]	*θ* [°]	*d* [Å]
1	*27.22*	*15.53*	*1.702*

Figure 2-5. Optimized structure (left: front view, right: side view) of **1**

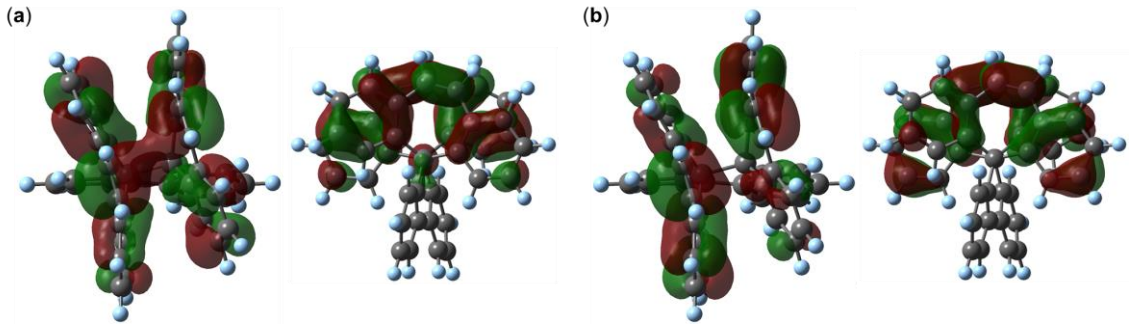

Figure 2-6. (**a**) HOMO and (**b**) HOMO-1 of **1** by DFT calculations (B3LYP/6-31G(d)).

2-2-2. Preparation and X-ray analysis

With 2,2'-diiodobiphenyl as a starting material, diol **4** was prepared by successive reactions with BuLi followed by the addition of dibenzosuberenone.[18] Upon treatment of **4** with HBF_4 in trifluoroacetic anhydride (TFAA), the dication salt $\mathbf{1}^{2+}(BF_4^-)_2$ was isolated as a deep purple powder with 85% yield. When dication $\mathbf{1}^{2+}$ was reduced with Zn powder, the newly designed dispiro Ar_4DHP **1** with two dibenzocycloheptatriene units was obtained quantitatively as a white solid (Scheme 2-1).

X-ray analysis was performed by using a single crystal of **1** (Figure 2-7). Consistent with the results of DFT calculations, **1** adopts a nearly eclipsed geometry. For the DHP skeleton, the torsion angle α over the C_9–C_{10} bond is 23.78(13)° and the dihedral angle θ for the biphenyl unit is only 3.7°. Due to the lack of skewing deformation to reduce the "front" strain, the C_9–C_{10} bond is expanded. The length of 1.6665(17) Å is greater than any values ever reported for Ar_4DHPs.[19]

Scheme 2-1. Preparation of newly designed Ar_4DHP **1**.

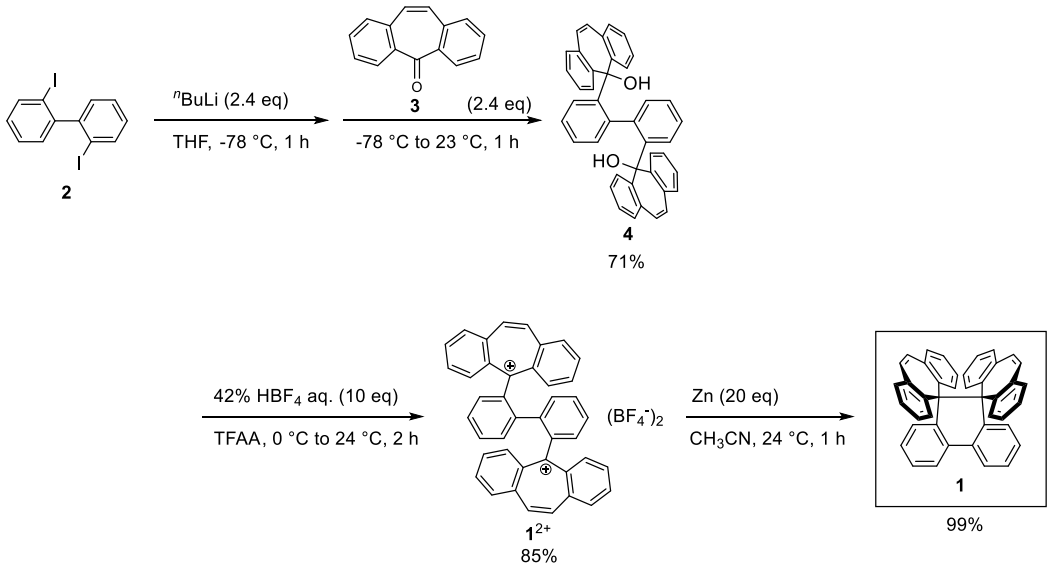

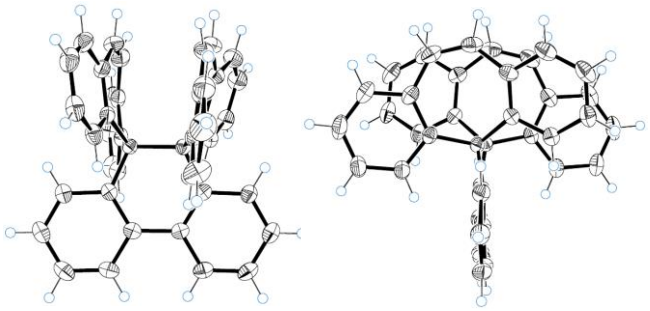

	1
α [°]	23.78(13)
θ [°]	3.7
d [Å]	1.6665(17)

Figure 2-7. ORTEP drawings (left: front view, right: side view) of **1** at 150 K. Thermal ellipsoids are shown at the 50% probability level.

2-2-3. Redox behavior

To investigate the electron-donating properties and reversibility of the redox behavior of **1**, redox potentials were measured by cyclic voltammetry in CH_2Cl_2 (Figure 2-8). The one-wave two-electron oxidation peak was observed, which corresponds to the formation of the dication $\mathbf{1}^{2+}$ accompanied by C_9–C_{10} bond cleavage. The corresponding reduction peak of $\mathbf{1}^{2+}$ appeared at +0.42 V. Such a separation of redox peaks is characteristic of *dyrex* systems. When scanning was repeated twice, no change was observed in the voltammogram, which indicates highly reversible interconversion between **1** and $\mathbf{1}^{2+}$.

The electron-donating properties of hydrocarbon **1** are striking. The oxidation potential (+0.95 V) is far less positive than that of $(4\text{-}CH_3OC_6H_4)_4DHP$ (+1.44 V) measured under similar conditions.[3] Such a change can be qualitatively accounted for by the different HOMO levels calculated by the DFT method, which demonstrates the validity of the concept for raising the HOMO level of Ar_4DHPs through TBI without the aid of heteroatoms.

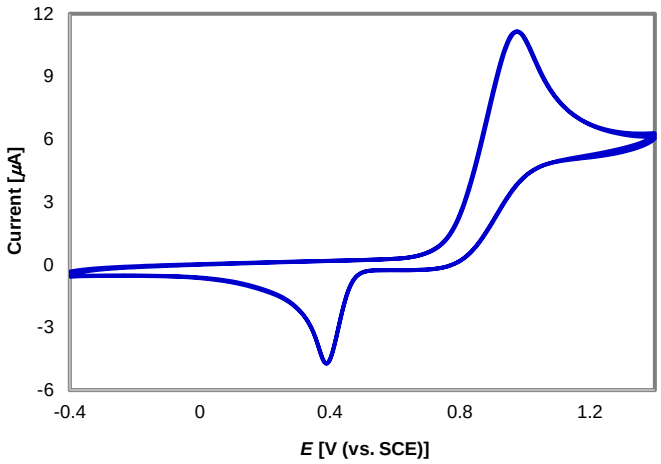

	E^{ox} [V]	E^{red} [V]
1	+0.95	-
$\mathbf{1}^{2+}$	-	+0.42
cf. 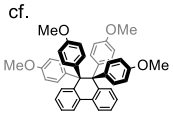	+1.44	-
cf. 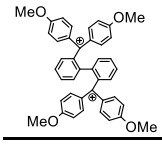	-	+0.21

Figure 2-8. Cyclic voltammogram of **1** in CH_2Cl_2 containing 0.1 M Bu_4NBF_4 as a supporting electrolyte (scan rate 100 mV s^{-1}, Pt electrodes).

2-2-4. Electrochromic behavior

Upon the electrochemical oxidation of **1** in CH_2Cl_2, an electrochromic response from colorless to red was observed with an isosbestic point at 252 nm. The final UV/Vis spectrum is identical to that of the isolated dication $\mathbf{1}^{2+}(BF_4^-)_2$ (Figure 2-9a). Regeneration of **1** with a drastic color change from red to colorless was attained by reverse electrolysis of the as-prepared dicationic solution (Figure 2-9b). This is a rare successful demonstration of electrochromic behavior based on pure hydrocarbon redox species.[1]

Quantitative interconversion between donor **1** and dication $\mathbf{1}^{2+}$ can be conducted in a preparative manner by chemical oxidation and reduction. Thus, upon treatment of **1** with two equivalents of $(4\text{-}BrC_6H_4)_3N^{+\bullet}SbCl_6^-$ in CH_2Cl_2, dication $\mathbf{1}^{2+}$ was isolated quantitatively as a stable salt (Scheme 2-2). The X-ray structural analysis of $\mathbf{1}^{2+}(SbCl_6^-)_2 \cdot 2(CH_2Cl_2)$ crystal shows that there is a π–π stacking interaction between two dibenzotropylium units [dihedral angle: 12.1°; closest C–C contact: 3.31(2) Å] (Figure 2-11a). The biphenyl unit in $\mathbf{1}^{2+}$ is twisted by 70.6°.

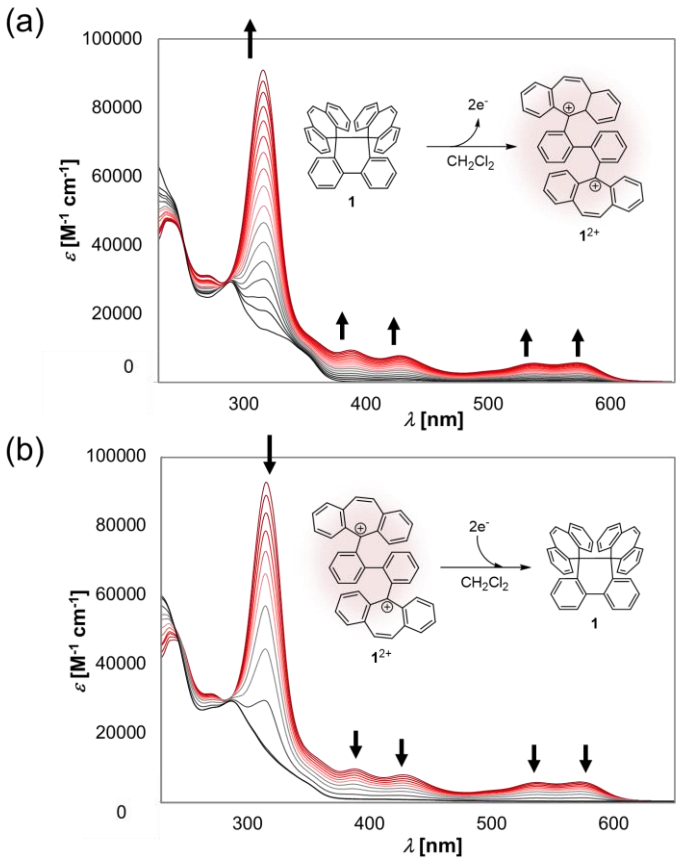

Figure 2-9. (a) A change in UV/Vis spectrum upon electrochemical oxidation (20 μA) of **1** in CH_2Cl_2 containing 0.05 M Bu_4NBF_4 as a supporting electrolyte (every 4 min). (b) A change in UV/Vis spectrum upon electrochemical reduction (20 μA) of as-prepared $\mathbf{1}^{2+}$ in CH_2Cl_2 containing 0.05 M Bu_4NBF_4 as a supporting electrolyte (every 4 min).

Scheme 2-2. Redox interconversion of **1**/**1**$^{2+}$.

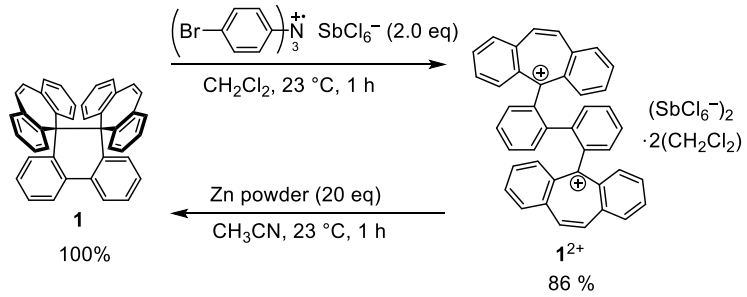

While **1**$^{2+}$ was persistent in CH_2Cl_2, it underwent facile transformation into spiro(fluorene)-type monocation **5**$^{+}$ in CH_3CN. When this conversion was followed by UV/Vis spectroscopy at 23 °C, several isosbestic points were observed (Figure 2-10), from which a reaction rate of 5.0×10^{-4} s^{-1} was deduced. Friedel–Crafts-type cyclization also proceeded cleanly in a preparative scale, and **5**$^{+}$ was isolated as a stable salt in 94% yield (Scheme 2-3). The spiro-structure was unambiguously determined by X-ray analysis of the **5**$^{+}$($SbCl_6^{-}$)·(CH_3CN) crystal (Figure 2-11b).

Many dicationic dyes with a biphenyl-2,2'-diyl skeleton adopt a twisted structure similar to that of **1**$^{2+}$ with a π–π stacking arrangement, for which solvent polarity affects the twisting angle: more acute in a non-polar/less polar solvent and nearly perpendicular in a polar solvent.[20,21] The observed solvent effects for the Friedel–Crafts-type cyclization of **1**$^{2+}$ might be related to this difference in conformation of dication depending on the solvent. Facile degradation to the monocation **5**$^{+}$ in CH_3CN may be related to the largely twisted conformation to facilitate nucleophilic addition of a benzene ring to the cationic center. The lack of further spiro cyclization of **5**$^{+}$ might be related to the ring strain of the 4,8-dihydrocyclopenta[*def*]fluorene structure.[22]

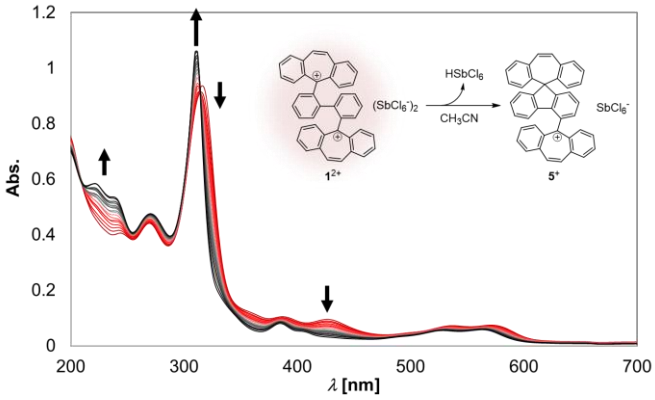

Figure 2-10. A change in UV/Vis spectrum of **1**$^{2+}$ upon standing at 23 °C in CH_3CN (0-12 min, every 2 min; 12-36 min, every 4 min; 36-52 min, every 8 min; 52-84 min, every 16 min).

Scheme 2-3. Irreversible cyclization of $\mathbf{1}^{2+}$.

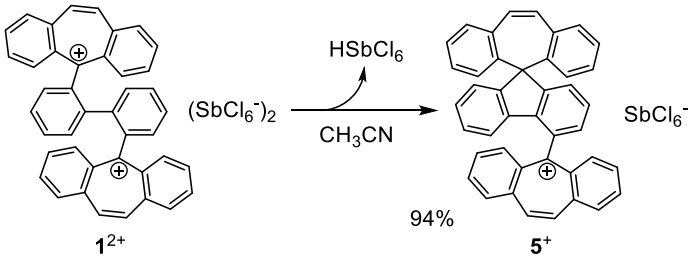

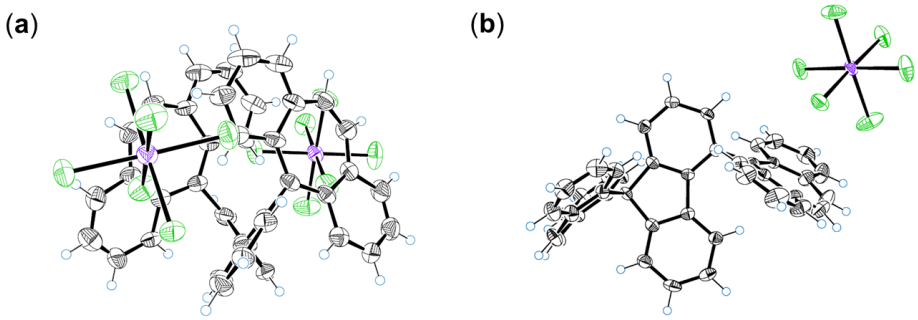

Figure 2-11. ORTEP drawings of (**a**) $\mathbf{1}^{2+}(SbCl_6^-)_2 \cdot 2(CH_2Cl_2)$ and (**b**) $\mathbf{5}^{+}(SbCl_6^-) \cdot (CH_3CN)$ at 150 K. Solvent molecules are omitted for clarity and thermal ellipsoids are shown at the 50% probability level.

2-3. Conclusion

Based on a molecular design that maximizes the effects of TBI, the novel Ar_4DHP **1** with two spiro(dibenzocycloheptatriene) units was designed and synthesized as a hydrocarbon with a stronger electron-donating ability. A highly strained structure of **1** due to unique steric hindrance of seven-membered ring skeleton was confirmed by X-ray analysis as reflected by nearly eclipsed conformation and an elongated "ethane" bond [bond length: 1.6665(17) Å] which is greater than any values ever reported for 9,9,10,10-tetraaryl-9,10-dihydrophenanthrene derivatives. This weakened bond was cleaved upon two-electron oxidation to generate the deeply colored dication, where the oxidation potential (+0.95 V vs. SCE in CH_2Cl_2) is far less positive than that of its analogue with four 4-methoxyphenyl groups (+1.44 V), indicating that the molecular design was appropriate to raise HOMO level effectively without aid of heteroatoms. Based on the reversible interconversion between Ar_4DHP **1** and bis(dibenzotropylium)-type dicationic dye $\mathbf{1}^{2+}$ accompanied by C–C bond formation/cleavage (*dyrex* behavior), the present redox pair exhibits electrochromism with a vivid change in color, and thus represents a class of less well-developed hydrocarbon-based systems. Furthermore, in contrast to the case of reversible process in CH_2Cl_2, the clean irreversible transformation from the dication to monocation with a spiro ring by Friedel–Crafts-type cyclization was observed in polar acetonitrile, Ar_4DHP **1** with dibenzocycloheptatriene units is a unique response system, in which reversible and irreversible switching process can be controlled by a solvent polarity.

2-4. Experimental Section

2-4-1. General

All reactions were carried out under an argon atmosphere. All commercially available compounds were used without further purification unless otherwise indicated. Dry CH_3CN was obtained by distillation from CaH_2 prior to use. Column chromatography was performed on silica gel I-6-40 (YMC) of particle size 40-63 μm. ^1H and ^{13}C NMR spectra were recorded on a BRUKER Ascend^{TM} 400 (^1H/400 MHz and ^{13}C/100 MHz) spectrometer. IR spectra were measured as a KBr pellet on a JEOL JIR-WINSPEC100 FT/IR spectrophotometer. Mass spectra were recorded on a JEOL JMS-T100GCV spectrometer in FD mode (GC-MS&NMR Laboratory, Research Faculty of Agriculture, Hokkaido University). Melting points were measured on a Yamato MP-21 or Yanagimoto micro melting point apparatus and are uncorrected. UV/Vis spectra were recorded on a Hitachi U-3500 spectrophotometer. DFT calculations were performed with the Gaussian 09W program package. The geometries of the compounds were optimized by using the B3LYP method in combination with the 6-31G(d) basis set. Redox potentials (E^{ox} and E^{red}) were measured a BAS ALS-600A by cyclic voltammetry in dry CH_2Cl_2 containing 0.1 M Bu_4NBF_4 as a supporting electrolyte. All of the values shown in the text are in E/V versus SCE measured at a scan rate of 100 mV s^{-1}. Pt electrodes were used as the working (disk) and counter electrodes. The working electrode was polished using a water suspension of aluminum oxide (0.05 μm) before use. The irreversible half-wave potentials were estimated from the anodic peak potentials (E_{pa}) as $E^{ox} = E_{pa} - 0.03$ or the cathodic peak potentials (E_{pc}) as $E^{red} = E_{pc} + 0.03$.

2-4-2. Synthetic procedures

Dispiro(dibenzo[*a*,*d*]cycloheptatriene-5,9'-phenanthrene-10',5''-dibenzo[*a*,*d*]cycloheptatriene) 1

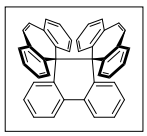

From $\mathbf{1}^{2+}(BF_4^-)_2$

To a solution of $\mathbf{1}^{2+}(BF_4^-)_2$ (265 mg, 375 μmol) in dry CH_3CN (8.5 mL) was added activated zinc powder (496 mg, 7.59 mmol) at 24 °C. The mixture was stirred for 1 h at 24 °C, and then diluted with water. The whole mixture was extracted with CH_2Cl_2 three times. The combined organic layers were washed with water and brine, and dried over anhydrous Na_2SO_4. After filtration through silica gel, the solvent was concentrated under reduced pressure to give **1** (198 mg) as a white solid in 99% yield.

From $\mathbf{1}^{2+}(SbCl_6^-)_2$

To a solution of $\mathbf{1}^{2+}(SbCl_6^-)_2$ (46.3 mg, 38.5 μmol) in dry CH_3CN (1.8 mL) was added activated zinc powder (50.7 mg, 775 μmol) at 25 °C. The mixture was stirred for 15 min, and then diluted with water. The whole mixture was extracted with CH_2Cl_2 three times. The combined organic layers were washed with water and brine, and dried over anhydrous Na_2SO_4. After filtration, the solvent was concentrated under reduced pressure. The crude product was purified by column chromatography on silica gel (CH_2Cl_2) to give **1** (20.4mg) as a white solid in 100% yield.

1; Mp: 259-260 °C (decomp.); ^{1}H NMR ($CDCl_3$): δ/ppm 8.10 (2H, dd, *J* = 1.2, 8.2Hz), 7.33 (2H, ddd, *J* = 1.3, 7.0, 8.2 Hz), 7.02 (2H, ddd, *J* = 1.2, 7.0, 8.1 Hz), 6.90 (2H, dd, *J* = 1.3, 8.1 Hz), 6.83 (4H, ddd, *J* = 1.1, 6.8, 7.8 Hz), 6.74 (4H, dd, *J* = 1.7, 7.8 Hz), 6.43 (4H, ddd, *J* = 1.7, 6.8, 8.5 Hz), 6.32 (4H, dd, *J* = 1.1, 8.5 Hz), 6.08 (4H, s); ^{13}C NMR ($CDCl_3$): δ/ppm 147.13, 143.59, 137.58, 137.15, 136.80, 133.25, 131.63, 131.26, 127.29, 126.56, 125.63, 125.34, 121.29, 70.50; IR (KBr): ν/cm^{-1} 3049, 3030, 1952, 1591, 1491, 1457, 1441, 1426, 1306, 1285, 1172, 1159, 1071, 1053, 954, 880, 870, 797, 767, 746, 725; LR-MS (FD) m/z (%): 534.26 (11), 533.26 (45), 532.25 (M^+, bp), 267.13 (2), 266.63 (10), 266.13 (22); HR-MS (FD) Calcd. for $C_{42}H_{28}$: 532.21910; Found: 532.22084; UV/Vis (CH_2Cl_2): λ_{max}/nm (ε/M^{-1}cm^{-1}) 347 (9600), 290 (29000), 246 (49200).

5,5'-([1,1'-Biphenyl]-2,2'-diyl)bis(5*H*-dibenzo[*a*,*d*]cycloheptatrien-5-ylium) bis(tetrafluoroborate) $\mathbf{1}^{2+}(BF_4^-)_2$

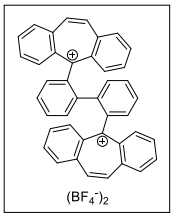

To a solution of diol **5** (252 mg, 445 μmol) in TFAA (4.7 mL) was added 42% HBF_4 aq (670 μL, 4.45 mmol) at 0 °C to give a deep red solution, and the mixture was stirred for 2 h at 24 °C. The addition of dry ether led to precipitation of the dication salt. The precipitates were filtered, washed with dry ether three times, and dried in vacuo to give $\mathbf{1}^{2+}(BF_4^-)_2$ (267 mg) as a red powder in 85% yield.

$\mathbf{1}^{2+}(BF_4^-)_2$; ^{1}H NMR and ^{13}C NMR spectra are identical to those of $\mathbf{1}^{2+}(SbCl_6^-)_2$; IR (KBr):

ν/cm^{-1} 3063, 1609, 1602, 1517, 1476, 1429, 1385, 1337, 1223, 1177, 1163, 1068, 897, 850, 836, 801, 781, 751, 735; LR-MS (FD) m/z (%): 548.22 (9), 534.23 (10), 533.23 (47), 532.22 (M^+, bp), 531.22 (7), 266.61 (10), 266.11 (M^{2+}, 21); HR-MS (FD) Calcd. for $C_{42}H_{28}$: 532.21910; Found: 532.21844; UV/Vis (CH_3CN): λ_{max}/nm (ε/M^{-1}cm^{-1}) 567 (4550), 534 (4330), 432 (4360), 386 (6760), 313 (76900), 269 (26200).

5,5'-(1,1'-Biphenyl-2,2'-diyl)bis(5*H*-dibenzo[*a*,*d*]cycloheptatrien-5-ylium) bis(hexachloroantimonate) $\mathbf{1}^{2+}(SbCl_6^-)_2$

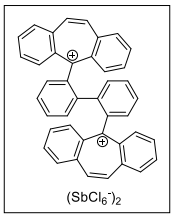

To a solution of **1** (225 mg, 422 μmol) in dry CH_2Cl_2 (10 mL) was added (4-$BrC_6H_4)_3N^{+\bullet}SbCl_6^-$ (680 mg, 833 μmol) at 23 °C, and the mixture was stirred for 1 h. The addition of dry ether led to precipitation of the dication salt. The precipitates were filtered, washed with dry ether three times, and dried in vacuo to give $\mathbf{1}^{2+}(SbCl_6^-)_2 \cdot 2(CH_2Cl_2)$ (500 mg) as a red powder in 86% yield.

$\mathbf{1}^{2+}(SbCl_6^-)_2$; ^{1}H NMR ($CH_3CN$): δ/ppm 8.98 (4H, brs), 8.49 (4H, brt, *J* = 7.0 Hz), 8.42 (4H, brt, *J* = 7.0 Hz), 7.80 (4H, brs), 7.61-7.53 (4H, m), 7.50 (4H, brs), 7.46 (2H, brt, *J* = 7.4 Hz), 7.06 (2H, brd, *J* = 7.4 Hz); ^{13}C NMR (CH_3CN): δ/ppm 180.00, 146.66, 145.95, 141.64, 140.49, 140.15, 139.40, 138.51, 136.97, 134.76, 134.14, 132.92, 130.99, 128.48; IR (KBr): ν/cm^{-1} 3055, 2931, 1636, 1600, 1512, 1473, 1426, 1383, 1335, 1253, 1222, 1164, 829, 847, 829, 796, 750, 730; LR-MS (FD) m/z (%): 534.26 (11), 533.26 (45), 532.25 (M^+, bp), 267.13 (2), 266.63 (10), 266.13 (M^{2+}, 22); HR-MS (FD) Calcd. for $C_{42}H_{28}$: 266.10955 (M^{2+}); Found: 266.10863 (M^{2+}); UV/Vis (CH_3CN): λ_{max}/nm (ε/M^{-1}cm^{-1}) 569 (5000), 535 (4780), 425 (61700), 387 (7740), 314 (85600), 270 (43000).

2,2'-Bis(5-hydroxydibenzo[*a*,*d*]cycloheptatriene-5-yl)biphenyl 4[18]

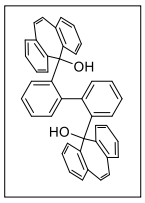

To a solution of 2,2'-diiodobiphenyl **2**[23] (1.13 g, 2.78 mmol) in dry THF (10 mL) was added ^{n}BuLi (1.55 M in hexane, 4.3 mL, 6.67 mmol) dropwise over 2 min at –78 °C. After stirring at –78 °C for 1 h, dibenzosuberenone **3** (1.38 g, 6.67 mmol) was added to the suspension and the mixture was warmed to 23 °C. The resulting solution was stirred for 1 h at 23 °C, and then diluted with water. The whole mixture was extracted with EtOAc three times. The combined organic layers were washed with water and brine, and dried over anhydrous Na_2SO_4. After filtration, the solvent was concentrated under reduced pressure. The crude product was washed with methanol to give diol **4** (1.12 mg) as a white solid in 71% yield.

4; ^{1}H NMR ($CDCl_3$): δ/ppm 8.13 (2H, dd, *J* = 1.2, 7.9 Hz), 7.50 (2H, ddd, *J* = 1.8, 6.8, 7.9 Hz), 7.39 (2H, dd, *J* = 1.3, 8.0 Hz), 7.30 (2H, dt, *J* = 1.2, 6.8 Hz), 7.02 (2H, dd, *J* = 1.8, 6.8 Hz), 6.98 (2H, dd, *J* = 1.3, 7.3 Hz), 6.86 (2H, dt, *J* = 1.3, 7.3 Hz), 6.79 (2H, ddd, *J* = 1.3, 7.3, 8.0 Hz),

6.67(4H, s), 6.61 (2H, ddd, *J* = 1.5, 7.5, 8.7 Hz), 6.46 (2H, dt, *J* = 1.2, 7.5 Hz), 6.39 (2H, dd, *J* = 1.2, 8.7 Hz), 6.05 (2H, dd, *J* = 1.5, 7.5 Hz), 5.04 (2H, s)

5-(Spiro[dibenzo[*a*,*d*]cycloheptatriene-5,9'-fluoren]-4'-yl)-5*H*-dibenzo[*a*,*d*]cycloheptatriene-5-ylium hexachloroantimonate $5^{+}(SbCl_6^{-})$

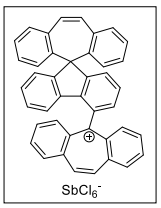

A solution of $\mathbf{1}^{2+}(SbCl_6^{-})_2$ (83.9 mg, 69.8 μmol) in dry CH_3CN (3 mL) was stirred for 2 days at 22 °C. The addition of dry ether led to precipitation of the monocation salt. The precipitates were filtered, washed with dry ether three times, and dried in vacuo to give $\mathbf{5}^{+}(SbCl_6^{-})$ (56.7 mg) as a red powder in 94% yield.

$\mathbf{5}^{+}(SbCl_6^{-})$; ^{1}H NMR (acetone-$d_6$): δ/ppm 9.71 (2H, s), 9.14 (2H, dd, *J* = 1.2, 8.1 Hz), 8.80 (2H, ddd, *J* = 1.0, 7.2, 8.1 Hz), 8.65 (2H, d, *J* = 8.9 Hz), 8.45 (1H, dd, *J* = 0.9, 7.7 Hz), 8.29 (2H, ddd, *J* = 1.2, 7.2, 8.9 Hz), 7.95 (1H, d, *J* = 7.7 Hz), 7.75 (1H, t, *J* = 7.7 Hz), 7.58 (2H, dd, *J* = 1.6, 7.3 Hz), 7.57 (1H, dd, *J* = 0.9, 7.7 Hz), 7.38 (2H, dt, *J* = 1.0, 7.3 Hz), 7.16 (2H, ddd, *J* = 1.6, 7.3, 8.3 Hz), 7.15 (2H, s), 7.13 (1H, dt, *J* = 0.9, 7.7 Hz), 7.03 (2H, dd, *J* = 1.0, 8.3 Hz), 6.68 (1H, dt, *J* = 0.9, 7.7 Hz), 5.78 (1H, d, *J* = 7.7 Hz); ^{13}C NMR (acetone-d_6): δ/ppm 181.17, 154.51, 154.39, 147.39, 145.88, 141.66, 141.23, 138.85, 138.12, 136.78, 136.75, 136.66, 136.02, 135.89, 134.09, 133.20, 132.88, 129.89, 128.78, 128.73, 128.46, 128.34, 128.16, 127.96, 127.84, 127.32, 122.72, 66.00; IR (KBr): ν/cm^{-1} 3061, 2935, 2859, 2360, 1600, 1513, 1479, 1428, 1385, 1337, 1258, 1177, 892, 848, 833, 801, 752, 734; LR-MS (FD) m/z (%): 588.24 (6), 566.19 (6), 533.23 (11), 532.23 (47), 531.22 (M^+, bp); HR-MS (FD) Calcd. for $C_{42}H_{27}$: 531.21128; Found: 531.21124; UV/Vis (CH_2Cl_2): λ_{max}/nm (ε/M^{-1}cm^{-1}) 567 (5200), 533 (4680), 406 (6310), 388 (7980), 315 (104500), 275 (35800), 242 (46700).

2-4-3. Crystal data

Data were collected with a Rigaku Mercury 70 diffractometer (Mo-Kα radiation, λ = 0.71075 Å). The structure was solved by the direct method (SIR2004) and refined by the full-matrix least-squares method on F^2 with anisotropic temperature factors for non-hydrogen atoms. All the hydrogen atoms were located at the calculated positions and refined with riding.

1: Crystals were obtained by recrystallization from $CHCl_3$/hexane. MF: $C_{42}H_{28}$, FW: 532.68, colorless block, 0.20 × 0.20 × 0.20 mm^3, monoclinic $P2_1/c$, a = 13.3661(12) Å, b = 12.6558(11) Å, c = 16.166(2) Å, β = 95.8567(13)°, V = 2720.4(5) Å^3, ρ (Z = 4) = 1.301 g cm^{-3}. A total 20359 reflections ($2\theta_{max}$ = 55.0°) were measured at T = 150 K. Numerical absorption correction was applied (μ = 0.735 cm^{-1}). The final *R1* and *wR2* values are 0.0439 (I > 2σI) and 0.1179 (all data) for 5332 reflections and 379 parameters. Estimated standard deviations are 0.0017-0.003 Å for bond lengths and 0.09-0.17° for bond angles. CCDC 1580196.

1^{2+}($SbCl_6^-$)$_2$·2(CH_2Cl_2): Crystals were obtained by recrystallization from CH_2Cl_2/ether. MF: $C_{44}H_{32}Cl_{16}Sb_2$, FW: 1371.48, red platelet, 0.60 × 0.10 × 0.10 mm^3, monoclinic $P2_1/c$, a = 11.109(2) Å, b = 15.074(3) Å, c = 30.901(6) Å, β= 91.693(3)°, V = 5172(2) Å^3, ρ (Z = 4) = 1.761 g cm^{-3}. A total 31500 reflections ($2\theta_{max}$ = 55.0°) were measured at T = 150 K. Numerical absorption correction was applied (μ = 19.007 cm^{-1}). The final *R1* and *wR2* values are 0.0983 (I > 2σI) and 0.2428 (all data) for 8942 reflections and 559 parameters. Estimated standard deviations are 0.004-0.03 Å for bond lengths and 0.13-0.8° for bond angles. CCDC 1580197.

5$^+$($SbCl_6^-$)·(CH_3CN): Crystals were obtained by recrystallization from CH_3CN/ether. MF: $C_{44}H_{30}Cl_6NSb$, FW: 907.20, red platelet, 0.80 × 0.20 × 0.10 mm^3, triclinic $P\bar{1}$, a = 9.518(7) Å, b = 13.5559(10) Å, c = 15.433(11) Å, α = 98.195(9)°, β = 92.202(13)°, γ = 102.889(11)°, V = 1916(2) Å^3, ρ (Z = 2) = 1.572 g cm^{-3}. A total 14621 reflections ($2\theta_{max}$ = 55.0°) were measured at T = 150 K. Numerical absorption correction was applied (μ = 11.707 cm^{-1}). The final *R1* and *wR2* values are 0.0415 (I > 2σI) and 0.1049 (all data) for 7454 reflections and 454 parameters. Estimated standard deviations are 0.0013-0.007 Å for bond lengths and 0.04-1.2° for bond angles. CCDC 1580199.

2-5. References

(1) Harimoto, T.; Ishigaki, Y. Redox-Active Hydrocarbons: Isolation and Structural Determination of Cationic States toward Advanced Response Systems. *ChemPlusChem,* **2022**, *87*, e202200013 (pp 1-14), DOI: 10.1002/cplu.202200013.

(2) Suzuki, T.; Nishida, J.; Tsuji, T. Hexaphenylethane derivatives exhibiting novel electrochromic behavior. *Angew. Chem. Int. Ed. Engl.* **1997**, *36*, 1329–1331, DOI: 10.1002/anie.199713291.

(3) Suzuki, T.; Nishida, J.; Tsuji, T. A new type of tricolor electrochromic system based on the dynamic redox properties of hexaarylethane derivatives. *Chem. Commun.* **1998**, 2193–2194, DOI: 10.1039/a806037a.

(4) Suzuki, T.; Ono, K.; Nishida, J.; Takahashi, H.; Tsuji, T. Preparation and molecular structures of 9,10-dihydrophenanthrenes: substituent effects on the long bond length. *J. Org. Chem.* **2000**, *65*, 4944–4948, DOI: 10.1021/jo0003697.

(5) Suzuki, T.; Migita, A.; Higuchi, H.; Kawai, H.; Fujiwara, K.; Tsuji, T. A novel redox switch for fluorescence: Drastic UV–vis and fluorescence spectral changes upon electrolysis of a hexaphenylethane derivative of 10,10′-dimethylbiacridan. *Tetrahedron Lett.* **2003**, *44*, 6837–6840, DOI: 10.1016/S0040-4039(03)01717-9.

(6) Suzuki, T.; Ohta, K.; Nehira, T.; Higuchi, H.; Ohta, E.; Kawai, H.; Fujiwara, K. Unprecedented four-way-output molecular response system based on biphenyl-2,2′-diyldiacridiniums: Induction of axial chirality through intramolecular hydrogen bonds between chiral amide groups. *Tetrahedron Lett.* **2008**, *49*, 772–776, DOI: 10.1016/j.tetlet.2007.11.179.

(7) Suzuki, T.; Tamaoki, H.; Nishida, J.; Higuchi, H.; Iwai, T.; Ishigaki, Y.; Hanada, K.; Katoono, R.; Kawai, H.; Fujiwara, K.; et al. Redox-mediated reversible σ-bond formation/cleavage. In *Organic Redox Systems*; John Wiley & Sons, Inc: Hoboken, NJ, USA, 2015; pp. 13–37, ISBN: 9781118858981.

(8) Hounshell, W.D.; Dougherty, D.A.; Hummel, J.P.; Mislow, K. Structure of hexaphenylethane and congeners as determined by empirical force field calculations. *J. Am. Chem. Soc.* **1977**, *99*, 1916–1924, DOI: 10.1021/ja00448a038.

(9) Wittig, G.; Petri, H. Über das 9, 10-Tetraphenyl-dihydrophenanthren und 4,5-Dimethoxy-9, 10-tetraphenyl-dihydrophenanthren. (V. Mitt. über Ringschluß und Radikalbildung. *Eur. J. Org. Chem.* **1933**, *505*, 17–41, DOI: 10.1002/jlac.19335050103.

(10) Suzuki, T.; Takeda, T.; Kawai, H.; Fujiwara, K. Ultralong C-C bonds in hexaphenylethane derivatives. *Pure Appl. Chem.* **2008**, *80*, 547–553, DOI: 10.1351/pac200880030547.

(11) Wittig, G.; Schoch, W. Propellane des Dibenzo[g.p]chrysen-Systems. *Eur. J. Org. Chem.* **1971**, *749*, 38–48, DOI: 10.1002/jlac.19717490106.

(12) Debroy, P.; Lindeman, S.V.; Rathore, R. Hexabenzo[4.4.4]propellane: A helical molecular platform for the construction of electroactive materials. *Org. Lett.* **2007**, *9*, 4091–4094, DOI: 10.1021/ol7015466.

(13) Dyker, G.; Körning, J.; Jones, P.G.; Bubenitschek, P. Palladium-catalyzed arylation of tetrasubstituted double bonds: A simple synthesis of annelated propellanes. *Angew. Chem. Int. Ed. Engl.* **1993**, *32*, 1733–1735, DOI: 10.1002/anie.199317331.

(14) Frisch, M.J.; Trucks, G.W.; Schlegel, H.B.; Scuseria, G.E.; Robb, M.A.; Cheeseman, J.R.; Scalmani, G.; Barone, V.; Mennucci, B.; Petersson, G.A.; et al. *Gaussian 09, Revision E.01*; Gaussian, Inc.: Wallingford, CT, USA, 2013.

(15) Kahr, B.; Van Engen, D.; Mislow, K. Length of the ethane bond in hexaphenylethane and its derivatives. *J. Am. Chem. Soc.* **1986**, *108*, 8305–8307, DOI: 10.1021/ja00286a053.

(16) Atoji, M.; Oda, T.; Watanabé, T. On the crystal structure of cubic hexachloroethane. *Acta Crystallogr.* **1953**, *6*, 868–868, DOI: 10.1107/S0365110X53002520.

(17) Hoffmann, R. Interaction of orbitals through space and through bonds. *Acc. Chem. Res.* **1971**, *4*, 1–9, DOI: 10.1021/ar50037a001.

(18) Weber, E.; Wierig, A.; Skobridis, K. Crystalline diol hosts featuring a bulky biphenyl framework—Host Synthesis and Formation of Inclusion Compounds. *Adv. Synth. Catal.* **1996**, *338*, 553–557, DOI: 10.1002/prac.199633801104.

(19) Wada, K.; Takeda, T.; Kawai, H.; Katoono, R.; Fujiwara, K.; Suzuki, T. Geometrical remote steric effects in 4,5-disubstituted-9,10-dihydrophenanthrenes: expansion of prestrained C^9–C^{10} bond in di(spiroacridan) derivatives. *Chem. Lett.* **2013**, *42*, 1194–1196, DOI: 10.1246/cl.130502.

(20) Suzuki, T.; Iwai, T.; Ohta, E.; Kawai, H.; Fujiwara, K. Electrochiroptical systems based on biphenyl-2,2′-diyl-type dicationic dyes: Strong chiroptical signals through the transmission of point chirality to axial chirality. *Tetrahedron Lett.* **2007**, *48*, 3599–3603, DOI: 10.1016/j.tetlet.2007.03.080.

(21) Suzuki, T.; Ishigaki, Y.; Iwai, T.; Kawai, H.; Fujiwara, K.; Ikeda, H.; Kano, Y.; Mizuno, K. Multi-input/multi-output molecular response system based on the dynamic redox behavior of 3,3,4,4-tetraaryldihydro[5]helicene derivatives: reversible formation/destruction of chiral fluorophore and modulation of chiroptical properties by solvent polarity. *Chemistry* **2009**, *15*, 9434–9441, DOI: 10.1002/chem.200900968.

(22) Trost, B.M.; Kinson, P.L.; Maier, C.A.; Paul, I.C. Structure of 4,8-dihydrodibenzo[*cd*,*gh*] pentalene. *J. Am. Chem. Soc.* **1971**, *93*, 7275–7281, DOI: 10.1021/ja00755a026.

(23) Neugebauer, W.; Kos, A.J.; von Ragué Schleyer, P. Regioselektive dimetallierung von aromaten. Bequemer zugang zu 2,2′-disubstituierten biphenylderivaten. *J. Organomet. Chem.* **1982**, *228*, 107–118, DOI: 10.1016/S0022-328X(00)87089-8.

Chapter 3

ON/OFF Switching of Oxidative Properties Based on "Photo/Thermal" Isomerization

" Compound numbers are independent in each Chapter."

3-1. Introduction

In contrast to normal alkenes with a planar geometry, a molecule in which the dibenzocycloheptatrienylidene moieties are connected by a C=C double bond, cannot adopt a planar geometry around the C=C unit. Deviation from standard planarity happens with an energy loss of π-conjugation to give strained molecules as in other overcrowded ethylenes (OCEs),[1–6] in which the C=C double bond is surrounded by bulky substituents. Since OCEs can often adopt multiple configurations such as folded and/or twisted form(s), many OCEs exhibit photo- and thermochromic behavior upon exposure to external stimuli such as light and heat (Figure 3-1). The author envisaged that advanced electrochromic OCEs could be realized, which could be activated/deactivated by light/heat by incorporating characteristic photo/thermal interconversion as a switching mechanism.

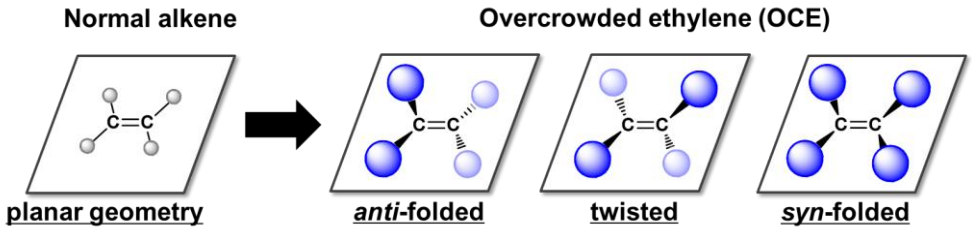

Figure 3-1. Multiple configurations of OCE.

Several dibenzocycloheptatrienylidene-based OCEs that include tetrabenzoheptafulvalene (TBHF)[7] have been reported. The parent TBHF exhibits photo- and thermal isomerization between their *anti*- and *syn*-folded isomers because flipping of a seven-membered ring is hampered by steric hindrance in the overcrowded fjord region around the central C=C double bond (Scheme 3-1a).[8–11] This observation can also be found in other types of TBHFs, as reported by Miao *et al*. (Scheme 3-1b).[12] The formation of a dication was observed for the parent TBHF; however, it was not isolated but only detected by NMR and UV-Vis spectroscopies,[13,14] because the spatial intimacy of two positive charges results in instability of the dicationic species. Thus, electrochromic behavior was not realized in those molecules.

On the other hand, redox-active OCEs with several configurations have been developed based on bistricyclic aromatic enes (BAEs) such as bianthrones (Scheme 3-2a)[1,2] and

bisthiaxanthylidenes (Scheme 3-2b)[4,5] by Evans *et al*. and Feringa *et al*. These BAEs have *syn*/*anti*-folded and twisted forms, where every form with different configurations has different redox potentials. Although the redox potential can be switched by heat or light, higher-energy forms are kinetically unstable and easily converted to the most stable configuration under ambient conditions, so that activation/deactivation by light/heat could not be applied for switching.

Scheme 3-1. Previously reported (a) TBHF[7–11,13,14] and (b) its derivatives[12] exhibiting photo- and thermal isomerization between *anti*- and *syn*-folded isomers.

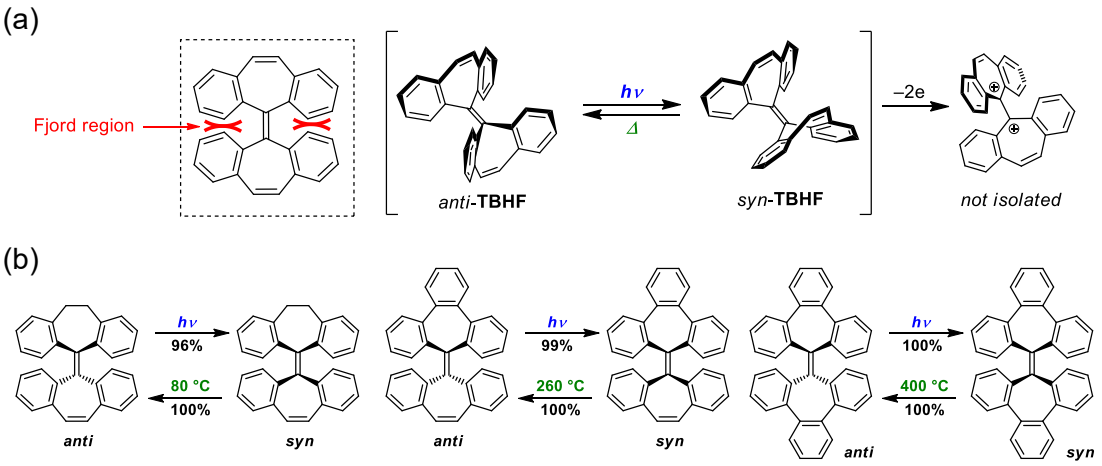

Scheme 3-2. Previously reported examples with different redox potentials depending on their configurations.

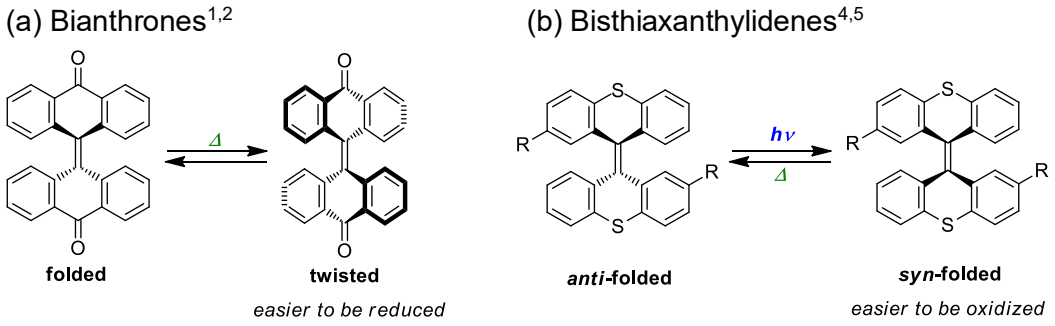

Scheme 3-3. Previously reported Ar_4AQDs exhibiting *dyex* behavior.[16]

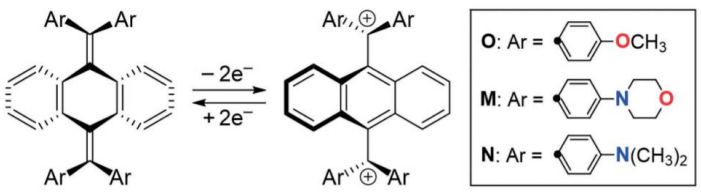

In this study, to create novel response systems in which oxidative properties can be completely activated/deactivated by light/heat, the author designed hydrocarbon-based OCE **1** by insertion of anthraquinodimethane (AQD) skeleton into TBHF (Scheme 3-4). The AQD skeleton would be expected to work as a proper spacer, which can stabilize corresponding dicationic species $\mathbf{1}^{2+}$ to realize redox interconversion between neutral form and cationic species, as exemplified by recent studies on the dication of tetraarylanthraquinodimethanes (Ar_4AQDs) in the author's group (Scheme 3-3).[15,16] Newly designed molecule **1** would exhibit two or more patterns of structural changes derived from reversible isomerization between *syn/anti*-folded isomers upon photoirradiation and heating. The resulting configurational isomers would be expected to be isolated as stable entity and could not undergo thermal isomerization under ambient conditions, thanks to the large steric hindrance in the overcrowded fjord region around the central C=C double bond caused by seven-membered rings of dibenzocycloheptatrienylidene units, as in the case of TBHFs. These isomers would have different electron-donating properties due to the difference in deformation of the conjugation, and thus the applied electric potential needed to give the corresponding cationic species would be different. To observe the enhanced switching properties, **2** with two tribenzocycloheptatrienylidene units, and greater steric hindrance, was also designed. It is expected that these OCEs **1** and **2** show quantitative photo- and thermal interconversion among the isolable configurational isomers with different oxidation potentials, which can selectively undergo redox interconversion with $\mathbf{1}^{2+}$ and $\mathbf{2}^{2+}$.

As shown above, few examples in which redox-active OCEs adopt two or more configurations in the neutral state have been reported, however, ON/OFF switching of redox properties has never been demonstrated.[1,2,4,5] In this dissertation, the author reports the first description of what oxidative properties among isomers were completely switched upon photoirradiation and heating, thus demonstrating light/heat-induced activation/deactivation of redox reactions based on isolable conformers.

Scheme 3-4. Molecular design for **1** and **2**.

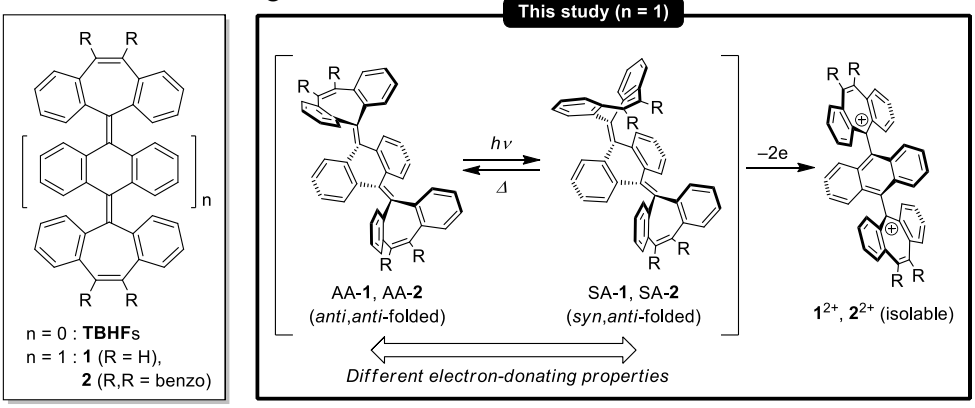

3-2. Results and Discussion

3-2-1. DFT calculations

Based on the above molecular design, a theoretical study was conducted for hydrocarbon **1**. There are five possible structures [relative energy E_{rel}/kcal mol^{-1}: 0 for *anti*,*anti*-**1** (AA-**1**), +4.75 for *syn*,*anti*-**1** (SA-**1**), +13.4 for *syn*,*syn*-**1** (SS-**1**), +40.9 for twisted **1** (T-**1**), and +22.9 for singlet/triplet diradical **1**$^{\bullet\bullet}$ (D-**1**$^{\bullet\bullet}$)] in the neutral state optimized by density functional theory (DFT) calculations[17] at the (U)B3LYP/6-31G(d) level (Figure 3-2a-d). Similar results were obtained for **2** [E_{rel}/kcal mol^{-1}: 0 for AA-**2**, +4.63 for SA-**2**, +23.4 for SS-**2**, +56.7 for T-**2**, and +36.7 for D-**2**$^{\bullet\bullet}$], and the data are summarized in Figure 3-2e-h. By considering the relative energies, the author expected that *anti,anti*- and *syn,anti*-isomers could be isolated but *syn,syn*-isomer and twisted species might not be, and thus the author started synthetic studies.

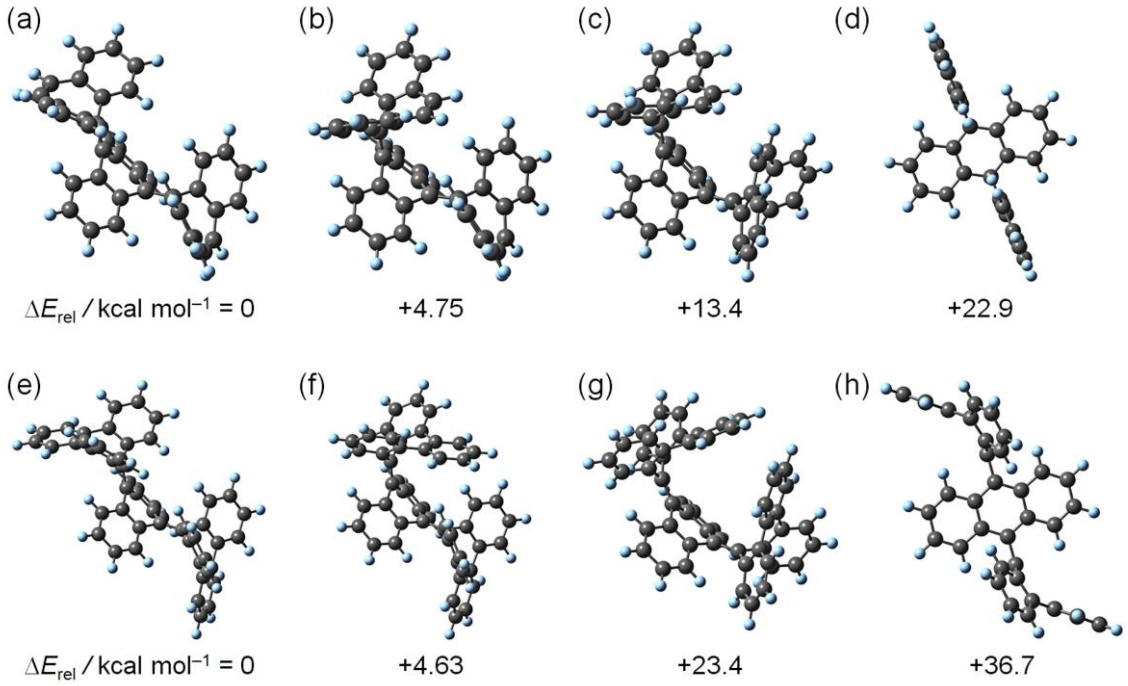

Figure 3-2. Optimized structures of (a) AA-**1**, (b) SA-**1**, (c) SS-**1**, (d) D-**1**$^{\bullet\bullet}$, (e) AA-**2**, (f) SA-**2**, (g) SS-**2**, and (h) D-**2**$^{\bullet\bullet}$ based on DFT calculations at the (U)B3LYP/6-31G(d) level.

3-2-2. Preparation and X-ray analysis

As shown in Scheme 3-5, diol **3** was prepared by lithiation of 9,10-dibromoanthracene followed by the addition of dibenzosuberenone. Upon treatment of **3** with acidic conditions, dication salt $\mathbf{1}^{2+}(BF_4^-)_2$ was isolated in 96% yield as a red powder, the structure of which was identified by X-ray analysis (Figure 3-3a). The dication $\mathbf{1}^{2+}$ adopts an almost orthogonally twisted structure and the dihedral angle between dibenzotropylium and anthracene units was determined to be 84.7°, which is in good agreement with the simulated value of 90.0° (Figure 3-3b). The dication salt $\mathbf{1}^{2+}(BF_4^-)_2$ exhibits strong absorption in the visible region (λ_{max} = 567 nm, log ε = 3.96 in CH_3CN), and the color persists for a long time in solution (Figure 3-4a). When dication $\mathbf{1}^{2+}$ was reduced with Zn powder, target compound **1** was quantitatively obtained as a mixture of two isomers (1:1 ratio). These two isomers were partially separated by column chromatography on silica gel. The first and second eluted samples exhibit resonances corresponding to C_{2v}-symmetric and C_s-symmetric species, respectively, characterized by ^{1}H NMR spectroscopy. X-ray analyses revealed that the former compound is AA-**1** and the latter is SA-**1** (Figure 3-5a,b). The details of bond lengths for both isomers of **1** are summarized in Table 3-1, showing that these isomers obviously adopt quinoidal forms but not diradical species.

The observed product ratio of *anti*,*anti*- and *syn*,*anti*-isomers could be accounted for by the Hammond postulate: in exergonic reactions, a transition-state structure should be similar to that of the starting material with a potential energy that is close to that in the transition state. Because the potential energy of twisted diradical $\mathbf{1}^{\bullet\bullet}$ would be much higher than those of AA-**1** and SA-**1**, the difference between the energy levels for the transition states toward both folded isomers would be negligibly small, so that the two isomers were produced in almost the same ratio.

On the other hand, when tribenzosuberenone[12] was used as the electrophile instead of dibenzosuberenone, AA-**2** and SA-**2**, whose structures were determined by X-ray analyses (Figure 3-5c,d), were obtained as a mixture (1:2 ratio). The details of bond lengths for both isomers of **2** are summarized in Table 3-2, showing that these isomers obviously adopt quinoidal forms but not diradical species as in the case of **1**. The corresponding dication salt $\mathbf{2}^{2+}(BF_4^-)_2$ was isolated in 86% yield as a green powder. As shown in Figure 3-4b, the dication salt in CH_3CN containing 10 vol% trifluoroacetic anhydride (TFAA) exhibits deep green (λ_{max} = 610 nm, log ε = 4.00). This means that the color of dicationic dyes can be controlled by changing the hydrocarbon skeleton without any heteroatoms. Though $\mathbf{2}^{2+}(BF_4^-)_2$ was relatively stable under an ambient atmosphere in a solid state, it gradually decomposed in solution such as CH_3CN. Thus, NMR and UV−Vis spectroscopic measurements were performed with the addition of TFAA to completely remove water from the solution for stabilizing the dication.

Scheme 3-5. Preparation scheme for **1** and **2**.

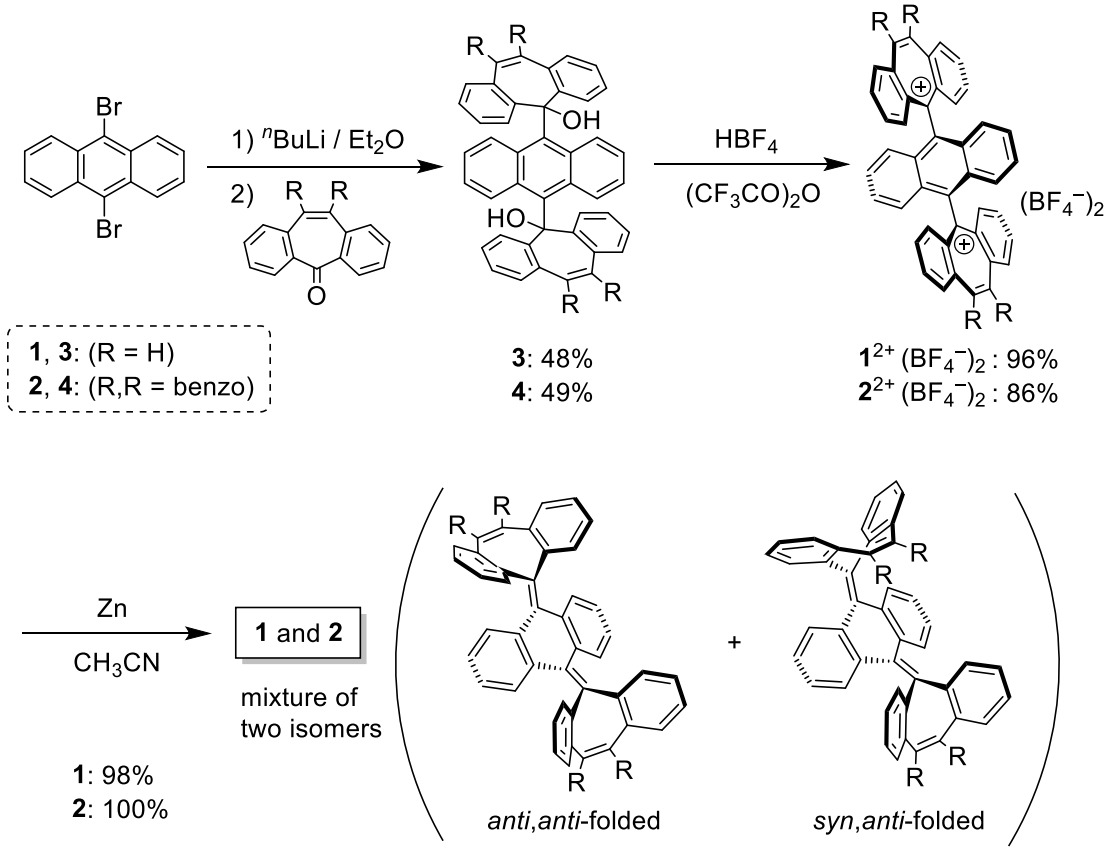

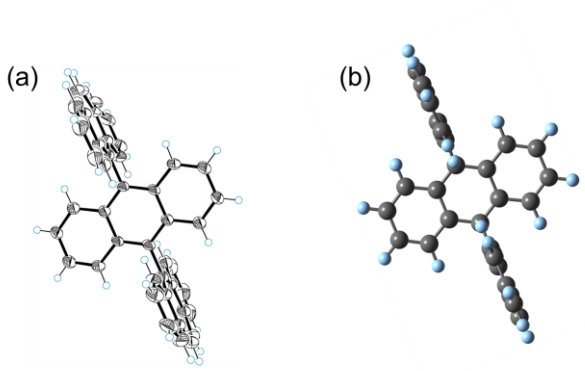

Figure 3-3. (a) ORTEP drawing of $\mathbf{1}^{2+}(BF_4^-)_2$. The counterions are omitted for clarity. Thermal ellipsoids are shown at the 50% probability level. (b) Optimized structure of dication $\mathbf{1}^{2+}$ based on DFT calculations at the B3LYP/6-31G(d) level.

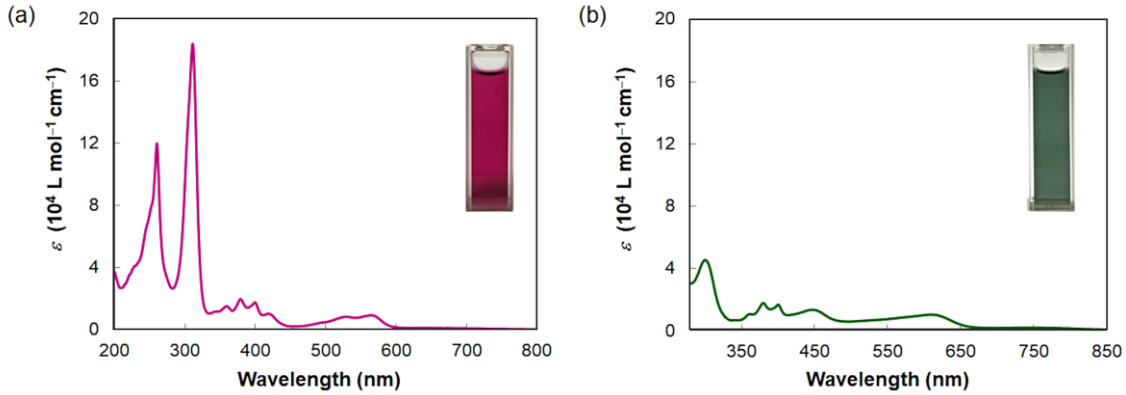

Figure 3-4. UV-Vis spectra of dication salts. (a) $\mathbf{1}^{2+}(BF_4^-)_2$ in CH_3CN and (b) $\mathbf{2}^{2+}(BF_4^-)_2$ in CH_3CN containing 10 vol% TFAA.

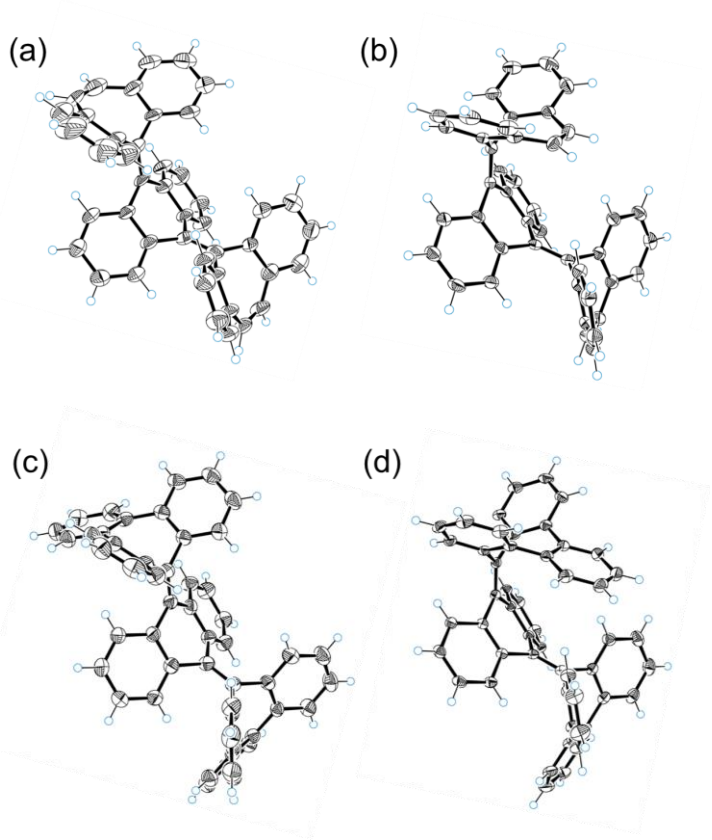

Figure 3-5. ORTEP drawings of (a) AA-**1**, (b) SA-**1**, (c) AA-**2**, and (d) SA-**2**. Solvent molecules are omitted for clarity. Thermal ellipsoids are shown at the 50% probability level.

Table 3-1. Bond lengths of AA-**1** and SA-**1** obtained by X-ray analyses and by DFT study.

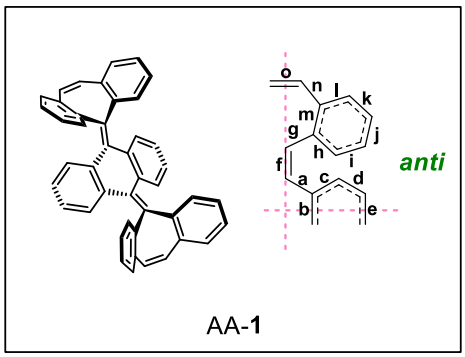

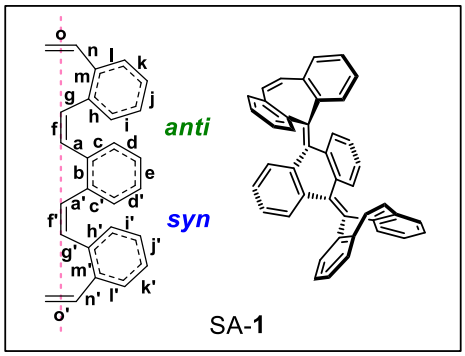

AA-**1**					SA-**1**				
Expt. (X-ray)			*Calcd.*		Expt. (X-ray)			*Calcd.*	
bond length/Å			bond length/Å		bond length/Å			bond length/Å	
a	1.503(7)	1.477(7)	a	*1.492*	a	1.492(4)	1.487(3)	a	*1.492*
	1.492(7)	1.497(7)			a'	1.486(4)	1.496(4)	a'	*1.494*
b	1.411(7)	1.401(7)	b	*1.415*	b	1.406(3)	1.399(3)	b	*1.416*
c	1.387(8)	1.394(7)	c	*1.402*	c	1.393(4)	1.400(4)	c	*1.401*
	1.409(7)	1.381(7)			c'	1.395(4)	1.397(3)	c'	*1.400*
d	1.392(7)	1.382(8)	d	*1.392*	d	1.384(4)	1.378(3)	d	*1.393*
	1.382(8)	1.392(7)			d'	1.382(4)	1.383(4)	d'	*1.394*
e	1.394(8)	1.384(8)	e	*1.397*	e	1.384(3)	1.381(3)	e	*1.395*
f	1.361(7)	1.358(7)	f	*1.361*	f	1.346(3)		f	*1.359*
					f'	1.349(3)		f'	*1.358*
g	1.481(7)	1.494(7)	g	*1.493*	g	1.488(3)	1.497(4)	g	*1.493*
	1.487(8)	1.481(7)			g'	1.487(3)	1.489(4)	g'	*1.495*
h	1.392(7)	1.396(7)	h	*1.403*	h	1.394(3)	1.388(4)	h	*1.403*
	1.379(9)	1.396(7)			h'	1.391(4)	1.393(3)	h'	*1.401*
i	1.368(9)	1.382(8)	i	*1.392*	i	1.383(3)	1.382(4)	i	*1.392*
	1.389(9)	1.387(8)			i'	1.386(4)	1.377(4)	i'	*1.393*
j	1.389(10)	1.393(11)	j	*1.398*	j	1.383(4)	1.383(4)	j	*1.398*
	1.377(11)	1.391(8)			j'	1.380(3)	1.381(4)	j'	*1.398*
k	1.370(8)	1.372(9)	k	*1.390*	k	1.378(3)	1.373(4)	k	*1.389*
	1.368(12)	1.392(8)			k'	1.376(4)	1.376(3)	k'	*1.390*
l	1.393(9)	1.396(8)	l	*1.409*	l	1.397(3)	1.400(4)	l	*1.409*
	1.412(10)	1.384(8)			l'	1.406(4)	1.397(4)	l'	*1.408*
m	1.407(7)	1.417(7)	m	*1.416*	m	1.408(3)	1.404(3)	m	*1.416*
	1.418(9)	1.417(7)			m'	1.406(3)	1.408(4)	m'	*1.417*
n	1.456(9)	1.442(7)	n	*1.463*	n	1.469(3)	1.461(4)	n	*1.463*
	1.452(11)	1.477(7)			n'	1.461(4)	1.460(3)	n'	*1.464*
o	1.354(11)	1.348(9)	o	*1.352*	o	1.337(4)		o	*1.352*
					o'	1.343(4)		o'	*1.355*

Table 3-2. Bond lengths of AA-**2** and SA-**2** obtained by X-ray analyses and by DFT study.

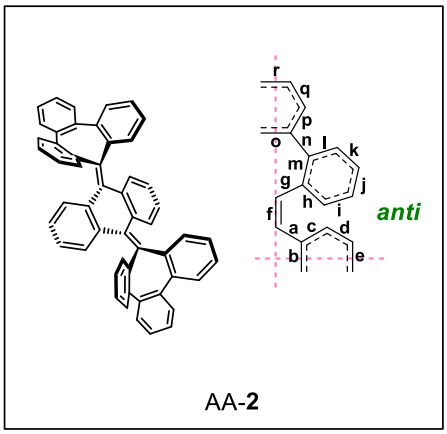

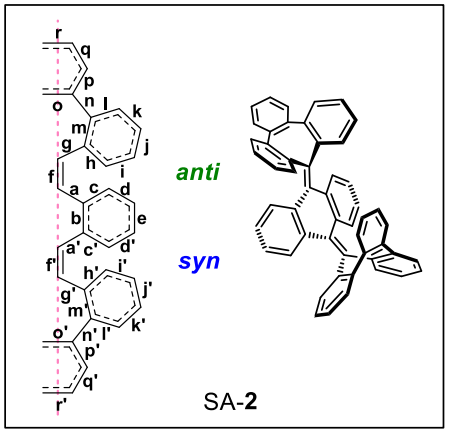

AA-**2**				SA-**2**			
Expt. (X-ray) bond length/Å		*Calcd.* bond length/Å		Expt. (X-ray) bond length/Å		*Calcd.* bond length/Å	
a	1.479(7)	a	*1.490*	a	1.486(2) 1.486(2)	a	*1.489*
				a'	1.493(2) 1.491(2)	a'	*1.493*
b	1.414(6)	b	*1.415*	b	1.410(2) 1.411(2)	b	*1.417*
c	1.394(7) 1.404(8)	c	*1.402*	c	1.397(2) 1.394(2)	c	*1.402*
				c'	1.399(2) 1.397(2)	c'	*1.401*
d	1.384(9) 1.390(7)	d	*1.392*	d	1.385(2) 1.386(2)	d	*1.393*
				d'	1.386(3) 1.385(3)	d'	*1.393*
e	1.398(7)	e	*1.397*	e	1.388(3) 1.389(3)	e	*1.395*
f	1.344(7)	f	*1.358*	f	1.347(2)	f	*1.359*
				f'	1.349(2)	f'	*1.359*
g	1.494(6) 1.496(7)	g	*1.494*	g	1.489(2) 1.491(2)	g	*1.495*
				g'	1.494(2) 1.498(2)	g'	*1.497*
h	1.392(9) 1.391(8)	h	*1.403*	h	1.395(3) 1.394(3)	h	*1.403*
				h'	1.396(2) 1.400(2)	h'	*1.401*
i	1.393(7) 1.401(9)	i	*1.392*	i	1.389(3) 1.388(3)	i	*1.392*
				i'	1.388(3) 1.391(3)	i'	*1.393*
j	1.374(8) 1.381(9)	j	*1.396*	j	1.385(3) 1.384(3)	j	*1.396*
				j'	1.385(2) 1.386(2)	j'	*1.395*
k	1.384(10) 1.370(9)	k	*1.392*	k	1.383(3) 1.382(4)	k	*1.392*
				k'	1.384(3) 1.384(3)	k'	*1.392*
l	1.389(6) 1.404(8)	l	*1.406*	l	1.403(3) 1.402(3)	l	*1.406*
				l'	1.397(3) 1.399(3)	l'	*1.406*
m	1.399(6) 1.410(7)	m	*1.413*	m	1.404(3) 1.406(3)	m	*1.413*
				m'	1.409(2) 1.409(2)	m'	*1.414*
n	1.495(8) 1.481(8)	n	*1.487*	n	1.486(3) 1.483(3)	n	*1.487*
				n'	1.485(2) 1.485(3)	n'	*1.487*
o	1.417(8)	o	*1.419*	o	1.411(2)	o	*1.419*
				o'	1.409(3)	o'	*1.421*
p	1.391(8) 1.396(9)	p	*1.407*	p	1.400(3) 1.402(3)	p	*1.407*
				p'	1.398(3) 1.400(3)	p'	*1.407*
q	1.385(10) 1.367(9)	q	*1.391*	q	1.383(3) 1.381(3)	q	*1.391*
				q'	1.391(3) 1.394(3)	q'	*1.392*
r	1.382(8)	r	*1.395*	r	1.385(3)	r	*1.395*
				r'	1.373(3)	r'	*1.395*

3-2-3. One-way thermal isomerization from *syn,anti*- to *anti,anti*-isomers

To investigate thermal interconversion, the mixture of isomers **1** was heated to reflux in dimethylsulfoxide (DMSO) for 1.5 h, and pure AA-**1** was obtained. This result is consistent with the theoretical prediction, which indicates AA-**1** is thermodynamically stable isomer. Thus, AA-**1** can be selectively obtained upon heating (one-way thermal isomerization to AA-**1**). To gain further insight into the thermal isomerization process for **1**, isomerization from pure SA-**1** to AA-**1** was monitored by ^{1}H NMR spectroscopy. Upon heating at 170 °C in DMSO-d_6, thermal isomerization proceeded cleanly to give AA-**1** (Figure 3-6). Based on the change in the isomer ratio, the rate constant k was determined to be 1.55×10^{-4} s^{-1} as a first-order reaction. In a similar manner, the rate constants k of isomerization at 150, 160, 180, and 185 °C were determined and are summarized in Figure 3-7a. According to an Arrhenius plot (Figure 3-7b) using these values, the energy barrier for the thermal isomerization of SA-**1** was estimated to be 30.5 kcal mol^{-1}, which is in accord with the fact that such isomerization does not occur at ambient temperature.

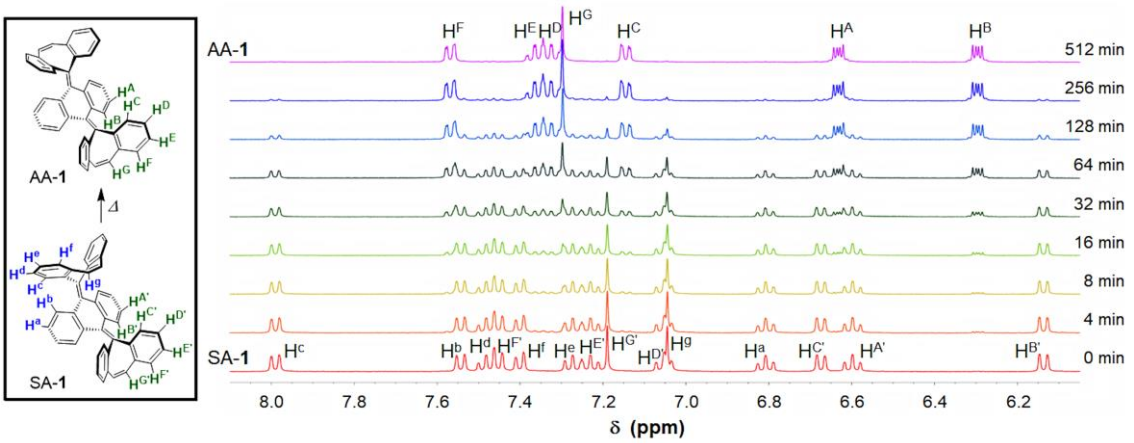

Figure 3-6. A change in ^{1}H NMR spectrum of SA-**1** in DMSO-d_6 upon heating at 170 °C.

(a)

from SA-1 to AA-1 in DMSO	
T (°C)	*k* (s^{-1})
185	5.33 x 10^{-4}
180	4.82 x 10^{-4}
170	1.55 x 10^{-4}
160	1.02 x 10^{-4}
150	3.40 x 10^{-5}

(b)

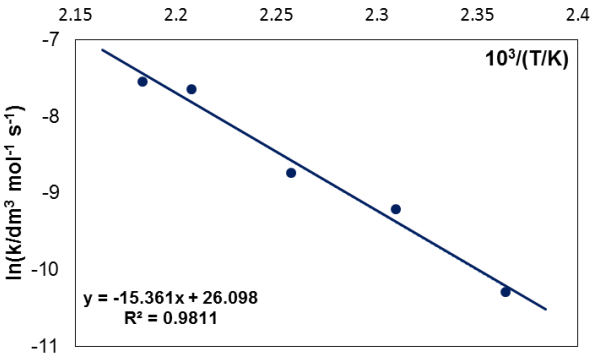

Figure 3-7. (a) Table of the rate constants k and (b) Arrhenius plot for thermal isomerization of SA-**1**.

For SA-**2**, one-way thermal isomerization that was similar to that for SA-**1** quantitatively occurred when hexamethylphosphoramide (HMPA) was used as a higher-boiling solvent. A detailed NMR study was performed with pure SA-**2** in HMPA, which was removed by extraction before NMR measurements. Upon heating at 230 °C, thermal isomerization proceeded cleanly to give AA-**2** (Figure 3-8), and the rate constant k was determined to be 8.86×10^{-4} s^{-1}. In a similar manner, the rate constants k of isomerization at 190, 200, 210, and 220 °C were determined (Figure 3-9a) and the energy barrier for the thermal isomerization of SA-**2** was calculated to be 40.9 kcal mol^{-1} (Figure 3-9b). This value for SA-**2** is greater than that for SA-**1** because increasing rigidity and steric hindrance around the cycloheptatriene ring make ring-flipping more difficult.

For both **1** and **2**, quantitative thermal isomerization from *syn*,*anti*-isomer to *anti*,*anti*-isomer proceeded in a preparative scale by heating to reflux in DMSO and heating at 220 °C in HMPA, respectively.

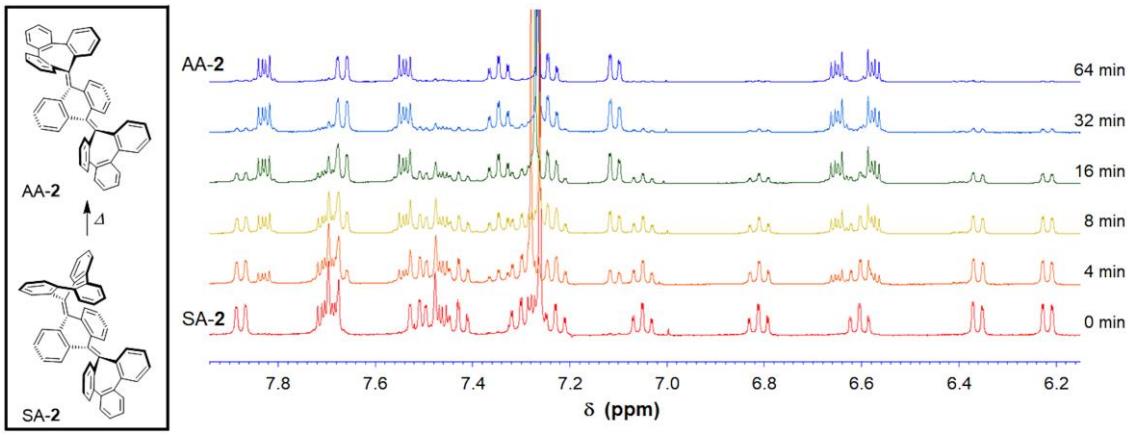

Figure 3-8. A change in ^{1}H NMR spectrum of SA-**2** in $CDCl_3$ upon thermal isomerization. After thermal isomerization of SA-**2** in HMPA upon heating at 230 °C, HMPA was removed by extraction.

(a)

from SA-2 to AA-2 in HMPA	
T (°C)	*k* (s^{-1})
230	8.86×10^{-4}
220	4.18×10^{-4}
210	1.64×10^{-4}
200	8.75×10^{-5}
190	2.36×10^{-5}

(b)

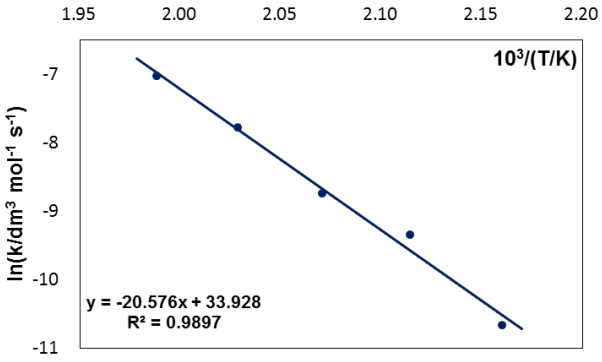

Figure 3-9. (a) Table of the rate constants k and (b) Arrhenius plot for thermal isomerization of SA-**2**.

3-2-4. One-way photoisomerization from *anti,anti*- to *syn,anti*-isomers.

Under photoirradiation conditions, *anti,anti*- and *syn,anti*-isomers of **1** were found to be interconvertible. To gain insight into the photostationary state, the author photoirradiated a solution of pure SA-**1** at 279 nm, which is an isosbestic point. As a result, the isomer ratio converged to 19:81 of AA-**1** and SA-**1** in the photostationary state. Although the absolute quantum yield (Φ) was not determined, $\Phi_{\text{AA-1}\rightarrow\text{SA-1}}$ is about 4 times as large as $\Phi_{\text{SA-1}\rightarrow\text{AA-1}}$.

Furthermore, UV spectra for AA-**1** and SA-**1** measured in CH_2Cl_2 (Figure 3-10a) show that the absorption-edge wavelengths are 380 and 360 nm, respectively. This means that selective photoexcitation of AA-**1** is possible to induce one-way photoisomerization into SA-**1** when the solution of **1** is irradiated with UV light at a wavelength longer than 360 nm. In fact, one-way isomerization upon photoirradiation of 365 nm for **1** was confirmed by UV spectroscopy, in which the UV spectrum exhibits a continuous change with several isosbestic points from AA-**1** to SA-**1** (Figure 3-10b).

To elucidate the details of photoisomerization, the author investigated the isomerization of AA-**1** in CD_2Cl_2 by using NMR. Thus, SA-**1** was obtained quantitatively, which was demonstrated by ^{1}H NMR spectroscopy as shown in Figure 3-10c. To confirm the absence of another isomer such as SS-**1** in the photoreactions, the solution of SA-**1** was irradiated with UV light at around 350 nm, which is the absorption-edge of SA-**1**. The UV spectrum showed an increase only for the signals of AA-**1**, suggesting that incorporation of a higher-energy isomer was not involved.

Such photoisomerization can also be found in **2** because of the similarity of UV absorption properties (Figure 3-11a). The absorption-edge wavelengths of AA-**2** and SA-**2** are 370 and 355 nm, respectively. The behavior of isomerization upon photoirradiation of 365 nm for **2** was confirmed by UV spectroscopy as well as ^{1}H NMR spectroscopy as in the case of **1** (Figure 3-11b,c).

Furthermore, for both **1** and **2**, quantitative photoisomerization was achieved in a preparative scale by photoirradiation at a wavelength longer than 360 nm. Based on these experimental results in combination with thermal reactivity, photo- and thermal isomerization proceed reversibly and quantitatively, which enables one-way isomerization between *anti,anti*- and *syn,anti*-isomers for both **1** and **2**.

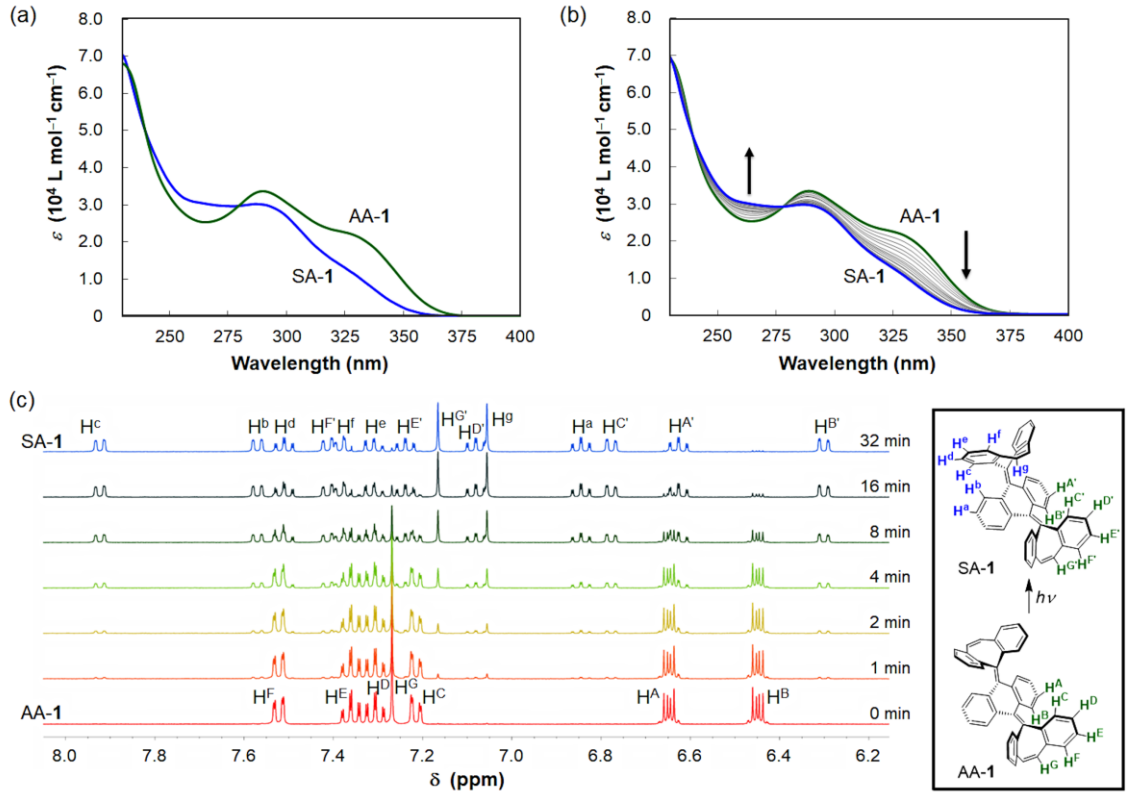

Figure 3-10. (a) UV spectra of AA-**1** (green) and SA-**1** (blue) in CH_2Cl_2. (b) A change in UV spectrum of AA-**1** (green) to SA-**1** (blue) in CH_2Cl_2 (0-20 min, every 2 min; 20-40 min, every 4 min) and (c) a change in ^{1}H NMR spectrum of AA-**1** in CD_2Cl_2 upon photoirradiation at 365 nm [spectrofluorometer: 150 W Xe lamp, slit width (b) 5 nm and (c) 10 nm].

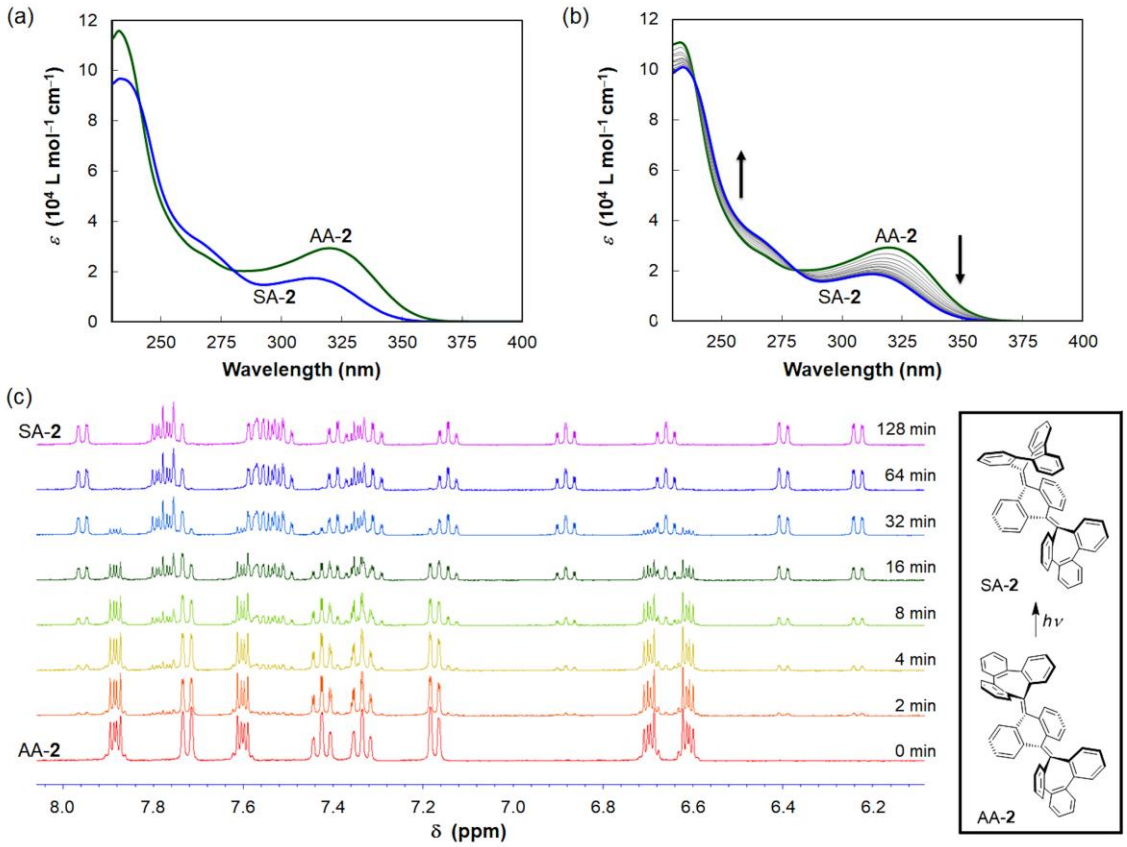

Figure 3-11. (a) UV spectra of AA-**2** (green) and SA-**2** (blue) in CH_2Cl_2. (b) A change in UV spectrum of AA-**2** (green) to SA-**2** (blue) in CH_2Cl_2 (every 8 min) and (c) a change in ^1H NMR spectrum of AA-**2** in CD_2Cl_2 upon photoirradiation at 365 nm [spectrofluorometer: 150 W Xe lamp, slit width (b) 5 nm and (c) 10 nm].

3-2-5. Redox behavior.

The redox potentials of two isomers for **1** were measured by cyclic voltammetry in CH_2Cl_2 (Figure 3-12a,c). As a result of the different configurations for **1**, *anti,anti*- and *syn,anti*-isomers undergo electrochemical oxidation at different potentials (E^{ox}/V vs SCE: +1.66 for AA-**1**, +1.54 for SA-**1**) to produce the same twisted dication $\mathbf{1}^{2+}$. The two-electron process for oxidation was confirmed by using ferrocene as an external standard. Upon the electrochemical oxidation of SA-**1** in $CH_2Cl_2/(CF_3)_2CHOH$ (9:1), clean conversion to $\mathbf{1}^{2+}$ (electrochromism) was observed with an isosbestic point (Figure 3-13a), thus confirming the presence of a one-wave two-electron oxidation process. Though electrochromic behavior of AA-**1** was also observed under the same conditions, the conversion to dication for AA-**1** was slower than that for SA-**1**, probably due to higher oxidation potential of AA-**1** (Figure 3-13b).

On the other hand, reduction of the dication $\mathbf{1}^{2+}$ occurred via a two-step one-electron process. Conversion of the diradical into AA-**1** and SA-**1** proceeds rather slowly. In fact, two-step one-electron oxidation of the corresponding radical species was observed in the second cycle, indicating that the lifetime of twisted diradical $\mathbf{1}^{\bullet\bullet}$ is longer than several seconds because of the large structural change between twisted diradical $\mathbf{1}^{\bullet\bullet}$ and butterfly-shaped folded isomers **1**.

Similar redox behavior was observed for SA-**2** (Figure 3-12b,c), and the oxidation peak appeared in the more anodic region (E^{ox} = +1.73 V) due to the lower aromatization energy of tribenzotropylium in $\mathbf{2}^{2+}$ compared to that of dibenzotropylium in $\mathbf{1}^{2+}$, which is accounted for by considering the addition of π-extended benzene rings to **1**. Notably, AA-**2** could not be oxidized even when the potential was scanned up to +2.30 V, which is a limit of CH_2Cl_2, and thus enhanced switching properties were observed in **2** when the potential difference was more than 0.5 V.

In the case of dication $\mathbf{2}^{2+}$, one-wave two-electron reduction was observed, but an oxidation process of corresponding radical species was not found in the second cycle, unlike **1**. This means that conversion of the diradical into folded isomers proceeds fast probably due to instability of distorted diradical $\mathbf{2}^{\bullet\bullet}$.

To gain further insight into the different donating abilities of *anti,anti*- and *syn,anti*-isomers, theoretical calculations were conducted by the DFT method. The HOMO levels of *anti,anti*- and *syn,anti*-isomers are calculated to be −5.36 and −5.40 eV for **1** and −5.46 and −5.46 eV for **2**, respectively, at the B3LYP/6-31G(d) level. When the M06-2X method with the 6-31G(d) or cc-pVTZ basis set was used for calculations, no significant change was observed (Table 3-3). The nearly identical HOMO levels for the *anti,anti*- and *syn,anti*-isomers in both **1** and **2** seem incompatible with the experimental results regarding the different redox potentials. It is most probable that the discrepancy between the redox potentials and HOMO levels can be accounted for by the drastic structural change during two-electron transfer. Thus, *syn,anti*-isomers can be

more easily oxidized than *ant,anti*-isomers due to large steric strain release after one-electron oxidation, which may facilitate the subsequent electrochemical event in *syn,anti*-isomers.

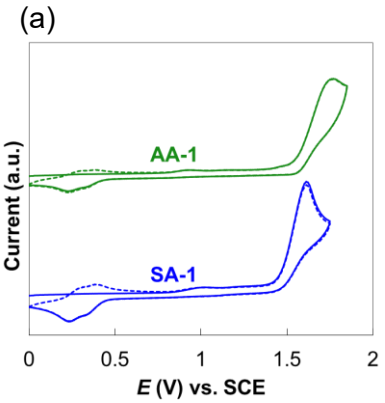

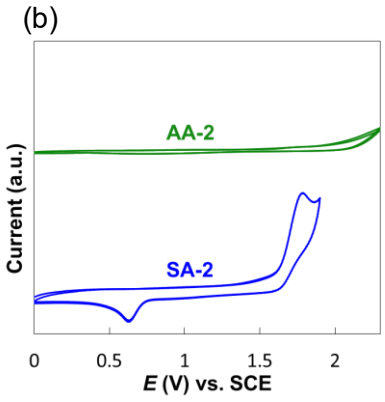

(c)

	E^{ox} (V)	E^{red} (V)
AA-**1**	+1.66	-
SA-**1**	+1.54	-
$\mathbf{1}^{2+}/\mathbf{1}^{+\cdot}$	= E^{red}	+0.39
$\mathbf{1}^{+\cdot}/\mathbf{1}$	= E^{red}	+0.28
AA-**2**	> +2.30	-
SA-**2**	+1.73	-
$\mathbf{2}^{2+}$	-	+0.74

Figure 3-12. Cyclic voltammograms of (a) AA-**1** (green) and SA-**1** (blue), and (b) AA-**2** (green) and SA-**2** in CH_2Cl_2 containing 0.1 M Bu_4NBF_4 as a supporting electrolyte (scan rate 0.5 V s^{-1}, Pt electrodes). The second cycles are shown by dotted line. The redox potentials for these hydrocarbons are summarized in (c) (scan rate 0.1 V s^{-1}). The irreversible redox potentials were estimated from the anodic peak potentials (E^{pa}) as $E^{ox} = E^{pa}$–0.03 or the cathodic peak potentials (E^{pc}) as $E^{red} = E^{pc}$+0.03.

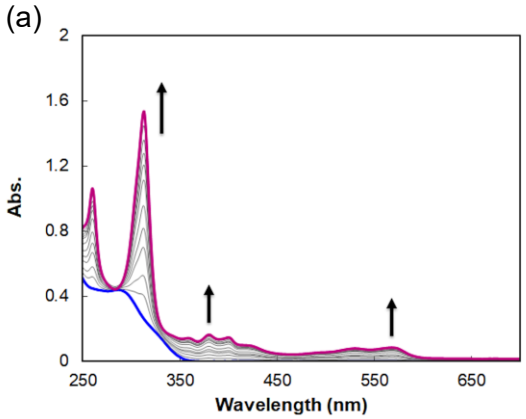

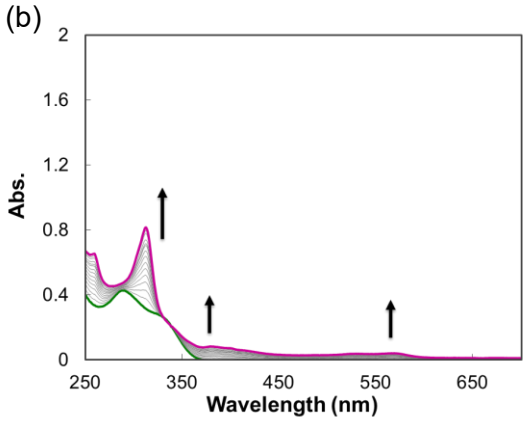

Figure 3-13. Changes in the UV-vis spectra of (a) SA-**1** (blue) to $\mathbf{1}^{2+}$ (violet) and (b) AA-**1** (green) to $\mathbf{1}^{2+}$ (violet) upon constant current electrochemical oxidation (80 μA, every 2 min) in CH_2Cl_2/1,1,1,3,3,3-hexafluoro-2-propanol (9:1) containing 0.05 M Bu_4NBF_4 as a supporting electrolyte.

Table 3-3. HOMO levels (eV) of **1** and **2** estimated by DFT calculations.

functional	basis set	AA-1	SA-1	AA-2	SA-2
B3LYP	6-31G(d)	–5.36	–5.40	–5.46	–5.46
CAM-B3LYP	6-31G(d)	–6.71	–6.76	–	–
M06-2X	6-31G(d)	–6.62	–6.67	–6.72	–6.72
M06-2X	cc-pVTZ	–6.91	–6.96	–	–

3-2-6. Redox interconversion and selective oxidation.

To confirm redox interconversion between folded isomers and twisted dication, both AA-**1** and SA-**1** were treated with two equivalents of $(2,4\text{-}Br_2C_6H_3)_3N^{+\bullet}SbCl_6^-$ as one-electron oxidant.[18] As a result, the same dication $\mathbf{1}^{2+}(SbCl_6^-)_2$, the structure of which is shown in Figure 3-14, was obtained quantitatively. As suggested by the voltammetric analyses, the two configurational isomers AA-**1** and SA-**1** exhibited quite different behaviors upon redox interconversion with $\mathbf{1}^{2+}$. By considering the lower oxidation potential between two isomers, SA-**1** could be selectively oxidized by weaker oxidant, $(4\text{-}BrC_6H_4)_3N^{+\bullet}SbCl_6^-$ (Magic Blue). In fact, upon treatment of SA-**1** with two equivalents of Magic Blue, the dication $\mathbf{1}^{2+}(SbCl_6^-)_2$ was obtained quantitatively, while AA-**1** did not react under the same conditions and was completely recovered (Scheme 3-6a).

Neither AA-**2** nor SA-**2** were oxidized by using Magic Blue, due to lower HOMO levels of **2** than those of **1**. When $(2,4\text{-}Br_2C_6H_3)_3N^{+\bullet}SbCl_6^-$ was used as stronger oxidant, the dication $\mathbf{2}^{2+}SbCl_6^-$ was obtained from SA-**2**, while AA-**2** did not react under the same conditions and was recovered (Scheme 3-6a).

It is noteworthy that such selective oxidation of *syn,anti*-isomers was achieved even when a 1:1 mixture of *anti,anti*- and *syn,anti*-isomers was treated with two equivalents of Magic Blue and $(2,4\text{-}Br_2C_6H_3)_3N^{+\bullet}SbCl_6^-$ for *syn,anti*-isomers in compound **1** and **2**, respectively. In the case of a 1:1 mixture of AA-**2** and SA-**2**, AA-**2** was quantitatively recovered, while some decomposition was observed when pure AA-**2** was treated with $(2,4\text{-}Br_2C_6H_3)_3N^{+\bullet}SbCl_6^-$ (Scheme 3-6a). It is highly likely that SA-**2** was preferentially oxidized rather than AA-**2**.

This is a quite rare example of well-controlled redox switchable OCE because *syn,anti*-isomers obtained by photoirradiation can be selectively oxidized, whereas *anti,anti*-isomers obtained by heat treatment remains intact. From the above, the author realized ON/OFF switching of oxidative properties based on photochemical activation and thermal deactivation by molecular isomerization for the first time (Scheme 3-6b).

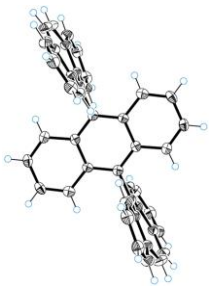

Figure 3-14. ORTEP drawing of $\mathbf{1}^{2+}(SbCl_6^-)_2$. The counterions and solvent molecules are omitted for clarity. Thermal ellipsoids are shown at the 50% probability level.

Scheme 3-6. (a) Selective oxidation between *anti*,*anti*- and *syn*,*anti*-isomers. i) (4-$BrC_6H_4)_3N^{+\bullet}SbCl_6^-$ (2.0 eq) in CH_2Cl_2 and ii) (2,4-$Br_2C_6H_3)_3N^{+\bullet}SbCl_6^-$ (2.0 eq) in CH_2Cl_2. (b) The activation/deactivation process by light/heat and redox cycle for the hydrocarbons **1** (R = H) and **2** (R,R = benzo).

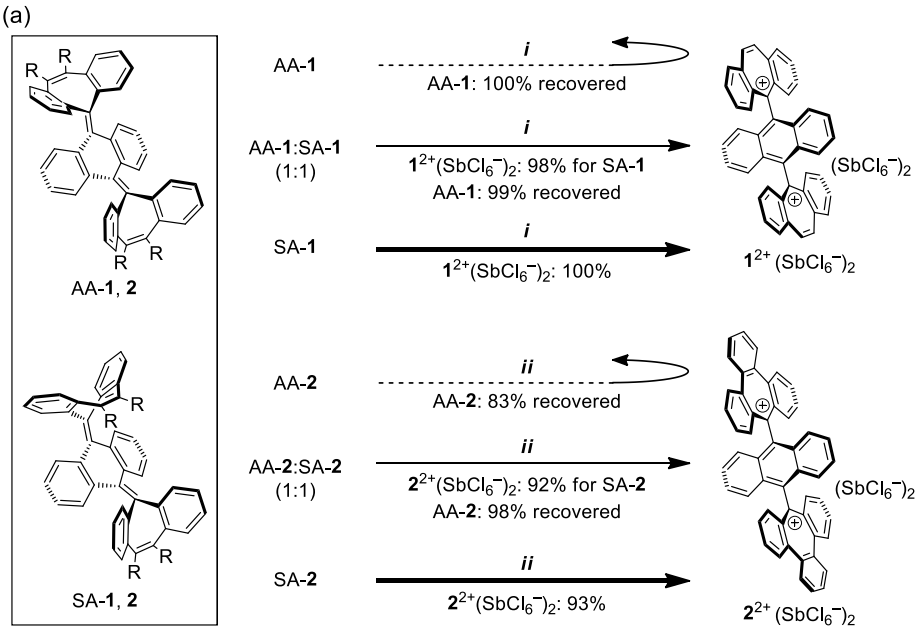

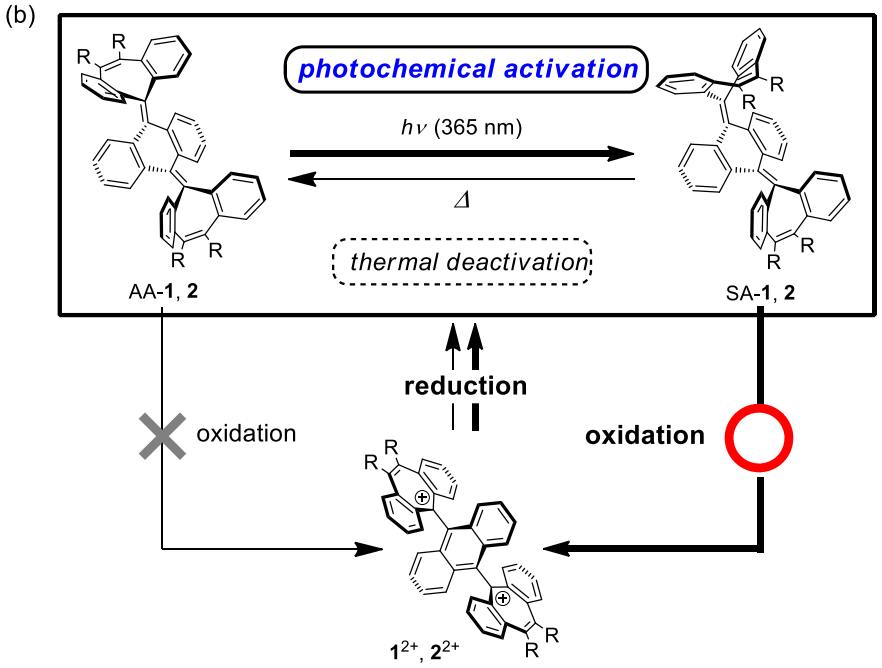

3-3. Conclusion

The author has designed and prepared redox-active OCEs **1** and **2**, for which both *anti,anti*- and *syn,anti*-folded isomers exist as stable entities due to rigid seven-membered rings as the key framework. These isomers do not interconvert at ambient temperature due to energy barriers greater than 30 kcal mol^{-1}. One-way thermal isomerization from *syn,anti*- to *anti,anti*-isomers and one-way photoisomerization from *anti,anti*- to *syn,anti*-isomers proceed quantitatively for both **1** and **2**. Furthermore, these hydrocarbons undergo two-electron oxidation to give twisted dications and exhibit *dyrex* behavior with a large separation of redox potentials, which gives favorable conditions for constructing electrochromic materials.

Moreover, the much easier oxidation of SA-**1** (ΔE = ca. 0.1 V) than of AA-**1** enables, in principle, activation/deactivation of the electrochromic properties of **1** by light/heat (Scheme 3-6b). Since photo- and thermal interconversion seldom changes the color, light and heat could be used only for the switching of electrochromism. As demonstrated by the larger difference in redox potentials (ΔE > 0.5 V) and the higher thermal activation energy in tribenzo derivative **2**, the activation/deactivation process by light/heat can be tuned by proper molecular design. Thus, the completely selective oxidation between *anti,anti*- and *syn,anti*-folded isomers, which can be switched by photo- and thermal isomerization, represents a new molecular concept for the design of smart functional devices.

3-4. Experimental Section

3-4-1. General

All reactions were carried out under an argon atmosphere. All commercially available compounds were used without further purification unless otherwise indicated. Dry CH_3CN was obtained by distillation from CaH_2 prior to use. Column chromatography was performed on silica gel 60N (KANTO KAGAKU, spherical neutral) of particle size 40–50 μm or Wakogel® 60N (neutral) of particle size 38–100 μm. ^1H and ^{13}C NMR spectra were recorded on a BRUKER Ascend™ 400 (^1H/400 MHz and ^{13}C/100 MHz) spectrometer. IR spectra were measured as a KBr pellet on a JEOL JIR-WINSPEC100 FT/IR spectrophotometer. Mass spectra were recorded on a JMS-T100GCV spectrometer in FD mode (GC-MS & NMR Laboratory, Research Faculty of Agriculture, Hokkaido University). Melting points were measured on a Yamato MP-21 and are uncorrected. UV-vis spectra were recorded on a Hitachi U-3500 spectrophotometer. Fluorescence spectra were measured on a Hitachi F-7000 spectrofluorometer. Fluorescence quantum yields were determined by using 9,10-diphenylanthracene (Φ_F = 0.97) as an external standard.[19] For photoisomerization reaction, the Hitachi F-7000 spectrofluorometer was used in a NMR tube and an Ushiospax SX-UID501XAMQ light source device was used with a CORNING COLOR FILTER (No. 0-51) in a preparative scale. Redox potentials (E^{ox} and E^{red}) were measured on a BAS ALS-600A by cyclic voltammetry in dry CH_2Cl_2 containing 0.1 M Bu_4NBF_4 as a supporting electrolyte. All of the values shown in the text are in E/V vs. SCE measured at the scan rate of 100 $mV \cdot s^{-1}$. Pt disk electrodes were used as the working and counter electrodes. The working electrode was polished using a water suspension of aluminum oxide (0.05 μm) before use. The irreversible half-wave potentials were estimated from the anodic peak potentials (E^{pa}) as $E^{ox} = E^{pa} - 0.03$ or the cathodic peak potentials (E^{pc}) as $E^{red} = E^{pc} + 0.03$. DFT calculations were performed with the Gaussian 16W program package.[17] The geometries of the compounds were optimized by using the (U)B3LYP method in combination with the 6-31G* basis set unless otherwise indicated.

3-4-2. Synthetic procedures

5,5'-(Anthracene-9,10-diyl)bis(5*H*-dibenzo[*a*,*d*]cycloheptatrien-5-ol) 3.

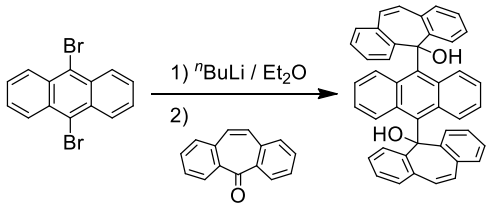

3: 48%

To a solution of 9,10-dibromoanthracene (3.10 g, 9.23 mmol) in dry Et_2O (100 mL) was added ^{n}BuLi (1.55 M in hexane, 13.7 mL, 21.2 mmol) dropwise over 10 min at –20 °C. After stirring at –20 °C for 1 h, dibenzosuberenone (4.37 g, 21.2 mmol) was added to the suspension and the mixture was warmed to 23 °C. The resulting solution was stirred at 23 °C for 1 h, and then diluted with water. The precipitates were filtered and washed with water (x 3) and methanol (x 3). The crude product was suspended in $CHCl_3$ and heated at 60 °C for 5 min. After cooling to 23 °C, the suspension was filtered and the solid was dried in vacuo to give diol **3** (5.45 g) as a yellow solid in 48% yield.

3; Mp: 293-300 °C (decomp.); ^{1}H NMR (DMSO-d_6): δ/ppm 8.36 (4H, dd, *J* = 1.0 Hz, 8.0 Hz), 7.53 (4H, ddd, *J* = 1.5 Hz, 6.8 Hz, 8.0 Hz), 7.46 (4H, dd, *J* = 3.4 Hz, 7.1 Hz), 7.31 (2H, s), 7.17 (4H, ddd, *J* = 1.0 Hz, 6.8 Hz, 7.6 Hz), 7.13 (4H, dd, *J* = 1.5 Hz, 7.6 Hz), 6.45 (4H, s), 6.37 (4H, dd, *J* = 3.4 Hz, 7.1 Hz); ^{13}C NMR (DMSO-d_6): δ/ppm 146.74, 137.81, 131.92, 131.50, 130.10, 128.43, 128.11, 126.17, 125.37, 122.74, 121.08, 78.47; IR (KBr): ν/cm^{-1} 3549, 3107, 3062, 3018, 1954, 1924, 1827, 1594, 1523, 1482, 1434, 1302, 1211, 1184, 1174, 1153, 1114, 1035, 989, 886, 877, 865, 822, 800, 763, 748, 743, 735, 682, 655, 627, 606; LR-MS (FD) m/z (%): 592.29 (13), 591.28 (48), 590.28 (M^+, bp); HR-MS (FD) Calcd. for $C_{44}H_{30}O_2$: 590.22458; Found: 590.22547.

5,5'-(Anthracene-9,10-diyl)bis(5*H*-dibenzo[*a*,*d*]cycloheptatrien-5-ylium) bis(tetrafluoroborate) $1^{2+}(BF_4^-)_2$.

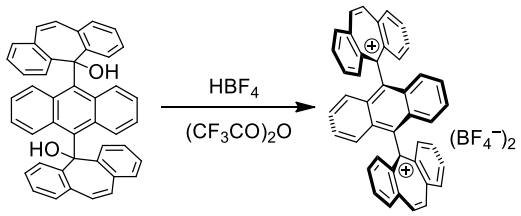

3 $1^{2+}(BF_4^-)_2$: 96%

To a solution of diol **3** (2.62 g, 4.44 mmol) in TFAA (65 mL) was added 42% HBF_4 aq. (6.68 mL, 44.4 mmol) at 0 °C to give a deep red solution, and the mixture was stirred at 22 °C for 2 h. The addition of dry Et_2O led to precipitation of the dication salt. The precipitates were filtered,

washed with dry Et_2O three times, and dried in vacuo to give $\mathbf{1}^{2+}(BF_4^-)_2$ (3.11 g) as a red powder in 96% yield.

$\mathbf{1}^{2+}(BF_4^-)_2$; Mp: > 300 °C; ^{1}H NMR (CD_3CN): δ/ppm 9.63 (4H, s), 9.05 (4H, dd, *J* = 1.1 Hz, 8.0 Hz), 8.72 (4H, ddd, *J* = 0.86 Hz, 7.0 Hz, 8.0 Hz), 8.41 (4H, dd, *J* = 0.86 Hz, 8.5 Hz), 8.19 (4H, ddd, *J* = 1.1 Hz, 7.0 Hz, 8.5 Hz), 7.30 (4H, dd, *J* = 3.2 Hz, 6.8 Hz), 7.13 (4H, dd, *J* = 3.2 Hz, 6.8 Hz); ^{13}C NMR (CD_3CN): δ/ppm 180.41, 147.90, 147.03, 142.18, 140.45, 139.34, 138.05, 137.47, 135.21, 130.84, 128.81, 127.25; IR (KBr): ν/cm^{-1} 3113, 3012, 2937, 2862, 2735, 1759, 1610, 1602, 1531, 1515, 1473, 1445, 1428, 1385, 1321, 1285, 1251, 1204, 1178, 1136, 1057, 983, 934, 904, 886, 837, 787, 760, 736, 664, 645, 606, 598, 531, 520, 508, 478; LR-MS (FD) m/z (%): 670.26 (8), 669.26 (15), 645.27 (9), 644.27 (36), 643.27 (78), 642.27 (17), 572.26 (6), 571.25 (9), 558.27 (14), 557.27 (48), 556.27 (M^{2+}+e, bp), 543.26 (7), 279.14 (6), 278.63 (26), 278.13 (M^{2+}, 54), 81.05 (13); HR-MS (FD) Calcd. for $C_{44}H_{28}$: 556.21910; Found: 556.22106; UV-vis (CH_3CN): λ_{max}/nm (ε/L mol^{-1} cm^{-1}) 563 (9210), 527 (8230), 418 (10200), 399 (17500), 379 (19500), 359 (15100), 311 (184000), 260 (120000).

9,10-Bis(5*H*-dibenzo[*a*,*d*]cycloheptatrien-5-ylidene)-9,10-dihydroanthracene 1.

Reduction of $\mathbf{1}^{2+}(BF_4^-)_2$ to **1**:

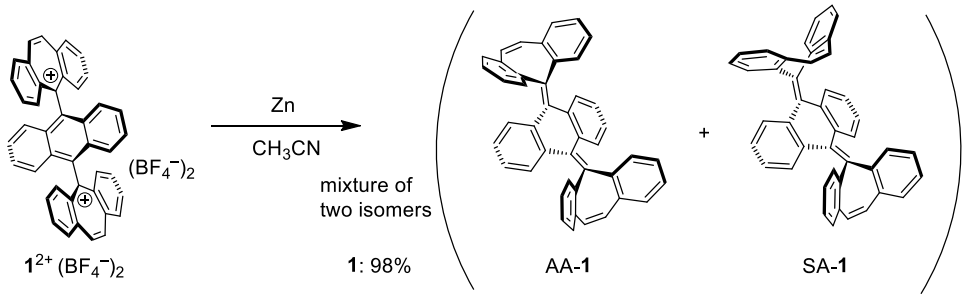

To a solution of $\mathbf{1}^{2+}(BF_4^-)_2$ (2.92 g, 4.00 mmol) in dry CH_3CN (85 mL) was added activated zinc powder (5.24 g, 80.2 mmol) at 23 °C. The mixture was stirred at 23 °C for 1 h, and then diluted with water. The whole mixture was extracted with CH_2Cl_2 three times. The combined organic layers were washed with water and brine, and dried over anhydrous Na_2SO_4. After filtration through silica gel, the solvent was concentrated under reduced pressure to give ca. 1:1 mixture (2.18 g) of AA-**1** (*anti*,*anti*-folded) and SA-**1** (*syn*,*anti*-folded) as a white solid in 98% yield. AA-**1** (Rf = 0.26) and SA-**1** (Rf = 0.22) were isolated by column chromatography on silica gel (hexane/CH_2Cl_2 = 4).

AA-**1**; Mp: > 300 °C; ^{1}H NMR ($CDCl_3$): δ/ppm 7.46 (4H, dd, *J* = 1.2 Hz, 7.5 Hz), 7.29 (4H, ddd, *J* = 1.4 Hz, 7.5 Hz, 7.5 Hz), 7.23 (4H, ddd, *J* = 1.2 Hz, 7.5 Hz, 7.5 Hz), 7.19 (4H, s), 7.16 (4H, dd, *J* = 1.4 Hz, 7.5 Hz), 6.61 (4H, dd, *J* = 3.3 Hz, 5.8 Hz), 6.41 (4H, dd, *J* = 3.3 Hz, 5.8 Hz); ^{13}C NMR ($CDCl_3$): δ/ppm 139.21, 137.54, 137.05, 135.63, 135.04, 131.51, 129.16, 128.55,

128.22, 127.91, 126.87, 124.89; IR (KBr): ν/cm^{-1} 3058, 3018, 1957, 1924, 1616, 1593, 1485, 1457, 1449, 1430, 1270, 1160, 1110, 1038, 948, 895, 830, 800, 782, 773, 758, 733, 646, 622, 604; LR-MS (FD) m/z (%): 559.28 (2), 558.28 (12), 557.27 (48), 556.27 (M^+, bp), 278.14 (M^{2+}, 1); HR-MS (FD) Calcd. for $C_{44}H_{28}$: 556.21910; Found: 556.22075; UV-vis (CH_2Cl_2): λ_{max}/nm (ε/L mol^{-1} cm^{-1}) 333 (20500), 289 (33600); Fluorescence (λ_{ex} = 290 nm): λ_{em}/nm (Φ_F) 407 (0.24).

SA-**1**; Mp: > 300 °C; ^{1}H NMR ($CDCl_3$): δ/ppm 7.86 (2H, dd, *J* = 1.0 Hz, 7.5 Hz), 7.50 (2H, dd, *J* = 0,9 Hz, 7.7 Hz), 7.44 (2H, ddd, *J* = 1.2 Hz, 7.5 Hz, 7.5 Hz), 7.34 (2H, dd, *J* = 1.0 Hz, 7.6 Hz), 7.30 (2H, dd, *J* =1.2 Hz, 7.5 Hz), 7.23 (2H, ddd, *J* = 1.0 Hz, 7.5 Hz, 7.5 Hz), 7.17 (2H, ddd, *J* = 1.1 Hz, 7.6 Hz, 7.6 Hz), 7.09 (2H, s), 6.98 (2H, ddd, *J* = 1.0 Hz, 7.6 Hz, 7.6 Hz), 6.97 (2H, s), 6.79 (2H, ddd, *J* = 0.9 Hz, 7.7 Hz, 7.7 Hz), 6.74 (2H, dd, *J* = 1.1 Hz, 7.6 Hz), 6.59 (2H, ddd, *J* = 0.9 Hz, 7.7 Hz, 7.7 Hz), 6.27 (2H, dd, *J* = 0.9 Hz, 7.7 Hz); ^{13}C NMR ($CDCl_3$): δ/ppm 139.04, 138.55, 137.90, 137.21, 137.13, 136.36, 135.98, 135.49, 135.27, 133.52, 131.36, 130.83, 129.45 (2C), 128.11, 127.92, 127.46, 127.36, 127.33, 126.79, 126.57, 126.45, 124.97, 124.88; IR (KBr): ν/cm^{-1} 3058, 3015, 1920, 1592, 1483, 1457, 1450, 1430, 1293, 1213, 1153, 1112, 1037, 948, 895, 828, 798, 792, 780, 768, 755, 734, 705, 668, 643, 622, 604; LR-MS (FD) m/z (%): 559.28 (2), 558.28 (12), 557.27 (47), 556.27 (M^+, bp), 278.14 (M^{2+}, 2); HR-MS (FD) Calcd. for $C_{44}H_{28}$: 556.21910; Found: 556.22072; UV-vis (CH_2Cl_2): λ_{max}/nm (ε/L mol^{-1} cm^{-1}) 287 (30300); Fluorescence (λ_{ex} = 290 nm): λ_{em}/nm (Φ_F) 417 (0.26).

Reduction of **1**$^{2+}$($SbCl_6^-$)$_2$ to **1**:

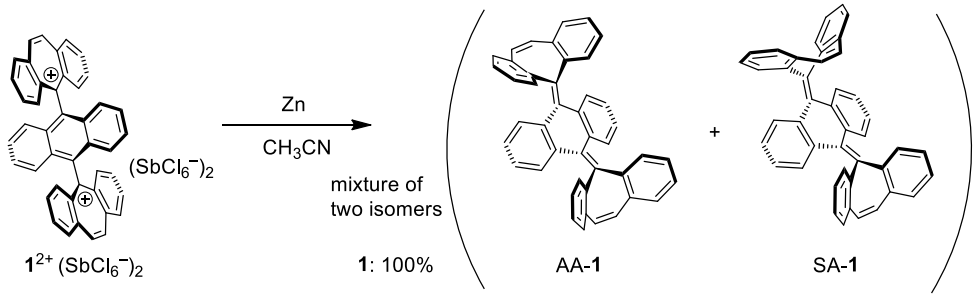

To a solution of **1**$^{2+}$($SbCl_6^-$)$_2$ (139 mg, 113 μmol) in dry CH_3CN (5.0 mL) was added activated zinc powder (148 mg, 2.26 mmol) at 23 °C. The mixture was stirred for 1 h, and then diluted with water. The whole mixture was extracted with CH_2Cl_2 three times. The combined organic layers were washed with water and brine, and dried over anhydrous Na_2SO_4. After filtration through silica gel, the solvent was concentrated under reduced pressure to give ca. 1:1 mixture (63.0 mg) of AA-**1** and SA-**1** as a white solid in 100% yield.

Thermal isomerization of SA-**1** to AA-**1**:

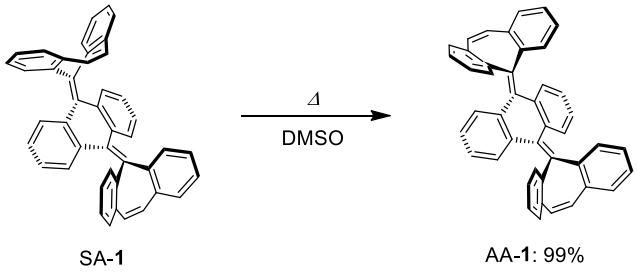

A solution of SA-**1** (50.0 mg, 89.8 μmol) in dimethylsulfoxide (DMSO, 7.0 mL) was refluxed for 1.5 h. After cooling to 23 °C, the resulting solution was diluted with water. The whole mixture was extracted with CH_2Cl_2 three times. The combined organic layers were washed with water and brine, and dried over anhydrous Na_2SO_4. After filtration through silica gel, the solvent was concentrated under reduced pressure to give AA-**1** (49.7 mg) as a white solid in 99% yield.

Photoisomerization of AA-**1** to SA-**1**:

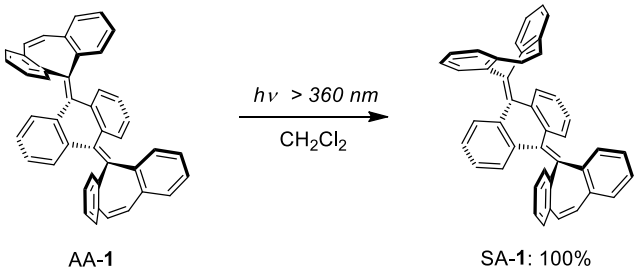

A solution of AA-**1** (83.0 mg, 149 μmol, 2.5×10^{-3} mol L^{-1}) in CH_2Cl_2 (60 mL) was degassed by Ar bubbling, and then stirred at 17 °C for 7 h upon photoirradiation ($h\nu > 360$ nm). The solvent was concentrated under reduced pressure to give SA-**1** (83.5 mg) as a white solid in 100% yield.

5,5'-(Anthracene-9,10-diyl)bis(5*H*-dibenzo[*a*,*d*]cycloheptatrien-5-ylium)bis(hexachloroantimonate) $\mathbf{1^{2+}(SbCl_6^-)_2}$

Oxidation of SA-**1** with $(4\text{-}BrC_6H_4)_3N^{+\bullet}SbCl_6^-$:

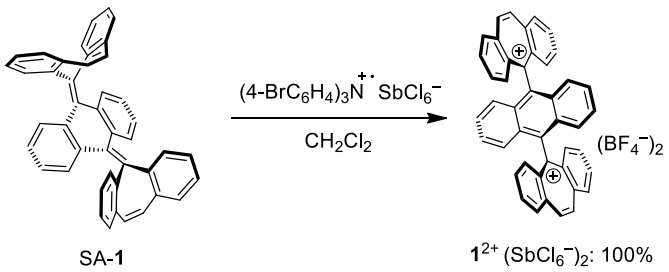

To a solution of SA-**1** (18.9 mg, 34.0 μmol) in dry CH_2Cl_2 (1.0 mL) was added $(4\text{-}BrC_6H_4)_3N^{+\bullet}SbCl_6^-$ (55.4 mg, 67.9 μmol) at 25 °C, and the mixture was stirred for 1 h. The addition of dry Et_2O led to precipitation of the dication salt. The supernatant solution was removed

by decantation, washed with dry Et_2O three times, and dried in vacuo to give $\mathbf{1}^{2+}(SbCl_6^-)_2$ (44.0 mg) as a red powder in 100% yield.

$\mathbf{1}^{2+}(SbCl_6^-)_2$; Mp: 241-242 °C (decomp.); ^{1}H NMR and ^{13}C NMR spectra are identical to those of $\mathbf{1}^{2+}(BF_4^-)_2$; IR (KBr): ν/cm^{-1} 3059, 2359, 1610, 1530, 1514, 1478, 1442, 1426, 1386, 1319, 1249, 1203, 1170, 1132, 886, 833, 784, 758, 730, 665, 639, 606, 597; LR-MS (FD) m/z (%): 629.21 (6), 628.21 (13), 627.21 (8), 626.21 (16), 592.23 (5), 591.23 (7), 590.23 (9), 559.26 (6), 558.26 (19), 557.27 (47), 556.27 (M^{2+}+e, bp), 530.25 (9), 278.64 (5), 278.13 (M^{2+}, 9), 81.05 (23), 80.04 (10); HR-MS (FD) Calcd. for $C_{44}H_{28}$: 556.21910; Found: 556.21855.

Oxidation of AA-**1** with $(4\text{-}BrC_6H_4)_3N^{+\bullet}SbCl_6^-$:

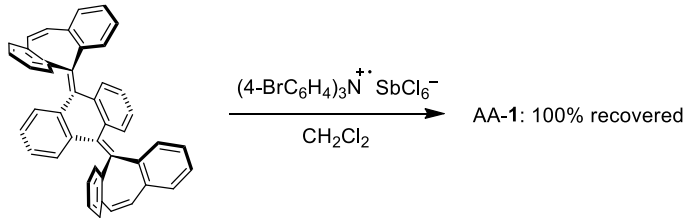

To a solution of AA-**1** (45.3 mg, 81.4 μmol) in dry CH_2Cl_2 (2.0 mL) was added $(4\text{-}BrC_6H_4)_3N^{+\bullet}SbCl_6^-$ (133 mg, 163 μmol) at 25 °C, and the mixture was stirred for 1 h. The addition of dry Et_2O led to precipitation, and the precipitation was removed by decantation. Then, the residue was dissolved in dry CH_2Cl_2, and these procedures were repeated 3 times. The resulting filtrate was evaporated under reduced pressure and dried in vacuo to recover AA-**1** (45.1 mg) as a white solid in 100% yield.

Oxidation of AA-**1** with $(2,4\text{-}Br_2C_6H_3)_3N^{+\bullet}SbCl_6^-$:

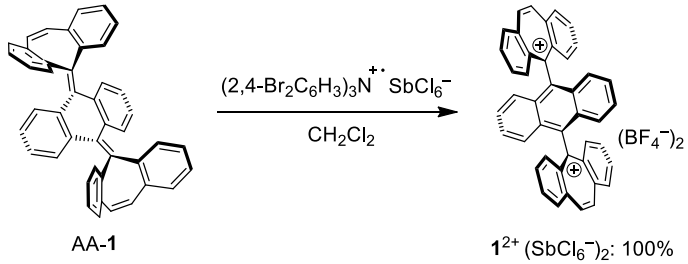

To a solution of AA-**1** (18.1 mg, 33.0 μmol) in dry CH_2Cl_2 (1.0 mL) was added $(2,4\text{-}Br_2C_6H_3)_3N^{+\bullet}SbCl_6^-$ (68.5 mg, 65.0 μmol) at 25 °C, and the mixture was stirred for 1 h. The addition of dry Et_2O led to precipitation of the dication salt. The supernatant solution was removed by decantation, washed with dry Et_2O three times, and dried in vacuo to give $\mathbf{1}^{2+}(SbCl_6^-)_2$ (40.0 mg) as a red powder in 100% yield.

Oxidation of SA-**1** with $(2,4\text{-}Br_2C_6H_3)_3N^{+\bullet}SbCl_6^-$:

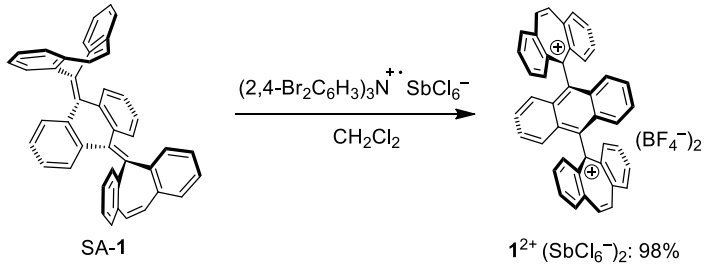

To a solution of SA-**1** (15.1 mg, 27.1 μmol) in dry CH_2Cl_2 (1.0 mL) was added $(2,4\text{-}Br_2C_6H_3)_3N^{+\bullet}SbCl_6^-$ (57.3 mg, 54.2 μmol) at 23 °C, and the mixture was stirred for 1 h. The addition of dry Et_2O led to precipitation of the dication salt. The supernatant solution was removed by decantation, washed with dry Et_2O three times, and dried in vacuo to give $\mathbf{1}^{2+}(SbCl_6^-)_2$ (32.6 mg) as a red powder in 98% yield.

Oxidation of a mixture of AA-**1** and SA-**1** with $(4\text{-}BrC_6H_4)_3N^{+\bullet}SbCl_6^-$:

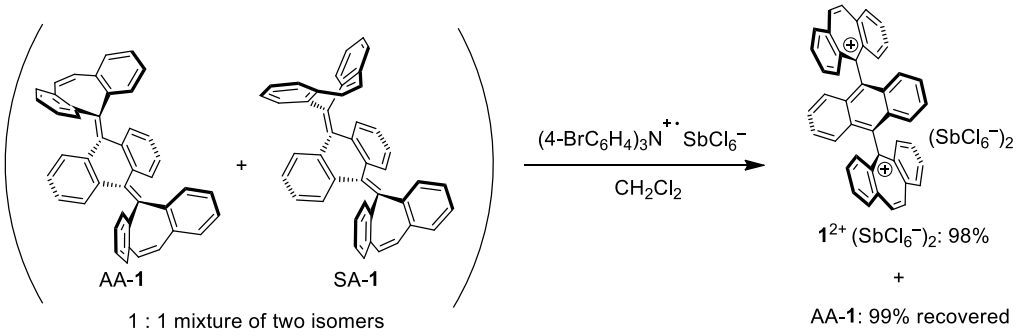

To a solution of mixture of AA-**1** (18.6 mg, 33.4 μmol) and SA-**1** (18.6 mg, 33.4 μmol) in dry CH_2Cl_2 (2.0 mL) was added $(4\text{-}BrC_6H_4)_3N^{+\bullet}SbCl_6^-$ (54.6 mg, 66.8 μmol) at 24 °C, and the mixture was stirred for 1 h. The addition of dry Et_2O led to precipitation of the dication salt. The supernatant solution was removed by decantation. Then, the residue was again dissolved in dry CH_2Cl_2, and these procedures were repeated 3 times. The resulting residue was dried in vacuo to give $\mathbf{1}^{2+}(SbCl_6^-)_2$ (40.2 mg) as a red powder in 98% yield for SA-**1**. On the other hand, the combined filtrate was evaporated under reduced pressure. The residue was washed with hexane three times to remove $(4\text{-}BrC_6H_4)_3N$ as a byproduct and dried in vacuo to recover AA-**1** (18.5 mg) as a white solid in 99% yield for AA-**1**.

5,5'-(Anthracene-9,10-diyl)bis(9*H*-tribenzo[*a*,*c*,*e*]cycloheptatrien-9-ol) 4.

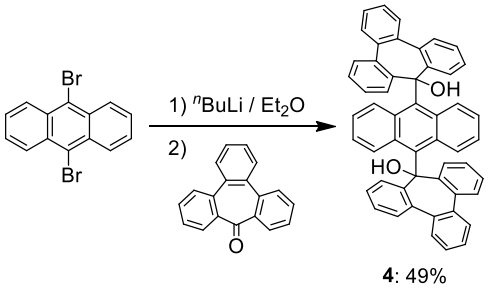

4: 49%

To a solution of 9,10-dibromoanthracene (297 mg, 0.883 mmol) in dry Et_2O (8 mL) was added ^{n}BuLi (1.57 M in hexane, 1.35 mL, 2.12 mmol) dropwise over 3 min at –20 °C. After stirring at –20 °C for 1 h, tribenzosuberenone[12,20] (543 mg, 2.12 mmol) was added to the suspension and the mixture was warmed to 24 °C. The resulting solution was stirred at 24 °C for 2 h, and then diluted with water. The precipitates were filtered and washed with water (x 3) and methanol (x 3). The crude product was washed with $CHCl_3$ and the suspension was filtered. The resulting solid was dried in vacuo to give diol **4** (234 mg) as a yellow solid. The filtrate was purified by column chromatography on silica gel (CH_2Cl_2/hexane = 4/5) to give diol **4** (66.0 mg). A total yield is 49% (300 mg).

4; Mp: 293-296 °C (decomp.); ^{1}H NMR ($CDCl_3$): δ/ppm 8.26 (4H, dd, *J* = 1.1 Hz, 8.0 Hz), 7.43 (4H, ddd, *J* = 1.3 Hz, 7.4 Hz, 8.0 Hz), 7.31 (4H, dd, *J* = 3.3 Hz, 7.2 Hz), 7.10 (4H, ddd, *J* = 1.1 Hz, 7.4 Hz, 7.4 Hz), 6.88 (4H, dd, *J* = 1.3 Hz, 7.4 Hz), 6.57 (4H, dd, *J* = 3.4 Hz, 5.7 Hz), 6.46 (4H, dd, *J* = 3.3 Hz, 7.2 Hz), 6.06 (4H, dd, *J* = 3.4 Hz, 5.7 Hz), 2.97 (2H, s); ^{13}C NMR ($CDCl_3$): δ/ppm 150.87, 138.55, 134.24, 132.93, 129.93, 129.34, 127.62, 125.97, 125.85, 125.55, 125.34, 120.68, 120,40, 79.67; IR (KBr): ν/cm^{-1} 3618, 3593, 3056, 1929, 1672, 1621, 1597, 1578, 1522, 1483, 1472, 1435, 1300, 1173, 1157, 1123, 1053, 1037, 992, 887, 861, 765, 746, 733, 683, 676, 647, 618, 602; LR-MS (FD) m/z (%): 693.19 (5), 692.18 (21), 691.18 (67), 690.58 (5), 690.18 (M^+, bp); HR-MS (FD) Calcd. for $C_{52}H_{34}O_2$: 690.25588; Found: 690.25624.

9,9'-(Anthracene-9,10-diyl)bis(9*H*-tribenzo[*a*,*c*,*e*]cycloheptatrien-9-ylium) bis(tetrafluoroborate) $2^{2+}(BF_4^-)_2$.

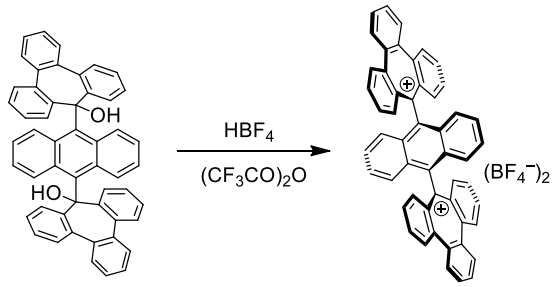

4 2^{2+} $(BF_4^-)_2$: 86%

To a solution of diol **4** (200 mg, 0.289 mmol) in TFAA (5.0 mL) was added 42% HBF_4 aq. (0.44 mL, 2.89 mmol) at 0 °C to give a deep green solution, and the mixture was stirred at 25 °C for 1 h. The addition of dry Et_2O at 0 °C led to precipitation of the dication salt. The precipitates were filtered, washed with dry Et_2O three times, and dried in vacuo to give $\mathbf{2}^{2+}(BF_4^-)_2$ (206 mg) as a green powder in 86% yield.

$\mathbf{2}^{2+}(BF_4^-)_2$; Mp: > 210-215 °C (decomp.); ^{1}H NMR (CD_3CN containing 5 vol% TFAA): δ/ppm 8.86 (4H, dd, *J* = 0.9 Hz, 8.3 Hz), 8.64 (4H, dd, *J* = 3.4 Hz, 6.2 Hz), 8.50 (4H, ddd, *J* = 1.2 Hz, 7.0 Hz, 8.3 Hz), 8.31 (4H, dd, *J* = 1.2 Hz, 8.3 Hz), 8.25 (4H, dd, *J* = 3.4 Hz, 6.2 Hz), 7.84 (4H, ddd, *J* = 0.9 Hz, 7.0 Hz, 8.3 Hz), 7.39 (4H, dd, *J* = 3.2 Hz, 6.8 Hz), 7.13 (4H, dd, *J* = 3.2 Hz, 6.8Hz); ^{13}C NMR (CD_3CN containing 5 vol% TFAA): δ/ppm 192.46, 150.14, 145.03, 141.23, 140.06, 138.93, 136.64, 133.44, 133.25, 132.91, 132.17, 131.14, 129.31, 127.19; IR (KBr): ν/cm^{-1} 3059, 1729, 1663, 1588, 1534, 1476, 1443, 1372, 1333, 1285, 1266, 1240, 1210, 1172, 1145, 1059, 996, 915, 879, 784, 769, 742, 713, 669, 658, 637, 617, 599, 572, 543, 519; LR-MS (FD) m/z (%): 769.23 (8), 673.26 (11), 672.25 (21), 658.27 (17), 657.25 (60), 656.26 (M^{2+}+e, bp), 433.16 (9), 432.15 (23); HR-MS (FD) Calcd. for $C_{52}H_{32}$: 656.25040; Found: 656.25125; UV-vis (CH_3CN containing 10 vol% TFAA): λ_{max}/nm (ε/L mol^{-1} cm^{-1}) 752 (1900), 610 (10100), 448 (13200), 401 (16500), 380 (17500), 362 (10600), 301 (45000).

9,10-Bis(9*H*-tribenzo[*a*,*c*,*e*]cycloheptatrien-9-ylidene)-9,10-dihydroanthracene 2.

Reduction of $\mathbf{2}^{2+}(BF_4^-)_2$ to **2**:

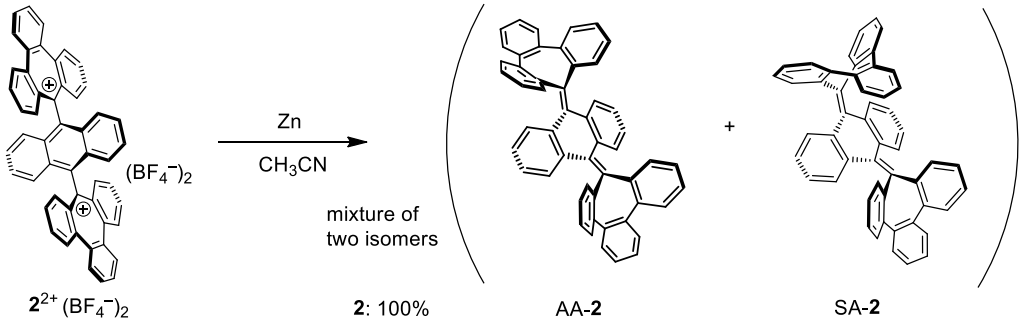

To a solution of $\mathbf{2}^{2+}(BF_4^-)_2$ (186.5 mg, 0.225 mmol) in dry CH_3CN (5 mL) was added activated zinc powder (294 g, 4.49 mmol) at 25 °C. The mixture was stirred at 25 °C for 1 min, and then diluted with water. The whole mixture was extracted with CH_2Cl_2 three times. The combined organic layers were washed with water and brine, and dried over anhydrous $MgSO_4$. After filtration through silica gel, the solvent was concentrated under reduced pressure to give ca. 1:2 mixture of AA-**2** and SA-**2** (148 mg) as a white solid in 100% yield.

AA-**2**; Rf = 0.29 (hexane/$CHCl_3$ = 2, silica gel); Mp: > 300 °C; ^{1}H NMR ($CDCl_3$): δ/ppm 7.83 (4H, dd, *J* = 3.4 Hz, 5.8 Hz), 7.67 (4H, dd, *J* = 1.0 Hz, 7.8 Hz), 7.54 (4H, dd, *J* = 3.4 Hz, 5.8 Hz), 7.35 (4H, ddd, *J* = 1.2 Hz, 7.8 Hz, 7.8 Hz), 7.25 (4H, ddd, *J* = 1.0 Hz, 7.8 Hz, 7.8 Hz), 7.11 (4H,

dd, *J* = 1.2 Hz, 7.8 Hz), 6.65 (4H, dd, *J* = 3.4 Hz, 6.0 Hz), 6.58 (4H, dd, *J* = 3.4 Hz, 6.0 Hz); ^{13}C NMR ($CDCl_3$): δ/ppm 144.11, 139.28, 138.63, 137.66, 136.56, 133.34, 129.82, 129.23, 128.06, 127.92, 127.77, 127.53, 127.29, 125.22; IR (KBr): ν/cm^{-1} 3060, 2360, 1956, 1922, 1628, 1593, 1478, 1460, 1450, 1431, 1273, 1216, 1166, 1152, 1045, 1006, 946, 779, 757, 746, 733, 705, 646, 618; LR-MS (FD) m/z (%): 658.16 (18), 657.16 (61), 656.16 (M^+, bp); HR-MS (FD) Calcd. for $C_{52}H_{32}$: 656.25040; Found: 656.25326; UV-vis (CH_2Cl_2): λ_{max}/nm (ε/L mol^{-1} cm^{-1}) 233 (116000), 321 (29300); Fluorescence (λ_{ex} = 320 nm): λ_{em}/nm (Φ_F) 398 (0.73).

SA-**2**; Rf = 0.24 (hexane/$CHCl_3$ = 2, silica gel); Mp: > 300 °C; ^{1}H NMR ($CDCl_3$): δ/ppm 7.89 (2H, dd, *J* = 1.0 Hz, 7.6 Hz), 7.71 (2H, dd, *J* = 3.4 Hz, 5.8 Hz), 7.69 (2H, dd, *J* = 2.6 Hz, 5.0Hz), 7.69 (2H, dd, *J* = 1.1 Hz, 7.6 Hz), 7.52 (2H, dd, *J* = 1.1 Hz, 8.8 Hz), 7.49 (2H, dd, *J* = 1.2 Hz, 7.5 Hz), 7.47 (2H, dd, *J* = 3.4 Hz, 5.8 Hz), 7.43 (2H, ddd, *J* = 1.2 Hz, 7.6 Hz, 7.6 Hz), 7.30 (2H, ddd, *J* = 1.0 Hz, 7.6 Hz, 7.6 Hz), 7.28 (2H, dd, *J* = 2.6 Hz, 5.0Hz), 7.23 (2H, ddd, *J* = 1.2 Hz, 8.8 Hz, 8.8 Hz), 7.05 (2H, ddd, *J* = 1.1 Hz, 8.8 Hz, 8.8 Hz), 6.81 (2H, ddd, *J* = 1.1 Hz, 7.6 Hz, 7.6 Hz), 6.60 (2H, ddd, *J* = 1.1 Hz, 7.6 Hz, 7.6 Hz), 6.36 (2H, dd, *J* = 1.1 Hz, 7.6 Hz), 6.22 (2H, dd, *J* = 1.2 Hz, 8.8 Hz); ^{13}C NMR ($CDCl_3$): δ/ppm 143.74, 143.05, 139.21, 138.83, 138.10, 137.04, 136.96, 136.81, 136.42, 135.55, 134.61, 132.58, 129.69,129.40, 129.06, 128.89, 128.73, 128.58, 128.07, 127.83, 127.68, 127.55, 127.19, 126.97, 126.90, 126.36, 125.25, 125.19; IR (KBr): ν/cm^{-1} 3057, 1959,1923, 1627, 1593, 1477, 1449, 1429, 1271, 1217, 1158, 1101, 1040, 1006, 975, 947, 892, 878, 858, 782, 761, 746, 703, 644, 624; LR-MS (FD) m/z (%): 672.25 (5), 658.28 (17), 657.27 (58), 656.27 (M^+, bp); HR-MS (FD) Calcd. for $C_{52}H_{32}$: 656.25040; Found: 656.25120; UV-vis (CH_2Cl_2): λ_{max}/nm (ε/L mol^{-1} cm^{-1}) 233 (96800), 268 (30800), 313 (17470); Fluorescence (λ_{ex} = 320 nm): λ_{em}/nm (Φ_F) 399 (0.44).

Reduction of **2**$^{2+}$($SbCl_6^-$)$_2$ to **2**:

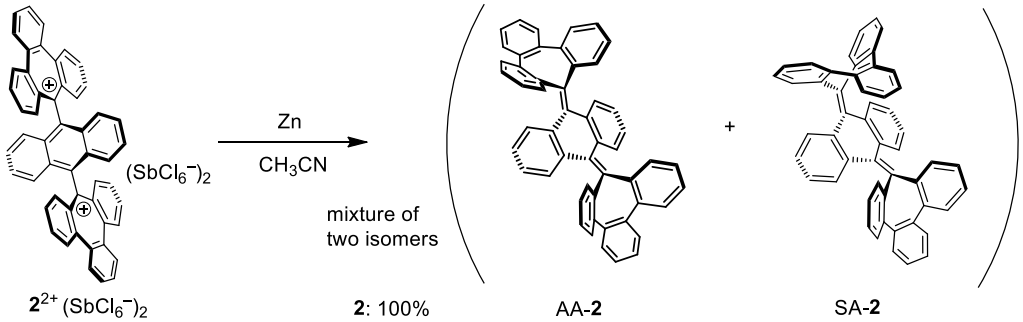

To a solution of **2**$^{2+}$($SbCl_6^-$)$_2$ (51.2 mg, 38.6 μmol) in dry CH_3CN (1.0 mL) was added activated zinc powder (50.5 mg, 772 μmol) at 24 °C. The mixture was stirred for 1 min, and then diluted with water. The whole mixture was extracted with CH_2Cl_2 three times. The combined organic layers were washed with water and brine, and dried over anhydrous $MgSO_4$. After filtration through silica gel, the solvent was concentrated under reduced pressure to give ca. 1:2 mixture of

AA-**2** and SA-**2** (26.4 mg) as a white solid in 100% yield.

Thermal isomerization of SA-**2** to AA-**2**:

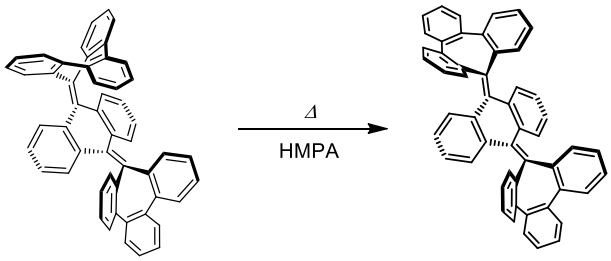

A solution of SA-**2** (24.9 mg, 37.9 μmol) in hexamethylphosphoramide (HMPA, 7.0 mL) was heated at 220 °C for 3 h. After cooling to 24 °C, the resulting solution was diluted with 1.0 M HCl aq. The whole mixture was extracted with CH_2Cl_2 three times. The combined organic layers were washed with water and brine, and dried over anhydrous $MgSO_4$. After filtration through silica gel, the solvent was concentrated under reduced pressure to give AA-**2** (24.7 mg) as a white solid in 99% yield.

Photoisomerization of AA-**2** to SA-**2**:

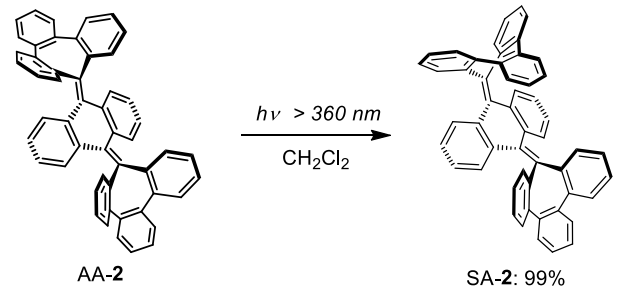

A solution of AA-**2** (57.5 mg, 87.5 μmol, 2.5×10^{-3} mol L^{-1}) in CH_2Cl_2 (35 mL) was degassed by Ar bubbling, and then stirred at 25 °C for 6 h upon photoirradiation (hν > 360 nm). The solvent was concentrated under reduced pressure to give SA-**2** (57.2 mg) as a white solid in 99% yield.

9,9'-(Anthracene-9,10-diyl)bis(9*H*-tribenzo[*a*,*c*,*e*]cycloheptatrien-9-ylium)bis(hexachloroantimonate) $2^{2+}(SbCl_6^-)_2$

Oxidation of SA-**2** with $(2,4\text{-}Br_2C_6H_3)_3N^{+\bullet}SbCl_6^-$:

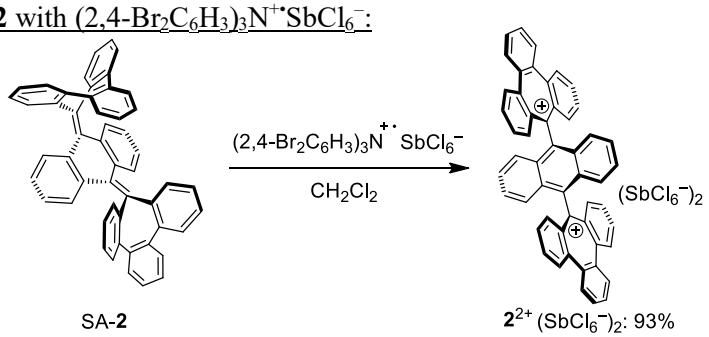

To a solution of SA-**2** (26.1 mg, 39.7 μmol) in dry CH_2Cl_2 (1.0 mL) was added $(2,4\text{-}Br_2C_6H_3)_3N^{+\bullet}SbCl_6^-$ (83.7 mg, 79.5 μmol) at 0 °C, and the mixture was stirred for 30 min. The addition of dry Et_2O led to precipitation of the dication salt. The supernatant solution was removed by decantation, washed with dry Et_2O three times, and dried in vacuo to give $\mathbf{2}^{2+}(SbCl_6^-)_2$ (49.1 mg) as a deep red powder in 93% yield.

$\mathbf{2}^{2+}(SbCl_6^-)_2$; Mp: 215-218 °C (decomp); ^{1}H NMR and ^{13}C NMR spectra are identical to those of $\mathbf{2}^{2+}(BF_4^-)_2$; IR (KBr): ν/cm^{-1} 3062, 1660, 1586, 1531, 1473, 1441, 1366, 1331, 1285, 1264, 1236, 1211, 1170, 1144, 997, 914, 881, 782, 768, 737, 728, 711, 668, 636, 571, 543; LR-MS (FD) m/z (%): 672.19 (5), 671.21 (5), 658.23 (15), 657.21 (59), 656.21 (M^{2+}+e, bp), 432.21 (8); HR-MS (FD) Calcd. for $C_{52}H_{32}$: 656.25040; Found: 656.24849.

Oxidation of AA-**2** with $(2,4\text{-}Br_2C_6H_3)_3N^{+\bullet}SbCl_6^-$:

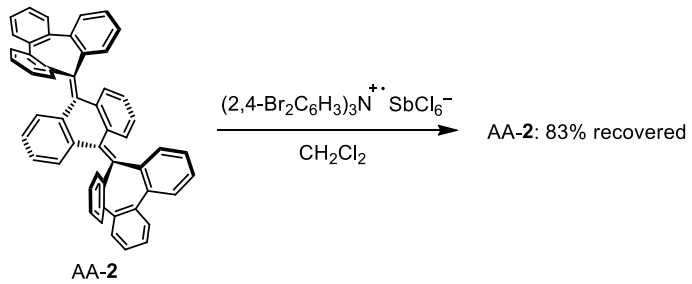

To a solution of AA-**2** (17.7 mg, 26.9 μmol) in dry CH_2Cl_2 (3.0 mL) was added $(2,4\text{-}Br_2C_6H_3)_3N^{+\bullet}SbCl_6^-$ (56.7 mg, 53.8 μmol) at 0 °C, and the mixture was stirred for 30 min. The addition of dry Et_2O led to precipitation, and the precipitation was removed by decantation. Then, the residue was dissolved in dry CH_2Cl_2, and these procedures were repeated 3 times. The resulting filtrate was filtered through silica gel and evaporated under reduced pressure. The residue was washed with hexane three times, and dried in vacuo to recover AA-**2** (14.7 mg) as a white solid in 83% yield.

Oxidation of a mixture of AA-**2** and SA-**2** with $(2,4\text{-}Br_2C_6H_3)_3N^{+\bullet}SbCl_6^-$:

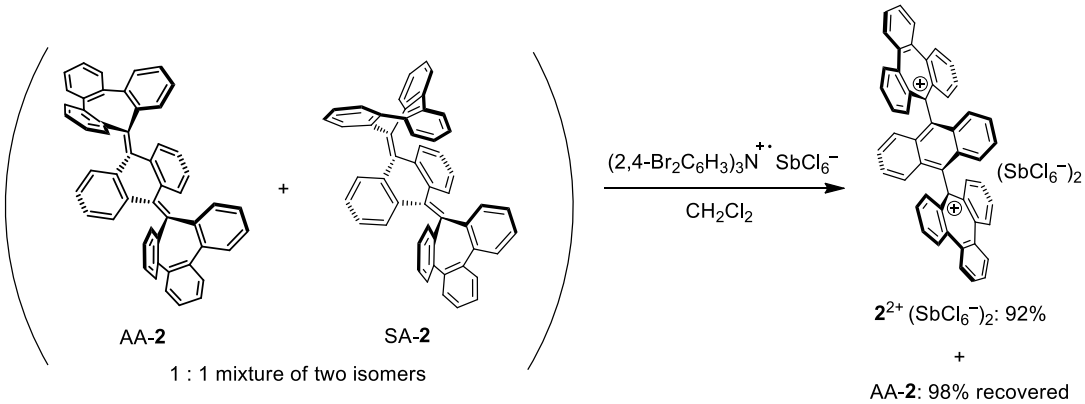

To a solution of mixture of AA-**2** (30.5 mg, 46.1 μmol) and SA-**2** (30.3 mg, 46.1 μmol) in dry CH_2Cl_2 (2.0 mL) was added $(2,4\text{-}Br_2C_6H_3)_3N^{+\bullet}SbCl_6^-$ (97.1 mg, 92.2 μmol) at 0 °C, and the mixture was stirred for 30 min. The addition of dry Et_2O led to precipitation of the dication salt. The supernatant solution was removed by decantation. Then the residue was again dissolved in dry CH_2Cl_2, and these procedure were repeated 3 times. The resulting residue was dried in vacuo to give $\mathbf{2}^{2+}(SbCl_6^-)_2$ (56.2 mg) as a deep red powder in 92% yield for SA-**2**. On the other hand, the combined filtrate was evaporated under reduced pressure. The residue was washed with hexane three times, and dried in vacuo to recover AA-**2** (29.9 mg) as a white solid in 98% yield for AA-**2**.

3-4-3. Crystal data

Data were collected with a Rigaku Mercury 70 diffractometer (Mo-Kα radiation, λ = 0.71075 Å) for $\mathbf{1}^{2+}(BF_4^-)_2$, AA-**1**, SA-**1**, and $\mathbf{1}^{2+}(SbCl_6^-)_2$ and a Rigaku XtaLAB Synergy (Cu-Kα radiation, λ = 1.54184 Å) for AA-**2** and SA-**2**. The structure was solved by the direct method (SIR2004) or ShelXT (Sheldrick) and refined by the full-matrix least-squares method on F^2 with anisotropic temperature factors for non-hydrogen atoms. All the hydrogen atoms were located at the calculated positions and refined with riding.

Crystal data of $\mathbf{1}^{2+}(BF_4^-)_2$:

Crystals were obtained by recrystallization from CH_3CN/Et_2O. MF: $C_{44}H_{28}B_2F_8$, FW: 730.31, purple plate, 0.30 × 0.30 × 0.05 mm^3, monoclinic $P2_1/n$, a = 10.326(2) Å, b = 14.178(3) Å, c = 11.546(2) Å, β = 99.37(2)°, V = 1667.8(6) Å^3, ρ (Z = 2) = 1.454 g cm^{-3}. A total 11532 reflections were measured at T = 150 K. Numerical absorption correction was applied (μ = 1.136 cm^{-1}). The final *R1* and *wR*2 values are 0.0764 (I > 2σI) and 0.2095 (all data) for 3260 reflections and 262 parameters. Estimated standard deviations are 0.005-0.017 Å for bond lengths and 0.3-1.1° for bond angles. CCDC 1950059

Crystal data of AA-**1**:

Crystals were obtained by recrystallization from CH_2Cl_2/hexane. MF: $C_{44}H_{28}$, FW: 556.71, colorless rod, 0.30 × 0.10 × 0.10 mm^3, monoclinic $P2_1/n$, a = 10.138(10) Å, b = 11.360(11) Å, c = 26.59(3) Å, β = 96.68(2)°, V = 3041(6) Å^3, ρ (Z = 4) = 1.216 g cm^{-3}. A total of 14226 reflections were measured at T = 150 K. Numerical absorption correction was applied (μ = 0.688 cm^{-1}). The final *R*1 and *wR*2 values are 0.0983 (I > 2σI) and 0.2596 (all data) for 5241 reflections and 397 parameters. Estimated standard deviations are 0.007-0.011 Å for bond lengths and 0.4-0.7° for bond angles. CCDC 1950060

Crystal data of SA-**1**:

Crystals were obtained by recrystallization from CH_2Cl_2/Et_2O. MF: $C_{44}H_{28}$, FW: 556.71, colorless platelet, 0.40 × 0.20 × 0.05 mm^3, triclinic $P\bar{1}$, a = 9.916(3) Å, b = 12.574(4) Å, c = 13.151(4) Å, α = 93.674(3)°, β = 103.439(4)°, γ = 107.172(4)°, V = 1508.1(8) Å^3, ρ (Z = 2) = 1.226 g cm^{-3}. A total 11265 reflections were measured at T = 150 K. Numerical absorption correction was applied (μ = 0.693 cm^{-1}). The final *R1* and *wR*2 values are 0.0554 (I > 2σI) and 0.1317 (all data) for 5855 reflections and 397 parameters. Estimated standard deviations are 0.003-0.004 Å for bond lengths and 0.16-0.3° for bond angles. CCDC 1950061

Crystal data of $\mathbf{1}^{2+}(SbCl_6^-)_2 \cdot 2(CH_3CN)$:

Crystals were obtained by recrystallization from CH_3CN/Et_2O. MF: $C_{48}H_{34}Cl_{12}N_2Sb_2$, FW: 1307.75, purple block, 0.30 × 0.20 × 0.10 mm^3, triclinic $P\overline{1}$, a = 9.5813(5) Å, b = 9.7045(4) Å, c = 14.8304(7) Å, α = 71.271(4)°, β = 76.563(4)°, γ = 84.617(4)°, V = 1269.91(11) Å^3, ρ (Z = 1) = 1.710 g cm^{-3}. A total 8899 reflections were measured at T = 150 K. Numerical absorption correction was applied (μ = 17.290 cm^{-1}). The final *R1* and *wR*2 values are 0.042 (I > 2σI) and 0.1295 (all data) for 4894 reflections and 289 parameters. Estimated standard deviations are 0.006-0.008 Å for bond lengths and 0.4-0.5° for bond angles. CCDC 1950062

Crystal data of AA-**2**:

Crystals were obtained by recrystallization from CH_2Cl_2/pentane. MF: $C_{52}H_{32}$, FW: 656.77, clear light colorless plate, 0.30 × 0.20 × 0.05 mm^3, monoclinic $C2$, a = 18.0595(6) Å, b = 6.7674(2) Å, c = 14.6897(6) Å, β = 104.488(4)°, V = 1738.22(11) Å^3, ρ (Z = 2) = 1.255 g cm^{-3}. A total of 4913 reflections were measured at T = 293 K. Numerical absorption correction was applied (μ = 0.540 mm^{-1}). The final *R*1 and *wR*2 values are 0.1191 (I > 2σI) and 0.3010 (all data) for 2418 reflections and 235 parameters. Estimated standard deviations are 0.006-0.010 Å for bond lengths and 0.4-0.6° for bond angles. CCDC 1950063

Crystal data of SA-$\mathbf{2} \cdot CH_2Cl_2$:

Crystals were obtained by recrystallization from CH_2Cl_2/hexane. MF: $C_{53}H_{34}Cl_2$, FW: 741.70, clear light colorless plate, 0.40 × 0.25 × 0.10 mm^3, monoclinic $P2_1/n$, a = 8.73705(6) Å, b = 16.80505(11) Å, c = 25.89795(19) Å, β = 96.3243(7)°, V = 3779.37(5) Å^3, ρ (Z = 4) = 1.304 g cm^{-3}. A total 23170 reflections were measured at T = 150 K. Numerical absorption correction was applied (μ = 1.827 mm^{-1}). The final *R1* and *wR*2 values are 0.0595 (I > 2σI) and 0.1604 (all data) for 7628 reflections and 520 parameters. Estimated standard deviations are 0.002-0.02 Å for bond lengths and 0.13-0.19° for bond angles. CCDC 1950064

3-5. References

(1) Olsen, B. A.; Evans, D. H. Electron-Transfer Reactions and Conformational Changes Associated with the Reduction of Bianthrone. *J. Am. Chem. Soc*. **1981**, *103* (4), 839–843, DOI: 10.1021/ja00394a018.

(2) Evans, D. H.; Busch, R. W. Electron-Transfer Reactions and Associated Conformational Changes. Extended Redox Series for Some Bianthrones, Lucigenin, and Dixanthylene. *J. Am. Chem. Soc*. **1982**, *104* (19), 5057–5062, DOI: 10.1021/ja00383a011.

(3) Suzuki, T.; Fukushima, T.; Miyashi, T.; Tsuji, T. Isolation and X-Ray Structural Determination of Both Folded and Twisted Conformers of Bis{4H,8H-4-(Dicyanomethylene)-Benzo[1,2-c:4,5-C']Bis[1,2,5]Thiadiazol-8-Ylidene}, an Overcrowded Ethylene with High Electron Affinity. *Angew. Chem. Int. Ed. Engl*. **1997**, *36* (22), 2495–2497, DOI: 10.1002/anie.199724951.

(4) Browne, W. R.; Pollard, M. M.; de Lange, B.; Meetsma, A.; Feringa, B. L. Reversible Three-State Switching of Luminescence: A New Twist to Electro- and Photochromic Behavior. *J. Am. Chem. Soc*. **2006,** *128* (38), 12412–12413, DOI: 10.1021/ja064423y.

(5) Ivashenko, O.; Logtenberg, H.; Areephong, J.; Coleman, A. C.; Wesenhagen, P. V.; Geertsema, E. M.; Heureux, N.; Feringa, B. L.; Rudolf, P.; Browne, W. R. Remarkable Stability of High Energy Conformers in Self-Assembled Monolayers of a Bistable Electro- and Photoswitchable Overcrowded Alkene. *J. Phys. Chem. C* **2011**, *115* (46), 22965–22975, DOI: 10.1021/jp206889y.

(6) Matsuo, Y.; Wang, Y.; Ueno, H.; Nakagawa, T.; Okada, H. Mechanochromism, Twisted/Folded Structure Determination, and Derivatization of (N-Phenylfluorenylidene)Acridane. *Angew. Chem. Int. Ed*. **2019**, *58* (26), 8762–8767, DOI: 10.1002/anie.201902636.

(7) Bergmann, E. D.; Ginsburg, D.; Hirshberg, Y.; Mayor, M.; Pullman, A.; Pullman, B. Fulvenes and Thermochromic Ethylenes. XIII. The Heptafulvenes and Their Tetrabenzo Derivatives. *Bull. Soc. Chim. Fr.* **1951**, *18*, 697–701.

(8) Schönberg, A.; Sodtke, U.; Praefcke, K. Über Stereoisomere Und Photochemie Des 2.3; 6.7;2'3';6',7'-Tetrabenzo-Heptafulvalens. *Tetrahedron Lett*. **1968**, *9* (29), 3253‑3256, DOI: 10.1016/S0040-4039(00)89540-4.

(9) Schönberg, A.; Sodtke, U.; Praefcke, K. Darstellung, Reaktionen Und Stereochemie Der 2.3;6.7;2'3';6',7'-Tetrabenzo-Heptafulvalene. *Chem. Ber*. **1969**, *102* (5), 1453‑1467, DOI: 10.1002/cber.19691020504.

(10) Dichmann, K. S.; Nyburg, S. C.; Pickard, F. H.; Potworowski, J. A. The Crystal and Molecular Structures of Two Stereoisomers of $\delta^{5,5'}$-Bi-5H-Dibenzo[a,d]Cycloheptene(2,3;6,7;2'3';6',7'-Tetrabenzoheptafulvalene). *Acta Crystallogr. Sect. B Struct. Crystallogr. Cryst. Chem*. **1974**, *30* (1), 27–36, DOI: 10.1111/j.1600-5740.1974.tb00006.x.

(11) Agranat, I.; Suissa, M. R. Syn, Anti Isomerization of 5,5'-Bis-5H-Dibenzo[a,d]Cyclohepten-5-Ylidene. *Struct. Chem*. **1993**, *4* (1), 59–66, DOI: 10.1007/BF00672100.

(12) Luo, J.; Song, K.; Gu, F. long; Miao, Q. Switching of Non-Helical Overcrowded Tetrabenzoheptafulvalene Derivatives. *Chem. Sci*. **2011**, *2* (10), 2029–2034, DOI: 10.1039/C1SC00340B.

(13) Malandra, J. L.; Mills, N. S.; Kadlecek, D. E.; Lowery, J. A. Dications of Tetrabenzofulvalenes. Paratropicity and .Sigma. Donation in Perpendicular Antiaromatic Systems. *J. Am. Chem. Soc*. **1994**, *116* (25), 11622–11623, DOI: 10.1021/ja00104a074.

(14) Mills, N. S.; Levy, A.; Plummer, B. F. Antiaromaticity in Fluorenylidene Dications. Experimental and Theoretical Evidence for the Relationship between the HOMO/LUMO Gap and Antiaromaticity. *J. Org. Chem*. **2004**, *69* (20), 6623–6633, DOI: 10.1021/jo0499266.

(15) Sakano, Y.; Katoono, R.; Fujiwara, K.; Suzuki, T. Preparation, Redox Properties, and X-Ray Structures of Electrochromic 11,11,12,12-Tetraarylanthraquinodimethane and Its Bianthraquinodimethane Analogue: Drastic Geometrical Changes upon Interconversion with Dicationic Dyes. *Chem. Lett*. **2014**, *43* (7), 1143–1145, DOI: 10.1246/cl.140393.

(16) Ishigaki, Y.; Sugawara, K.; Yoshida, M.; Kato, M.; Suzuki, T. Two-Way Chromic Systems Based on Tetraarylanthraquinodimethanes: Electrochromism in Solution and Mechanofluorochromism in a Solid State. *Bull. Chem. Soc. Jpn*. **2019**, *92* (7), 1211–1217, DOI: 10.1246/bcsj.20190094.

(17) *Gaussian 16, Revision A.03*; Frisch, M. J.; Trucks, G. W.; Schlegel, H. B.; Scuseria, G. E.; Robb, M. A.; Cheeseman, J. R.; Scalmani, G.; Barone, V.; Petersson, G. A.; Nakatsuji, H.; Li, X.; et al., Gaussian, Inc., Wallingford CT, 2016.

(18) Aranzaes, J. R.; Daniel, M.-C.; Astruc, D. Metallocenes as References for the Determination of Redox Potentials by Cyclic Voltammetry – Permethylated Iron and Cobalt Sandwich Complexes, Inhibition by Polyamine Dendrimers, and the Role of Hydroxy-Containing Ferrocenes. *Can. J. Chem*. **2006**, *84* (2), 288–299, DOI: 10.1139/v05-262.

(19) Suzuki, K.; Kobayashi, A.; Kaneko, S.; Takehira, K.; Yoshihara, T.; Ishida, H.; Shiina, Y.; Oishi, S.; Tobita, S. Reevaluation of Absolute Luminescence Quantum Yields of Standard Solutions Using a Spectrometer with an Integrating Sphere and a Back-Thinned CCD Detector. *Phys. Chem. Chem. Phys*. **2009**, *11*, 9850, DOI: 10.1039/B912178A.

(20) Tochtermann, W. Hexabenzooctalene from Tribenzotropone. *Angew. Chem. Int. Ed. Engl.* **1963**, *2*, 265–266, DOI: 10.1002/anie.196302653.

Chapter 4

Cation-capped Orthogonal Approach Enabling Isolation and Examination of a Series of Hydrocarbons with Multiple 14π-Aromatic Units

” Compound numbers are independent in each Chapter.”

4-1. Introduction

The linking of several π-conjugated carbon skeletons, especially those in which the same units are connected by C-C single bonds, is of special interest, since unique properties that are not possessed by the original skeleton can appear due to the accumulation of simple π-conjugated scaffolds (Figure 4-1).[1–5] For example, oligophenylene-[6–15] and oligonaphthylene[16–23]-based frameworks with various topologies such as linear and cyclic structures have been developed by accumulating simple planar π-systems (benzene and naphthalene, respectively), which has led to the discovery of numerous functions and physical properties.

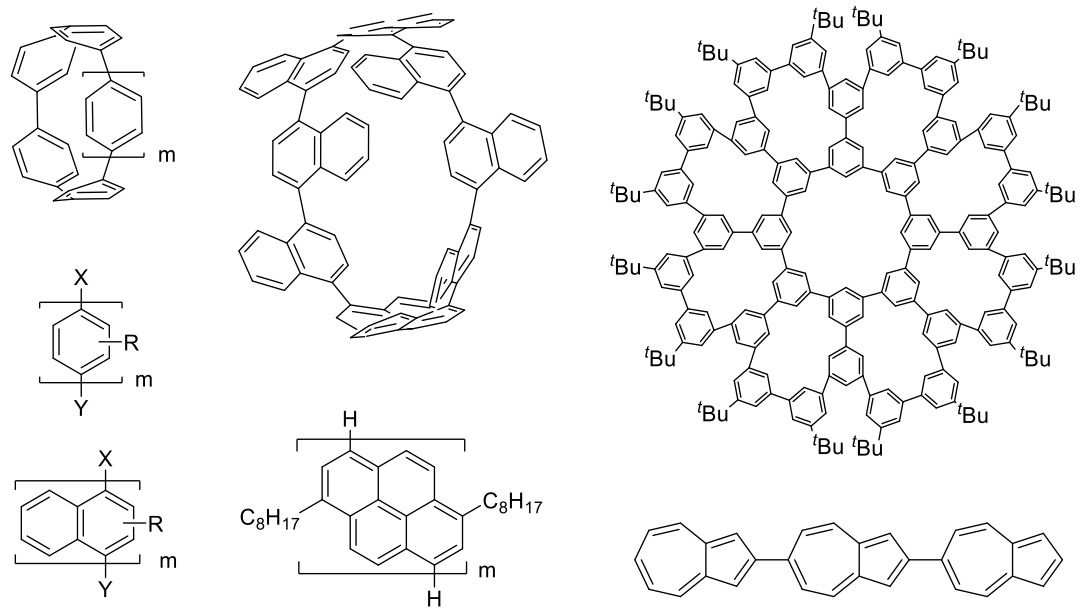

Figure 4-1. Some examples of oligomers composed of several same π-conjugated carbon skeletons connected by C-C single bonds.

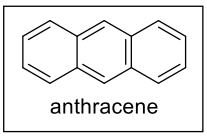

Anthracene is a highly attractive carbon π-skeleton with intrinsic photophysical and electrochemical properties that has attracted attention since its discovery in 1832.[24] It has been widely used as an essential component in the development of smart functional materials such as organic light-emitting diodes, organic solar cells, and organic thin-film transistors.[25–27] Since anthracene can be a key building block for a variety of organic molecules, several oligoanthrylenes [X-$(C_{14}H_8)_m$-Y] with multiple anthracenes linked at arbitrary positions have been reported (Figure 4-2a).[28–30] Especially, 9,9'-bianthracene (Figure 4-2b: m = 2; X, Y, R and R' = H) [31–34] and its derivatives,[35–39] in which two anthracene units are directly linked to each other at the 9-position, have been investigated for their unique physical properties such as their emission behavior based on twisted intramolecular charge transfer states in their excited states.[40]

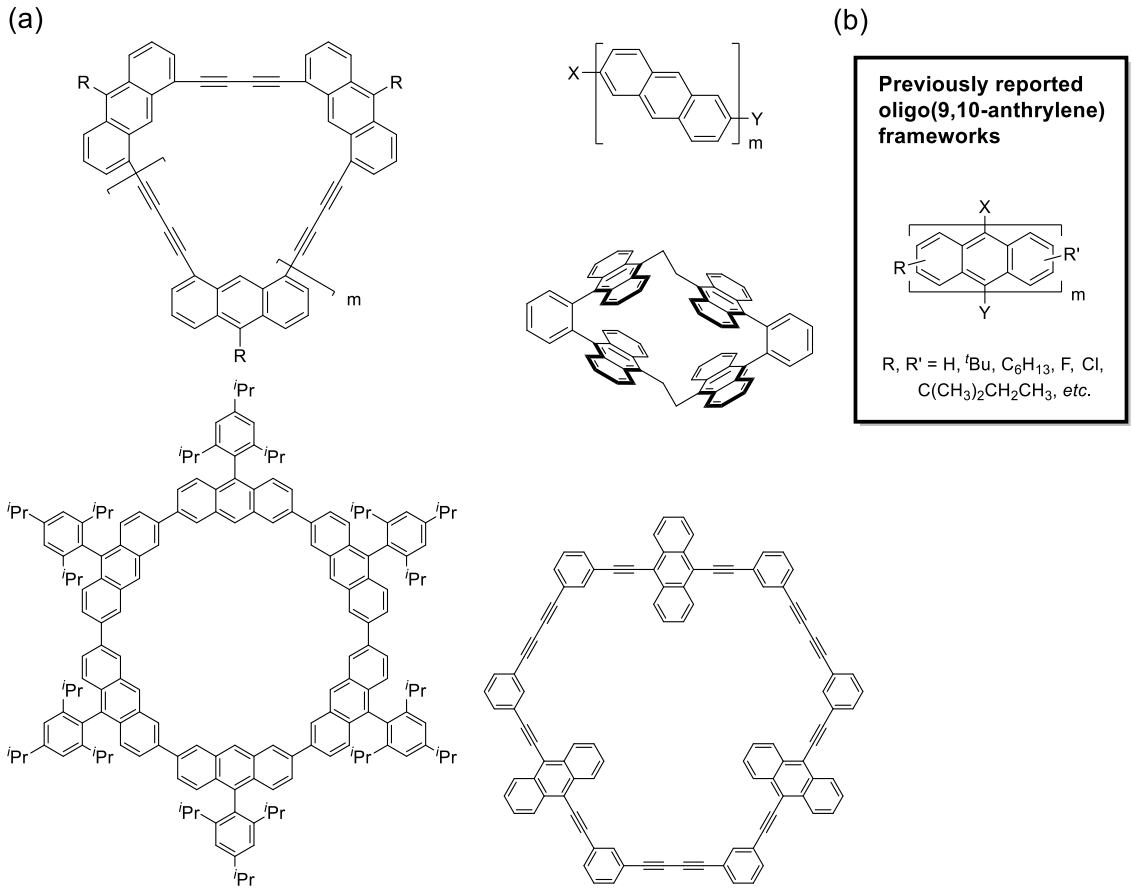

Figure 4-2. Some examples of anthracene oligomers.

Compared to the plethora of studies on bianthracenes, there have been only a few reported examples of oligo(9,10-anthrylene) derivatives of $m \geq 3$, in which anthracene units are connected at 9,10-positions in a linear manner (Figure 4-2b). In the 1990s, Müllen *et al*. synthesized several derivatives (m = 3 and 4) and reported their photophysical properties, such as the absorption and emission behavior of neutral species.[41–45] The magnetic properties of the corresponding anion radical species obtained upon treatment with potassium metal showed that high-spin states are stabilized due to the orthogonally twisted structure between anthrylene units, which can suppress electron delocalization over the connected anthrylene units. In addition, several other derivatives with three or four anthrylene units have been studied by Baumgarten *et al*.,[46] Ajibade *et al.*,[47,48] Wu *et al*.,[49] Kubo *et al*.[50] and Ruffieux *et al*.,[51,52] and have recently been used as starting materials for the bottom-up synthesis of nanocarbon materials by Kubo *et al*.,[53,54] Yamada *et al.*[55] and Amsharov *et al*.[56] However, most of these structures have only been determined by mass spectrometry (MS) and/or NMR measurements. There are no reports in which the geometrical features of oligo(9,10-anthrylene)s with more than three anthrylene units have been determined by X-ray analyses. A much longer analogue was reported, though its NMR spectrum is rather broad and its identity was just confirmed only by field desorption (FD) MS.[42] Besides, while oligophenylenes and oligonaphthylenes without substituents on the π-skeletons are soluble enough to be isolated and were investigated in detail, the introduction of multiple substituents on the anthrylene skeletons is required to make the previously reported oligo(9,10-anthrylene)s soluble, so that the effects of attached substituents must always be taken into account when considering the properties of longer derivatives. Therefore, there have been no studies on the redox behavior of oligo(9,10-anthrylene)s, especially for longer derivatives of $m > 4$, without substituents on the anthrylenes. It is still challenging to evaluate the relationship between the number of anthrylene units and the redox behavior of oligoanthrylenes. For this purpose, a new concept is necessary for the molecular design of oligo(9,10-anthrylene)s, which would enable detailed spectroscopic and voltammetric analyses for elongated analogues (e.g., m = 6) by providing high solubility as well as crystallographic analyses by providing high crystallinity.

In this study, a series of dications $\mathbf{1}^{2+}$, $\mathbf{2}^{2+}$, $\mathbf{3}^{2+}$, $\mathbf{4}^{2+}$, $\mathbf{5}^{2+}$, and $\mathbf{6}^{2+}$ with non-substituted oligo(9,10-anthrylene) backbone(s) (n = 1-6) were designed by end-capping with a dibenzotropylium skeleton at each end of the molecules, which is a stable and planar cation unit (Scheme 4-1). These compounds are expected to be easily handled in solution despite their huge size (molecular formula: $C_{130}H_{100}$, molecular weight of $\mathbf{6}^{2+}$: 1660.78 excepting anions) since aggregation and/or precipitation would be suppressed due to the electrostatic repulsion between charged moieties. These dications would adopt an orthogonally twisted structure between all 14π-aromatic units, which would also increase solubility in common organic solvents. A change of counter anions would enable easy modification of the solubility of dicationic salts. Thus, the author envisaged

that the electronic properties of non-substituted oligo(9,10-anthrylene)s could be readily clarified by spectroscopic measures in solution. Although the cationic moieties at both ends act as electron-withdrawing groups, their effects on the electronic structure of the oligo(9,10-anthrylene)s would be minimized (e.g., only Coulombic effects) due to the orthogonal geometry. Thus, the relationship between the electron-donating properties of oligo(9,10-anthrylene)s and the number of anthrylene units could be elucidated in detail, thanks to the number-dependent localization of HOMO on certain anthrylene units. Another concern is the conversion of oligo(9,10-anthrylene)s into oligo(9,10-anthraquinodimethane)s. Thus, upon reduction, due to the unique rigidity of the seven-membered carbon ring, a dibenzotropylium moiety would be transformed into a planar dibenzocycloheptatrienyl radical or a folded dibenzocycloheptatrienylidene structure. Accordingly, the neutral species generated upon two-electron (2e) reduction of $\mathbf{1}^{2+}$-$\mathbf{6}^{2+}$ would be an anthrylene-based bis(dibenzocycloheptatrienyl) biradical as an open-shell species while maintaining the orthogonally twisted structure as in the original dications. However, they would, if possibly, be isomerized into oligo(anthraquinodimethane)-based bis(dibenzoheptafulvene) as closed-shell species, in which all of the anthracene units adopt a folded structure. By tuning the number of anthrylene unit(s) between two dibenzotropyliums, the preference of one isomeric structure over the other could be controlled with a drastic change in their properties.

Scheme 4-1. Target dications $\mathbf{1}^{2+}$, $\mathbf{2}^{2+}$, $\mathbf{3}^{2+}$, $\mathbf{4}^{2+}$, $\mathbf{5}^{2+}$, and $\mathbf{6}^{2+}$ and their redox behavior.

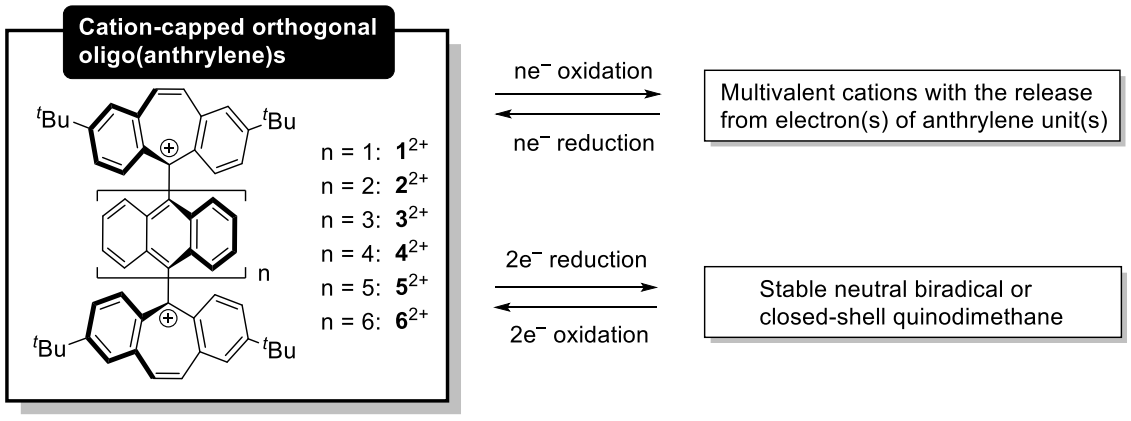

Herein, the author reveals that an oligo(9,10-anthrylene) scaffold with dibenzotropyliums is one of the best strategies for examining the potential functions and tunability of structures and properties based on the orthogonally twisted structure with multiple π-conjugated carbon backbones. In particular, this "cation-capped orthogonal approach" in linearly connected oligomers would enable the observation of potentially unstable electronic states such as multi-cationic and/or open-shell states that are short-lived without adopting this strategy (Figure 4-3). Therefore, this approach, which allows to isolate a family of compounds with a non-substituted oligo(9,10-anthrylene) and to elucidate their structures and properties, represents an important tool for the future design and development of unique molecules with an extended π-conjugated backbone.

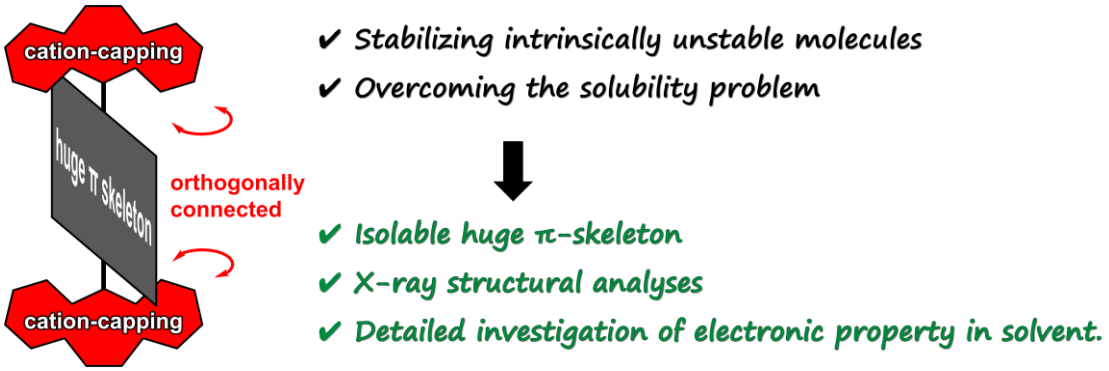

Figure 4-3. Design concept, "cation-capped orthogonal approach".

4-2. Results and Discussion

4-2-1. Preparation of dications $1^{2+}(BF_4^-)_2$-$6^{2+}(BF_4^-)_2$

At first, to prepare target dications, ketone **13**, one of the key building blocks, was newly synthesized from 1-bromo-4-(*tert*-butyl)-2-methylbenzene **7**[57] (Scheme 4-2). Extended ketone **16** was obtained by the Barton-Kellogg reaction of thioketone **14**, which was prepared from **13**, and 10-diazoanthracen-9(10*H*)-one followed by the treatment of PBu_3.[58] Further extended ketone **19**, the structure of which is shown in Figure 4-4, was synthesized in a similar manner from ketone **16**.

Next, six kinds of dication salts with odd and even numbers of anthrylene units were synthesized from 9,10-dibromoanthracene and 10,10'-dibromo-9,9'-bianthracene, respectively (Scheme 4-3). Diol precursors **1-OH**, **2-OH**, **3-OH**, **4-OH**, **5-OH** and **6-OH** were prepared by dilithiation of the dibromides followed by addition of the corresponding ketones **13**, **16** and **19** for **1-OH** and **2-OH**, **3-OH** and **4-OH**, and **5-OH** and **6-OH**, respectively. In contrast to **1-OH** and **2-OH** synthesized as single diastereomers, **3-OH**, **4-OH**, **5-OH** and **6-OH** were obtained as mixtures of diastereomers, each of which was identified to be one of the diastereomers by FD-MS. Upon treatment of these diols with tetrafluoroboric acid in the presence of trifluoroacetic anhydride (TFAA), BF_4^- salts of the desired dications were cleanly isolated as red powders in high yield for all derivatives, even when mixtures of multiple diastereomers were used as in the cases of **3-OH**–**6-OH**. These dications salts $\mathbf{1}^{2+}(BF_4^-)_2$-$\mathbf{6}^{2+}(BF_4^-)_2$ were fully characterized by ^{1}H NMR and ^{13}C NMR spectroscopy, FD-MS or ESI-MS, and single-crystal X-ray structure analyses (*vide infra*). They are stable enough to be easily handled under air at ambient temperature in both the solid state and solution. This is the first example of the synthesis of a family of compounds with one to six non-substituted oligoanthrylene units that could be isolated as stable entities.

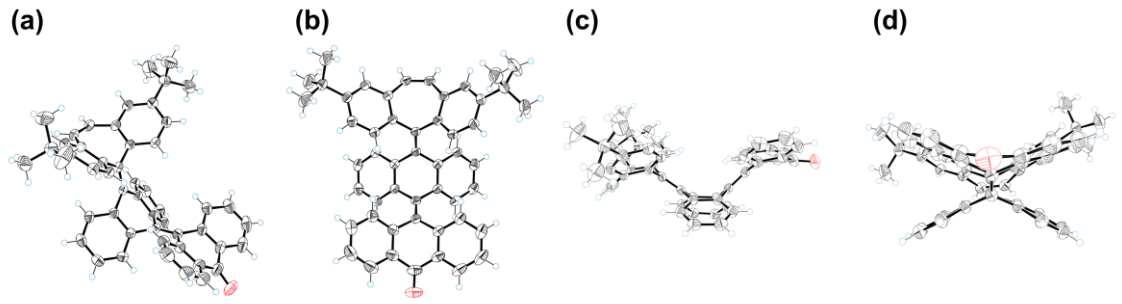

Figure 4-4. ORTEP drawings of **19**: (a) best view, (b) front view, (c) side view and (d) top view. Solvent molecule is omitted for clarity. Thermal ellipsoids are shown at the 50% probability level.

Scheme 4-2. Preparation of key building blocks, ketones **13**, **16** and **19**.

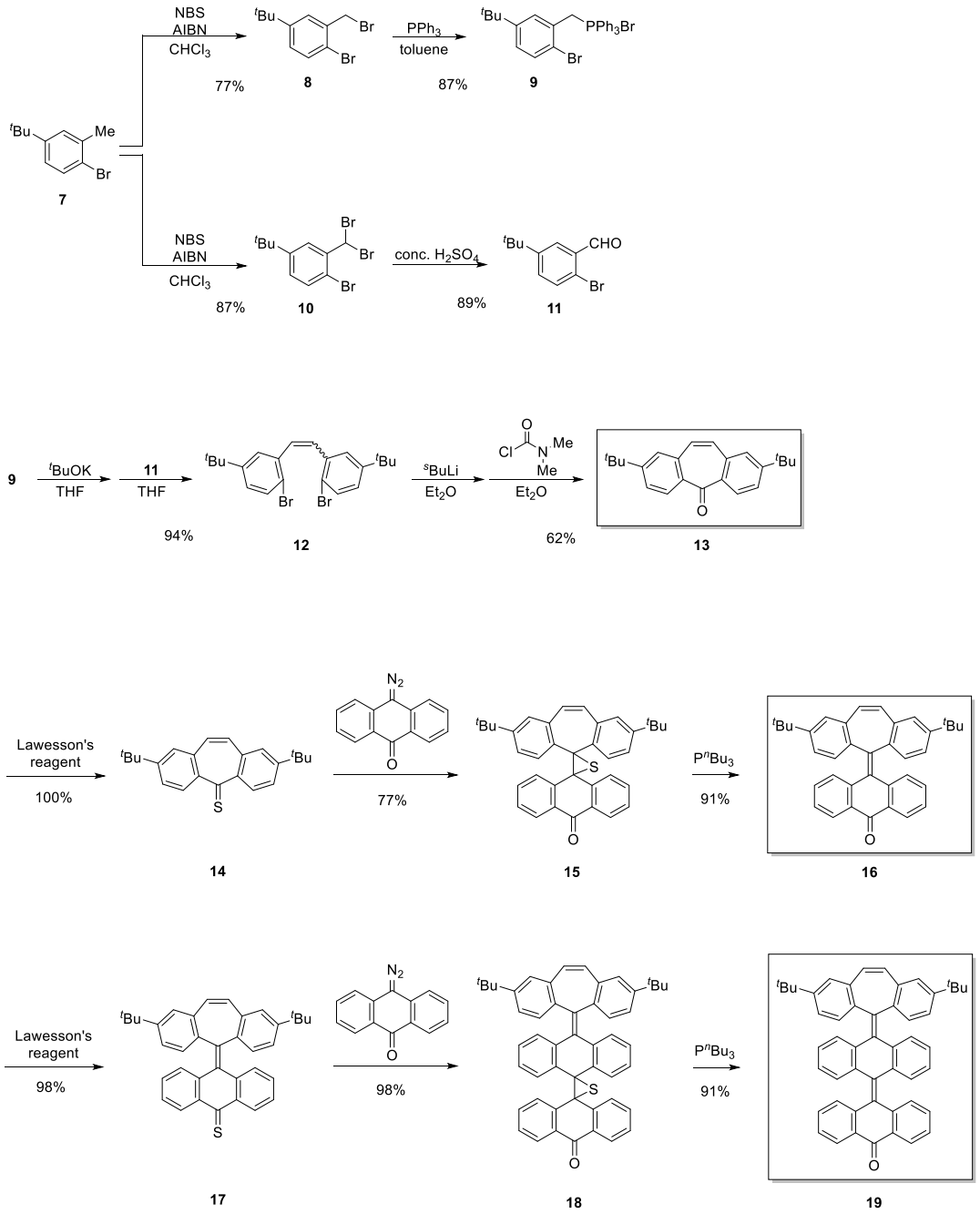

Scheme 4-3. Preparation of dications $\mathbf{1}^{2+}(BF_4^-)_2$ - $\mathbf{6}^{2+}(BF_4^-)_2$.

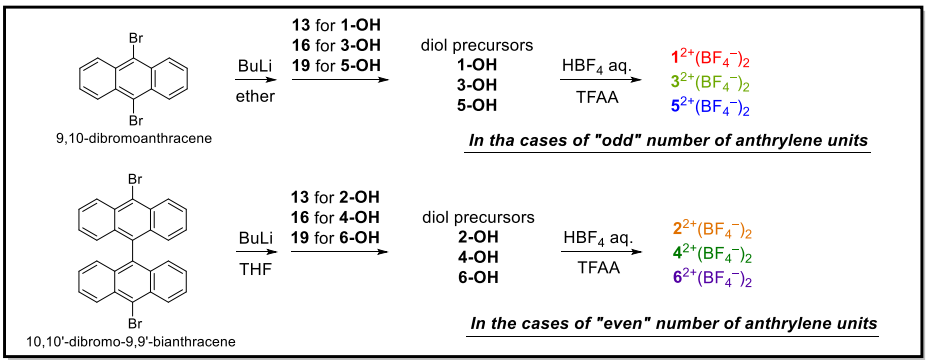

diol precursors	dication salts with odd number of anthrylene units
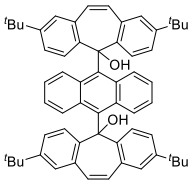 **1-OH**, 43%	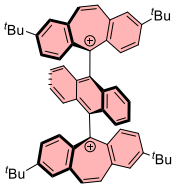 $\mathbf{1}^{2+}(BF_4^-)_2$, 93%
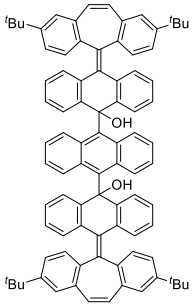 **3-OH**, 41%	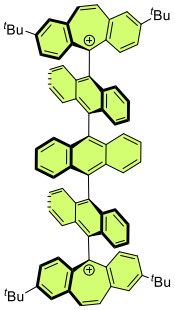 $\mathbf{3}^{2+}(BF_4^-)_2$, 100%
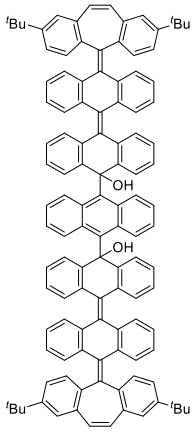 **5-OH**, 45%	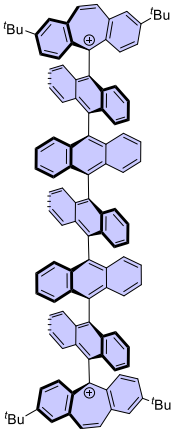 $\mathbf{5}^{2+}(BF_4^-)_2$, 100%

diol precursors	dication salts with even number of anthrylene units
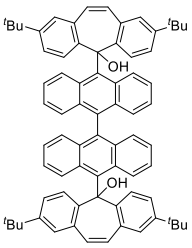 **2-OH**, 49%	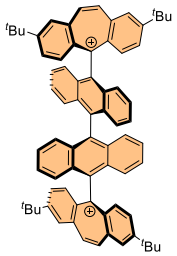 $\mathbf{2}^{2+}(BF_4^-)_2$, 100%
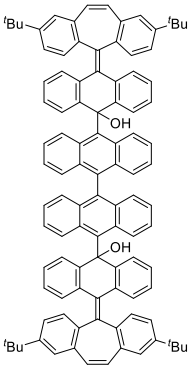 **4-OH**, 37%	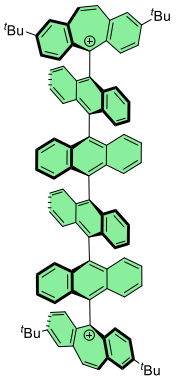 $\mathbf{4}^{2+}(BF_4^-)_2$, 100%
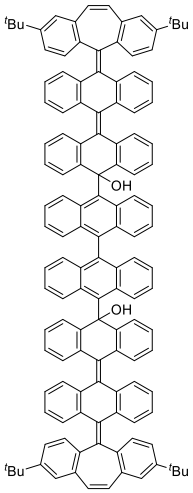 **6-OH**, 58%	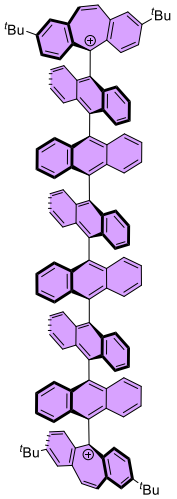 $\mathbf{6}^{2+}(BF_4^-)_2$, 100%

4-2-2. Single-crystal X-ray structure analyses of dications

The structures of dications $\mathbf{1}^{2+}$, $\mathbf{2}^{2+}$, $\mathbf{3}^{2+}$, $\mathbf{4}^{2+}$, and $\mathbf{6}^{2+}$ were successfully determined by single-crystal X-ray structure analyses, for which single crystals of $\mathbf{1}^{2+}$, $\mathbf{3}^{2+}$, and $\mathbf{4}^{2+}$ were obtained as BF_4^- salts. Dications $\mathbf{2}^{2+}$ and $\mathbf{6}^{2+}$ were prepared by using PF_6^- and bis(trifluoromethanesulfonyl)imide (NTf_2^-) as counter anions, respectively, to achieve better crystallinity (Figure 4-5). Previous studies were limited only to determining the X-ray structures of bianthracene (m = 2)[31–33,35–39] and teranthracene derivatives (m = 3),[43,50–52,55] the latter of which have multiple substituents on the anthrylene units. In contrast, the molecular design in this study actually allowed to determine the X-ray structures of the longer oligoanthrylene series of $\mathbf{3}^{2+}$, $\mathbf{4}^{2+}$, and $\mathbf{6}^{2+}$ with an orthogonally twisted geometry of five to eight 14π-electron units connected in a linear manner, where the number of anthrylene units (three to six) is significantly greater than that previously reported. These results demonstrated that the "cation-capped orthogonal approach" offers a significant benefit for obtaining the structure of a huge carbon skeleton such as oligoanthrylene, which would serve as a valuable strategy for studying novel π-conjugated carbon frameworks.

Based on the results of X-ray analyses, the dihedral angles between adjacent 14π-electron units were determined based on the mean planes defined by the 14 (anthrylene) or 15 (dibenzotropylium) carbon atoms that compose each aromatic unit (Table 4-1). The author confirmed that all dications adopt an almost orthogonally twisted structure for each pair of 14π-aromatic units in the crystal of their salts, which is in good agreement with the optimized structures obtained by density functional theory (DFT) calculations at the CAM-B3LYP/6-31G(d) level, which gave all the dihedral angles of 90.0 ° for all of the dications (Figure 4-26 in p 106). The maximum deviation of the dihedral angles from the calculated value is only 11.77(3) ° in $\mathbf{2}^{2+}$, indicating that the orthogonality between neighboring units is highly retained. Thus, the molecules of $\mathbf{1}^{2+}$, $\mathbf{2}^{2+}$, $\mathbf{3}^{2+}$, $\mathbf{4}^{2+}$, and $\mathbf{6}^{2+}$ are less perturbed by the crystal packing force. This is because no obvious intermolecular interactions between anthrylene units are observed in the crystals of these dication salts, due to the orthogonally twisted structures (closest distance between carbon atoms > 3.4 Å). Furthermore, the bulky ^{t}Bu groups effectively suppress intermolecular π-π stacking and C-H···π contacts between the dibenzotropylium units at both ends. The scarcity of intermolecular interactions is the key for a high enough solubility of these dications to perform various measurements for a series of oligoanthrylenes composed of rigid and planar anthrylene units without any substituents.

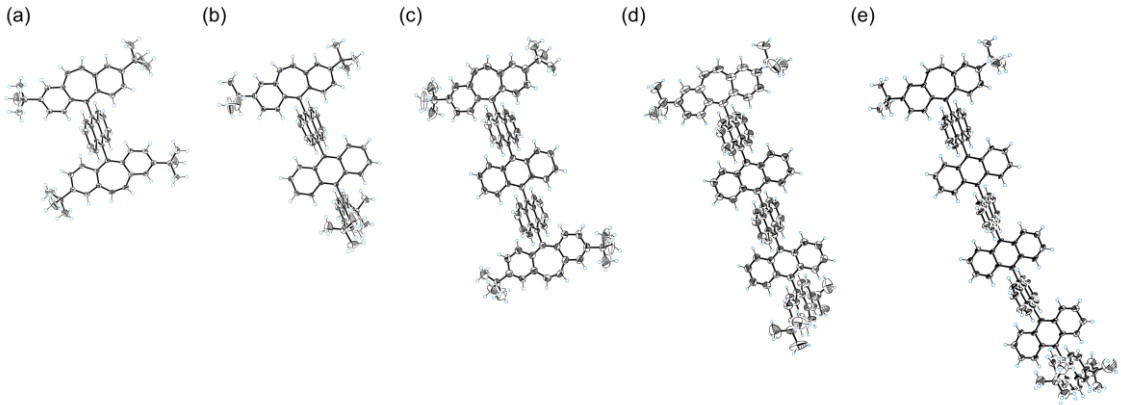

Figure 4-5. ORTEP drawings of (a) $\mathbf{1}^{2+}(BF_4^-)_2$, (b) $\mathbf{2}^{2+}(PF_6^-)_2$, (c) $\mathbf{3}^{2+}(BF_4^-)_2$, (d) $\mathbf{4}^{2+}(BF_4^-)_2$, and (e) $\mathbf{6}^{2+}(NTf_2^-)_2$. The counterions and solvent molecules are omitted for clarity. Thermal ellipsoids are shown at the 50% probability level for (a), (b), (c), and (e), and the 30% probability level for (d).

Table 4-1. The dihedral angles between adjacent 14π-electron units determined by X-ray analyses based on the mean planes defined by the 14 (anthrylene) or 15 (dibenzotropylium) carbon atoms that compose each aromatic unit.

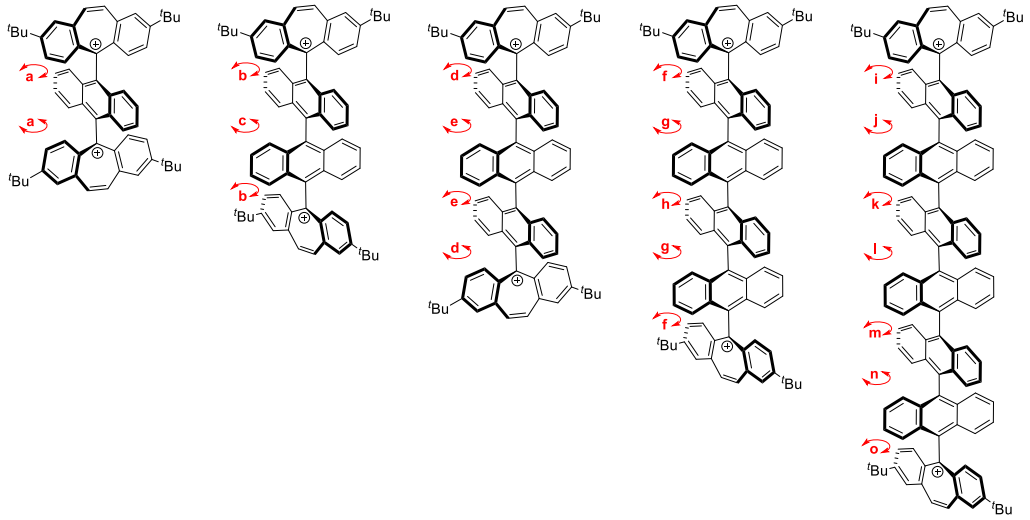

$\mathbf{1}^{2+}(BF_4^-)_2$	$\mathbf{2}^{2+}(PF_6^-)_2$		$\mathbf{3}^{2+}(BF_4^-)_2$		$\mathbf{4}^{2+}(BF_4^-)_2$		
a	b	c	d	e	f	g	h
83.89(3)°	81.04(2)°	78.23(3)°	88.52(5)°	88.63(5)°	89.20(5)°	88.51(5)°	90°

$\mathbf{6}^{2+}(NTf_2^-)_2$						
i	j	k	l	m	n	o
89.91(4)°	89.95(4)°	84.59(4)°	82.79(4)°	83.75(5)°	82.85(5)°	89.45(5)°

4-2-3. UV-Vis-NIR absorption properties of dications

Since anthrylene unit(s) as well as the terminal dibenzotropylium units are almost orthogonally connected to each other in the crystals of $\mathbf{1}^{2+}$-$\mathbf{6}^{2+}$, each anthrylene unit can be considered to be electronically independent due to a negligible overlap of their p orbitals between neighboring units. To gain insight into whether or not the oligo(9,10-anthrylene)-based dications would maintain this orthogonally twisted geometry even in solution, the author investigated the electronic properties of $\mathbf{1}^{2+}$-$\mathbf{6}^{2+}$ in solution. First, UV-Vis-NIR absorption spectra of BF_4^- salts of dications $\mathbf{1}^{2+}$-$\mathbf{6}^{2+}$ were measured in CH_3CN (Figure 4-6, Table 4-2). Characteristic absorption bands in the UV region show a nearly equally-spaced increase in molar absorption coefficient values with an increase in the number of anthrylene units, where a vibrational structure assigned to absorptions of the anthrylene skeleton was clearly observed (λ_{max} = 250-258 nm, 378-383 nm and 400-407 nm in CH_3CN). The absorption bands in the UV-Vis region that show hardly any change in molar absorption coefficients among the derivatives with different numbers of anthrylene units can be assigned to the absorptions of the dibenzotropylium skeleton (peak wavelength: 320-321 nm, 433-434 nm, 514-519 nm and 543-546 nm in CH_3CN) because all of the dications have the same two cationic chromophores. Since no change in the peak wavelengths of the main absorption bands was observed among dications $\mathbf{1}^{2+}(BF_4^-)_2$-$\mathbf{6}^{2+}(BF_4^-)_2$, there is no significant electronic interaction between anthrylene units even in solution.

On the other hand, quite weak absorption bands attributed to forbidden charge-transfer (CT) transitions from anthrylene unit(s) to dibenzotropyliums were observed in the NIR region. Time-dependent (TD) DFT calculations were conducted on all dications $\mathbf{1}^{2+}$-$\mathbf{6}^{2+}$ at the CAM-B3LYP/6-31G(d) level, which can predict the origin of the lowest-energy electronic transitions (pp 133-138, Figures 4-27, 4-28 and 4-29 in pp 130-132). According to TD-DFT calculations, these CT absorption bands are assigned to be electronic transitions from the anthrylene unit, which is placed next to the dibenzotropylium unit, to the dibenzotropylium. The molar absorption coefficients of these CT bands for $\mathbf{1}^{2+}$-$\mathbf{6}^{2+}$ were considerably smaller than those observed in other anthrylene-based derivatives with more flexible diarylmethylium moieties,[59] indicating that the orthogonally twisted structures in $\mathbf{1}^{2+}$-$\mathbf{6}^{2+}$ are robust to suppress the interaction between anthrylene unit(s) and terminal dibenzotropyliums.

These results showed that the orthogonally twisted structures of all 14π-conjugated units are highly preserved in solution thanks to the oligo(9,10-anthrylene) scaffold in combination with the end-capping with two rigid dibenzotropyliums, and thus electronic interaction between 14π-aromatic units is weak for all dications $\mathbf{1}^{2+}$-$\mathbf{6}^{2+}$, as designed.

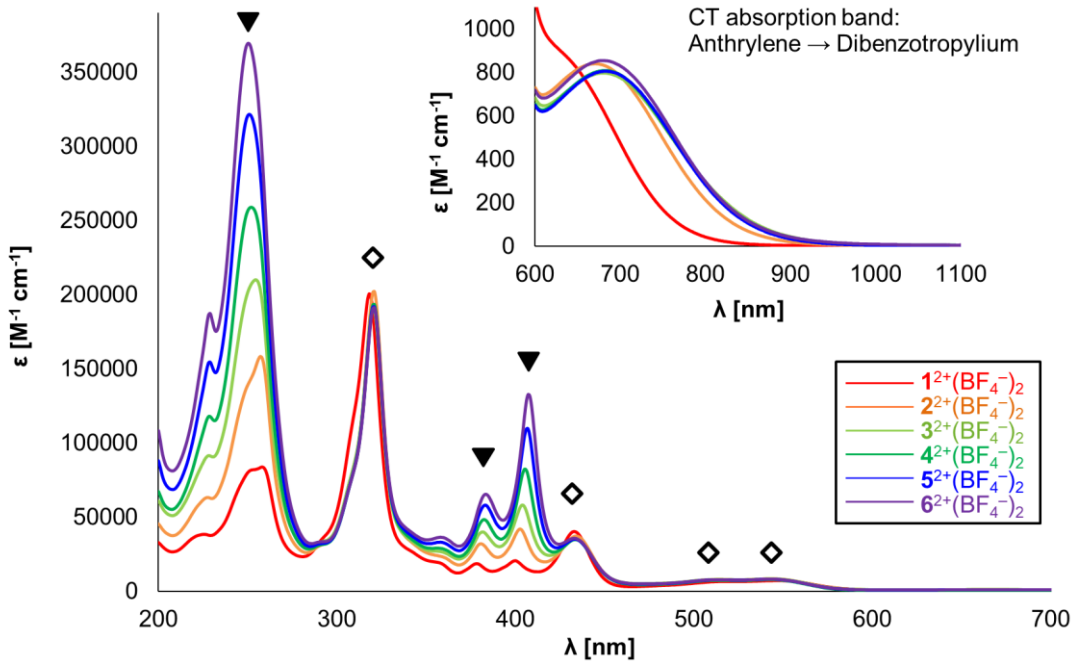

Figure 4-6. UV-Vis-NIR spectra of dications $\mathbf{1}^{2+}(BF_4^-)_2$, $\mathbf{2}^{2+}(BF_4^-)_2$, $\mathbf{3}^{2+}(BF_4^-)_2$, $\mathbf{4}^{2+}(BF_4^-)_2$, $\mathbf{5}^{2+}(BF_4^-)_2$, and $\mathbf{6}^{2+}(BF_4^-)_2$ in CH_3CN. Triangle and diamond-marked absorption peaks were mainly assigned to the absorptions of the anthrylene units and the dibenzotropylium skeleton, respectively.

Table 4-2. Maximum absorption wavelengths λ_{max} and molar absorption coefficients ε of dications $\mathbf{1}^{2+}(BF_4^-)_2$-$\mathbf{6}^{2+}(BF_4^-)_2$ in CH_3CN.

dications	λ_{max} [nm] (ε [M^{-1} cm^{-1}])								
$\mathbf{1}^{2+}(BF_4^-)_2$	646 (833)	546 (7460)	519 (6840)	433 (40500)	400 (20800)	378 (18800)	318 (201000)	258 (83900)	228 (38000)
$\mathbf{2}^{2+}(BF_4^-)_2$	670 (840)	544 (8080)	515 (7550)	434 (37200)	403 (41800)	381 (31900)	321 (202000)	257 (158000)	228 (63200)
$\mathbf{3}^{2+}(BF_4^-)_2$	680 (797)	543 (7880)	514 (7390)	434 (35000)	404 (58000)	382 (39900)	320 (192000)	254 (210000)	228 (91400)
$\mathbf{4}^{2+}(BF_4^-)_2$	682 (808)	543 (7960)	514 (7500)	434 (35000)	405 (83400)	382 (48500)	321 (193000)	252 (259000)	229 (118000)
$\mathbf{5}^{2+}(BF_4^-)_2$	682 (805)	543 (7590)	514 (7510)	433 (35000)	407 (110000)	383 (58000)	321 (192000)	251 (322000)	229 (154000)
$\mathbf{6}^{2+}(BF_4^-)_2$	679 (854)	543 (7940)	514 (7510)	433 (35600)	407 (132000)	383 (65200)	321 (191000)	250 (369000)	229 (187000)

4-2-4. Oxidation behavior of dications and formation of multivalent cations

Next, the author conducted voltammetric analyses of the BF_4^- salts of dications by differential pulse voltammetry (DPV) in CH_2Cl_2 (Figure 4-7a,b) to elucidate the electron-donating properties of oligo(9,10-anthrylene)s end-capped with two dibenzotropyliums (Figures 4-9 and 4-10). This should give insight into the oxidative properties of the oligo(9,10-anthrylene)s. These analyses revealed that each dication underwent stepwise oxidation in a reversible manner, where the maximum number of electron(s) released was in accordance with the number of orthogonally connected anthrylene units, resulting in the formation of multivalent cations.

The first oxidation wave, measured as a reversible process for all derivatives, shifted to a less positive potential with an increase in the number of anthrylene units [+1.80 V vs SCE for $\mathbf{1}^{2+}(BF_4^-)_2$, +1.65 V for $\mathbf{2}^{2+}(BF_4^-)_2$, +1.52 V for $\mathbf{3}^{2+}(BF_4^-)_2$, +1.48 V for $\mathbf{4}^{2+}(BF_4^-)_2$, +1.46 V for $\mathbf{5}^{2+}(BF_4^-)_2$, and +1.45 V for $\mathbf{6}^{2+}(BF_4^-)_2$], suggesting an increase in the HOMO level of dications $\mathbf{1}^{2+}$-$\mathbf{6}^{2+}$ in the order of the number of anthrylene units. To clarify this point, the distributions of HOMO for the dications were estimated by DFT calculations at the CAM-B3LYP/6-31G(d) level (Figures 4-27, 4-28 and 4-29 in pp 130-132). For $\mathbf{1}^{2+}$, $\mathbf{3}^{2+}$, and $\mathbf{5}^{2+}$, with an odd number of anthrylene unit(s), the HOMO was located on the anthrylene unit at the very center, which is furthest away from the two terminal dibenzotropylium units. For $\mathbf{2}^{2+}$, $\mathbf{4}^{2+}$, and $\mathbf{6}^{2+}$, with an even number of anthrylene units, the HOMO and HOMO-1 are degenerated, and both orbitals are distributed on the two central anthrylene units, which are apart from the dibenzotropylium units at both termini. Therefore, the first oxidation wave in the voltammogram can be accounted for by the release of an electron from the anthrylene unit(s) located in the center of the molecule. A linear correlation (R^2=0.9987) was observed when the values of the oxidation potential for these dications were plotted against the sum of $1/r^2$ where r is the distance between the center of gravity of the dibenzotropylium unit and the central anthrylene unit(s) in the optimized structures. As shown in Figure 4-8a, the value of the intercept (+1.42) indicates the oxidation potential for a compound with an infinite number of anthrylene units. This intercept is very close to the experimentally measured oxidation potential of the parent anthracene (+1.36 V), with a difference of only 0.06 V, demonstrating that the change in HOMO levels for anthrylene-based dications $\mathbf{1}^{2+}$-$\mathbf{6}^{2+}$ follows Coulomb's law.[60,61] Similar behavior was observed when the voltammetric analyses were conducted in more polar solvents such as CH_3CN or 1,1,1,3,3,3-hexafluoro-2-propanol (HFIP) (Figures 4-9a,b and 4-10). The differences between the value of the intercept and the oxidation potential of the parent anthracene (+1.17 V and +0.92 V) are only 0.05 V and 0.02 V, respectively, in CH_3CN and HFIP (Figure 4-8b,c). These results show that neither significant overlap of orbitals nor delocalization of electrons occur between the neighboring anthrylene units, which is in accord with the results of the UV-Vis-NIR absorption measurements (*vide supra*).

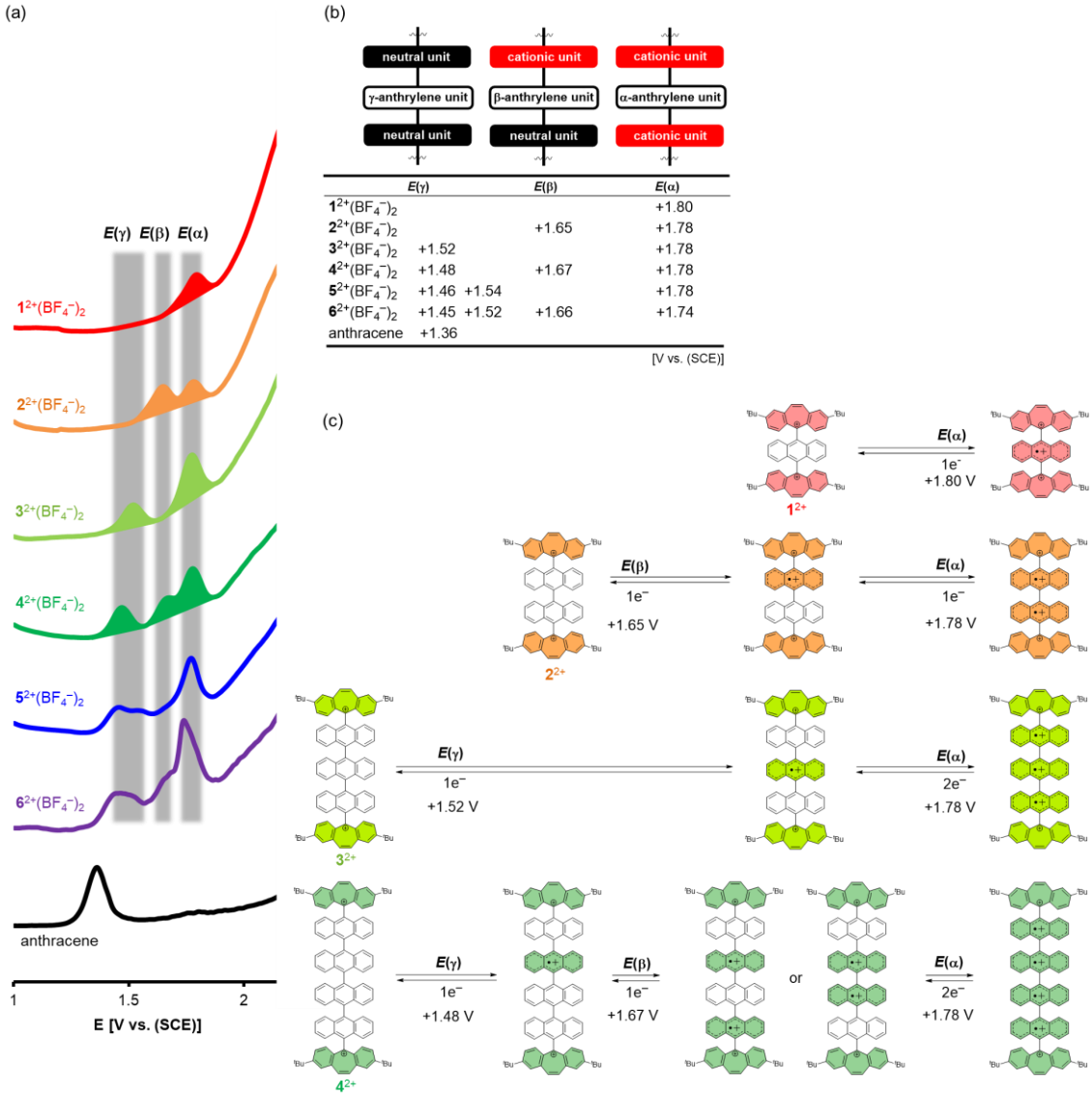

Figure 4-7. (a) Differential pulse voltammograms of dications $\mathbf{1}^{2+}(BF_4^-)_2$, $\mathbf{2}^{2+}(BF_4^-)_2$, $\mathbf{3}^{2+}(BF_4^-)_2$, $\mathbf{4}^{2+}(BF_4^-)_2$, $\mathbf{5}^{2+}(BF_4^-)_2$, $\mathbf{6}^{2+}(BF_4^-)_2$, and anthracene in 0.2 mM CH_2Cl_2 solution containing 0.1 M Bu_4NBF_4 as a supporting electrolyte (Pt electrode). (b) All oxidation potentials of dications assignable to the release of electrons from α-anthrylene unit, β-anthrylene unit or γ-anthrylene unit. (c) Schematic diagram of stepwise oxidation process of dications $\mathbf{1}^{2+}(BF_4^-)_2$ - $\mathbf{4}^{2+}(BF_4^-)_2$. Cationic units were colored in the scheme.

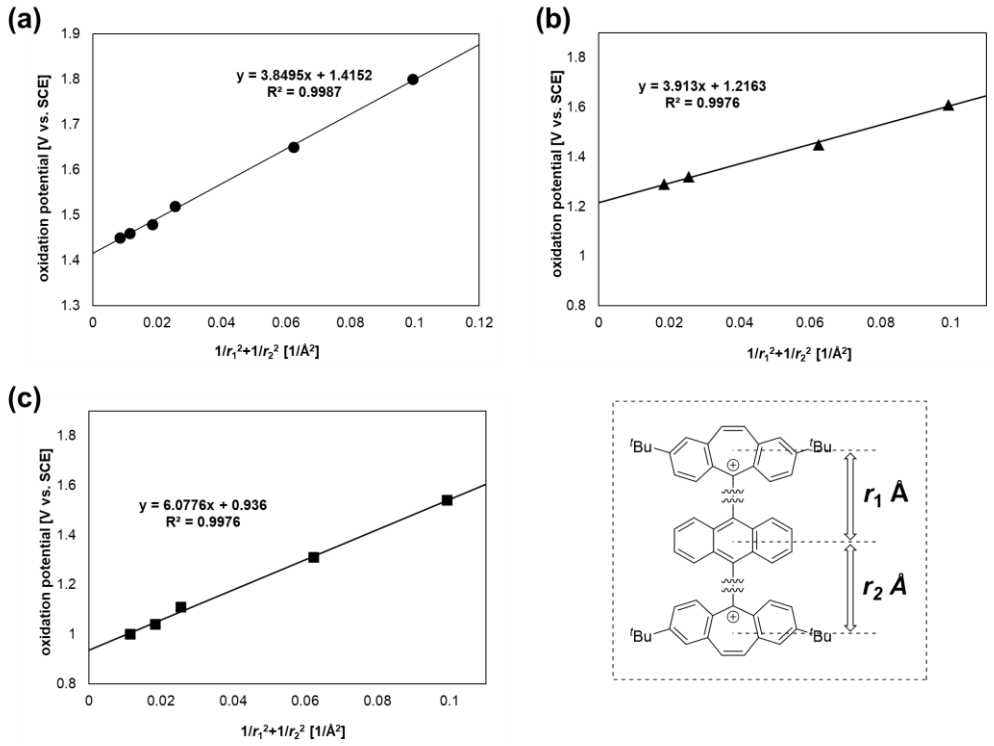

Figure 4-8. The plot of the oxidation potential for dications (a) $\mathbf{1}^{2+}(BF_4^-)_2$-$\mathbf{6}^{2+}(BF_4^-)_2$ in CH_2Cl_2, (b) $\mathbf{1}^{2+}(BF_4^-)_2$-$\mathbf{4}^{2+}(BF_4^-)_2$ in CH_3CN and (c) $\mathbf{1}^{2+}(BF_4^-)_2$-$\mathbf{5}^{2+}(BF_4^-)_2$ in HFIP against the sum of $1/r^2$ where r is the distance between the center of gravity of the dibenzotropylium unit and the central anthrylene unit(s) in the optimized structures.

Furthermore, if the orthogonally twisted structures are preserved even after the one-electron oxidation of dications, Coulombic considerations can also be applied to further oxidation processes during the formation of higher multivalent cations. Focusing on the relationship between the oxidation potentials and the anthrylene units involved in the next oxidation, the anthrylene unit undergoing the next oxidation can be classified into three types by considering the charge state of the adjacent tricyclic units: (α) anthrylene between two cationic units, (β) anthrylene between cationic and neutral units, and (γ) anthrylene between two neutral units (Figure 4-7b). Based on the Coulombic effects for the three anthrylene units of (α), (β), or (γ) from the adjacent units, the oxidation potential should be more positive in the order $E(\alpha) > E(\beta) > E(\gamma)$. In fact, in terms of the observed values of the first oxidation wave for $\mathbf{1}^{2+}(BF_4^-)_2$-$\mathbf{6}^{2+}(BF_4^-)_2$, the first oxidation process of $\mathbf{1}^{2+}(BF_4^-)_2$ [$E(\alpha)$ = +1.80 V], $\mathbf{2}^{2+}(BF_4^-)_2$ [$E(\beta)$ = +1.65 V] and $\mathbf{3}^{2+}(BF_4^-)_2$ [$E(\gamma)$ = +1.52 V] can be explained in terms of the oxidation of α, β and γ-anthrylene units, respectively (Figure 4-7b,c). The fact that the first oxidation of $\mathbf{3}^{2+}(BF_4^-)_2$-$\mathbf{6}^{2+}(BF_4^-)_2$ occurs at almost the same potential region (+1.52 - +1.45 V) due to the oxidation of γ-anthrylene units also indicates that the above three classifications are reasonable.

In this way, the oxidation potentials after the first oxidation wave can be estimated just by considering the position of an anthrylene unit that would be involved in the next oxidation while considering that an α, β, or γ-anthrylene unit is oxidized at its unique potential region [E(α) = +1.74 - +1.80 V, E(β) = +1.65 - +1.67 V, and E(γ) = +1.45 - +1.52 V] (Figure 4-7c). In fact, the second oxidation wave of $\mathbf{2}^{2+}(BF_4^-)_2$ and $\mathbf{3}^{2+}(BF_4^-)_2$ appeared at almost the same potential because the second wave in each corresponds to the oxidation of the α-anthrylene unit, while that of $\mathbf{4}^{2+}(BF_4^-)_2$ appeared at a less positive region corresponding to oxidation of the β-anthrylene unit. The third oxidation wave of $\mathbf{4}^{2+}(BF_4^-)_2$ was observed at a potential similar to the second one of $\mathbf{2}^{2+}(BF_4^-)_2$ and $\mathbf{3}^{2+}(BF_4^-)_2$ due to involvement of an α-anthrylene unit in these oxidation processes. This explanation allows to understand the subsequent oxidative behavior after the first oxidation of longer dications $\mathbf{5}^{2+}(BF_4^-)_2$ and $\mathbf{6}^{2+}(BF_4^-)_2$. These results indicated that the orthogonally twisted structure is preserved in multivalent cations as well as in dications. The author have found a previously unreported simple and straightforward rule for orthogonally connected oligo(9,10-anthrylene)s, which is based solely on Coulombic considerations.

In terms of the number of electrons released upon oxidation with the formation of multivalent cations, the second oxidation wave of $\mathbf{3}^{2+}(BF_4^-)_2$ and the third oxidation wave of $\mathbf{4}^{2+}(BF_4^-)_2$ exhibited a larger peak area than others (Figure 4-7a). Thus, these oxidation processes should correspond to a one-wave 2e-oxidation. Due to the similar one-wave multi-electron-oxidation process, some oxidation peaks get broad in $\mathbf{5}^{2+}(BF_4^-)_2$ and $\mathbf{6}^{2+}(BF_4^-)_2$. Still, it is highly likely that $\mathbf{5}^{2+}$and $\mathbf{6}^{2+}$ are oxidized up to $\mathbf{5}^{7+}$ and $\mathbf{6}^{8+}$ based on the systematic voltammetric analyses of $\mathbf{1}^{2+}$-$\mathbf{6}^{2+}$. Therefore, all anthrylene units were oxidized in CH_2Cl_2 in all of the derivatives with an increase in the oxidation number by n at most. In addition, almost the same behavior was observed in polar CH_3CN (Figure 4-9c). Furthermore, voltammetric analyses revealed that all of the oxidation processes are reversible. No further oxidation wave was observed while the potential was swept up to 2.5 V beyond the E(α) region.

Particularly noteworthy is the finding that the reversible formation of multivalent cations can be observed by end-capping with dibenzotropylium units, because many papers to date have reported that condensation reactions easily proceeded on anthrylene skeletons upon oxidation of bianthracenes or higher analogues.[38,43,51–56,62,63] This work is the first to demonstrate the relationship between the number of π units and their redox behaviors for a series of linearly connected π-compounds. This study demonstrated that multivalent cations can be effectively stabilized by the sophisticated use of orthogonally twisted structures between tricyclic units under a “cation-capped orthogonal approach”.

(a)

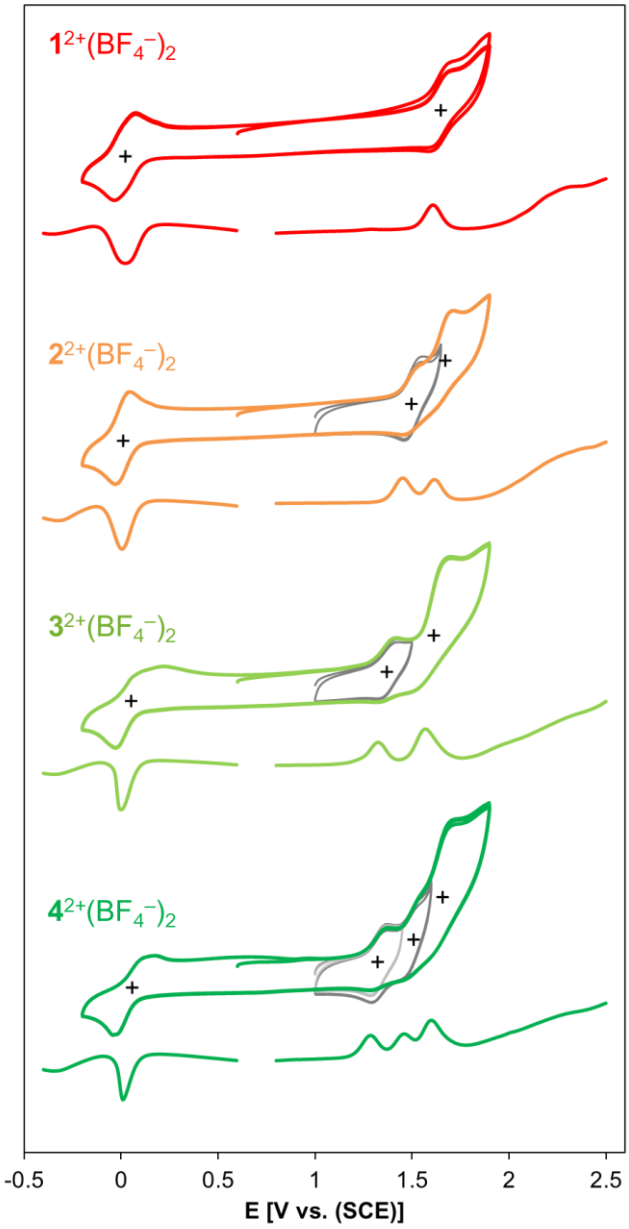

(b)

	E^{red}	$E(\gamma)$	$E(\beta)$	$E(\alpha)$
$1^{2+}(BF_4^-)_2$	+0.02			+1.61
$2^{2+}(BF_4^-)_2$	+0.00		+1.45	+1.62
$3^{2+}(BF_4^-)_2$	+0.00	+1.32		+1.57
$4^{2+}(BF_4^-)_2$	+0.01	+1.29	+1.46	+1.60
Anthracene		+1.17		

[V vs. (SCE)]

(c)

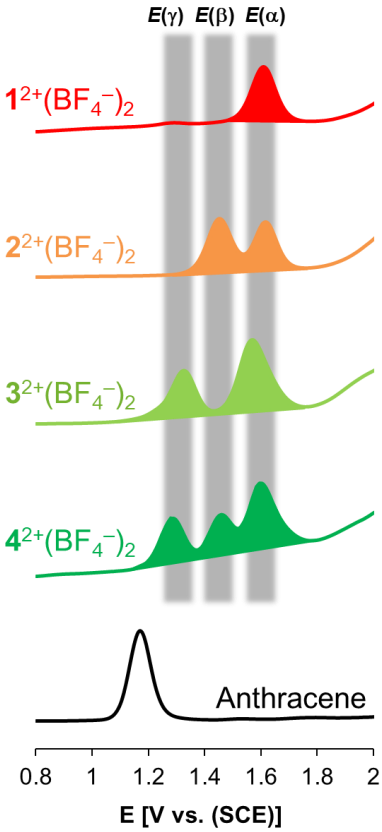

Figure 4-9. (a) Cyclic voltammograms (scan rate 100 mVs^{-1}) and differential pulse voltammograms of dications $\mathbf{1}^{2+}(BF_4^-)_2$-$\mathbf{4}^{2+}(BF_4^-)_2$ (1.0 mM) in CH_3CN containing 0.1 M Et_4NClO_4 as a supporting electrolyte (Pt electrode) and (b) their redox potentials. (c) The oxidation potentials are classified into three types by considering the charge state of the adjacent tricyclic units.

(a)

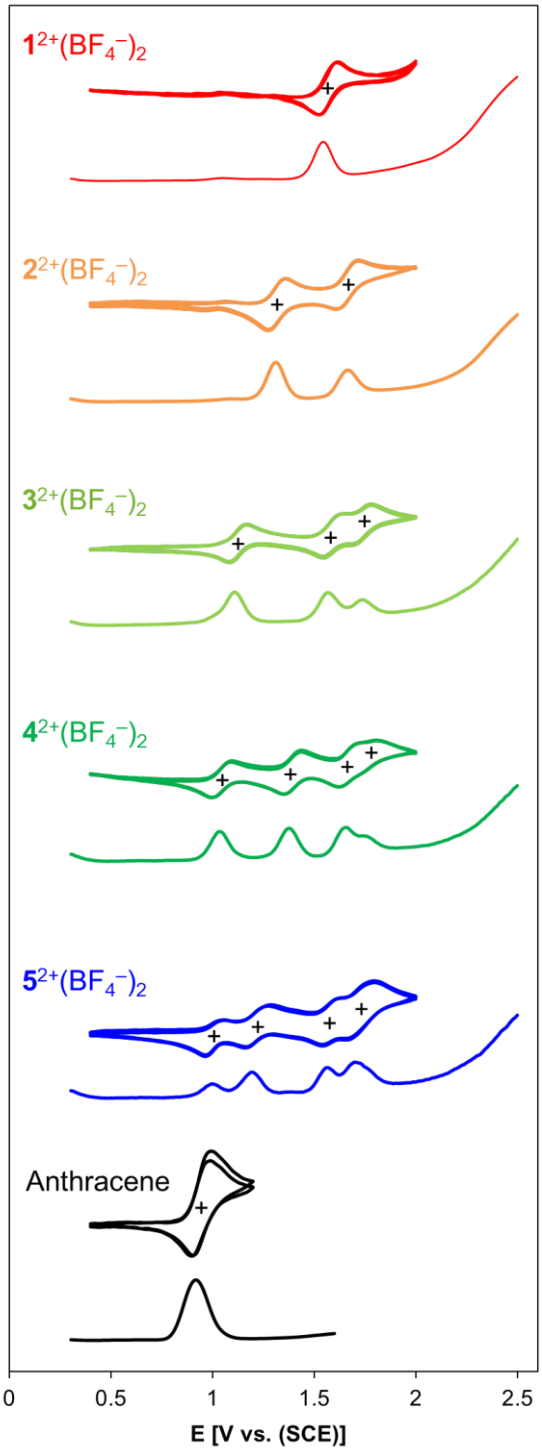

(b)

	E(γ)		*E*(β)	*E*(α)	
$1^{2+}(BF_4^-)_2$				+1.54	
$2^{2+}(BF_4^-)_2$			+1.31	+1.67	
$3^{2+}(BF_4^-)_2$	+1.11			+1.57	+1.74
$4^{2+}(BF_4^-)_2$	+1.04		+1.38	+1.66	+1.74
$5^{2+}(BF_4^-)_2$	+1.00	+1.19		+1.56	+1.70
Anthracene	+0.92				

[V vs. (SCE)]

Figure 4-10. (a) Cyclic voltammograms (scan rate 100 mVs^{-1}) and differential pulse voltammograms of dications $\mathbf{1}^{2+}(BF_4^-)_2$-$\mathbf{5}^{2+}(BF_4^-)_2$ (1.0 mM) and anthracene (1.0 mM) in HFIP containing 0.1 M Bu_4NBF_4 as a supporting electrolyte (Pt electrode) and (b) their redox potentials. Backgrounds were subtracted for all cyclic voltammograms.

4-2-5. Reduction behavior of dications and formation of two types of neutral species

The author next investigated the reduction behavior of dications $\mathbf{1}^{2+}$ - $\mathbf{6}^{2+}$ to gain insight into the structure of 2e-reduced species. Based on the unique rigidity of the seven-membered carbon ring, the dibenzotropylium moiety can be reduced to give planar dibenzocycloheptatrienyl radical or a butterfly-shaped dibenzocycloheptatrienylidene structure as an open-shell or closed-shell species, respectively. Accordingly, 2e-reduction of $\mathbf{1}^{2+}$ - $\mathbf{6}^{2+}$ with two dibenzotropylium moieties would produce an open-shell twisted (**T**) or closed-shell folded (**F**) form with anthrylene(s) or anthraquinodimethane(s) in the center of the molecules. To estimate which form is the most thermodynamically stable structure as a reduced product from $\mathbf{1}^{2+}$ - $\mathbf{6}^{2+}$, the author performed DFT calculations at the (U)B3LYP/6-31G(d) level (Figures 4-30 to 4-37 in pp 139-146). Although there are many isomers for the **F**-form by adopting either *anti*- or *syn*-type configurations, since closed-shell **1**-**6** have two or more overcrowded alkene units, only the most favorable all-*anti*-type folded forms among the configurational isomers were chosen to be calculated. As can be seen from the relative energies of the **F**- and **T**-forms, the **F**-form was predicted to be more stable than the **T**-form for **1** and **2** with one and two anthrylene units, respectively, while the **T**-form was estimated to be more stable than the **F**-form for **3**-**6** with three to six anthrylene units (Table 4-3). For **2** and **3**, both forms would be observed by considering the small energy difference, and thus the author sought to clarify the structures of the corresponding reduced species.

The reduction behavior of the dications was first investigated by voltammetric analyses in CH_2Cl_2 (Figure 4-11a). Reversible 2e-reduction waves were observed in the range +0.09 - +0.18 V (vs. SCE) for all BF_4^- salts of dications. These results indicate that the perpendicular geometries of not only $\mathbf{3}^{2+}$-$\mathbf{6}^{2+}$, but also $\mathbf{1}^{2+}$ and $\mathbf{2}^{2+}$ do not change under the measurement conditions. Thus, **1T** and **2T** with a twisted geometry similar to the structure of dications should be kinetically produced with a longer lifetime than a few seconds at least.

To clarify the properties and identities of 2e-reduced species, a series of electrochemical reductions were conducted for $\mathbf{3}^{2+}(BF_4^-)_2$, $\mathbf{4}^{2+}(BF_4^-)_2$, $\mathbf{5}^{2+}(BF_4^-)_2$ and $\mathbf{6}^{2+}(BF_4^-)_2$ in CH_3CN, and the results were monitored by UV-Vis spectroscopy (Figure 4-11d,e,f,g). According to the calculation, the 2e-reduced state for each compound prefers to adopt the **T**-form rather than the **F**-form. For $\mathbf{3}^{2+}(BF_4^-)_2$ and $\mathbf{4}^{2+}(BF_4^-)_2$, only the absorptions that originated from the dibenzotropylium skeletons disappeared upon electrochemical reduction and clean conversion was observed with isosbestic points (Figure 4-11d,e). In addition, the vibrational structure in the region of 350-410 nm assigned to the electronic transition of the anthrylene skeletons exhibited almost no change. These results indicated that the structures of the oligo(anthrylene)s in the molecules were maintained upon 2e-reduction, meaning that open-shell **3T** and **4T** with

orthogonally connected anthrylene units were certainly produced. For $\mathbf{5}^{2+}(BF_4^-)_2$ and $\mathbf{6}^{2+}(BF_4^-)_2$, similar behavior was observed upon electrochemical reduction, even though there was a sign that a reduced species was deposited on an electrode surface (Figure 4-11f,g).

Table 4-3. The relative energies of possible isomers for neutral species based on DFT calculations at the (U)B3LYP/6-31G(d) level (0 kcal/mol for open-shell triplet **T**-form). For **2F**-**6F**, the most favorable all-*anti*-type folded forms among the configurational isomers were chosen to be calculated.

	1T(triplet)	**1T(singlet)**	**1F$_{anti,anti}$**	**1F$_{syn,anti}$**
Δ*E* (kcal/mol)	0.00	0.00	-21.22	-16.34

	2T(triplet)	**2T(singlet)**	**2F**
Δ*E* (kcal/mol)	0.00	0.00	-8.72

	3T(triplet)	**3T(singlet)**	**3F**
Δ*E* (kcal/mol)	0.00	0.00	3.93

	4T(triplet)	**4T(singlet)**	**4F**
Δ*E* (kcal/mol)	0.00	0.00	16.63

	5T(triplet)	**5T(singlet)**	**5F**
Δ*E* (kcal/mol)	0.00	0.00	29.29

	6T(triplet)	**6T(singlet)**	**6F**
Δ*E* (kcal/mol)	0.00	0.00	42.02

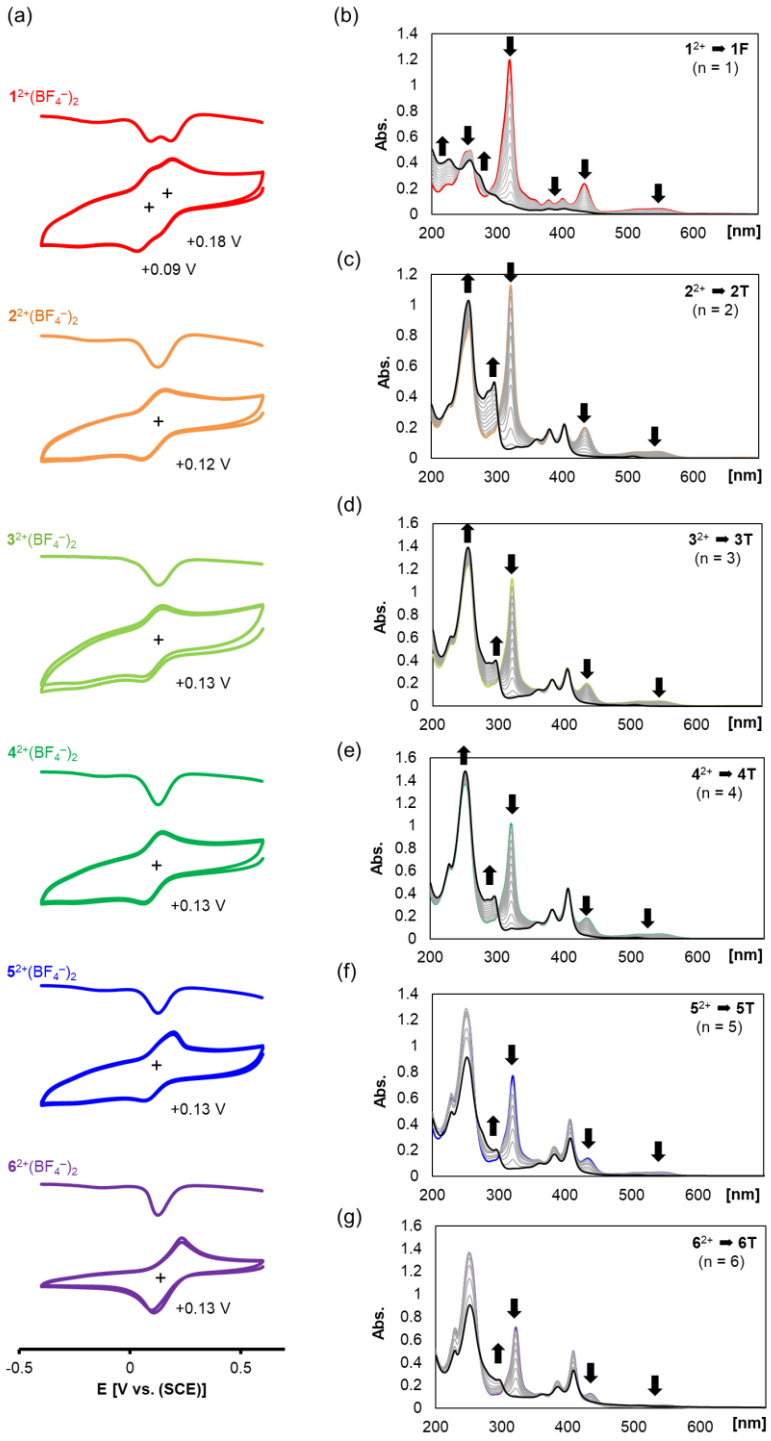

Figure 4-11. (a) Cyclic voltammograms (scan rate 100 mVs^{-1}) and differential pulse voltammograms of 0.2 mM solution of dications $\mathbf{1}^{2+}(BF_4^-)_2$, $\mathbf{2}^{2+}(BF_4^-)_2$, $\mathbf{3}^{2+}(BF_4^-)_2$, $\mathbf{4}^{2+}(BF_4^-)_2$, $\mathbf{5}^{2+}(BF_4^-)_2$, and $\mathbf{6}^{2+}(BF_4^-)_2$ in CH_2Cl_2. (b-g) Changes in UV-Vis spectra upon electrochemical reduction (20 µA) of (b) $\mathbf{1}^{2+}(BF_4^-)_2$ (5.96 µM), (c) $\mathbf{2}^{2+}(BF_4^-)_2$ (5.59 µM), (d) $\mathbf{3}^{2+}(BF_4^-)_2$ (5.81 µM), (e) $\mathbf{4}^{2+}(BF_4^-)_2$ (5.28 µM), (f) $\mathbf{5}^{2+}(BF_4^-)_2$ (4.02 µM) and (g) $\mathbf{6}^{2+}(BF_4^-)_2$ (3.73 µM) in CH_3CN containing 0.05 M Et_4NClO_4 as a supporting electrolyte (every 30 seconds).

Scheme 4-4. Two-electron reduction of dications to give neutral **T**-forms and thermal isomerization from **T**-forms to **F**-forms.

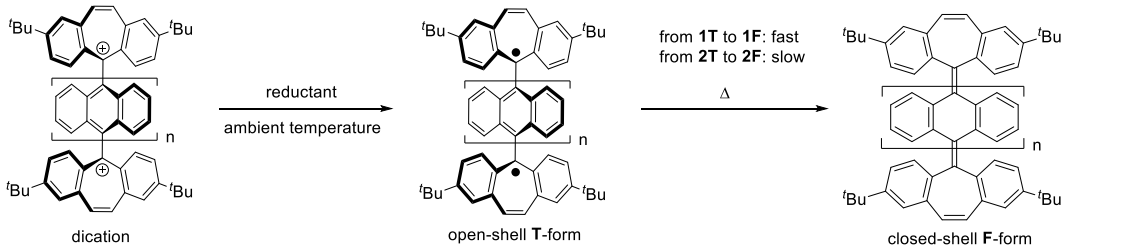

n = 1: **intermidiate**
n = 2: **kinetic product**
n = 3 - 6: **thermodynamically stable product**

n = 1: **thermodynamically stable product**
n = 2: **thermodynamically stable product**
n = 3 - 6: **not obtained**

	Chemical reduction of dications			Thermal isomerization from T-forms to F-forms	
n	dication	reductant	**T**-form	temperature	**F**-form
1	$\mathbf{1}^{2+}(BF_4^-)_2$	Zn	-	22 °C	**1F**, 100%
2	$\mathbf{2}^{2+}(BF_4^-)_2$	Zn	**2T**, 100%	100 °C	**2F**, 79%
3	$\mathbf{3}^{2+}(BF_4^-)_2$	Zn	**3T**, 100%	-	-
4	$\mathbf{4}^{2+}(BF_4^-)_2$	cobaltocene	**4T**, 90%	-	-
5	$\mathbf{5}^{2+}(BF_4^-)_2$	cobaltocene	**5T**, 88%	-	-
6	$\mathbf{6}^{2+}(BF_4^-)_2$	cobaltocene	**6T**, 100%	-	-

Upon chemical reduction of $\mathbf{3}^{2+}(BF_4^-)_2$ with zinc powder and $\mathbf{4}^{2+}(BF_4^-)_2$, $\mathbf{5}^{2+}(BF_4^-)_2$, and $\mathbf{6}^{2+}(BF_4^-)_2$ with cobaltocene in preparative-scale experiments, the resulting species were completely NMR-silent. In fact, ESR measurement of the solids showed signals characteristic of the presence of a dibenzocycloheptatrienyl radical (Scheme 4-4, Figure 4-12b,c,d,e). Formation of the neutral species was also confirmed by IR spectroscopy, which showed the disappearance of absorptions of BF_4^- ions in the reduction products (Figure 4-15c,d,e,f). The UV-Vis spectra of the isolated solids by chemical reduction are almost identical to those obtained by electrochemical reduction (Figures 4-13b,c,d and 4-14b,c,d,e). In particular, the intensity ratio of the strong peak around 250 nm and the absorption showing the vibrational structure of anthrylenes around 400 nm are almost the same, showing that electrolytic and chemical reduction of dications gave the same species. These results demonstrated that the biradical species **3T**, **4T**, **5T**, and **6T**, all of which were predicted to be the most stable configurational isomers by theoretical studies, were cleanly obtained upon 2e-reduction of dications. Notably, these open-shell **T**-forms are stable enough to be easily manipulated under air at ambient temperature. Furthermore, there was no change in the UV-Vis absorption spectrum of **3T** upon heating at 100 °C for 10 minutes in a toluene solution, indicating that **3T** has high thermal stability despite being an open-shell species composed of pure hydrocarbons (Figure 4-16).

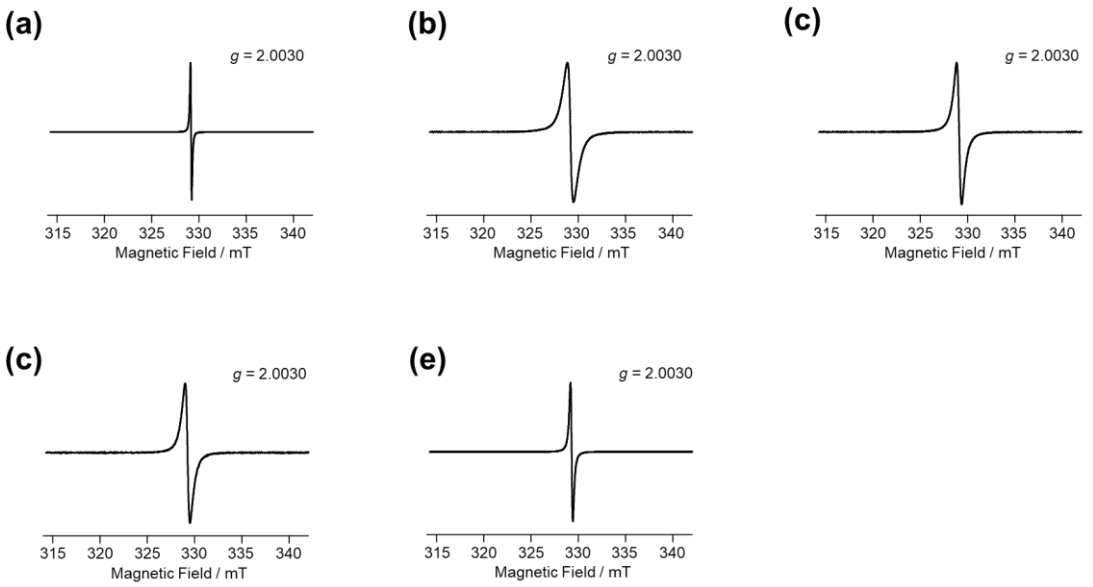

Figure 4-12. ESR spectra of biradicals: (a) **2T**, (b) **3T**, (c) **4T**, (d) **5T** and (e) **6T** in a solid state.

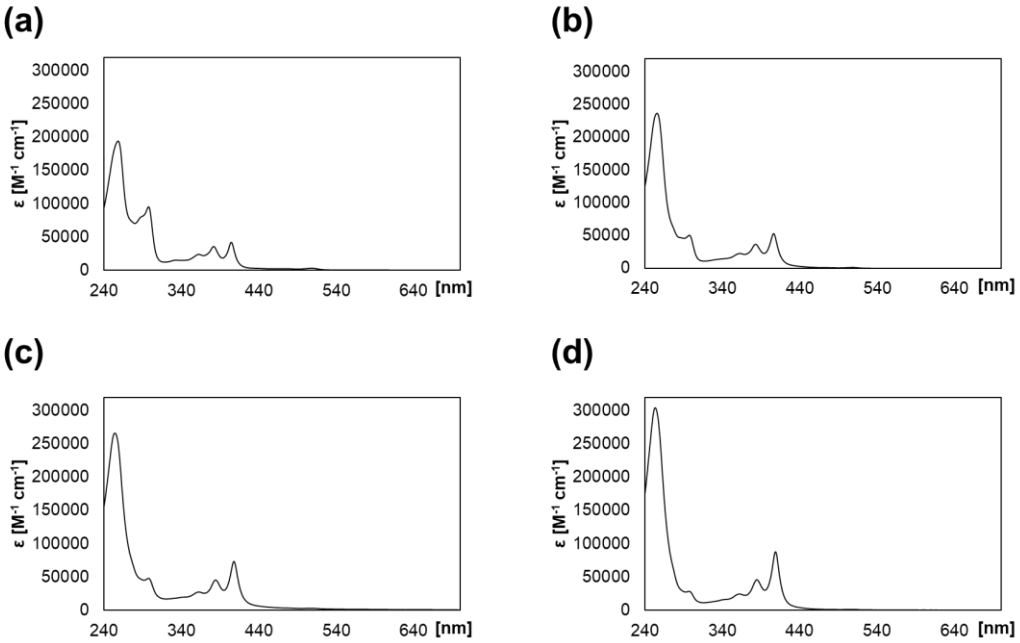

biradicals	λ_{max} [nm] (ε [M^{-1} cm^{-1}])					
2T	508 (2940)	404 (41900)	382 (35500)	362 (23800)	297 (95000)	258 (194000)
3T	508 (1440)	406 (53200)	383 (36800)	363 (22700)	297 (50600)	255 (237000)
4T	507 (2850)	408 (73100)	384 (45400)	362 (27200)	297 (47900)	254 (266000)
5T	507 (892)	409 (87400)	385 (45500)	362 (24200)	297 (28100)	253 (304000)

Figure 4-13. UV-Vis spectra of open-shell **T**-forms: (a) **2T**, (b) **3T**, (c) **4T** and (d) **5T** in THF.

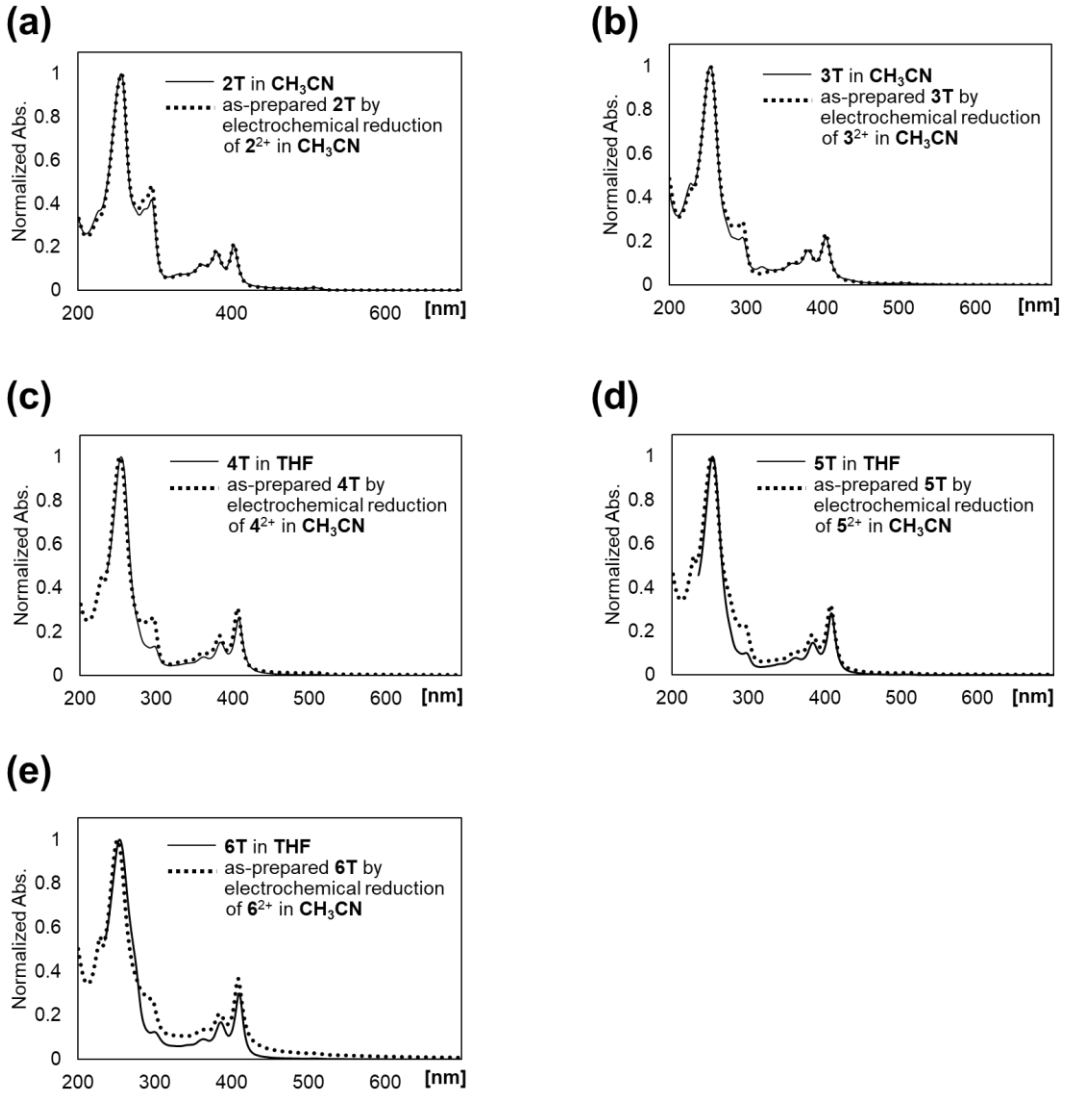

Figure 4-14. UV-Vis spectra of (a) isolated **2T** and as-prepared **2T** by electrochemical reduction of $\mathbf{2}^{2+}(BF_4^-)_2$ in CH_3CN, (b) isolated **3T** and as-prepared **3T** by electrochemical reduction of $\mathbf{3}^{2+}(BF_4^-)_2$ in CH_3CN, (c) isolated **4T** in THF and as-prepared **4T** by electrochemical reduction of $\mathbf{4}^{2+}(BF_4^-)_2$ in CH_3CN, (d) isolated **5T** in THF and as-prepared **5T** by electrochemical reduction of $\mathbf{5}^{2+}(BF_4^-)_2$ in CH_3CN and (e) isolated **6T** in THF and as-prepared **6T** by electrochemical reduction of $\mathbf{6}^{2+}(BF_4^-)_2$ in CH_3CN.

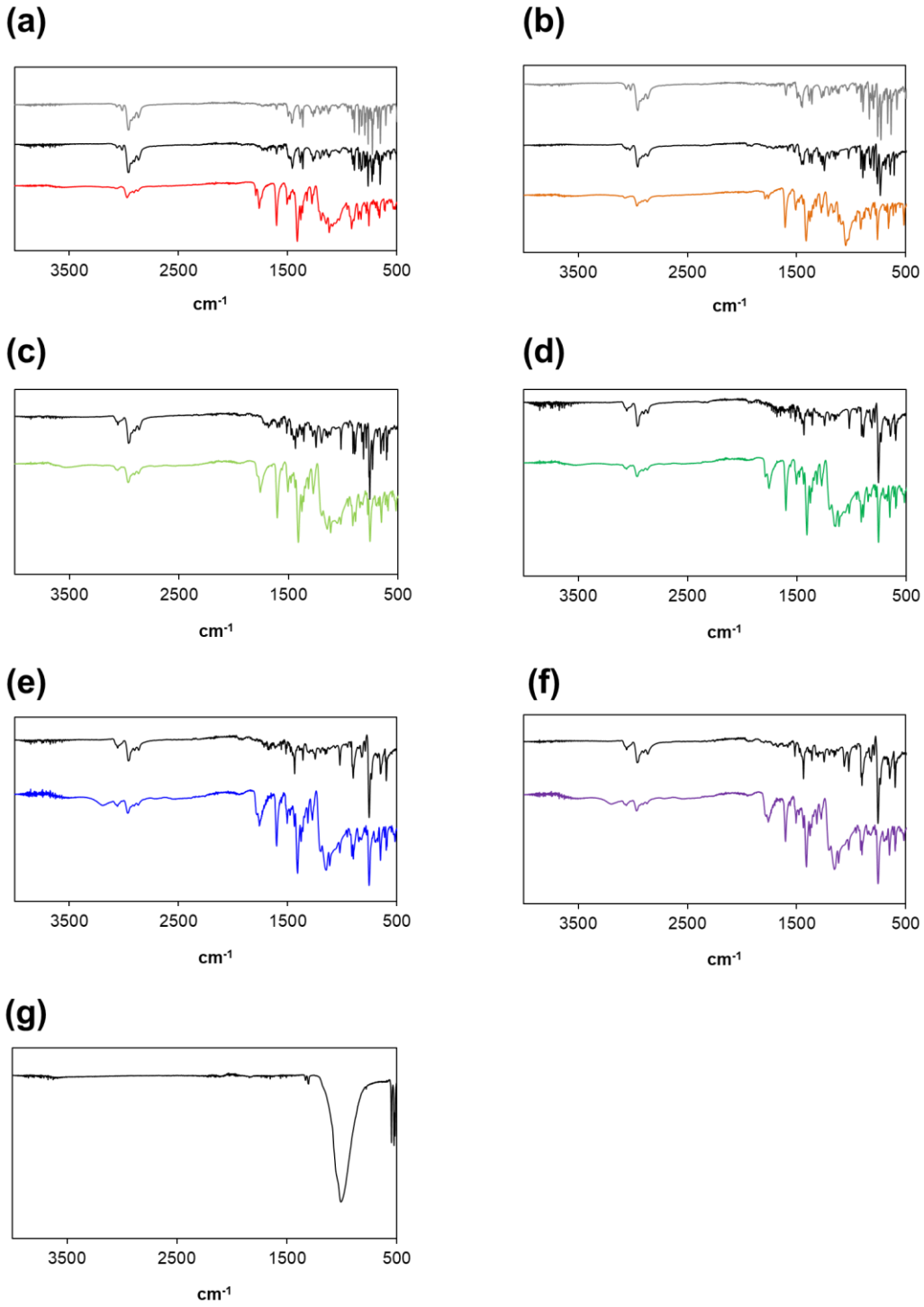

Figure 4-15. IR spectra of (a) $\mathbf{1}^{2+}(BF_4^-)_2$ (red), $\mathbf{1F}_{syn,anti}$ (black), and $\mathbf{1F}_{anti,anti}$ (gray), (b) $\mathbf{2}^{2+}(BF_4^-)_2$ (orange), **2T** (black), and **2F** (gray), (c) $\mathbf{3}^{2+}(BF_4^-)_2$ (olive) and **3T** (black), (d) $\mathbf{4}^{2+}(BF_4^-)_2$ (green) and **4T** (black), (e) $\mathbf{5}^{2+}(BF_4^-)_2$ (blue) and **5T** (black), (f) $\mathbf{6}^{2+}(BF_4^-)_2$ (purple) and **6T** (black), and (g) $NaBF_4$.

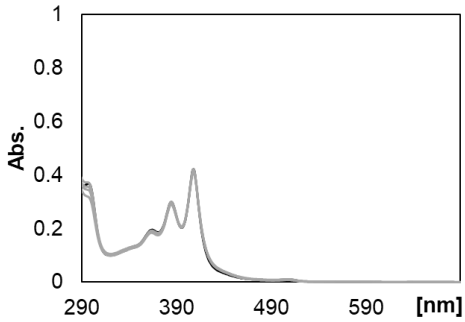

Figure 4-16. A change in UV-Vis spectrum of **3T** upon heating at 100 °C (0, 2, 4, 8, 16 min) in toluene.

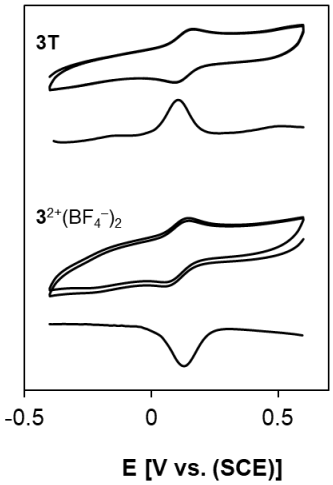

	E^{red}	E^{ox}
3T	+0.11	-
$\mathbf{3}^{2+}(BF_4^-)_2$	-	+0.13

[V vs. (SCE)]

Figure 4-17. Cyclic voltammograms (scan rate 100 mVs^{-1}) and differential pulse voltammograms of 0.2 mM solution of **3T** and $\mathbf{3}^{2+}(BF_4^-)_2$ in CH_2Cl_2 containing 0.1 M Bu_4NBF_4 as a supporting electrolyte (Pt electrode).

When electrochemical reduction was conducted for $\mathbf{2}^{2+}(BF_4^-)_2$, behavior similar to those for $\mathbf{3}^{2+}(BF_4^-)_2$-$\mathbf{6}^{2+}(BF_4^-)_2$ was observed, suggesting that open-shell **2T** was generated as a kinetically stable isomer even though the **F**-form was predicted to be more stable than the **T**-form for the neutral state of **2** (Figure 4-11c). Accordingly, reduction of $\mathbf{2}^{2+}(BF_4^-)_2$ with zinc powder quantitatively gave **2T** as a deep green solid, indicating the formation of biradical species (Scheme 4-4, Figures 4-12a, 4-13a, 4-14a, and 4-15b). In contrast to the previous report on the similar biradical,[37] the author found that biradical **2T** was converted to closed-shell species **2F** upon heating at 100 °C for 20 min in toluene, and **2F** was isolated in 79% yield (Scheme 4-4, Figure 4-19). The closed-shell **2F** adopts an all-*anti* configuration, as determined by single-crystal X-ray

structure analysis (Figure 4-18). To gain further insight into the thermal isomerization process, isomerization from **2T** to **2F** was monitored by UV-Vis spectroscopy (Figure 4-20). The absorption band assignable to the electronic transitions of anthrylenes for **2T** rapidly decayed upon heating at 100 °C, and the spectral pattern changed to that of isolated **2F**. By supposing first-order reaction kinetics, the rate constant *k* of isomerization was determined to be 6.08 x 10^{-4}, 1.34 x 10^{-3}, 4.02 x 10^{-3}, and 8.67 x 10^{-3} s^{-1} at 70, 80, 90, and 100 °C, respectively, based on the molar absorption coefficient at 297 nm showing the largest change (Figure 4-21). According to an Arrhenius plot, the activation energy for thermal isomerization was estimated to be 23.1 kcal mol^{-1}, suggesting that **2T** has a long half-life at ambient temperature (20 °C, 100 h). The persistence and kinetic stability of **2T** were also confirmed by measuring the cyclic voltammogram of the isolated solid of **2T**, which showed a reversible oxidation wave, which is similar to the oxidation process of twisted biradical species, as in **3T**-**6T** (Figures 4-17 and 4-25). There have been several reports for bianthracene derivatives exhibiting a change in conformation from the **T**-form to the **F**-form, however, it is difficult to isolate the metastable open-shell **T**-form due to its very short lifetime at ambient temperature under air. In contrast, the author revealed that all three states, the dication $\mathbf{2}^{2+}$, the open-shell biradical **2T**, and the closed-shell folded form **2F**, can be isolated as stable entities and mutually interconvert even at ambient conditions. These observations rely on the moderate rigidity of the seven-membered fused-ring structure and the orthogonally twisted structure of the oligoanthrylenes, which play important roles in both raising the activation energy for the change in configuration and kinetically stabilizing carbocations/radicals, which are typically considered to be unstable and reactive.

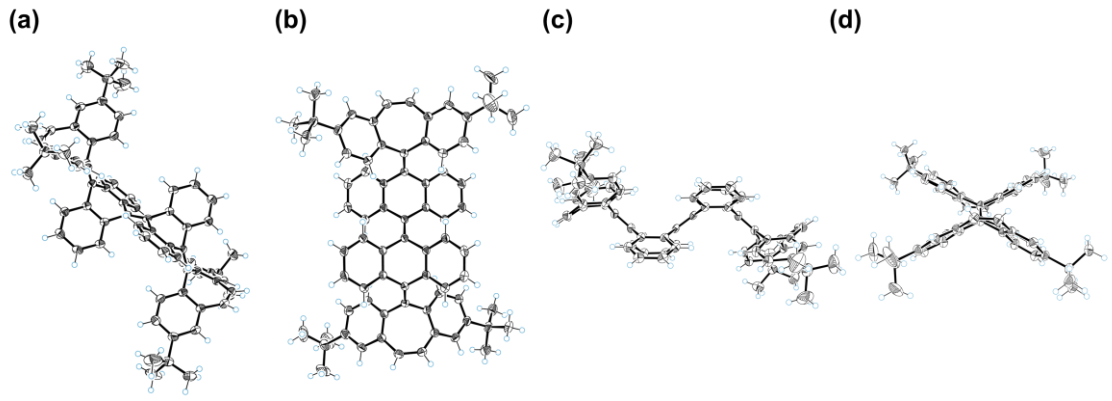

Figure 4-18. ORTEP drawings of **2F**: (a) best view, (b) front view, (c) side view and (d) top view. Solvent molecule is omitted for clarity. Thermal ellipsoids are shown at the 50% probability level.

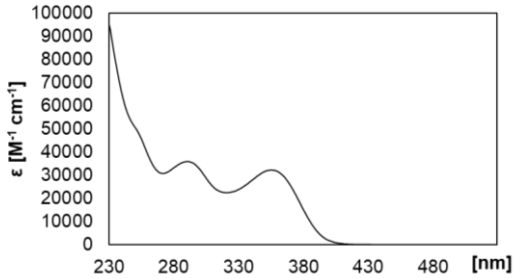

λ_{max} [nm]	(ε [M^{-1} cm^{-1}])
355 (32300)	290 (36000)

Figure 4-19. UV-Vis spectrum of closed-shell **2F** in CH_2Cl_2.

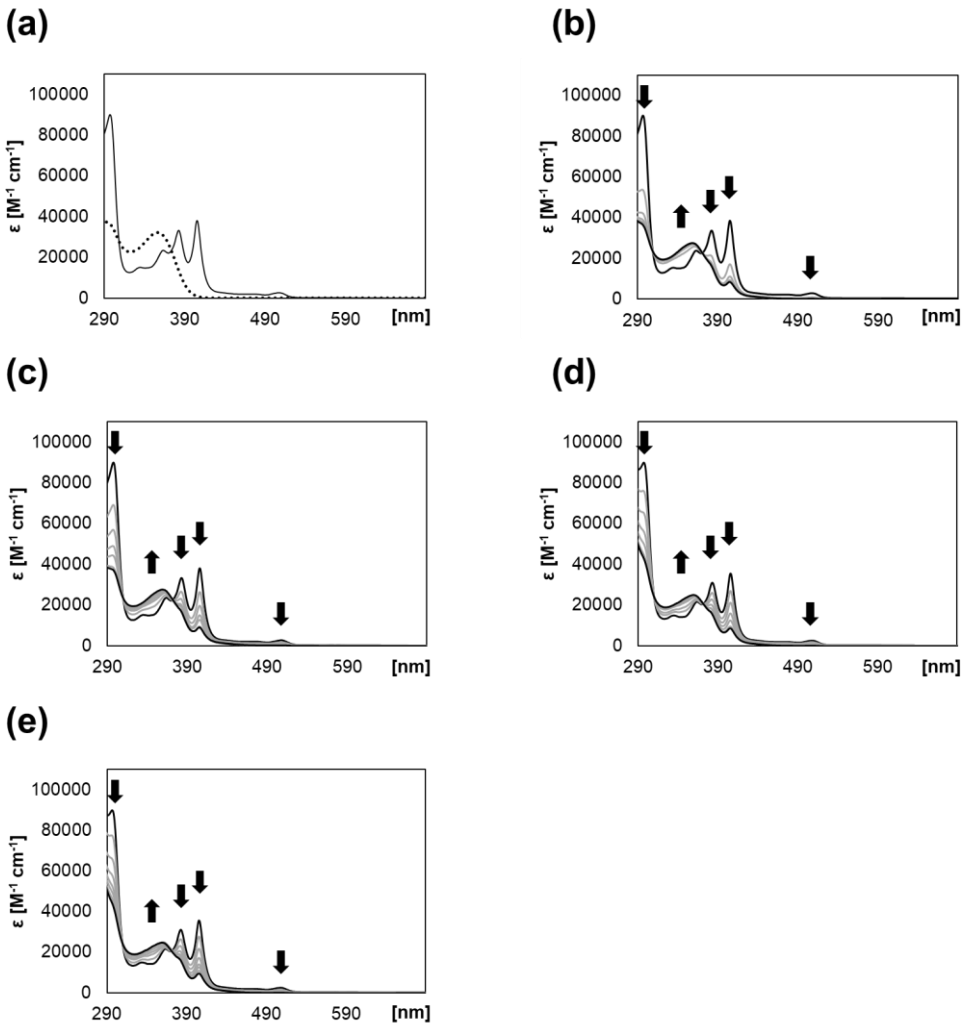

Figure 4-20. (a) UV-Vis spectra of **2T** (solid line) and **2F** (dotted line), and changes in UV-Vis spectra of (b) **2T** upon heating at 100 °C (0, 2, 4, 6, 8, 12, 16 min), (c) **2T** upon heating at 90 °C (0, 2, 4, 6, 8, 12, 16 min), (d) **2T** upon heating at 80 °C (0, 4, 8, 12, 16, 24, 32 min) and (e) **2T** upon heating at 70 °C (0, 8, 16, 24, 32, 40, 48, 64 min) in toluene.

from **2T** to **2F** in toluene	
T (°C)	k (s^{-1})
100	8.67 x 10^{-3}
90	4.02 x 10^{-3}
80	1.34 x 10^{-3}
70	6.08 x 10^{-4}

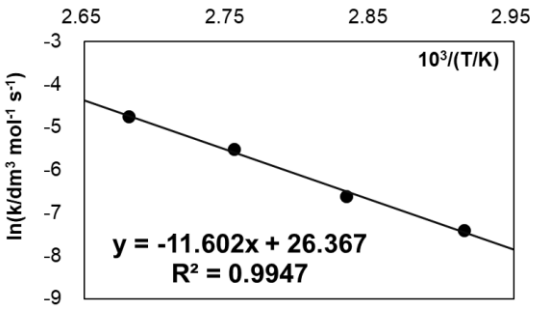

Figure 4-21. The rate constants k of thermal isomerization from **2T** to **2F** and an Arrhenius plot.

Upon electrochemical reduction of $\mathbf{1}^{2+}(BF_4^-)_2$, a continuous decrease not only in the absorptions assigned to the electronic transitions of dibenzotropyliums but also of the vibrational structure of the anthrylene skeleton was observed, which reflected the rapid formation of a closed-shell **F**-form, as expected based on the result of DFT calculations (Figure 4-11b). Although the generation of **1T** with a twisted geometry could be observed in the CV measurement (Figure 4-11a), the conversion of **1T** to **1F** is a much faster process than that of **2T** to **2F**. Thus, reduction of $\mathbf{1}^{2+}(BF_4^-)_2$ with zinc powder did not give **1T**, but rather a mixture of two isomers of **F**-forms quantitatively, $\mathbf{1F}_{anti,anti}$ and $\mathbf{1F}_{syn,anti}$, both of which are thermodynamically more stable than open-shell **1T** (Scheme 4-4, Figure 4-22). Upon heating a mixture of two isomers under reflux conditions in DMSO, the C_{2v}-symmetric $\mathbf{1F}_{anti,anti}$ was quantitatively obtained as the most stable isomer. Photoirradiation (λ >360 nm) of two **F**-forms quantitatively produces the C_s-symmetric $\mathbf{1F}_{syn,anti}$ as a metastable isomer, but not **1T**. This behavior is similar to the author's previous work (Chapter 3) as a molecular switch in response to heat and light to realize selective oxidation (Figure 4-23).

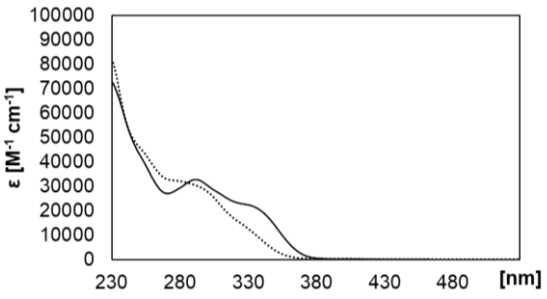

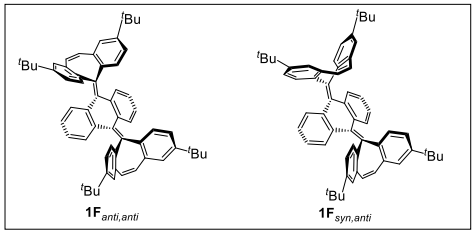

	λ_{max} [nm]	(ε [M^{-1} cm^{-1}])
$\mathbf{1F}_{anti,anti}$	331 (22300)	291 (32800)
$\mathbf{1F}_{syn,anti}$		295 (29600)

Figure 4-22. UV-Vis spectra of $\mathbf{1F}_{anti,anti}$ (solid line) and $\mathbf{1F}_{syn,anti}$ (dotted line) in CH_2Cl_2.

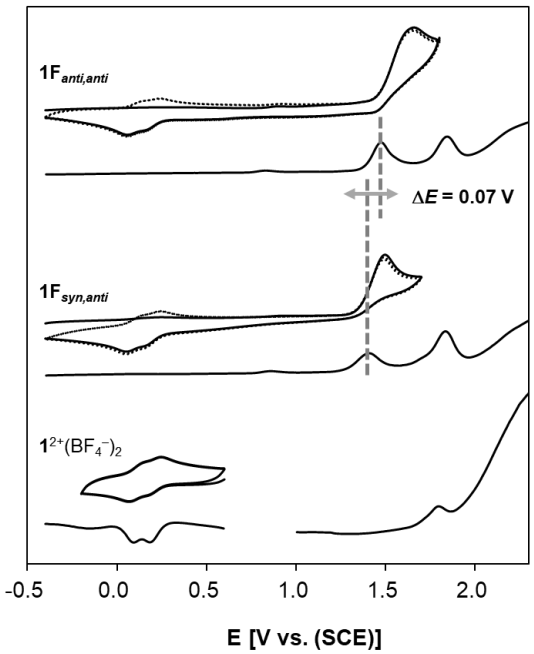

	E^{red}	E^{ox}	$E(\alpha)$
1F$_{anti,anti}$	-	+1.48	+1.84
as-prepared **1**$^{2+}$/**1**$^{+\bullet}$	+0.20	= E^{red}	-
as-prepared **1**$^{+\bullet}$/**1T**	+0.10	= E^{red}	-
1F$_{syn,anti}$	-	+1.41	+1.84
as-prepared **1**$^{2+}$/**1**$^{+\bullet}$	+0.20	= E^{red}	-
as-prepared **1**$^{+\bullet}$/**1T**	+0.09	= E^{red}	-
1^{2+}$(BF_4^-)_2$/**1**$^{+\bullet}$	+0.18	= E^{red}	+1.80
as-prepared **1**$^{+\bullet}$/**1T**	+0.09	= E^{red}	

[V vs. (SCE)]

Figure 4-23. (a) Cyclic voltammograms (scan rate 500 mVs^{-1}) and differential pulse voltammograms of 1.0 mM solution of **1F**$_{anti,anti}$, **1F**$_{syn,anti}$ and **1**$^{2+}$$(BF_4^-)_2$ in CH_2Cl_2 containing 0.1 M Bu_4NBF_4 as a supporting electrolyte (Pt electrode). Backgrounds were subtracted for all cyclic voltammograms. The second and third cycles are shown by dotted lines in the cyclic voltammograms of **1F**$_{anti,anti}$ and **1F**$_{syn,anti}$.

As mentioned above, the 2e-reduction of dications **1**$^{2+}$- **6**$^{2+}$ exhibited characteristic behavior depending on the number of anthrylene units. For **3**$^{2+}$, **4**$^{2+}$, **5**$^{2+}$, and **6**$^{2+}$, open-shell twisted **3T**, **4T**, **5T**, and **6T** were obtained as the thermodynamically most stable isomers. Despite the absence of bulky substituents such as mesityl groups, the 2e-reductions that generated these open-shell species proceeded almost quantitatively, and all neutral species could be handled as stable entities. In these biradicals, the oligoanthrylene skeleton acts as a rigid spacer, which separates two radical centers with a discrete increase in the distance of separation with an increase in the number of anthrylene units. On the other hand, during the reduction of dications **1**$^{2+}$ and **2**$^{2+}$, the biradical species **1T** and **2T** were generated as kinetic products in voltammetric analyses. Open-shell **1T** was quickly converted to the thermodynamically stable closed-shell **1F**$_{anti,anti}$ and **1F**$_{syn,anti}$ even at ambient temperature, whereas **2T** was isolated as a stable entity with an energy of 23.1 kcal mol^{-1} for isomerization. Upon heating of **2T** in a toluene solution, the most stable closed-shell isomer **2F** was obtained, and thus three states can be isolated for bianthrylene-type derivative **2**. In this way, oligoanthrylenes designed under the “cation-capped orthogonal approach" can lead to new functional materials.

4-2-6. Switching behavior between a dicationic state and a 2e-reduced state of oligoanthrylenes

Due to the persistence of biradical species **2T – 6T**, they could be used to construct spectral and magnetic switching systems when reversible interconversion with $\mathbf{2}^{2+}$- $\mathbf{6}^{2+}$ is possible. Upon electrochemical oxidation of as-prepared **2T** and **3T** in solution, regeneration of dications $\mathbf{2}^{2+}$ and $\mathbf{3}^{2+}$ was confirmed with the appearance of absorption assignable to the formation of dibenzotropiums with isosbestic points (Figure 4-24a,b). Based on the reversible redox interconversion between dications and biradicals, **2T** and **3T** exhibit clean electrochromism. For the electrochemical oxidation of as-prepared **4T**, **5T**, and **6T** in solution, almost the same spectral change was observed as in **2T** and **3T**, although conversion did not proceed completely probably due to deposition on the electrode surface (Figure 4-24c,d,e). In preparative-scale experiments, upon treatment of isolated open-shell **2T**-**6T** with two equivalents of $(4\text{-}BrC_6H_4)_3N^{+\bullet}BF_4^-$, original dications $\mathbf{2}^{2+}(BF_4^-)_2$ - $\mathbf{6}^{2+}(BF_4^-)_2$ were obtained quantitatively (Scheme 4-5). These results reveled that a family of dications $\mathbf{2}^{2+}$ - $\mathbf{6}^{2+}$ and **2T**-**6T** show high reversibility in terms of redox interconversion, and thus are potential candidates for the development of molecular switches with which color and magnetic properties can be controlled by applying an electric potential. In addition, treatment of closed-shell neutral species $\mathbf{1F}_{anti,anti}$/$\mathbf{1F}_{syn,anti}$ and **2F** with two equivalents of an appropriate oxidant, $(4\text{-}BrC_6H_4)_3N^{+\bullet}BF_4^-$ or $(2,4\text{-}Br_2C_6H_3)_3N^{+\bullet}SbCl_6^-$, quantitatively gave dications $\mathbf{1}^{2+}(BF_4^-)_2$, $\mathbf{1}^{2+}(SbCl_6^-)_2$ and $\mathbf{2}^{2+}(SbCl_6^-)_2$, respectively.

Scheme 4-5. Two-electron oxidation of isolated neutral species to reproduce original dications.

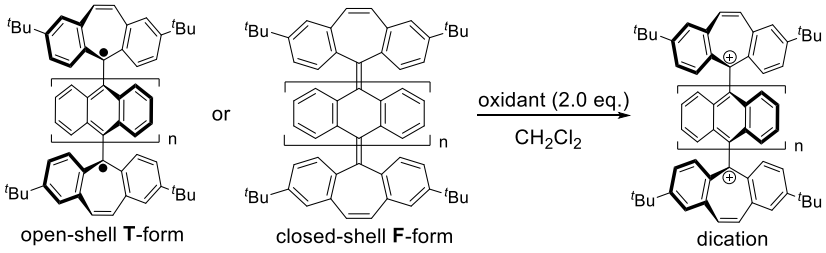

n	T-form	oxidant	dication
2	**2T**	$(4\text{-}BrC_6H_4)_3N^{+\bullet}BF_4^-$	$\mathbf{2}^{2+}(BF_4^-)_2$, 100%
3	**3T**	$(4\text{-}BrC_6H_4)_3N^{+\bullet}BF_4^-$	$\mathbf{3}^{2+}(BF_4^-)_2$, 96%
4	**4T**	$(4\text{-}BrC_6H_4)_3N^{+\bullet}BF_4^-$	$\mathbf{4}^{2+}(BF_4^-)_2$, 95%
5	**5T**	$(4\text{-}BrC_6H_4)_3N^{+\bullet}BF_4^-$	$\mathbf{5}^{2+}(BF_4^-)_2$, 99%
6	**6T**	$(4\text{-}BrC_6H_4)_3N^{+\bullet}BF_4^-$	$\mathbf{6}^{2+}(BF_4^-)_2$, 97%
n	**F**-form	oxidant	dication
1	$\mathbf{1F}_{anti,anti}$	$(2,4\text{-}Br_2C_6H_3)_3N^{+\bullet}SbCl_6^-$	$\mathbf{1}^{2+}(SbCl_6^-)_2$, 98%
1	$\mathbf{1F}_{syn,anti}$	$(4\text{-}BrC_6H_4)_3N^{+\bullet}BF_4^-$	$\mathbf{1}^{2+}(BF_4^-)_2$, 99%
2	**2F**	$(2,4\text{-}Br_2C_6H_3)_3N^{+\bullet}SbCl_6^-$	$\mathbf{2}^{2+}(SbCl_6^-)_2$, 100%

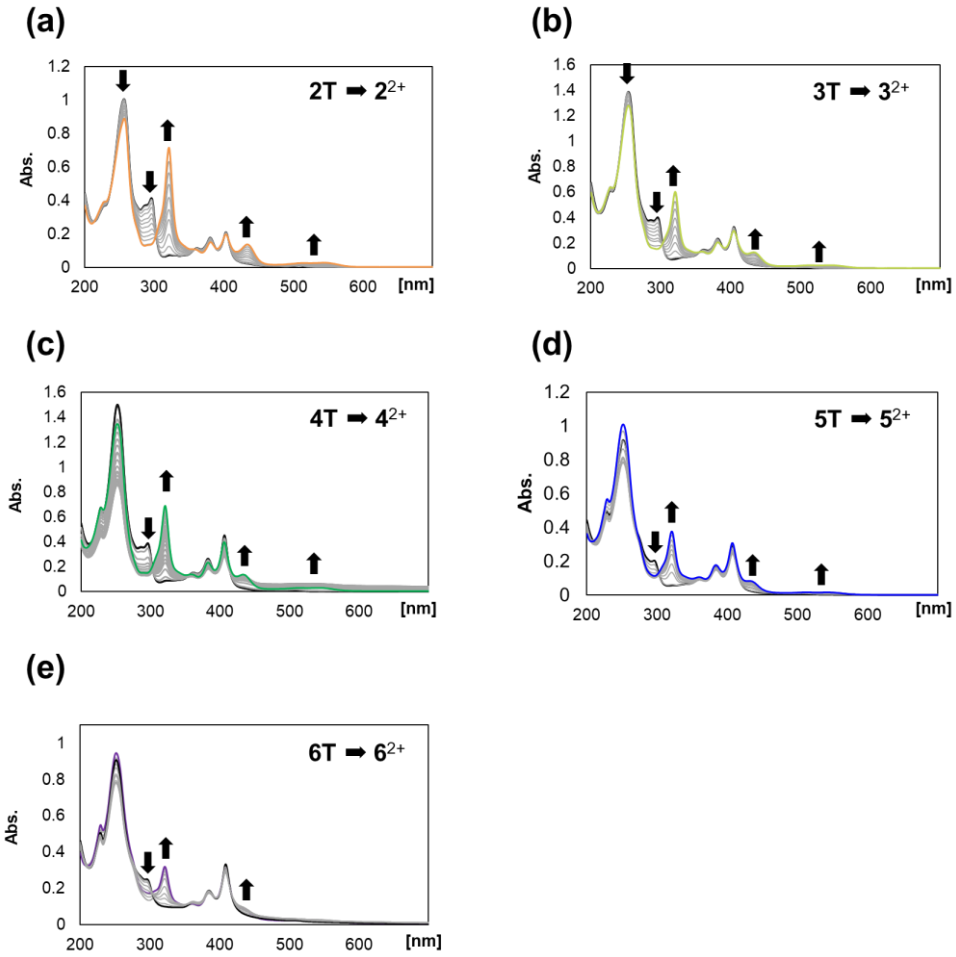

Figure 4-24. Changes in UV-Vis spectra upon electrochemical oxidation (20 μA) of as-prepared (a) **2T**, (b) **3T**, (c) **4T**, (d) **5T** and (e) **6T** in CH_3CN containing 0.05 M Et_4NClO_4 as a supporting electrolyte (every 30 seconds).

Based on the above results, the dications synthesized in this study can serve as key starting materials for making a series of unique molecular switches (Scheme 4-6). Dications $\mathbf{2}^{2+}$, $\mathbf{3}^{2+}$, $\mathbf{4}^{2+}$, $\mathbf{5}^{2+}$, and $\mathbf{6}^{2+}$ are suitable for ON/OFF switching of magnetic properties by redox interconversion between the dications and their corresponding open-shell **T**-forms. In the case of $\mathbf{2}^{2+}$, both the most stable closed-shell **2F** and metastable open-shell **2T** in the neutral state can be isolated and are stable enough even under ambient conditions so that the switching behavior among three states, $\mathbf{2}^{2+}$, **2T**, and **2F**, is completely controllable and a magnetic property can be changed not only by the redox interconversion between $\mathbf{2}^{2+}$ and **2T** but also by thermal conversion between **2T** and **2F**. Moreover, the difference between the oxidation potentials of **2T** and **2F** (ΔE = 1.32 V in CH_2Cl_2) is the largest change among the values reported to date (Figure 4-25).[64,65] In the case of n = 1, photo- and thermally controlled redox interconversion with $\mathbf{1}^{2+}$ occurs without magnetic switching, which is similar to previously reported behavior (Chapter 3).

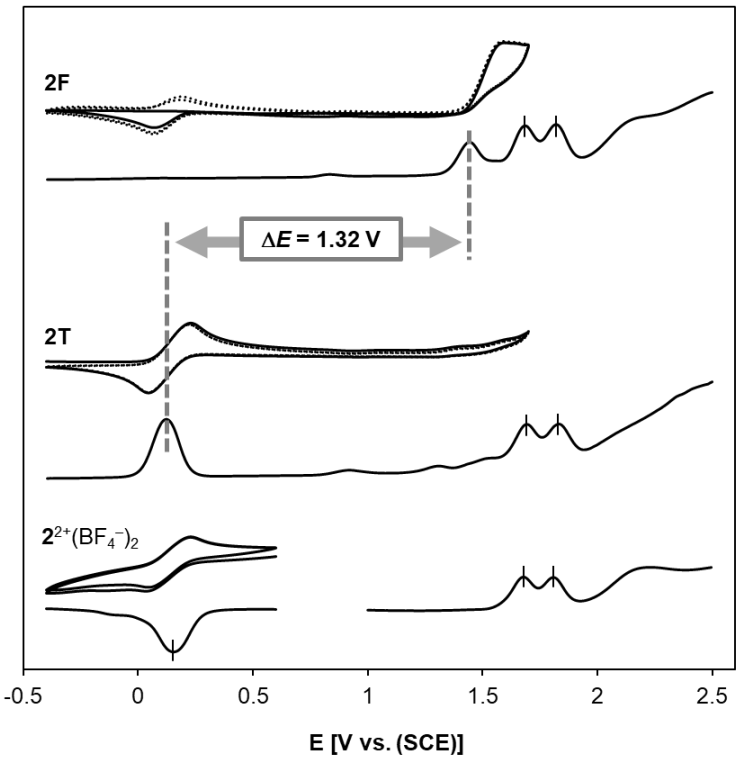

	E^{red}	E^{ox}	$E(\beta)$	$E(\alpha)$
2F	-	+1.44	+1.68	+1.82
as-prepared $\mathbf{2}^{2+}$/**2T**	+0.13	$=E^{red}$	-	-
2T	-	+0.12	+1.69	+1.83
$\mathbf{2}^{2+}(BF_4^-)_2$	+0.15	-	+1.68	+1.81

[V vs. (SCE)]

Figure 4-25. Cyclic voltammograms (scan rate 500 mVs^{-1}) and differential pulse voltammograms of 1.0 mM solution of **2F**, **2T**, and $\mathbf{2}^{2+}(BF_4^-)_2$ in CH_2Cl_2 containing 0.1 M Bu_4NBF_4 as a supporting electrolyte (Pt electrode). Backgrounds were subtracted for all cyclic voltammograms. The second and third cycles are shown by dotted lines in cyclic voltammograms of **2F** and **2T**.

Scheme 4-6. A family of molecular switches composed of 9,10-anthrylene(s), in which the switching behavior can be precisely tuned by selecting the number of anthrylene unit(s) between two dibenzotropyliums.

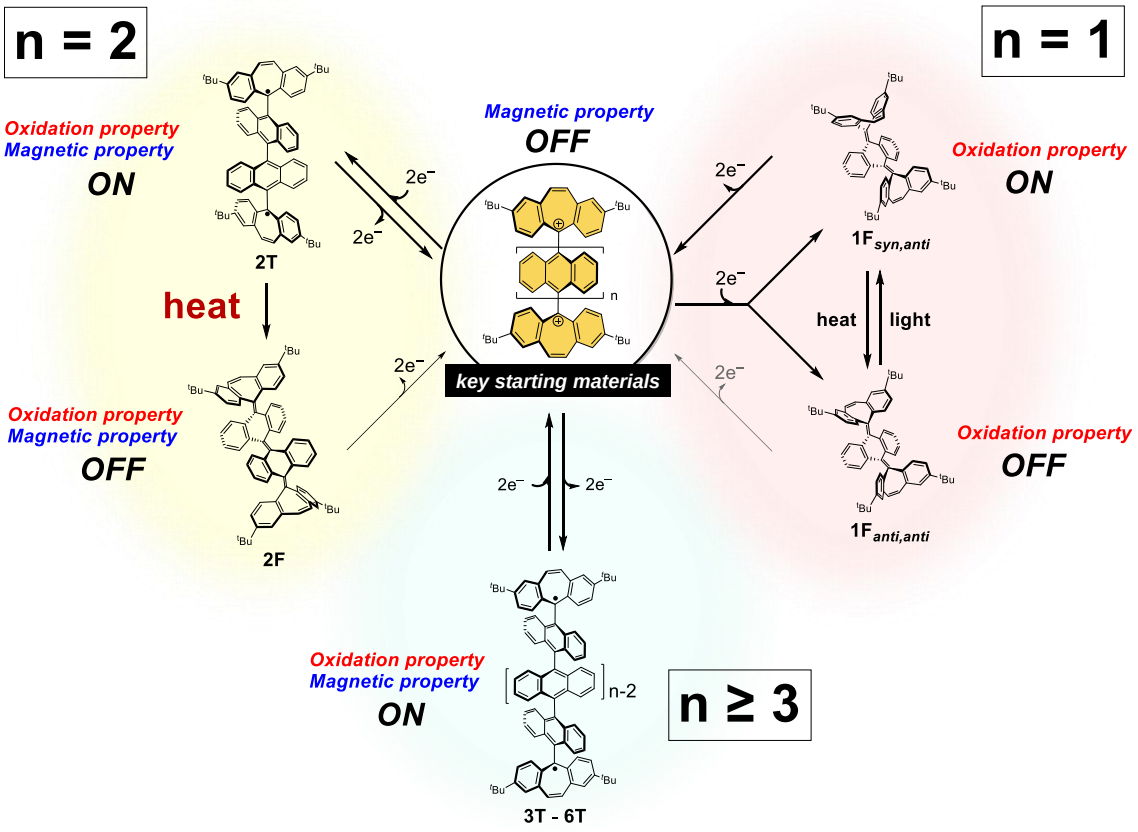

In this way, the author has constructed a family of molecular switches composed of 9,10-anthrylene(s), in which the switching behavior can be precisely tuned by selecting the number of anthrylene unit(s) between two dibenzotropyliums. The "cation-capped orthogonal approach" should provide valuable guidelines for the molecular design of arylene-based response systems, because preliminary DFT calculations indicated that the number of arylene units, which would be suitable for realizing three-state switching, could be tuned by modifying the anthrylene skeletons or changing the cationic moieties for end-capping while maintaining the orthogonally twisted structure.

4-3. Conclusion

The author has designed and synthesized a family of dications with one to six anthrylene unit(s) composed of pure hydrocarbons by end-capping with dibenzotropylium skeletons as key building blocks. This approach enabled isolation of the non-substituted oligo(9,10-anthrylene) derivatives even in the case of six anthrylene units, which is the largest number ever reported. Furthermore, they are soluble enough to perform various measurements due to the scarcity of intermolecular interactions in the crystal form, and thus the author was able to elucidate their orthogonally twisted structures and unique redox properties.

Based on voltammetric analyses of these dications, all derivatives exhibited reversible oxidation wave(s), where each anthrylene unit underwent one-by-one oxidation resulting in the formation of multivalent cations. These dications are appropriate systems for investigating the electronic properties of individual anthrylene units in oligoanthrylenes because the electronic interaction between each 14π-aromatic unit is very weak due to the orthogonally twisted structure. In fact, the relationship between the oxidation potentials and the number of anthrylene unit(s) in each oxidation process was clarified in detail. Therefore, this study should provide important insights into applications for molecular electronics such as single-molecule memory or transistors because these dications can be considered a suitable model, in which individual molecules are forced to be close to each other.

These dications undergo 2e-reduction to give the corresponding closed-shell and/or open-shell neutral species as stable entities depending on the number of anthrylene unit(s), which can be handled under air at ambient temperature. While switching between the dication and closed-shell folded species was observed for monoanthrylene derivative **1**, that between the dication and open-shell biradical species was demonstrated for longer derivatives **3**-**6** upon redox interconversion. Particularly in the case of bianthrylene derivative **2**, since neutral species were isolated as both a kinetically produced biradical and thermodynamically stable folded structure, changes in the color, oxidation properties, and magnetic properties were demonstrated based on three-state interconversion. Although some studies have sought to construct switching systems based on interconversion between anthrylene-based open-shell species and anthraquinodimethane-based closed-shell species,[65–71] the isolation of both structures is still challenging, especially under air at ambient temperature, and thus, a series of the molecular switches in this study could pave the way for the development of functional π-conjugated molecules.

In conclusion, the author demonstrated that molecular design under the “cation-capped orthogonal approach” could be a versatile strategy for stabilizing intrinsically unstable molecules and overcoming the solubility problem, so that this approach could provide valuable guidelines for constructing and investigating unexploited molecular skeletons.

4-4. Experimental Section

4-4-1. General

All reactions were carried out under an argon atmosphere. All commercially available compounds were used without further purification unless otherwise indicated. Dry MeCN was obtained by distillation from CaH_2 prior to use. Column chromatography was performed on silica gel 60N (KANTO KAGAKU, spherical neutral) of particle size 40–50 μm or Wakogel® 60N (neutral) of particle size 38-100 μm. ^{1}H and ^{13}C NMR spectra were recorded on a BRUKER Ascend™ 400 (^{1}H/400 MHz and ^{13}C/100 MHz) spectrometer. ESR spectra were recorded on a JEOL JES-FE2XG spectrometer. IR spectra were measured on a Shimadzu IRAffinity-1S spectrophotometer using the attenuated total reflection (ATR) mode. Mass spectra were recorded on a JEOL JMS-T100GCV spectrometer in FD mode, on a Thermo Fisher Scientific Q Exactive Plus spectrometer in ESI positive mode or on a BRUKER UltrafleXtreme-DHS2 TOF/TOF in MALDI positive mode with α-cyano-4-hydroxycinnamic acid (CHCA) as matrix by Dr. Eri Fukushi and Mr. Yusuke Takata (GC-MS&NMR Laboratory, Research Faculty of Agriculture, Hokkaido University). Melting points were measured on a Stanford Research Systems MPA100 Optimelt and are uncorrected. UV-Vis-NIR spectra were recorded on a JASCO V-770 spectrophotometer. Fluorescence spectra were measured on a Hitachi F-7000 spectrofluorometer. Fluorescence quantum yields were determined by using 9,10-diphenylanthracene (Φ_F = 0.97) as an external standard.[72] Redox potentials (E^{ox} and E^{red}) were measured on a BAS ALS-612EX by differential pulse voltammetry and cyclic voltammetry. Pt electrodes were used as the working (disk) and counter electrodes. The working electrode was polished using a water suspension of aluminum oxide (0.05 μm) before use. DFT calculations were performed with the Gaussian 16 W program package.[73] The geometries of the compounds were optimized by using the (U)B3LYP or (U)CAM-B3LYP method in combination with the 6–31G(d) basis set. Single-crystal X-ray structure analyses were performed by a Rigaku XtaLAB Synergy (Cu-Kα radiation, λ = 1.54184 Å) with HyPix diffractometer. Using Olex2,[74] the structure was solved with the SHELXT[75] structure solution program using Intrinsic Phasing and refined with the SHELXL[76] refinement package using Least Squares minimization. All the hydrogen atoms were located at the calculated positions and refined with riding.

4-4-2. Synthetic procedures

1-Bromo-2-(bromomethyl)-4-(*tert*-butyl)benzene 8

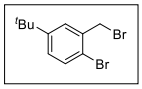

A solution of 1-bromo-4-(*tert*-butyl)-2-methylbenzene **7**[57] (6.14 g, 27.0 mmol), *N*-bromosuccinimide (NBS, 7.70 g, 43.2 mmol) and azobis(isobutyronitrile) (AIBN, 222 mg, 1.35 mmol) in $CHCl_3$ (90 mL) was heated at reflux under photoirradiation with 500 W halogen lamp for 15 h. The reaction mixture was allowed to cool to 24 °C, and then diluted with 5% $Na_2S_2O_3$ aqueous solution. The whole mixture was extracted with $CHCl_3$ three times. The combined organic layers were washed with water and brine, and dried over anhydrous $MgSO_4$. After filtration, the solvent was concentrated under reduced pressure. The crude product was purified by column chromatography on silica gel (hexane only, Rf = 0.44) to give **8** (6.39 g) as a pale-yellow oil in 77% yield.

8; ^{1}H NMR ($CDCl_3$): δ/ppm 7.48 (1H, d, *J*= 8.4 Hz), 7.45 (1H, d, *J*= 2.4 Hz), 7.19 (1H, dd, *J*= 2.4 Hz, 8.4 Hz), 4.61 (2H, s), 1.31 (9H, s); ^{13}C NMR ($CDCl_3$): δ/ppm 151.36, 136.34, 132.89, 128.38, 127.54, 121.22, 34.61, 33.95, 31.16; IR (ATR): ν/cm^{-1} 2964, 2904, 2868, 2369, 1902, 1773, 1654, 1559, 1478, 1461, 1436, 1395, 1363, 1264, 1218, 1158, 1109, 1025, 921, 889, 868, 820, 726, 699, 677, 661, 577, 546, 441, 419; LR-MS (FD) m/z (%): 308.98 (6), 307.98 (48), 306.99 (11), 305.98 (bp), 304.99 (6), 303.98 (M^+, 50); HR-MS (FD) Calcd. for $C_{11}H_{14}Br_2$: 303.94623; Found: 303.94744.

(2-Bromo-4-*tert*-butylbenzyl)-triphenylphosphonium bromide 9

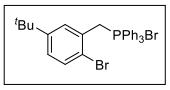

A suspension of **8** (10.0 g, 32.8 mmol) and triphenylphosphine (9.46 g, 36.1 mmol) in toluene (170 mL) was heated at reflux for 4 h. After cooling to 25 °C, the precipitates were filtered and washed with hexane three times. The resulting solid was dried in vacuo to give **9** (16.2 g) as a white solid in 87% yield.

9; Mp: 236.4-239.4 °C; ^{1}H NMR ($CDCl_3$): δ/ppm 7.81-7.77 (3H, m), 7.75-7.62 (12H, m), 7.43 (1H, dd, *J*= 2.4 Hz, 2.4 Hz), 7.28 (1H, dd, *J*= 0.8 Hz, 8.4 Hz), 7.12 (1H, ddd, *J*= 2.4 Hz, 2.4 Hz, 8.4 Hz), 5.69 (2H, d, *J*= 14.4 Hz), 1.05 (9H, s); ^{13}C NMR ($CDCl_3$): δ/ppm 151.71 (d, *J*= 3.7 Hz), 135.90 (d, *J*= 2.8 Hz), 134.43 (d, *J*= 10.0 Hz), 132.44 (d, *J*= 3.0 Hz), 130.76 (d, *J*= 5.1 Hz), 130.19 (d, *J*= 12.3 Hz), 127.25 (d, *J*= 3.8 Hz), 126.75 (d, *J*= 8.4 Hz), 123.69 (d, *J*= 7.3 Hz), 117.53 (d, *J*= 84.7 Hz), 34.55 (s), 31.25 (d, *J*= 47.8 Hz), 30.88 (s); IR (ATR): ν/cm^{-1} 3053, 3013, 2950, 2896, 2867, 2833, 2767, 1586, 1478, 1464, 1443, 1433, 1398, 1362, 1318, 1267, 1187, 1157, 1107, 1074, 1021, 995, 939, 908, 894, 836, 812, 761, 744, 726, 719, 689, 676, 629, 570, 516, 494, 450, 439; LR-MS (FD) m/z (%): 491.16 (6), 490.16 (32), 489.15 (bp), 488.16 (33), 487.16 (M^+, 99); HR-MS (FD) Calcd. for $C_{29}H_{29}BrP$: 487.11902; Found: 487.12059.

1-Bromo-4-(*tert*-butyl)-2-(dibromomethyl)benzene 10

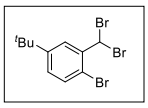

A solution of **7** (7.66 g, 33.7 mmol), NBS (18.0 g, 101 mmol) and AIBN (277 mg, 1.69 mmol) in $CHCl_3$ (110 mL) was heated at reflux under photoirradiation with 500 W halogen lamp for 20 h. The reaction mixture was allowed to cool to 24 °C, and then diluted with 5% $Na_2S_2O_3$ aqueous solution. The whole mixture was extracted with $CHCl_3$ three times. The combined organic layers were washed with water and brine, and dried over anhydrous $MgSO_4$. After filtration, the solvent was concentrated under reduced pressure. The crude product was purified by column chromatography on silica gel (hexane only, Rf = 0.57) to give **10** (11.3 g) as a colorless amorphous solid in 87% yield.

10; Mp: 50.8-53.4 °C; ^{1}H NMR ($CDCl_3$): δ/ppm 8.02 (1H, d, *J*= 2.4 Hz), 7.40 (1H, d, *J*= 7.6 Hz), 7.20 (1H, dd, *J*= 2.4 Hz, 7.6 Hz), 7.09 (1H, s), 1.35 (9H, s); ^{13}C NMR ($CDCl_3$): δ/ppm 152.04, 139.66, 132.04, 128.64, 128.21, 116.40, 40.43, 34.92, 31.11; IR (ATR): ν/cm^{-1} 3060, 3028, 2964, 2903, 2866, 2296, 1911, 1791, 1653, 1559, 1474, 1458, 1393, 1362, 1263, 1215, 1202, 1182, 1156, 1115, 1019, 954, 923, 897, 818, 727, 715, 676, 666, 590, 575, 419; LR-MS (FD) m/z (%): 387.90 (32), 386.90 (12), 385.90 (98), 384.90 (13), 383.90 (bp), 382.91 (5), 381.90 (M^+, 34), 304.96 (5); HR-MS (FD) Calcd. for $C_{11}H_{13}Br_3$: 381.85674; Found: 381.85826.

2-Bromo-5-*tert*-butylbenzaldehyde 11

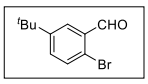

A suspension of **10** (10.4 g, 27.0 mmol) in concentrated sulfuric acid (110 mL) was heated at 60 °C for 3 h. The reaction mixture was allowed to cool to 0 °C, and then diluted with water. The whole mixture was extracted with ethyl acetate three times. The combined organic layers were washed with 5% NaOH aqueous solution, water and brine, and dried over anhydrous $MgSO_4$. After filtration, the solvent was concentrated under reduced pressure. The crude product was purified by column chromatography on silica gel (CH_2Cl_2/hexane = 1/4, Rf = 0.27) to give **11** (5.78 g) as a pale-yellow oil in 89% yield.

^{1}H NMR data were identical to those in literature.[77]

(*E*)-1,2-Bis(2-bromo-5-(*tert*-butyl)phenyl)ethene and (*Z*)-1,2-bis(2-bromo-5-(*tert*-butyl)phenyl)ethene 12

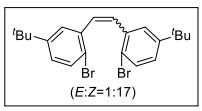

To a suspension of **9** (13.8 g, 24.3 mmol) in dry THF (300 mL) was added potassium *tert*-butoxide (3.28 g, 29.2 mmol) at 0 °C. After stirring at 0 °C for 30 min, a solution of **11** (5.87 g, 24.3 mmol) in dry THF (70 mL) was added to the suspension and the mixture was warmed to 22 °C. The resulting suspension was stirred at 22 °C for 14 h, and then diluted with water. The whole mixture was extracted with ethyl acetate three times. The combined organic layers were washed with water and brine, and dried over anhydrous $MgSO_4$. After filtration, the solvent was concentrated under reduced pressure. The crude product was

purified by column chromatography on silica gel (CH_2Cl_2/hexane = 1/10, Rf = 0.53) to give **12** (10.3 g, *E*:Z = 1:17) as a white solid in 94% yield.

12; Mp: 75.1-79.8 °C; ^{1}H NMR ($CDCl_3$): δ/ppm (*E*)-isomer 7.69 (2H, d, *J*= 2.4 Hz), 7.51 (2H, d, *J*= 8.4 Hz), 7.36 (2H, s), 7.19 (2H, dd, *J*= 2.4 Hz, 8.4 Hz), 1.36 (18H, s), (*Z*)-isomer 7.45 (2H, d, *J*= 8.4 Hz), 7.03 (2H, dd, *J*= 2.4 Hz, 8.4 Hz), 6.91 (2H, d, *J*= 2.4 Hz), 6.80 (2H, s), 1.01 (18H, s); ^{13}C NMR ($CDCl_3$): δ/ppm (*E*)-isomer 150.85, 136.37, 132.58, 130.41, 126.71, 124.24, 121.10, 34.68, 31.24, (*Z*)-isomer 150.03, 136.77, 131.91, 131.62, 128.67, 125.77, 120.49, 34.17, 30.92; IR (ATR): ν/cm^{-1} 2959, 2901, 2865, 1900, 1740, 1714, 1640, 1587, 1559, 1474, 1454, 1386, 1362, 1260, 1203, 1166, 1111, 1019, 963, 926, 900, 828, 820, 777, 750, 727, 708, 690, 638, 575, 530, 505, 475, 441; LR-MS (FD) m/z (%): 453.07 (13), 452.07 (50), 451.08 (25), 450.07 (bp), 449.08 (13), 448.07 (M^+, 51); HR-MS (FD) Calcd. for $C_{22}H_{26}Br_2$: 448.04013; Found: 448.03811.

2,8-Di-*tert*-butyl-dibenzosuberenone 13

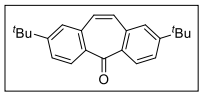

To a solution of **12** (*E*:*Z* = 1:17, 10.3 g, 22.9 mmol) in dry Et_2O (250 mL) was added *sec*-BuLi (1.03 M in hexane, 50.3 mL, 51.8 mmol) dropwise over 20 min at –78 °C. After stirring at –78 °C for 1 h, dimethylcarbamoyl chloride (2.38 ml, 25.9 mmol) was added to the suspension dropwise over 6 min at –78 °C and the mixture was warmed to 25 °C. The resulting solution was stirred at 25 °C for 13 h, and then diluted with water. The whole mixture was extracted with ethyl acetate three times. The combined organic layers were washed with water and brine, and dried over anhydrous $MgSO_4$. After filtration, the solvent was concentrated under reduced pressure. The crude product was purified by column chromatography on silica gel (CH_2Cl_2/hexane = 3/4, Rf = 0.20) to give **13** (4.51 g) as a white solid in 62% yield (for a mixture of *E*:*Z* isomers).

13; Mp: 155.0-156.4 °C; ^{1}H NMR ($CDCl_3$): δ/ppm 8.23 (2H, d, *J*= 8.4 Hz), 7.58 (2H, dd, *J*= 2.0 Hz, 8.4 Hz), 7.51 (2H, d, *J*= 2.0 Hz), 7.06 (2H, s), 1.38 (18H, s); ^{13}C NMR ($CDCl_3$): δ/ppm 191.74, 155.36, 136.22, 134.95, 132.08, 130.39, 127.52, 126.41, 34.93, 31.08; IR (ATR): ν/cm^{-1} 3071, 3031, 2960, 2903, 2868, 1623, 1593, 1461, 1389, 1383, 1362, 1307, 1268, 1204, 1166, 1135, 1118, 1029, 968, 949, 926, 907, 897, 891, 862, 851, 842, 804, 773, 706, 700, 681, 653, 567, 553, 509, 466, 449; LR-MS (FD) m/z (%): 319.20 (25), 318.20 (M^+, bp); HR-MS (FD) Calcd. for $C_{23}H_{26}O$: 318.19836; Found: 318.19920.

2,8-Di-*tert*-butyl-5*H*-dibenzo[*a,d*]cycloheptatriene-5-thione 14

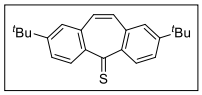

A solution of ketone **13** (1.10 g, 3.46 mmol) and 2,4-bis(4-methoxyphenyl)-1,3-dithia-2,4-diphosphetan-2,4-disulfide (Lawesson's reagent) (770 mg, 1.90 mmol) in dry toluene (35 mL) was heated to reflux for 4 h. After cooling to 25 °C, the resulting green solution was concentrated under reduced pressure. The crude product was purified by column chromatography on silica gel (CH_2Cl_2/hexane = 1/1, Rf = 0.60) to give thione **14** (1.21 g) as a green solid in 100% yield.

14; Mp: 124.0-126.3 °C; ^{1}H NMR ($CDCl_3$): δ /ppm 8.04 (2H, d, J= 8.4 Hz), 7.43 (2H, dd, J= 2.0 Hz, 8.4 Hz), 7.33 (2H, d, J= 2.0 Hz), 7.00 (2H, s), 1.34 (18H, s); ^{13}C NMR ($CDCl_3$): δ/ppm 238.15, 154.03, 146.92, 131.82, 130.63, 129.71, 126.21, 125.22, 34.82, 31.02; IR (ATR): ν/cm^{-1} 3051, 3025, 2960, 2901, 2864, 1917, 1772, 1668, 1641, 1597, 1539, 1476, 1458, 1381, 1361, 1311, 1294, 1271, 1253, 1235, 1196, 1177, 1149, 1112, 1020, 977, 961, 944, 900, 887, 843, 834, 799, 793, 740, 703, 694, 677, 661, 622, 539, 502, 456; LR-MS (FD) m/z (%): 669.39 (5), 668.38 (9), 336.19 (8) , 335.20 (25), 334.19 (M^+, bp), 318.22 (6); HR-MS (FD) Calcd. for $C_{23}H_{26}S$: 334.17552; Found: 334.17504.

2'',8''-Di-*tert*-butyl-10*H*-dispiro[anthracene-9,2'-thiirane-3',5''-dibenzo[*a,d*]cycloheptatrien]-10-one 15

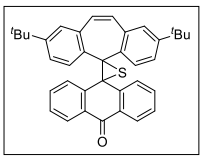

A solution of thione **14** (1.16 g, 3.46 mmol) and 10-diazoanthracen-9(10*H*)-one [58] (763 mg, 3.46 mmol) in dry THF (35 mL) was heated to reflux for 14 h. After cooling to 25 °C, the precipitates were collected and washed with ethanol three times. The resulting solid was dried in vacuo to give **15** (1.40 g) as a yellow solid in 77% yield.

15; Mp: 204.0-208.2 °C (decomp.); ^{1}H NMR ($CDCl_3$): δ /ppm 8.06 (2H, dd, J= 0.8 Hz, 7.2 Hz), 7.64 (2H, d, J= 8.0 Hz), 7.27 (2H, dd, J= 2.0 Hz, 8.0 Hz), 7.15 (2H, ddd, J= 0.8 Hz, 7.2 Hz, 7.2 Hz), 7.14 (2H, d, J= 7.2 Hz), 6.90 (2H, ddd, J= 0.8 Hz, 7.2 Hz, 7.2 Hz), 6.70 (2H, d, J= 2.0 Hz), 6.23 (2H, s), 1.16 (18H, s); ^{13}C NMR ($CDCl_3$): δ/ppm 184.90, 149.94, 139.84, 134.78, 134.09, 133.99, 132.03, 130.39, 129.17, 128.31, 127.11, 126.53, 124.86, 123.88, 68.53, 56.84, 34.28, 31.22; IR (ATR): ν/cm^{-1} 3062, 3028, 2957, 2901, 2866, 1667, 1595, 1496, 1477, 1457, 1387, 1361, 1317, 1278, 1244, 1198, 1171, 1161, 1112, 1091, 1044, 963, 950, 933, 910, 893, 878, 829, 821, 814, 785, 763, 717, 689, 678, 662, 646, 620, 613, 571, 535, 520, 497, 474, 452; LR-MS (FD) m/z (%): 528.25 (14), 527.25 (43), 526.25 (M^+, bp); HR-MS (FD) Calcd. for $C_{37}H_{34}OS$: 526.23304; Found: 526.23141.

10-(2,8-Di-*tert*-butyl-5*H*-dibenzo[*a,d*]cycloheptatrien-5-ylidene)anthracen-9(10*H*)-one 16

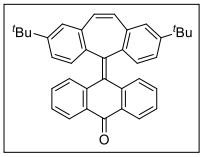

A solution of **15** (1.36 g, 2.58 mmol) and tri-*n*-butylphosphine (638 mg, 3.15 mmol) in dry toluene (30 mL) was heated to reflux for 15 h. After cooling to 25 °C, the precipitates were collected and washed with hexane three times. The resulting solid was dried in vacuo to give ketone **16** (1.16 g) as a pale-yellow solid in 91% yield.

16; Mp: 305.8-309.1 °C (decomp.); ^{1}H NMR ($CDCl_3$): δ /ppm 8.10 (2H, dd, J= 1.2 Hz, 7.6 Hz), 7.44 (2H, d, J= 2.0 Hz), 7.26 (2H, ddd, J= 1.2 Hz, 7.6 Hz, 7.6 Hz), 7.20 (2H, s), 7.14 (2H, dd, J= 2.0 Hz, 8.4 Hz), 6.96 (2H, ddd, J= 1.2 Hz, 7.6 Hz, 8.0 Hz), 6.70 (2H, d, J= 8.4 Hz), 6.52 (2H, dd, J= 1.2 Hz, 8.0 Hz), 1.31 (18H, s); ^{13}C NMR ($CDCl_3$): δ/ppm 186.26, 150.37, 142.49, 139.24, 135.89, 134.51, 133.46, 131.55, 129.86, 129.43, 128.88, 127.76, 127.01, 126.31, 126.16, 124.59, 34.57, 31.38; IR (ATR): ν/cm^{-1} 3062, 3027, 2952, 2902, 2864, 1772, 1659, 1597, 1465, 1457, 1384, 1360, 1306, 1282, 1202, 1173, 1162, 1151, 1135, 1114, 1092, 1037, 984, 963, 930, 908, 889, 858, 830, 822, 798, 779, 749, 717, 691, 679, 654, 642, 620, 603, 546, 509, 502, 458, 419; LR-MS (FD) m/z (%): 496.27 (9), 495.27 (42), 494.27 (M^+, bp); HR-MS (FD) Calcd. for $C_{37}H_{34}O$: 494.26096; Found: 494.26056.

10-(2,8-Di-*tert*-butyl-5*H*-dibenzo[*a,d*]cycloheptatrien-5-ylidene)anthracene-9(10*H*)-thione 17

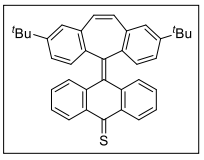

A solution of ketone **16** (1.27 g, 2.57 mmol) and 2,4-bis(4-methoxyphenyl)-1,3-dithia-2,4-diphosphetan-2,4-disulfide (Lawesson's reagent) (571 mg, 1.41 mmol) in dry toluene (27 mL) was heated to reflux for 4 h. After cooling to 26 °C, the resulting green solution was concentrated under reduced pressure. The crude product was purified by column chromatography on silica gel (CH_2Cl_2/hexane = 1/1, Rf = 0.65) to give thione **17** (1.29 g) as a green solid in 98% yield.

17; Mp: 273.5-274.3 °C (decomp.); ^{1}H NMR ($CDCl_3$): δ /ppm 8.31 (2H, dd, J= 1.2 Hz, 8.0 Hz), 7.44 (2H, d, J= 2.0 Hz), 7.20 (2H, s), 7.18 (2H, ddd, J= 1.2 Hz, 7.2 Hz, 8.0 Hz), 7.11 (2H, dd, J= 2.0 Hz, 8.0 Hz), 6.98 (2H, ddd, J= 1.2 Hz, 7.2 Hz, 8.0 Hz), 6.71 (2H, d, J= 8.0 Hz), 6.50 (2H, dd, J= 1.2 Hz, 8.0 Hz), 1.31 (18H, s); ^{13}C NMR ($CDCl_3$): δ/ppm 223.11, 150.40, 142.71, 141.64, 135.96, 134.34, 132.89, 131.55, 130.53, 129.44, 128.67, 128.12, 127.50, 126.89, 126.24, 124.60, 34.55, 31.34; IR (ATR): ν/cm^{-1} 3060, 3022, 2960, 2902, 2865, 1599, 1487, 1465, 1458, 1383, 1361, 1310, 1297, 1275, 1254, 1225, 1212, 1174, 1154, 1137, 1122, 1098, 1030, 959, 907, 886, 854, 829, 822, 796, 788, 771, 737, 705, 687, 656, 635, 621, 613, 607, 601, 505, 500, 452, 430; LR-MS (FD) m/z (%): 512.21 (15), 511.21 (43), 510.21 (M^+, bp); HR-MS (FD) Calcd. for $C_{37}H_{34}S$: 510.23812; Found: 510.23846.

10''-(2,8-Di-*tert*-butyl-5*H*-dibenzo[*a,d*]cycloheptatrien-5-ylidene)-10*H*,10''*H*-dispiro[anthracene-9,2'-thiirane-3',9''-anthracen]-10-one 18

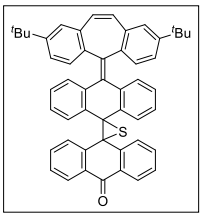

A solution of thione **17** (1.15 g, 2.25 mmol) and 10-diazoanthracen-9(10*H*)-one[58] (496 mg, 2.25 mmol) in dry THF (23 mL) was heated to reflux for 14 h. After cooling to 25 °C, the precipitates were collected and washed with ethanol three times. The resulting solid was dried in vacuo to give **18** (1.56 g) as a yellow solid in 98% yield.

18; Mp: 224.1-229.3 °C (decomp.); ^{1}H NMR ($CDCl_3$): δ /ppm 8.24-8.21 (2H, m), 7.98-7.95 (2H, m), 7.66 (2H, dd, J= 1.2 Hz, 8.0 Hz), 7.46-7.40 (4H, m), 7.25 (2H, d, J= 2.0 Hz), 6.96 (2H, s), 6.89 (2H, ddd, J= 1.2 Hz, 8.0 Hz, 8.0 Hz), 6.80 (2H, dd, J= 2.0 Hz, 8.0 Hz), 6.52 (2H, ddd, J= 1.2 Hz, 8.0 Hz, 8.0 Hz), 6.16 (2H, d, J= 8.0 Hz), 6.07 (2H, dd, J= 0.8 Hz, 8.0 Hz), 1.26 (18H, s); ^{13}C NMR ($CDCl_3$): δ/ppm 184.11, 149.48, 139.43 (2C), 138.06, 135.94, 135.48, 134.97, 134.45, 131.75, 131.58, 131.43, 129.45, 128.56, 128.27, 128.01, 127.69, 127.06, 125.65, 124.98, 124.58, 124.51, 66.63, 59.77, 34.33, 31.35; IR (ATR): ν/cm^{-1} 3056, 3025, 2962, 2902, 2866, 1667, 1596, 1466, 1457, 1383, 1362, 1312, 1267, 1204, 1172, 1159, 1135, 1116, 1092, 1042, 932, 900, 886, 851, 821, 801, 792, 782, 768, 750, 731, 704, 694, 688, 664, 649, 632, 610, 575, 519, 498, 475, 452, 436, 418; LR-MS (FD) m/z (%): 705.30 (9), 704.30 (24), 703.30 (60), 702.30 (M^{+}, bp); HR-MS (FD) Calcd. for $C_{51}H_{42}OS$: 702.29564; Found: 702.29704.

10'-(2,8-Di-*tert*-butyl-5*H*-dibenzo[*a,d*]cycloheptatrien-5-ylidene)-10*H*, 10'*H*-[9,9'-bianthracenylidene]-10-one 19

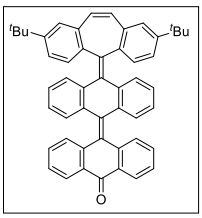

A solution of **18** (1.49 g, 2.12 mmol) and tri-*n*-butylphosphine (693 mg, 3.43 mmol) in dry toluene (20 mL) was heated to reflux for 14 h. After cooling to 25 °C, the precipitates were collected and washed with hexane three times. The resulting solid was dried in vacuo to give ketone **19** (1.29 g) as a pale yellow solid in 91% yield.

19; Mp: 196.9-206.3 °C (decomp.); ^{1}H NMR ($CDCl_3$): δ /ppm 8.19 (2H, dd, J= 1.2 Hz, 8.0 Hz), 7.46 (2H, d, J= 2.0 Hz), 7.45-7.41 (4H, m), 7.31 (2H, ddd, J= 1.2 Hz, 7.6 Hz, 9.2 Hz), 7.28 (2H, ddd, J= 2.0 Hz, 8.0 Hz), 7.19 (2H, s), 7.16 (2H, d, J= 8.0 Hz), 6.87-6.83 (2H, m), 6.77-6.72 (4H, m), 6.55-6.50 (2H, m), 1.36 (18H, s); ^{13}C NMR ($CDCl_3$): δ/ppm 186.61, 150.16, 139.37, 138.67, 137.96, 137.84, 137.81, 136.27, 135.01, 134.29, 134.11, 131.76, 130.04, 129.87, 128.97, 128.79, 127.89, 127.69, 126.79, 126.64, 125.90, 125.86, 125.00, 124.89, 34.58, 31.43; IR (ATR): ν/cm^{-1} 3064, 3022, 2955, 2903, 2867, 1663, 1598, 1496, 1457, 1450, 1383, 1361, 1305, 1275, 1202, 1170, 1144, 1092, 1038, 950, 931, 908, 896, 866, 844, 819, 798, 778, 766, 724,699, 688, 679, 657, 636, 590, 517, 499, 494, 454; LR-MS (FD) m/z (%): 673.35 (5), 672.35 (19), 671.34 (58), 670.34 (M^{+}, bp); HR-MS (FD) Calcd. for $C_{51}H_{42}O$: 670.32356; Found: 670.32242.

5,5'-(Anthracene-9,10-diyl)-bis(2,8-di-*tert*-butyl-5*H*-dibenzo[*a,d*]cycloheptatrien-5-ol) 1-OH

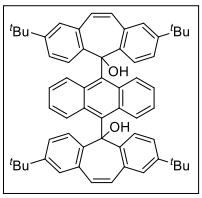

To a solution of 9,10-dibromoanthracene (233 mg, 0.694 mmol) in dry Et_2O (10 mL) was added ^{n}BuLi (1.58 M in hexane, 1.05 mL, 1.67 mmol) dropwise over 2 min at –20 °C. After stirring at –20 °C for 1 h, **13** (530 mg, 1.67 mmol) was added to the suspension and the mixture was warmed to 22 °C. The resulting solution was stirred at 22 °C for 1 h, and then diluted with water. The precipitates were collected and washed with water three times and with methanol three times. The resulting solid was washed with $CHCl_3$ dried in vacuo to give diol **1-OH** (241 mg) as a yellow solid in 43% yield.

1-OH; Mp: 233.0-251.2 °C (decomp.); ^{1}H NMR (DMSO-d_6): δ /ppm 8.23 (4H, d, J= 8.8 Hz), 7.58-7.54 (8H, m), 7.14 (2H, s), 7.06 (4H, d, J= 1.6 Hz), 6.41 (4H, s), 6.36 (4H, dd, J= 3.2 Hz, 7.2 Hz), 1.27 (36H, s); ^{13}C NMR (DMSO-d_6): δ/ppm 147.42, 144.74, 138.11, 131.68, 131.38, 130.16, 126.40, 125.67, 124.04, 122.40, 120.87, 78.39, 34.53, 31.72; IR (ATR): ν/cm^{-1} 3544, 3119, 3072, 3033, 3019, 2958, 2902, 2866, 1603, 1559, 1527, 1490, 1461, 1444, 1387, 1363, 1299, 1266, 1202, 1188, 1163, 1132, 1096, 1063, 1041, 990, 942, 905, 893, 829, 816, 801, 758, 736, 704, 699, 683, 653, 640, 622, 615, 547, 506, 482, 419; LR-MS (FD) m/z (%): 816.48 (20), 815.48 (66), 814.48 (M^+, bp), 576.19 (6), 574.19 (6), 497.28 (6), 496.28 (11), 318.20 (22); HR-MS (FD) Calcd. for $C_{60}H_{62}O_2$: 814.47498; Found: 814.47532.

5,5'-([9,9'-Bianthracene]-10,10'-diyl)-bis(2,8-di-*tert*-butyl-5*H*-dibenzo[*a,d*]cycloheptatrien-5-ol) 2-OH

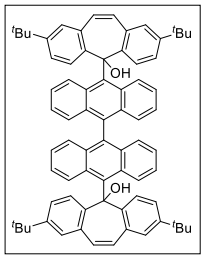

To a solution of 10,10'-dibromo-9,9'-bianthracene (362 mg, 0.706 mmol) in dry THF (8 mL) was added ^{n}BuLi (1.58 M in hexane, 1.07 mL, 1.69 mmol) dropwise over 2 min at –78 °C. After stirring at –78 °C for 1 h, **13** (538 mg, 1.69 mmol) was added to the suspension and the mixture was warmed to 21 °C. The resulting solution was stirred at 21 °C for 1 h, and then diluted with water. The whole mixture was extracted with EtOAc three times. The combined organic layers were washed with water and brine, and dried over anhydrous Na_2SO_4. After filtration, the solvent was concentrated under reduced pressure. The crude product was purified by column chromatography on silica gel (CH_2Cl_2/hexane = 1/1, Rf = 0.27) to give diol **2-OH** (340 mg) as a yellow solid in 49% yield.

2-OH; Mp: 221.9-225.4 °C (decomp.); ^{1}H NMR ($CDCl_3$): δ /ppm 8.43 (4H, d, J= 8.8 Hz), 7.66 (2H, dd, J= 0.8 Hz, 9.2 Hz), 7.62 (4H, dd, J= 1.6 Hz, 8.8 Hz), 7.42 (2H, dd, J= 0.8 Hz, 9.2 Hz), 6.98-6.88 (10H, m), 6.76 (2H, ddd, J= 0.8 Hz, 6.4 Hz, 8.4 Hz), 6.69 (2H, ddd, J= 2.4 Hz, 5.6 Hz, 9.2 Hz), 6.63 (2H, ddd, J= 1.6 Hz, 6.4 Hz, 9.2 Hz), 6.17 (4H, s), 3.70 (2H, s), 1.29 (18H, s), 1.28

(18H, s); ^{13}C NMR ($CDCl_3$): δ/ppm 148.42, 148.38, 143.77, 143.66, 136.37, 135.30, 131.61, 131.55, 131.24, 131.19, 130.93, 130.88, 130.18, 129.78, 126.67, 126.26, 125.81, 125.62, 125.56, 125.46, 124.78, 124.70, 124.37, 124.00, 122.52, 122.47, 121.66, 121.58, 79.87, 34.35, 31.43; IR (ATR): ν/cm^{-1} 3559, 3062, 3024, 2902, 2866, 1918, 1602, 1555, 1521, 1489, 1458, 1444, 1387, 1362, 1315, 1266, 1209, 1186, 1165, 1134, 1095, 1058, 1034, 991, 949, 906, 889, 883, 836, 821, 798, 756, 732, 699, 684, 676, 662, 633, 611, 578, 548, 507, 477, 449, 420; LR-MS (FD) m/z (%): 993.55 (10), 992.55 (36), 991.55 (83), 990.54 (M^+, bp),; HR-MS (FD) Calcd. for $C_{74}H_{70}O_2$: 990.53758; Found: 990.53711.

10,10''-Bis(2,8-di-*tert*-butyl-5*H*-dibenzo[*a,d*]cycloheptatrien-5-ylidene)-[9,9':10',9''-teranthracene]-9,9''(10*H*,10''*H*)-diol 3-OH

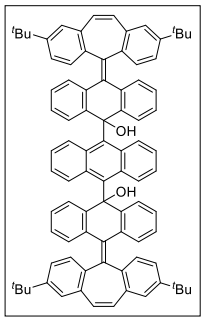

To a solution of 9,10-dibromoanthracene (300 mg, 0.894 mmol) in dry Et_2O (15 mL) was added ^{n}BuLi (1.58 M in hexane, 1.36 mL, 2.15 mmol) dropwise over 2 min at –20 °C. After stirring at –20 °C for 1 h, **16** (1.06 g, 2.15 mmol) was added to the suspension and the mixture was warmed to 21 °C. The resulting solution was stirred at 21 °C for 1 h, and then diluted with water. The whole mixture was extracted with CH_2Cl_2 three times. The combined organic layers were washed with water and brine, and dried over anhydrous Na_2SO_4. After filtration, the solvent was concentrated under reduced pressure. The crude product was purified by column chromatography on silica gel (toluene/hexane = 2/1, Rf = 0.067) to give diol **3-OH** (432 mg) as a yellow solid in 41% yield as a mixture of diastereomers, which were identified by FD-MS.

3-OH; Mp: 219.2-229.6 °C (decomp.); IR (ATR): ν/cm^{-1} 3531, 3060, 3022, 2954, 2902, 2866, 2367, 1675, 1601, 1495, 1458, 1444, 1383, 1361, 1304, 1284, 1269, 1252, 1202, 1169, 1135, 1116, 1079, 1030, 992, 951, 907, 890, 856, 838, 822, 795, 780, 758, 729, 700, 654, 631, 619, 501, 452, 425, 419; LR-MS (FD) m/z (%): 1170.61 (6), 1169.61 (18), 1168.61 (49), 1167.60 (99), 1166.60 (M^+, bp), 1151.61 (8), 1150.60 (12), 1149.59 (12), 673.35 (6), 672.34 (10), 583.80 (7), 495.27 (6), 494.26 (13); HR-MS (FD) Calcd. for $C_{88}H_{78}O_2$: 1166.60018; Found: 1166.60194.

10,10'''-Bis(2,8-di-*tert*-butyl-5*H*-dibenzo[*a,d*]cycloheptatrien-5-ylidene)-[9,9':10',9'':10'',9'''-quateranthracene]-9,9'''(10*H*,10'''*H*)-diol 4-OH

To a solution of 10,10'-dibromo-9,9'-bianthracene (393 mg, 0.767 mmol) in dry THF (10 mL) was added ^{n}BuLi (1.58 M in hexane, 1.16 mL, 1.84 mmol) dropwise over 2 min at –78 °C. After stirring at –78 °C for 1 h, **16** (911 mg, 1.84 mmol) was added to the suspension and the mixture was warmed to 26 °C. The resulting solution was stirred at 26 °C for 1 h, and then diluted with water. The whole mixture was extracted with CH_2Cl_2 three times. The combined organic layers

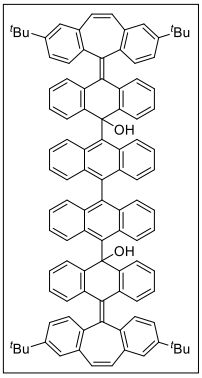

were washed with water and brine, and dried over anhydrous Na_2SO_4. After filtration, the solvent was concentrated under reduced pressure. The crude product was purified by column chromatography on silica gel (CH_2Cl_2/hexane = 2/1, Rf = 0.13) to give diol **4-OH** (378 mg) as a yellow solid in 37% yield as a mixture of diastereomers, which were identified by FD-MS.

4-OH; Mp: 271.0-281.1 °C (decomp.); IR (ATR): ν/cm^{-1} 3537, 3062, 3019, 2959, 2903, 2867, 1601, 1521, 1490, 1458, 1442, 1383, 1361, 1306, 1269, 1252, 1169, 1135, 1116, 1079, 1034, 992, 951, 908, 894, 871, 854, 838, 823, 796, 780, 761, 730, 679, 655, 627, 617, 605, 566, 536, 502, 451, 431, 419; LR-MS (FD) m/z (%): 1346.67 (8), 1345.67 (22), 1344.66 (56), 1343.66 (bp), 1342.66 (M^+, 89), 1327.66 (6), 1326.65 (9), 1325.65 (8), 671.83 (7), 671.33 (M^{2+}, 7), 496.28 (6), 495.27 (5), 494.26 (9); HR-MS (FD) Calcd. for $C_{102}H_{86}O_2$: 1342.66278; Found: 1342.66472.

10,10''''-Bis(2,8-di-*tert*-butyl-5*H*-dibenzo[*a,d*]cycloheptatrien-5-ylidene)-9'''*H*,10*H*,10'*H*, 10''''*H*-[9,9':10',9'':10'',9''':10''',9''''-quinqueanthracene]-9''',10'-diol 5-OH

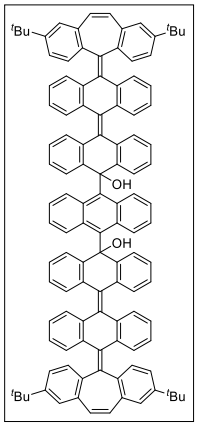

To a solution of 9,10-dibromoanthracene (236 mg, 0.702 mmol) in dry Et_2O (10 mL) was added ^{n}BuLi (1.58 M in hexane, 1.07 mL, 1.68 mmol) dropwise over 2 min at –20 °C. After stirring at –20 °C for 1 h, **19** (1.13 g, 1.68 mmol) was added to the suspension and the mixture was warmed to 24 °C. The resulting solution was stirred at 24 °C for 1 h, and then diluted with water. The whole mixture was extracted with CH_2Cl_2 three times. The combined organic layers were washed with water and brine, and dried over anhydrous Na_2SO_4. After filtration, the solvent was concentrated under reduced pressure. The crude product was purified by column chromatography on silica gel (toluene/hexane = 3/1, Rf = 0.089) to give diol **5-OH** (482 mg) as a yellow solid in 45% yield as a mixture of diastereomers, which were identified by FD-MS.

5-OH; Mp: 241.2-251.3 °C (decomp.); IR (ATR): ν/cm^{-1} 3567, 3061, 3021, 2960, 2903, 2865, 1675, 1599, 1490, 1457, 1448, 1384, 1361, 1304, 1284, 1264, 1252, 1203, 1170, 1118, 1093, 1039, 992, 951, 908, 891, 836, 818, 795, 759, 732, 700, 677, 664, 657, 633, 611, 582, 455; LR-MS (FD) m/z (%): 1522.71 (9), 1521.71 (28), 1520.70 (63), 1519.71 (bp), 1518.70 (M^+, 78), 1505.78 (6), 1504.71 (11), 1503.71 (18), 1502.70 (23), 1501.70 (18), 848.38 (6), 760.85 (5), 760.35 (9), 759.85 (M^{2+}, 14), 759.35 (11), 751.87 (6), 751.35 (7), 750.85 (5), 672.33 (5), 671.32 (6), 670.31 (7), 208.05 (6); HR-MS (FD) Calcd. for $C_{116}H_{94}O_2$: 1518.72538; Found: 1518.72590.

10,10''''-Bis(2,8-di-*tert*-butyl-5*H*-dibenzo[*a,d*]cycloheptatrien-5-ylidene)-9''''*H*,10*H*,10'*H*, 10''''*H*-[9,9':10',9'':10'',9''':10''',9'''':10'''',9''''':10''''',9''''''-sexianthracene]-9''''',10'-diol 6-OH

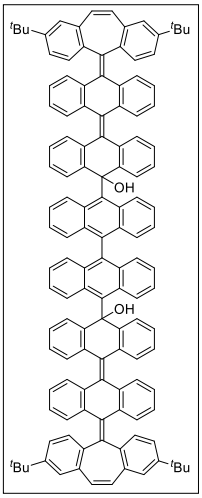

To a solution of 10,10'-dibromo-9,9'-bianthracene (354 mg, 0.691 mmol) in dry THF (8 mL) was added ^{n}BuLi (1.58 M in hexane, 1.05 mL, 1.66 mmol) dropwise over 2 min at –78 °C. After stirring at –78 °C for 1 h, **19** (1.11 g, 1.66 mmol) was added to the suspension and the mixture was warmed to 26 °C. The resulting solution was stirred at 26 °C for 1 h, and then diluted with water. The whole mixture was extracted with CH_2Cl_2 three times. The combined organic layers were washed with water and brine, and dried over anhydrous Na_2SO_4. After filtration, the solvent was concentrated under reduced pressure. The crude product was purified by column chromatography on silica gel (toluene/hexane = 3/1, Rf = 0.022) to give diol **6-OH** (682 mg) as a yellow solid in 58% yield as a mixture of diastereomers, which were identified by FD-MS.

6-OH; Mp: 283.5-296.7 °C (decomp.); IR (ATR): ν/cm^{-1} 3566, 3061, 3022, 2958, 2902, 2866, 1671, 1599, 1457, 1448, 1384, 1361, 1305, 1270, 1252, 1170, 1119, 1093, 1034, 993, 951, 932, 908, 890, 839, 818, 795, 760, 732, 711, 694, 676, 659, 637, 632, 606, 592, 583, 452; LR-MS (FD) m/z (%): 1698.74 (11), 1697.74 (38), 1696.74 (73), 1695.73 (bp), 1694.73 (M^+, 77), 1693.73 (8), 1682.78 (5), 1681.74 (10), 1680.75 (18), 1679.74 (31), 1678.74 (39), 1677.73 (29), 848.87 (5), 848.36 (8), 847.86 (11), 847.36 (M^{2+}, 8), 840.95 (5), 840.40 (10), 839.86 (14), 839.36 (15), 838.86 (10), 831.90 (6), 831.37 (8), 830.85 (8), 830.36 (6), 671.30 (11), 670.30 (16); HR-MS (FD) Calcd. for $C_{130}H_{102}O_2$: 1694.78798; Found: 1694.78725.

5,5'-(Anthracene-9,10-diyl)-bis(2,8-di-*tert*-butyl-5*H*-dibenzo[*a,d*]cycloheptatrien-5-ylium) bis(tetrafluoroborate) $\mathbf{1}^{2+}(BF_4^-)_2$

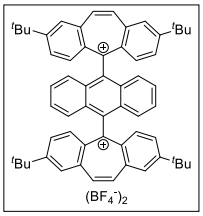

Dehydration of **1-OH** with HBF_4:

To a solution of diol **1-OH** (34.8 mg, 42.7 μmol) in trifluoroacetic anhydride (TFAA, 2.0 mL) was added 42% HBF_4 aq. (64 μL, 427 μmol) at 0 °C to give a deep red solution, and the mixture was stirred at 25 °C for 2 h. The addition of dry Et_2O led to precipitation of the dication salt. The supernatant solution was removed by decantation, and the precipitates were washed with dry Et_2O three times, and dried in vacuo to give $\mathbf{1}^{2+}(BF_4^-)_2$ (38.0 mg) as a red powder in 93% yield.

Oxidation of $\mathbf{1F}_{syn,anti}$ with $(4\text{-}BrC_6H_4)_3N^{+\bullet}BF_4^-$:

To a solution of $\mathbf{1F}_{syn,anti}$ (12.6 mg, 17.5 μmol) in dry CH_2Cl_2 (1 mL) was added $(4\text{-}BrC_6H_4)_3N^{+\bullet}BF_4^-$ (20.0 mg, 35.1 μmol) at 20 °C, and the mixture was stirred for 2 h. The addition of dry hexane led to precipitation of the dication salt. The supernatant solution was removed by

decantation, and the precipitates were washed with dry hexane three times, and dried in vacuo to give $\mathbf{1}^{2+}(BF_4^-)_2$ (16.6 mg) as a red powder in 99% yield.

$\mathbf{1}^{2+}(BF_4^-)_2$; Mp: 302.3-308.8 °C (decomp.); ^{1}H NMR (CD_3CN): δ /ppm 9.48 (4H, s), 8.95 (4H, dd, J= 1.2 Hz, 1.2 Hz), 8.22 (8H, d, J= 1.2 Hz), 7.32 (4H, dd, J= 3.2 Hz, 7.2 Hz), 7.16 (4H, dd, J= 3.2 Hz, 7.2 Hz), 1.58 (36H, s); ^{13}C NMR (CD_3CN): δ/ppm 177.47, 167.48, 147.67, 145.93, 139.06, 138.18, 137.85, 133.41, 133.22, 130.72, 128.82, 127.22, 37.34, 30.24; IR (ATR): ν/cm^{-1} 3061, 2969, 2908, 2872, 1792, 1761, 1601, 1505, 1478, 1412, 1380, 1363, 1322, 1277, 1194, 1147, 1120, 1088, 1065, 1027, 914, 851, 827, 780, 755, 693, 676, 667, 659, 615, 608, 531, 514, 442, 431, 419; LR-MS (FD) m/z (%): 870.55 (6), 869.55 (24), 868.54 (67), 867.54 ($M^{2+}BF_4^-$, bp), 866.54 (23), 851.53 (5), 850.53 (16), 849.53 (21), 782.53 (12), 781.53 (30), 780.53 (M^+, 43); HR-MS (FD) Calcd. for $C_{60}H_{60}$: 780.46950; Found: 780.46943.

5,5'-(Anthracene-9,10-diyl)-bis(2,8-di-*tert*-butyl-5*H*-dibenzo[*a,d*]cycloheptatrien-5-ylium) bis(hexachloroantimonate) $\mathbf{1}^{2+}(SbCl_6^-)_2$

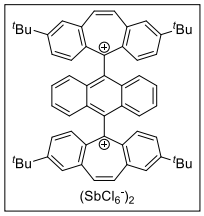

To a solution of $\mathbf{1F}_{anti,anti}$ (22.1 mg, 28.3 μmol) in dry CH_2Cl_2 (2 mL) was added $(2,4\text{-}Br_2C_6H_3)_3N^{+\bullet}SbCl_6^-$ (59.5 mg, 56.6 μmol) at 20 °C, and the mixture was stirred for 2 h. The addition of dry hexane led to precipitation of the dication salt. The supernatant solution was removed by decantation, and the precipitates were washed with dry hexane three times, and dried in vacuo to give $\mathbf{1}^{2+}(SbCl_6^-)_2$ (40.0 mg) as a red powder in 98% yield.

$\mathbf{1}^{2+}(SbCl_6^-)_2$; Mp: 247.8-250.4 °C (decomp.); ^{1}H NMR and ^{13}C NMR spectra are identical to those of $\mathbf{1}^{2+}(BF_4^-)_2$; IR (ATR): ν/cm^{-1} 3060, 2964, 2929, 2902, 2868, 2365, 1607, 1506, 1476, 1444, 1410, 1380, 1367, 1359, 1345, 1321, 1271, 1261, 1211, 1116, 1022, 957, 918, 909, 887, 855, 823, 778, 763, 731, 702, 694, 676, 669, 656, 613, 513, 436, 429; LR-MS (FD) m/z (%): 852.34 (7), 851.34 (8), 850.34 (9), 849.33 (6), 817.37 (5), 816.37 (10), 815.37 (12), 814.37 (14), 810.38 (6), 796.40 (8), 795.39 (9), 784.39 (6), 783.40 (16), 782.40 (38), 781.41 (69), 780.41 (M^+, bp), 768.40 (7), 767.40 (10), 755.40 (6), 754.39 (9), 391.20 (5), 390.70 (12), 390.20 (M^{2+}, 18); HR-MS (FD) Calcd. for $C_{60}H_{60}$: 780.46950; Found: 780.46775.

5,5'-([9,9'-Bianthracene]-10,10'-diyl)-bis(2,8-di-*tert*-butyl-5*H*-dibenzo[*a,d*]cycloheptatrien-5-ylium) bis(tetrafluoroborate) $\mathbf{2}^{2+}(BF_4^-)_2$

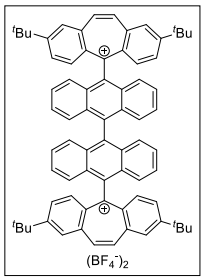

Dehydration of **2-OH** with HBF_4:

To a solution of diol **2-OH** (67.2 mg, 67.8 μmol) in trifluoroacetic anhydride (TFAA, 2.0 mL) was added 42% HBF_4 aq. (100 μL, 678 μmol) at 0 °C to give a deep red solution, and the mixture was stirred at 25 °C for 2 h. The addition of dry Et_2O led to precipitation of the dication salt. The

supernatant solution was removed by decantation, and the precipitates were washed with dry Et_2O three times, and dried in vacuo to give $\mathbf{2}^{2+}(BF_4^-)_2$ (77.5 mg) as a red powder in 100% yield.

Oxidation of **2T** with $(4\text{-}BrC_6H_4)_3N^{+\bullet}BF_4^-$:

To a solution of **2T** (20.5 mg, 21.4 μmol) in dry CH_2Cl_2 (1 mL) was added $(4\text{-}BrC_6H_4)_3N^{+\bullet}BF_4^-$ (24.3 mg, 42.8 μmol) at 20 °C, and the mixture was stirred for 2 h. The addition of dry hexane led to precipitation of the dication salt. The supernatant solution was removed by decantation, and the precipitates were washed with dry hexane three times, and dried in vacuo to give $\mathbf{2}^{2+}(BF_4^-)_2$ (24.3 mg) as a red powder in 100% yield.

$\mathbf{2}^{2+}(BF_4^-)_2$; Mp: 299.1-306.5 °C (decomp.); ^{1}H NMR (CD_3CN): δ /ppm 9.48 (4H, s), 8.96 (4H, d, J= 1.6 Hz), 8.27 (4H, d, J= 9.6 Hz), 8.23 (4H, dd, J= 1.6 Hz, 9.6 Hz), 7.70 (4H, dd, J= 1.2 Hz, 8.8 Hz), 7.46 (4H, ddd, J= 1.2 Hz, 6.4 Hz, 8.8 Hz),7.38 (4H, ddd, J= 1.2 Hz, 6.4 Hz, 8.8 Hz), 7.18 (4H, dd, J= 1.2 Hz, 8.8 Hz), 1.59 (36H, s); ^{13}C NMR (CD_3CN): δ/ppm 179.29, 167.40, 147.60, 145.75, 139.14, 138.52, 136.51, 136.09, 133.30, 133.20, 131.53, 131.30, 128.65, 127.83, 127.61, 127.17, 37.31, 30.26; IR (ATR): ν/cm^{-1} 3072, 2963, 2868, 1790, 1761, 1606, 1507, 1478, 1443, 1414, 1379, 1364, 1346, 1321, 1274, 1262, 1211, 1167, 1152, 1119, 1086, 1049, 1037, 1024, 957, 913, 878, 825, 780, 774, 760, 694, 685, 676, 660, 616, 593, 518, 440; LR-MS (FD) m/z (%): 959.60 (10), 958.60 (40), 957.59 (87), 956.59 (M^+, bp); HR-MS (FD) Calcd. for $C_{74}H_{68}$: 956.53210; Found: 956.53289.

5,5'-([9,9'-Bianthracene]-10,10'-diyl)-bis(2,8-di-*tert*-butyl-5*H*-dibenzo[*a,d*]cycloheptatrien-5-ylium) bis(hexafluorophosphate) $\mathbf{2}^{2+}(PF_6^-)_2$

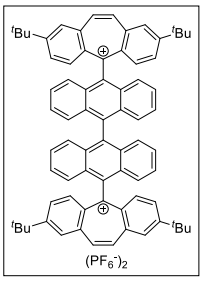

To a solution of diol **2-OH** (21.8 mg, 22.0 μmol) in trifluoroacetic anhydride (TFAA, 2.0 mL) was added 60% HPF_6 aq. (30 μL, 220 μmol) at 0 °C to give a deep red solution, and the mixture was stirred at 25 °C for 2 h. The addition of dry Et_2O led to precipitation of the dication salt. The supernatant solution was removed by decantation, and the precipitates were washed with dry Et_2O three times, and dried in vacuo to give $\mathbf{2}^{2+}(PF_6^-)_2$ (22.1 mg) as a red powder in 81% yield.

$\mathbf{2}^{2+}(PF_6^-)_2$; Mp: 223.6-242.9 °C (decomp.); ^{1}H NMR and ^{13}C NMR spectra are identical to those of $\mathbf{2}^{2+}(BF_4^-)_2$; IR (ATR): ν/cm^{-1} 3066, 2964, 2871, 1790, 1757, 1605, 1507, 1479, 1443, 1411, 1381, 1363, 1346, 1320, 1274, 1212, 1169, 1118, 1026, 957, 916, 877, 838, 831, 775, 762, 694, 675, 658, 615, 593, 556, 517, 495, 440; LR-MS (FD) m/z (%): 1105.58 (5), 1104.57 (11), 1103.57 (40), 1102.57 (88), 1101.57 ($M^{2+}PF_6^-$, bp), 973.59 (6), 972.58 (15), 971.58 (18), 959.59 (7), 958.60 (19), 957.59 (41), 956.59 (M^+, 47), 945.59 (5), 944.59 (12), 943.59 (13), 480.30 (6), 479.80 (12), 479.30 (28), 478.80 (51), 478.30 (M^{2+}, 55); HR-MS (FD) Calcd. for $C_{74}H_{68}$: 956.53210; Found: 956.53501.

5,5'-([9,9'-Bianthracene]-10,10'-diyl)-bis(2,8-di-*tert*-butyl-5*H*-dibenzo[*a,d*]cycloheptatrien-5-ylium) bis(hexachloroantimonate) $\mathbf{2}^{2+}(SbCl_6^-)_2$

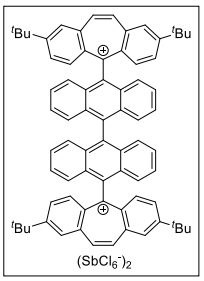

To a solution of **2F** (17.9 mg, 18.7 μmol) in dry CH_2Cl_2 (2 mL) was added $(2,4\text{-}Br_2C_6H_3)_3N^{+\bullet}SbCl_6^-$ (39.4 mg, 37.4 μmol) at 20 °C, and the mixture was stirred for 2 h. The addition of dry hexane led to precipitation of the dication salt. The supernatant solution was removed by decantation, and the precipitates were washed with dry hexane three times, and dried in vacuo to give $\mathbf{2}^{2+}(SbCl_6^-)_2$ (30.3 mg) as a red powder in 100% yield.

$\mathbf{2}^{2+}(SbCl_6^-)_2$; Mp: 215.7-219.1 °C (decomp.); ^{1}H NMR and ^{13}C NMR spectra are identical to those of $\mathbf{2}^{2+}(BF_4^-)_2$; IR (ATR): ν/cm^{-1} 3077, 3064, 2955, 2926, 2868, 2854, 1602, 1505, 1478, 1464, 1443, 1409, 1378, 1362, 1344, 1319, 1272, 1261, 1223, 1212, 1169, 1118, 1024, 957, 910, 893, 876, 822, 778, 773, 757, 694, 675, 657, 615, 588, 553, 518, 438, 426; LR-MS (FD) m/z (%): 972.46 (5), 960.47 (6), 959.47 (15), 958.48 (42), 957.48 (83), 956.47 (M^+, bp), 931.46 (6), 930.46 (7), 478.73 (6), 478.23 (M^{2+}, 7), 41.02 (5); HR-MS (FD) Calcd. for $C_{74}H_{68}$: 956.53210; Found: 956.53416.

5,5'-([9,9':10',9''-Teranthracene]-10,10''-diyl)-bis(2,8-di-*tert*-butyl-5*H*-dibenzo[*a,d*]cycloheptatrien-5-ylium) bis(tetrafluoroborate) $\mathbf{3}^{2+}(BF_4^-)_2$

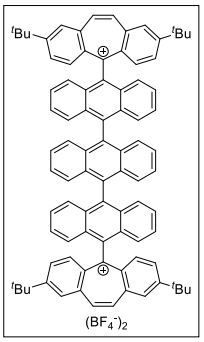

Dehydration of **3-OH** with HBF_4:

To a solution of diol **3-OH** (49.7 mg, 42.6 μmol) in trifluoroacetic anhydride (TFAA, 2 mL) was added 42% HBF_4 aq. (64 μL, 0.426 mmol) at 0 °C to give a deep red solution, and the mixture was stirred at 26 °C for 2 h. The addition of dry Et_2O led to precipitation of the dication salt. The supernatant solution was removed by decantation, and the precipitates were washed with dry Et_2O three times, and dried in vacuo to give $\mathbf{3}^{2+}(BF_4^-)_2$ (55.2 mg) as a red powder in 99% yield.

Oxidation of **3T** with $(4\text{-}BrC_6H_4)_3N^{+\bullet}BF_4^-$:

To a solution of **3T** (14.0 mg, 12.4 μmol) in dry CH_2Cl_2 (1 mL) was added $(4\text{-}BrC_6H_4)_3N^{+\bullet}BF_4^-$ (14.0 mg, 24.7 μmol) at 19 °C, and the mixture was stirred for 2 h. The addition of dry hexane led to precipitation of the dication salt. The supernatant solution was removed by decantation, and the precipitates were washed with dry hexane three times, and dried in vacuo to give $\mathbf{3}^{2+}(BF_4^-)_2$ (15.5 mg) as a red powder in 96% yield.

$\mathbf{3}^{2+}(BF_4^-)_2$; Mp: 310.5-336.4 °C (decomp.); ^{1}H NMR (CD_3CN): δ /ppm 9.47 (4H, s), 8.96 (4H, d, J= 1.6 Hz), 8.28 (4H, d, J= 9.2 Hz), 8.24 (4H, dd, J= 1.6 Hz, 9.2 Hz), 7.69 (4H, dd, J= 3.6 Hz, 7.2 Hz), 7.67 (4H, dd, J= 1.2 Hz, 8.4 Hz), 7.51 (4H, dd, J= 3.6 Hz, 7.2 Hz), 7.44 (4H, ddd, J= 1.2 Hz, 6.4 Hz, 8.4 Hz),7.38 (4H, ddd, J= 1.2 Hz, 6.4 Hz, 8.4 Hz), 7.18 (4H, dd, J= 1.2 Hz, 8.4 Hz),

1.59 (36H, s); ^{13}C NMR (CD_3CN): δ/ppm 179.56, 167.41, 147.59, 145.72, 139.17, 138.59, 137.66, 135.73, 134.23, 133.32, 133.19, 132.11, 131.70, 131.37, 128.62, 127.94, 127.80, 127.44, 127.37, 127.13, 37.32, 30.28; IR (ATR): ν/cm^{-1} 3060, 2966, 2907, 2870, 1759, 1604, 1506, 1479, 1441, 1412, 1379, 1363, 1319, 1275, 1197, 1148, 1117, 1056, 1025, 957, 914, 889, 850, 825, 778, 757, 694, 675, 654, 617, 599, 592, 520, 441, 420; LR-MS (FD) m/z (%): 1245.65 (8), 1220.67 (9), 1219.66($M^{2+}BF_4^-$, 9), 1203.68 (6), 1202.66 (13), 1201.66 (11), 1149.65 (8), 1148.65 (13), 1147.65 (17), 1136.66 (6), 1135.66 (22), 1134.67 (51), 1133.66 (bp), 1132.67 (M^+, 93), 1120.66 (9), 1119.66 (10), 780.51 (5), 711.44 (6), 670.37 (6), 656.39 (25), 655.38 (37), 567.83 (13), 567.33 (22), 566.84 (34), 566.33 (30); HR-MS (FD) Calcd. for $C_{88}H_{76}$: 1132.59470; Found: 1132.59360.

5,5'-([9,9':10',9'':10'',9'''-Quateranthracene]-10,10'''-diyl)-bis(2,8-di-*tert*-butyl-5*H*-dibenzo[*a,d*]cycloheptatrien-5-ylium) bis(tetrafluoroborate) $4^{2+}(BF_4^-)_2$

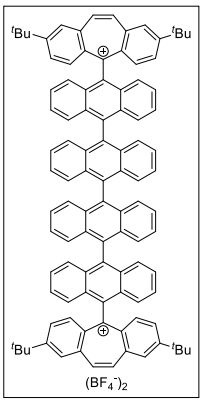

Dehydration of **4-OH** with HBF_4:

To a solution of diol **4-OH** (43.4 mg, 32.3 μmol) in trifluoroacetic anhydride (TFAA, 2 mL) was added 42% HBF_4 aq. (50 μL, 0.323 mmol) at 0 °C to give a deep red solution, and the mixture was stirred at 27 °C for 2 h. The addition of dry Et_2O led to precipitation of the dication salt. The supernatant solution was removed by decantation, and the precipitates were washed with dry Et_2O three times, and dried in vacuo to give $\mathbf{4}^{2+}(BF_4^-)_2$ (48.0 mg) as a red powder in 100% yield.

Oxidation of **4T** with $(4\text{-}BrC_6H_4)_3N^{+\bullet}BF_4^-$:

To a solution of **4T** (11.6 mg, 8.86 μmol) in dry CH_2Cl_2 (1 mL) was added $(4\text{-}BrC_6H_4)_3N^{+\bullet}BF_4^-$ (10.0 mg, 17.7 μmol) at 20 °C, and the mixture was stirred for 2 h. The addition of dry hexane led to precipitation of the dication salt. The supernatant solution was removed by decantation, and the precipitates were washed with dry hexane three times, and dried in vacuo to give $\mathbf{4}^{2+}(BF_4^-)_2$ (12.5 mg) as a red powder in 95% yield.

$\mathbf{4}^{2+}(BF_4^-)_2$; Mp: 292.9-306.0 °C (decomp.); ^{1}H NMR (CD_3CN): δ /ppm 9.48 (4H, s), 8.96 (4H, d, J= 2.0 Hz), 8.29 (4H, d, J= 9.2 Hz), 8.25 (4H, dd, J= 2.0 Hz, 9.2 Hz), 7.72-7.65 (12H, m), 7.53-7.48 (8H, m), 7.47 (4H, ddd, J= 1.2 Hz, 6.4 Hz, 8.4 Hz), 7.39 (4H, ddd, J= 1.2 Hz, 6.4 Hz, 8.4 Hz), 7.19 (4H, dd, J= 1.2 Hz, 8.4 Hz), 1.59 (36H, s); ^{13}C NMR (CD_3CN): δ/ppm 179.62, 167.40, 147.59, 145.71, 139.18, 138.60, 137.82, 135.68, 135.34, 133.79, 133.33, 133.19, 132.28, 132.15, 131.73, 131.38, 128.61, 127.97, 127.92, 127.76, 127.44, 127.33, 127.20, 127.13, 37.32, 30.28; IR (ATR): ν/cm^{-1} 3060, 2963, 2907, 2872, 1792, 1756, 1603, 1506, 1479, 1441, 1410, 1379, 1346, 1318, 1275, 1204, 1159, 1150, 1117, 1024, 956, 914, 896, 852, 826, 777, 756, 694, 675, 653, 616, 610, 599, 593, 519, 440, 420; LR-MS (FD) m/z (%): 1424.70 (8), 1423.71 (12), 1422.72 (18), 1421.71 (15), 1397.73 (6), 1396.72 (10), 1395.74 ($M^{2+}BF_4^-$, 11), 1380.71 (8), 1379.71 (15),

1378.73 (27), 1377.72 (23), 1324.74 (6), 1312.69 (9), 1311.71 (28), 1310.72 (64), 1309.72 (bp), 1308.72 (M^+, 83), 1296.71 (5), 1295.70 (5), 1133.67 (5), 944.44 (9), 943.42 (10), 847.43 (9), 846.44 (8), 833.47 (6), 832.45 (15), 831.45 (22), 655.87 (18), 655.38 (23), 654.87 (32), 654.37 (M^{2+}, 26), 479.31 (5); HR-MS (FD) Calcd. for $C_{102}H_{84}$: 1308.65730; Found: 1308.65617.

5,5'-([9,9':10',9'':10'',9''':10''',9''''-Quinqueanthracene]-10,10''''-diyl)-bis(2,8-di-*tert*-butyl-5*H*-dibenzo[*a,d*]cycloheptatrien-5-ylium) bis(tetrafluoroborate) $5^{2+}(BF_4^-)_2$

Dehydration of **5-OH** with HBF_4:

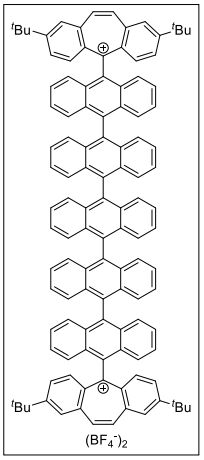

To a solution of diol **5-OH** (56.6 mg, 37.2 μmol) in trifluoroacetic anhydride (TFAA, 2 mL) was added 42% HBF_4 aq. (56 μL, 0.362 mmol) at 0 °C to give a deep red solution, and the mixture was stirred at 25 °C for 2 h. The addition of dry Et_2O led to precipitation of the dication salt. The supernatant solution was removed by decantation, and the precipitates were washed with dry Et_2O three times, and dried in vacuo to give $\mathbf{5}^{2+}(BF_4^-)_2$ (62.0 mg) as a red powder in 100% yield.

Oxidation of **5T** with $(4\text{-}BrC_6H_4)_3N^{+\bullet}BF_4^-$:

To a solution of **5T** (11.4 mg, 7.67 μmol) in dry CH_2Cl_2 (1 mL) was added $(4\text{-}BrC_6H_4)_3N^{+\bullet}BF_4^-$ (8.7 mg, 15.3 μmol) at 19 °C, and the mixture was stirred for 2 h. The addition of dry hexane led to precipitation of the dication salt. The supernatant solution was removed by decantation, and the precipitates were washed with dry hexane three times, and dried in vacuo to give $\mathbf{5}^{2+}(BF_4^-)_2$ (12.6 mg) as a red powder in 99% yield.

$\mathbf{5}^{2+}(BF_4^-)_2$; Mp: 285.9-288.7 °C (decomp.); ^{1}H NMR (CD_3CN): δ /ppm 9.48 (4H, s), 8.97 (4H, d, J= 1.6 Hz), 8.30 (4H, d, J= 9.6 Hz), 8.26 (4H, dd, J= 1.6 Hz, 9.6 Hz), 7.73-7.68 (16H, m), 7.53-7.48 (12H, m), 7.47 (4H, ddd, J= 1.2 Hz, 6.4 Hz, 8.4 Hz), 7.40 (4H, ddd, J= 1.2 Hz, 6.4 Hz, 8.4 Hz), 7.19 (4H, dd, J= 1.2 Hz, 8.4 Hz), 1.60 (36H, s); ^{13}C NMR (CD_3CN): δ/ppm 179.64, 167.41, 147.58, 145.70, 139.19, 138.60, 137.85, 135.67, 135.49, 134.89, 133.73, 133.33, 133.18, 132.33, 132.31, 132.17, 131.74, 131.38, 128.62, 127.98, 127.95, 127.88, 127.76, 127.45, 127.33, 127.20, 127.15, 127.13, 37.32, 30.28; IR (ATR): ν/cm^{-1} 3197, 3060, 2965, 2870, 1761, 1603, 1505, 1479, 1440, 1411, 1379, 1363, 1316, 1275, 1199, 1149, 1117, 1024, 956, 913, 900, 851, 826, 756, 694, 675, 652, 615, 599, 592, 519, 431, 416; LR-MS (ESI) m/z (%): 1486.72 (1), 1485.72 (1), 1484.72 (M^+, 1), 744.36 (8), 743.86 (27), 743.36 (61), 742.86 (bp), 742.36 (M^{2+}, 83), 655.34 (5), 453.17 (10), 415.21 (5), 316.21 (7); HR-MS (ESI) Calcd. for $C_{116}H_{92}$: 742.35940 (M^{2+}); Found: 742.35889.

5,5'-([9,9':10',9'':10'',9''':10''',9'''':10'''',9''''':10''''',9'''''-Sexianthracene]-10,10'''''-diyl)-bis(2,8-di-*tert*-butyl-5*H*-dibenzo[*a,d*]cycloheptatrien-5-ylium) bis(tetrafluoroborate) $\mathbf{6}^{2+}(BF_4^-)_2$

Dehydration of **6-OH** with HBF_4:

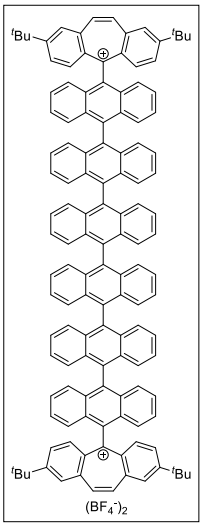

To a solution of diol **6-OH** (60.7 mg, 35.8 μmol) in trifluoroacetic anhydride (TFAA, 2 mL) was added 42% HBF_4 aq. (54 μL, 0.358 mmol) at 0 °C to give a deep red solution, and the mixture was stirred at 25 °C for 2 h. The addition of dry Et_2O led to precipitation of the dication salt. The supernatant solution was removed by decantation, and the precipitates were washed with dry Et_2O three times, and dried in vacuo to give $\mathbf{6}^{2+}(BF_4^-)_2$ (65.8 mg) as a red powder in 100% yield.

Oxidation of **6T** with $(4\text{-}BrC_6H_4)_3N^{+\bullet}BF_4^-$:

To a solution of **6T** (13.1 mg, 7.88 μmol) in dry CH_2Cl_2 (1 mL) was added $(4\text{-}BrC_6H_4)_3N^{+\bullet}BF_4^-$ (9.0 mg, 15.8 μmol) at 20 °C, and the mixture was stirred for 2 h. The addition of dry hexane led to precipitation of the dication salt. The supernatant solution was removed by decantation, and the precipitates were washed with dry hexane three times, and dried in vacuo to give $\mathbf{6}^{2+}(BF_4^-)_2$ (14.0 mg) as a red powder in 97% yield.

$\mathbf{6}^{2+}(BF_4^-)_2$; Mp: 287.9-296.8 °C (decomp.); ^{1}H NMR (CD_3CN): δ /ppm 9.48 (4H, s), 8.96 (4H, d, J= 2.0 Hz), 8.30 (4H, d, J= 9.26 Hz), 8.26 (4H, dd, J= 2.0 Hz, 9.6 Hz), 7.74-7.68 (20H, m), 7.54-7.50 (16H, m), 7.48 (4H, ddd, J= 0.8 Hz, 6.4 Hz, 8.8 Hz), 7.40 (4H, ddd, J= 0.8 Hz, 6.4 Hz, 8.4 Hz), 7.20 (4H, dd, J= 0.8 Hz, 8.4 Hz), 1.60 (36H, s); ^{13}C NMR (CD_3CN): δ/ppm 179.61, 167.43, 147.58, 145.67, 139.22, 138.63, 137.89, 137.43, 135.54, 135.05, 134.85, 133.73, 133.36, 133.20, 132.38, 132.36, 132.33, 132.19, 131.76, 131.38, 128.63, 128.01, 127.98, 127.91, 127.89, 127.76, 127.46, 127.34, 127.21, 127.16 (3C), 37.34, 30.29; IR (ATR): ν/cm^{-1} 3206, 3060, 2968, 2909, 2872, 1784, 1761, 1603, 1506, 1479, 1439, 1412, 1378, 1363, 1316, 1275, 1206, 1156, 1117, 1024, 956, 913, 903, 851, 823, 755, 700, 675, 651, 615, 599, 519, 440, 431, 419; LR-MS (ESI) m/z (%): 1662.79 (2), 1661.78 (3), 1660.78 (M^+, 2), 1023.45 (8), 832.40 (12), 831.89 (33), 831.39 (70), 830.89 (bp), 830.39 (M^{2+}, 66), 671.33 (11), 479.28 (5); HR-MS (ESI) Calcd. for $C_{130}H_{100}$: 830.39070 (M^{2+}); Found: 830.39020.

5,5'-([9,9':10',9'':10'',9''':10''',9'''':10'''',9''''':10''''',9'''''-Sexianthracene]-10,10'''''-diyl)-bis(2,8-di-*tert*-butyl-5*H*-dibenzo[*a,d*]cycloheptatrien-5-ylium) bis(trifluoromethanesulfonyl)imide $\mathbf{6}^{2+}(NTf_2^-)_2$

To a solution of diol **6-OH** (33.7 mg, 19.9 μmol) in CH_2Cl_2 (2 mL) was added bis(trifluoromethanesulfonyl)imide ($HNTf_2$) (36.0 mg, 0.128 mmol) at 0 °C to give a deep red solution, and the mixture was stirred at 25 °C for 2 h. The addition of dry Et_2O led to precipitation of the dication salt. The supernatant solution was removed by decantation, and the precipitates

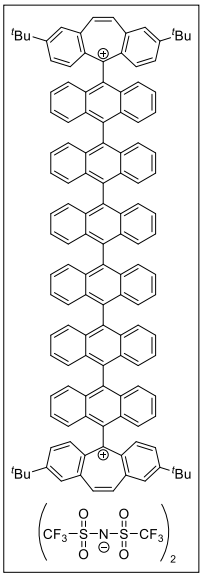

were washed with dry Et_2O three times, and dried in vacuo to give $\mathbf{6}^{2+}(NTf_2^-)_2$ (39.4 mg) as a red powder in 89% yield.

$\mathbf{6}^{2+}(NTf_2^-)_2$; Mp: 244.5-254.3 °C (decomp.); ^{1}H NMR and ^{13}C NMR spectra are identical to those of $\mathbf{6}^{2+}(BF_4^-)_2$; IR (ATR): ν/cm^{-1} 3060, 2967, 2908, 2870, 1799, 1706, 1603, 1506, 1479, 1439, 1412, 1379, 1345, 1316, 1275, 1224, 1181, 1132, 1117, 1054, 1024, 957, 914, 903, 825, 789, 779, 756, 738, 674, 651, 613, 598, 569, 507, 431, 419; LR-MS (FD) m/z (%): 1945.84 (5), 1944.88 (17), 1943.88 (38), 1942.87 (59), 1941.87 (73), 1940.87 ($M^{2+}NTf_2^-$, 42), 1677.91 (6), 1676.91 (5), 1675.90 (5), 1664.89 (5), 1663.96 (8), 1662.93 (11), 1661.95 (12), 1660.96 (M^+, 5), 1649.93 (5), 1647.92 (6), 1108.66 (5), 1057.55 (8), 1056.55 (19), 1055.54 (23), 1054.52 (20), 1053.52 (19), 1039.54 (5), 1038.54 (7), 1037.53 (6), 1026.45 (7), 1025.54 (14), 1024.55 (44), 1023.55 (88), 1022.54 (bp), 832.45 (20), 831.96 (28), 831.47 (48), 830.97 (62), 830.48 (M^{2+}, 40), 671.39 (9), 670.38 (14); HR-MS (FD) Calcd. for $C_{130}H_{100}$: 1660.78250; Found: 1660.78505.

9,10-Bis(2,8-di-*tert*-butyl-5*H*-dibenzo[*a,d*]cycloheptatrien-5-ylidene)-9,10-dihydroanthracene 1F$_{anti,anti}$

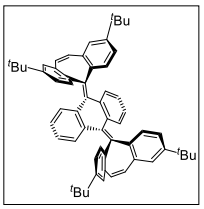

To a solution of $\mathbf{1}^{2+}(BF_4^-)_2$ (79.0 mg, 82.7 μmol) in dry CH_3CN (5 mL) was added activated zinc powder (108 mg, 1.65 mmol) at 22 °C. The mixture was stirred at 22 °C for 5 min under sonication, and then diluted with water. The whole mixture was extracted with CH_2Cl_2 three times. The combined organic layers were washed with water and brine, and dried over anhydrous Na_2SO_4. After filtration through silica gel, the solvent was concentrated under reduced pressure to give ca. 2:1 mixture of $\mathbf{1F}_{anti,anti}$ and $\mathbf{1F}_{syn,anti}$ as a white solid. Then, a solution of the whole mixture in dimethylsulfoxide (DMSO, 8 mL) was refluxed for 1.5 h. After cooling to 22 °C, the resulting solution was diluted with water. The whole mixture was extracted with CH_2Cl_2 three times. The combined organic layers were washed with water and brine, and dried over anhydrous Na_2SO_4. After filtration through silica gel, the solvent was concentrated under reduced pressure to give $\mathbf{1F}_{anti,anti}$ (64.5 mg) as a white solid in 100% yield.

$\mathbf{1F}_{anti,anti}$; Mp: 310.3-317.6 °C (decomp.); ^{1}H NMR ($CDCl_3$): δ /ppm 7.42 (4H, d, J= 1.6 Hz), 7.24 (4H, dd, J= 1.6 Hz, 8.0 Hz), 7.16 (4H, s), 7.05 (4H, d, J= 8.0 Hz), 6.57 (4H, dd, J= 3.2 Hz, 5.6 Hz), 6.42 (4H, dd, J= 3.2 Hz, 5.6 Hz), 1.34 (36H, s); ^{13}C NMR ($CDCl_3$): δ/ppm 149.66, 137.72, 136.83, 136.78, 135.11, 134.51, 131.78, 128.96, 127.96, 125.77, 124.85, 124.53, 34.52, 31.43; IR (ATR): ν/cm^{-1} 3065, 3014, 2958, 2928, 2902, 2866, 1601, 1495, 1462, 1386, 1361, 1282, 1265, 1251, 1204, 1193, 1173, 1163, 1125, 1112, 1042, 1026, 948, 906, 888, 846, 824, 818, 793, 785, 762, 749, 734, 723, 714, 672, 651, 601, 557, 545, 498, 460, 457, 423, 419; LR-MS (FD) m/z (%):

783.55 (5), 782.55 (25), 781.54 (68), 780.54 (M^+, bp); HR-MS (FD) Calcd. for $C_{60}H_{60}$: 780.46950; Found: 780.46835; Fluorescence (CH_2Cl_2, λ_{ex} = 290 nm): λ_{em}/nm (Φ_F) 429 (0.21).

9,10-Bis(2,8-di-*tert*-butyl-5*H*-dibenzo[*a,d*]cycloheptatrien-5-ylidene)-9,10-dihydroanthracene 1F$_{syn,anti}$

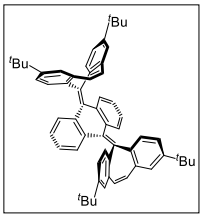

A solution of **1F**$_{anti,anti}$ (39.1 mg, 50.1 μmol, 2.5×10^{-3} mol L^{-1}) in CH_2Cl_2 (20 mL) was degassed by Ar bubbling, and then photoirradiated with an Ushiospax SX-UID501XAMQ light source device and a CORNING COLOR FILTER (No. O-51) at 24 °C for 5 h (λ> 360 nm). The solvent was concentrated under reduced pressure to give **1F**$_{syn,anti}$ (38.4 mg) as a white solid in 98% yield.

1F$_{syn,anti}$; Mp: 289.0-298.6 °C (decomp.); ^{1}H NMR ($CDCl_3$): δ /ppm 7.74 (2H, d, J= 8.0 Hz), 7.49 (2H, dd, J= 1.2 Hz, 7.6 Hz), 7.43 (2H, dd, J= 2.0 Hz, 8.0 Hz), 7.30 (2H, d, J= 2.0 Hz), 7.26 (2H, d, J= 2.0 Hz), 7.05 (2H, s), 6.93 (2H, dd, J= 2.0 Hz, 8.0 Hz), 6.91 (2H, s), 6.77 (2H, ddd, J= 1.2 Hz, 7.6 Hz, 7.6 Hz), 6.63 (2H, d, J= 8.0 Hz), 6.55 (2H, ddd, J= 1.2 Hz, 7.6 Hz, 7.6 Hz), 6.28 (2H, dd, J= 1.2 Hz, 7.6 Hz), 1.32 (18H, s), 1.26 (18H, s); ^{13}C NMR ($CDCl_3$): δ/ppm 149.34, 148.93, 138.26, 137.49, 137.36, 136.65, 136.59, 136.26, 135.75, 135.01, 135.01, 133.25, 131.62, 131.14, 129.40, 129.09, 127.38, 127.34, 125.04, 124.62, 124.54, 124.51, 123.95, 123.84, 34.47, 34.36, 31.42, 31.34; IR (ATR): ν/cm^{-1} 3062, 3016, 2958, 2902, 2865, 1601, 1540, 1490, 1478, 1458, 1384, 1361, 1266, 1252, 1203, 1168, 1122, 1025, 944, 910, 904, 888, 848, 827, 818, 795, 781, 763, 726, 714, 706, 693, 675, 664, 653, 632, 599, 559, 500, 452, 446, 429; LR-MS (FD) m/z (%): 783.56 (7), 782.56 (25), 781.56 (69),780.56 (M^+, bp); HR-MS (FD) Calcd. for $C_{60}H_{60}$: 780.46950; Found: 780.47042; Fluorescence (CH_2Cl_2, λ_{ex} = 290 nm): λ_{em}/nm (Φ_F) 443 (0.17).

5,5'-([9,9'-Bianthracene]-10,10'-diyl)-bis(2,8-di-*tert*-butyl-5*H*-dibenzo[*a,d*]cycloheptatrien-5-yl) 2T

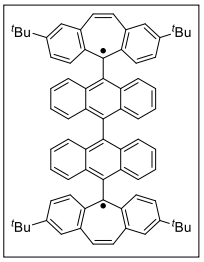

To a solution of $\mathbf{2}^{2+}(BF_4^-)_2$ (64.0 mg, 56.6 μmol) in dry CH_3CN (6 mL) was added activated zinc powder (74.2 mg, 1.13 mmol) at 26 °C. The mixture was stirred at 26 °C for 5 min under sonication, and then diluted with water. The whole mixture was extracted with CH_2Cl_2 three times. The combined organic layers were washed with water and brine, and dried over anhydrous Na_2SO_4. After filtration, the solvent was concentrated under reduced pressure to give **2T** (54.2 g) as a deep green solid in 100% yield.

2T; Mp: 240.7-274.1 °C (decomp.); IR (ATR): ν/cm^{-1} 3059, 3027, 2956, 2901, 2864, 1950, 1914, 1772, 1714, 1582, 1527, 1517, 1476, 1454, 1438, 1383, 1359, 1301, 1279, 1265, 1247, 1200, 1162, 1146, 1126, 1117, 1025, 954, 912, 894, 877, 854, 832, 824, 794, 767, 760, 734, 703, 685, 643, 608, 582, 436, 409; LR-MS (FD) m/z (%): 972.57 (5), 959.58 (12), 958.57 (37), 957.57

(84), 956.57 (M^+, bp); HR-MS (FD) Calcd. for $C_{74}H_{68}$: 956.53210; Found: 956.53321.

10,10'-Bis(2,8-di-*tert*-butyl-5*H*-dibenzo[a,d]cycloheptatrien-5-ylidene)-10*H*,10'*H*-9,9'-bianthracenylidene 2F

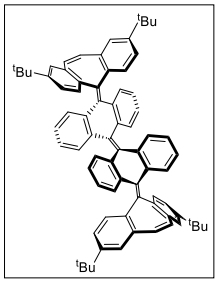

A solution of **2T** (19.0 mg, 19.8 μmol) in toluene (5 mL) was degassed by Ar bubbling, and then heated at 100 °C for 20 min. After cooling to 25 °C, the resulting solution was concentrated under reduced pressure. The resulting residue was washed with hexane three times, and dried in vacuo to give **2F** (15.0 mg) as a white solid in 79% yield.

2F; Mp: 333.5-350.5 °C (decomp.); ^{1}H NMR ($CDCl_3$): δ /ppm 7.45 (4H, d, J= 1.6 Hz), 7.25 (4H, dd, J= 1.6 Hz, 8.0 Hz), 7.21 (4H, dd, J= 1.2 Hz, 7.6 Hz), 7.20 (4H, s), 7.12 (4H, d, J= 8.0 Hz), 6.89 (4H, ddd, J= 1.2Hz, 7.6 Hz, 7.6 Hz), 6.75 (4H, dd, J= 1.2 Hz, 7.6 Hz, 7.6 Hz), 6.55 (4H, dd, J= 1.2 Hz, 7.6 Hz), 1.35 (36H, s); ^{13}C NMR ($CDCl_3$): δ/ppm 149.85, 138.30, 138.01, 137.18, 136.62, 135.06, 134.53, 132.09, 131.78, 129.06, 128.64, 128.30, 125.90, 125.25, 124.84, 124.81, 34.54, 31.43; IR (ATR): ν/cm^{-1} 3060, 3022, 2954, 2930, 2903, 2866, 1598, 1496, 1458, 1449, 1394, 1384, 1361, 1271, 1252, 1202, 1171, 1154, 1126, 1113, 1038, 1024, 948, 934, 910, 892, 835, 815, 799, 783, 758, 752, 729, 694, 678, 667, 652, 636, 583, 500, 453, 420; LR-MS (FD) m/z (%): 959.48 (9), 958.48 (36), 957.48 (83), 956.47 (M^+, bp); HR-MS (FD) Calcd. for $C_{74}H_{68}$: 956.53210; Found: 956.53410; Fluorescence (CH_2Cl_2, λ_{ex} = 290 nm): λ_{em}/nm (Φ_F) 450 (0.41).

5,5'-([9,9':10',9''-Teranthracene]-10,10''-diyl)-bis(2,8-di-*tert*-butyl-5*H*-dibenzo[*a,d*]cycloheptatrien-5-yl) 3T

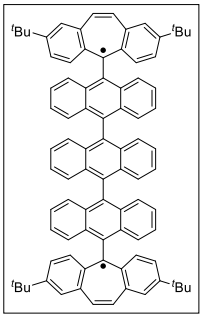

To a solution of $\mathbf{3}^{2+}(BF_4^-)_2$ (31.0 mg, 23.7 μmol) in dry CH_3CN (3 mL) was added activated zinc powder (31.0 mg, 0.474 mmol) at 23 °C. The mixture was stirred at 23 °C for 5 min under sonication, and then diluted with water. The whole mixture was extracted with CH_2Cl_2 three times. The combined organic layers were washed with water and brine, and dried over anhydrous Na_2SO_4. After filtration, the solvent was concentrated under reduced pressure to give **3T** (26.9 mg) as a light brown solid in 100% yield.

3T; Mp: 303.8-327.6 °C (decomp.); IR (ATR): ν/cm^{-1} 3059, 2961, 2926, 2905, 2867, 1723, 1675, 1583, 1517, 1477, 1456, 1438, 1380, 1362, 1281, 1250, 1201, 1159, 1144, 1119, 1022, 911, 897, 890, 832, 817, 792, 759, 734, 687, 656, 634, 607, 599, 414; LR-MS (FD) m/z (%): 1182.73 (5), 1181.73 (6), 1180.73 (6), 1179.75 (6), 1178.76 (7), 1177.78 (5), 1168.73 (6), 1167.74 (9), 1166.73 (16), 1165.73 (23), 1164.73 (29), 1163.72 (27), 1162.71 (26), 1153.73 (8), 1152.74 (13), 1151.74 (24), 1150.73 (43), 1149.73 (63), 1148.73 (79), 1147.73 (57), 1139.72 (6), 1138.73 (13),

1137.73 (27), 1136.73 (51), 1135.73 (77), 1134.73 (bp), 1133.74 (66), 1132.74 (M^+, 50), 1124.72 (6), 1123.73 (12), 1122.73 (25), 1121.73 (52), 1120.73 (79), 1119.73 (56), 1109.71 (6), 1108.72 (15), 1107.72 (28), 1106.71 (29), 780.57 (6), 670.41 (6), 656.43 (8), 655.42 (9), 642.41 (7), 567.37 (6); HR-MS (FD) Calcd. for $C_{88}H_{76}$: 1132.59470; Found: 1132.59640.

5,5'-([9,9':10',9'':10'',9'''-Quateranthracene]-10,10'''-diyl)-bis(2,8-di-*tert*-butyl-5*H*-dibenzo[*a,d*]cycloheptatrien-5-yl) 4T

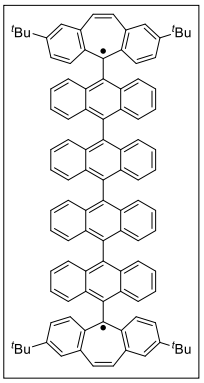

To a solution of $\mathbf{4}^{2+}(BF_4^-)_2$ (24.9 g, 16.8 μmol) in dry CH_3CN (4 mL) was added cobaltocene (6.4 mg, 33.8 μmol) at 25 ℃ to give a yellow suspension, and the mixture was stirred at 25 °C for 5 min under sonication. After the supernatant solution was removed by decantation, the precipitates were washed with dry CH_3CN three times and dried in vacuo to give **4T** (19.7 mg) as a brown powder in 90% yield.

4T; Mp: >400 °C; IR (ATR): ν/cm^{-1} 3057, 2961, 2903, 2865, 1559, 1517, 1473, 1457, 1438, 1380, 1362, 1303, 1249, 1201, 1158, 1144, 1118, 1023, 954, 911, 896, 831, 817, 791, 757, 733, 670, 648, 606, 599, 442, 417; LR-MS (MALDI) m/z (%): 1341.64 (7), 1340.64 (5), 1327.66 (11), 1326.65 (22), 1325.65 (35), 1324.64 (41), 1323.64 (35), 1312.66 (9), 1311.66 (24), 1310.66 (58), 1309.65 (bp), 1308.65 (M+, 91), 1298.65 (13), 1297.65 (38), 1296.64 (72), 1295.64 (65), 877.04 (5), 862.07 (5), 861.07 (11), 845.09 (9), 672.05 (11), 657.08 (12), 656.07 (42), 650.05 (8); HR-MS (MALDI) Calcd. for $C_{102}H_{84}$: 1308.65675; Found: 1308.65967.

5,5'-([9,9':10',9'':10'',9''':10''',9''''-Quinqueanthracene]-10,10''''-diyl)-bis(2,8-di-*tert*-butyl-5*H*-dibenzo[*a,d*]cycloheptatrien-5-yl) 5T

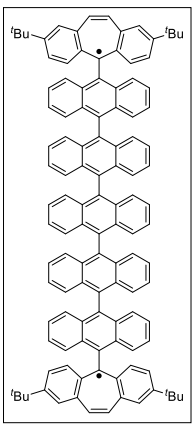

To a solution of $\mathbf{5}^{2+}(BF_4^-)_2$ (15.4 mg, 9.28 μmol) in dry THF (1 mL) was added cobaltocene (3.6 mg, 19.0 μmol) at 25 °C to give a yellow suspension, and the mixture was stirred at 25 °C for 5 min under sonication. After the supernatant solution was removed by decantation, the precipitates were washed with dry CH_3CN three times and dried in vacuo to give **5T** (12.2 mg) as a deep brown powder in 88% yield.

5T; Mp: >400 °C; IR (ATR): ν/cm^{-1} 3058, 2960, 2901, 2865, 1671, 1559, 1517, 1507, 1477, 1438, 1362, 1305, 1250, 1201, 1157, 1145, 1024, 953, 925, 901, 825, 819 791, 755, 735, 678, 652, 599, 468, 431, 416; LR-MS (MALDI) m/z (%): 1567.69 (6), 1566.69 (7), 1565.69 (7), 1552.71 (6), 1551.70 (13), 1550.70 (18), 1549.69 (16), 1548.68 (7), 1537.71 (5), 1536.71 (10), 1535.71 (21), 1534.70 (32), 1533.70 (30), 1532.69 (16), 1531.68 (12), 1521.70 (6), 1520.71 (9) 1519.71 (16) 1518.71 (25), 1517.70 (32) 1516.69

(26), 1515.69 (14), 1506.71 (7), 1505.71 (14), 1504.72 (29), 1503.72 (60), 1502.71 (94) 1501.71 (bp), 1500.70 (65) 1499.69 (48), 1490.70 (6) 1489.70 (13), 1488.70 (21), 1487.70 (25), 1486.71 (24), 1485.71 (35), 1484.70 (M^+, 25), 1475.71 (7), 1474.71 (19), 1473.70 (42), 1472.70 (68), 1471.69 (53), 1200.51 (6), 1199.51 (9), 1198.50 (6), 861.07 (5), 833.40 (6), 832.40 (20), 831.40 (28), 672.04 (5), 656.07 (15); HR-MS (MALDI) Calcd. for $C_{116}H_{92}$: 1484.71935; Found: 1484.72062.

5,5'-([9,9':10',9'':10'',9''':10''',9'''':10'''',9''''':10''''',9'''''-Sexianthracene]-10,10'''''-diyl)-bis(2,8-di-*tert*-butyl-5*H*-dibenzo[*a,d*]cycloheptatrien-5-yl) 6T

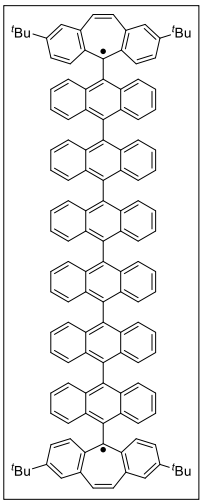

To a solution of $\mathbf{6}^{2+}(BF_4^-)_2$ (51.1 mg, 27.8 μmol) in dry THF (6 mL) was added cobaltocene (10.6 mg, 56.0 μmol) at 25 °C to give a yellow suspension, and the mixture was stirred at 25 °C for 5 min under sonication. After the supernatant solution was removed by decantation, the precipitates were washed with dry CH_3CN three times and dried in vacuo to give **6T** (46.1 mg) as a deep brown powder in 100% yield.

6T; Mp: 324.3-340.5 °C (decomp.); IR (ATR): ν/cm^{-1} 3058, 2960, 2902, 2865, 1582, 1517, 1477, 1438, 1394, 1382, 1361, 1322, 1305, 1249, 1201, 1157, 1145, 1065, 1024, 954, 910, 903, 831, 818, 793, 756, 735, 667, 649, 607, 599, 436, 420; LR-MS (MALDI) m/z (%): 1727.89 (5), 1726.89 (6), 1725.88 (6), 1712.89 (6), 1711.89 (10), 1710.89 (14), 1709.89 (15), 1708.88 (10), 1707.87 (8), 1697.88 (5), 1696.88 (8), 1695.89 (11), 1694.89 (14), 1693.89 (15), 1692.88 (13), 1691.87 (9), 1682.89 (6), 1681.89 (12), 1680.89 (21), 1679.89 (31), 1678.89 (36), 1677.89 (44), 1676.88 (42), 1675.88 (25), 1667.88 (5), 1666.88 (8), 1665.88 (15), 1664.88 (28), 1663.89 (40), 1662.89 (43), 1661.90 (46), 1660.90 (M^+, 31), 1651.88 (8), 1650.88 (18), 1649.89 (38), 1648.89 (57), 1647.88 (36), 1636.86 (6), 1635.86 (8), 877.14 (9), 862.17 (15), 861.16 (40), 847.19 (8), 846.19 (18), 845.19 (36), 686.53 (11), 685.53 (28), 671.42 (9), 670.41 (5), 666.11 (10), 657.17 (29), 656.16 (bp), 651.14 (10), 650.14 (39), 635.16 (8), 634.16 (23); HR-MS (MALDI) Calcd. for $C_{130}H_{100}$: 1660.78190; Found: 1660.78022.

4-4-3. Crystal data

	S7	**1**$^{2+}$$(BF_4^-)_2$	**2**$^{2+}$$(PF_6^-)_2$	**3**$^{2+}$$(BF_4^-)_2$	**4**$^{2+}$$(BF_4^-)_2$	**6**$^{2+}$$(NTf_2^-)_2$	**2F**
Recrystallization solvent	$CHCl_3$/hexane	CH_3NO_2/ether	CH_3NO_2/ether	CH_3CN/ether	CH_3CN/ether	CH_3CN/ether	CH_2Cl_2/hexane
Color and shape	Yellow plate	Red plate	Red block	Red block	Red block	Red needle	Colourless needle
Empirical formula	$C_{54}H_{49}O$	$C_{62}H_{66}N_2O_4B_2F_8$	$C_{82}H_{88}O_2F_{12}P_2$	$C_{88}H_{76}B_2F_8$	$C_{102}H_{84}B_2F_8$	$C_{134}H_{100}F_{12}N_2O_8S_4$	$C_{78}H_{77}Cl_2$
Formula weight	713.93	1076.78	1395.46	1307.1	1483.31	2222.39	1085.29
Temperature [K]	150	150	150	150	150	150	150
Crystal system	triclinic	monoclinic	monoclinic	triclinic	tetragonal	triclinic	triclinic
Space group	P-1	$P2_1/n$	P2/n	P-1	$I4_1/a$	P-1	P-1
a [Å]	11.08121(12)	16.6120(3)	18.4135(3)	8.8004(3)	15.5948(6)	15.3955(5)	12.92157(16)
b [Å]	13.4917(2)	9.5042(2)	9.93257(11)	15.9682(6)	15.5948(6)	21.2106(7)	15.04323(19)
c [Å]	16.1866(2)	17.6414(3)	20.6392(3)	16.1181(5)	37.677(3)	21.4503(6)	16.4212(2)
α [°]	95.6869(12)	90	90	84.118(3)	90	77.909(3)	96.0445(11)
β [°]	106.8765(11)	94.0685(18)	104.9946(14)	82.203(3)	90	85.462(2)	101.7699(11)
γ [°]	113.9838(13)	90	90	81.164(3)	90	70.337(3)	96.5757(10)
Volume [Å^3]	2049.54(5)	2778.25(10)	3646.24(8)	2209.73(14)	9162.9(10)	6449.5(4)	3077.03(7)
Z	2	2	2	1	4	2	2
ρ_{calc}g [cm^3]	1.157	1.287	1.271	0.982	1.075	1.144	1.171
μ [mm^{-1}]	0.507	0.81	1.194	0.544	0.58	1.264	1.27
Crystal size [mm^3]	0.3 × 0.2 × 0.05	0.4 × 0.3 × 0.03	0.2 × 0.15 × 0.1	0.3 × 0.2 × 0.1	0.2 × 0.1 × 0.05	0.3 × 0.03 × 0.03	0.8 × 0.06 × 0.03
Reflections collected	24787	16305	22464	23240	12762	78230	22481
Independent reflections	8254	5581	7366	7835	4488	25718	22481
R_{int}	0.0198	0.0583	0.0305	0.0839	0.0378	0.1195	0.0409
Data/restraints/parameters	8254/0/503	5581/0/322	7366/0/461	7835/0/448	4488/0/290	25718/0/1453	22481/0/792
GOF	1.075	1.073	1.081	1.726	1.357	1.227	1.06
R_1 [I>=2σ (I)]	0.0495	0.0863	0.0794	0.1623	0.1225	0.127	0.0538
wR_2 [I>=2σ (I)]	0.1486	0.2558	0.2228	0.4269	0.3585	0.3345	0.1516
R_1 [all data]	0.0533	0.0937	0.0847	0.1839	0.1624	0.1608	0.0611
wR_2 [all data]	0.1533	0.2655	0.2272	0.4467	0.4046	0.3682	0.1575
CCDC	2218480	2218481	2218482	2218483	2218484	2218485	2218486

[#]Solvent mask procedure was used for the analyses of **1**$^{2+}$$(BF_4^-)_2$, **3**$^{2+}$$(BF_4^-)_2$, **4**$^{2+}$$(BF_4^-)_2$, and **6**$^{2+}$$(NTf_2^-)_2$.

4-4-4. DFT calculations of dications at the CAM-B3LYP/6-31G(d) level

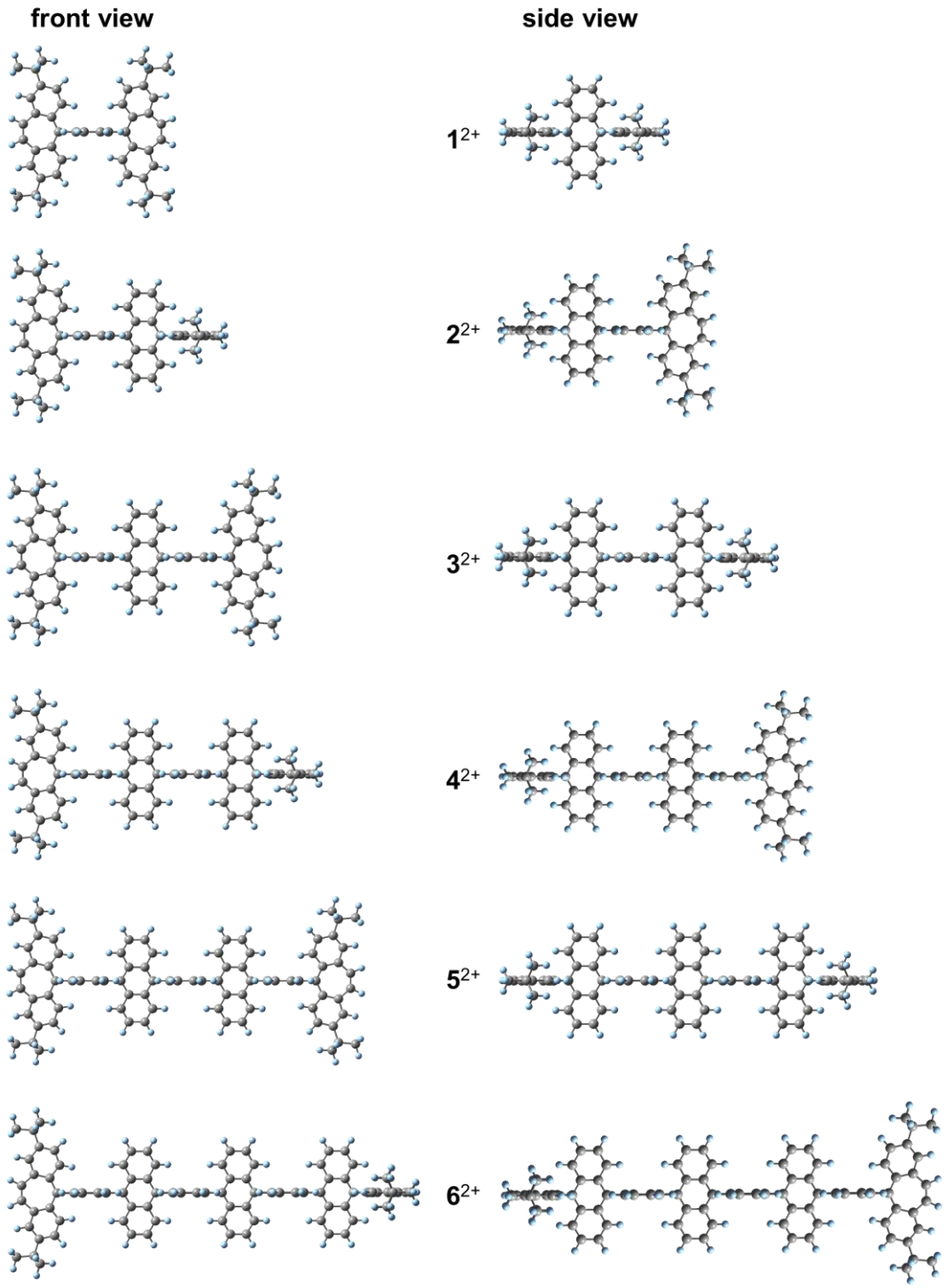

Figure 4-26. Optimized structures of dications $\mathbf{1}^{2+}$-$\mathbf{6}^{2+}$ based on DFT calculations at the CAM-B3LYP/6-31G(d) level.

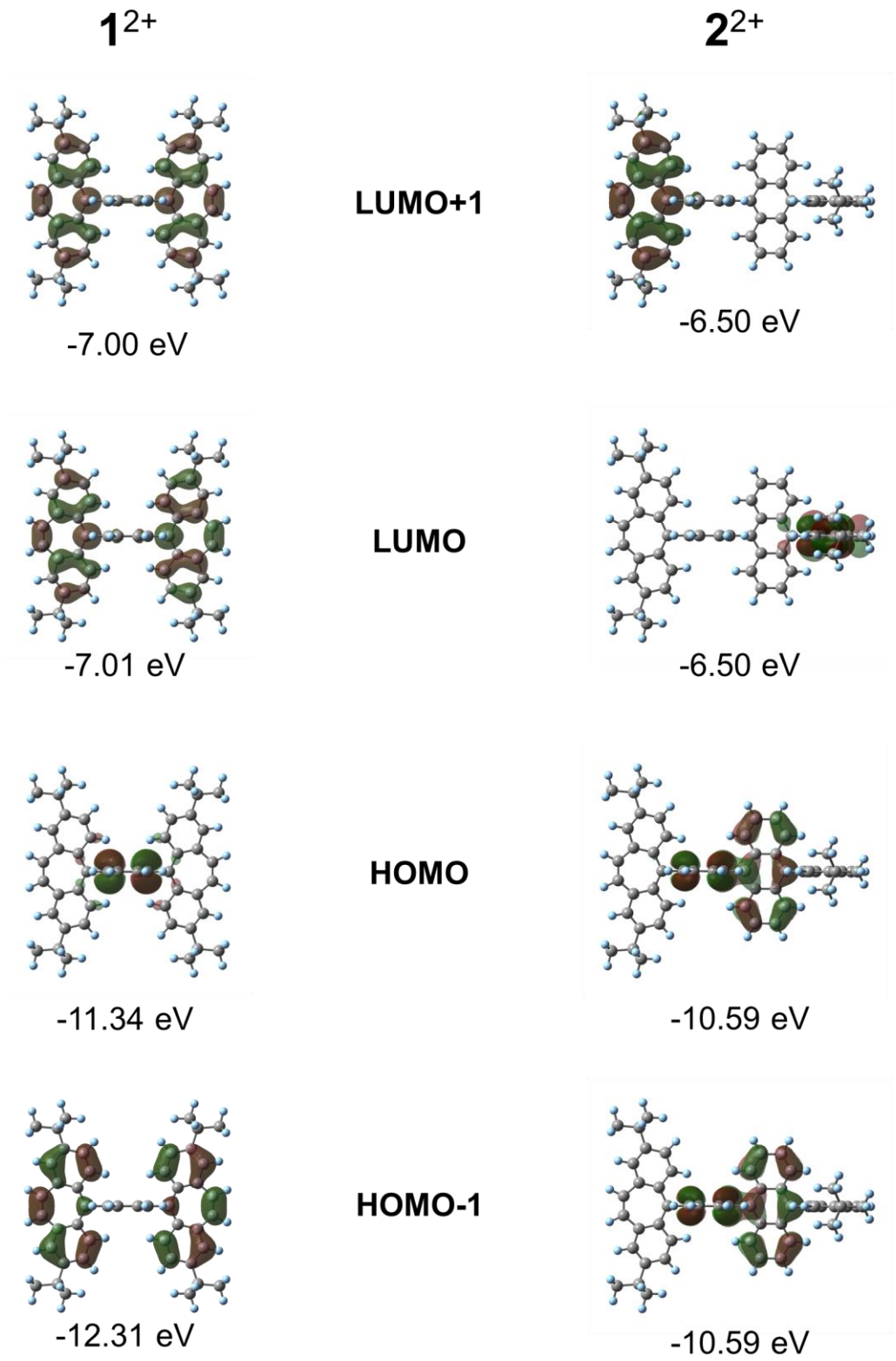

Figure 4-27. Molecular orbitals of dications $\mathbf{1}^{2+}$ and $\mathbf{2}^{2+}$ based on DFT calculations at the CAM-B3LYP/6-31G(d) level.

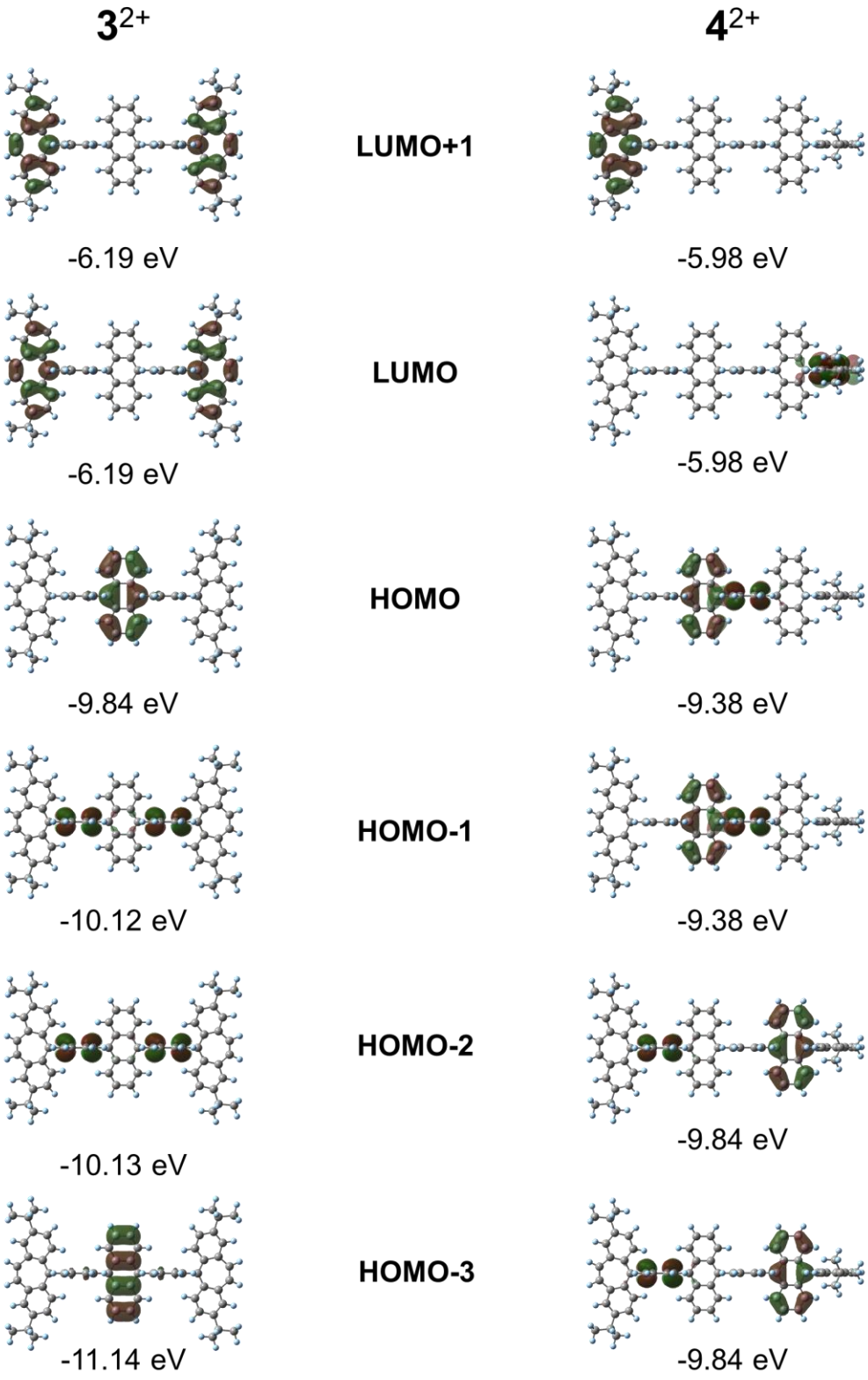

Figure 4-28. Molecular orbitals of dications $\mathbf{3}^{2+}$ and $\mathbf{4}^{2+}$ based on DFT calculations at the CAM-B3LYP/6-31G(d) level.

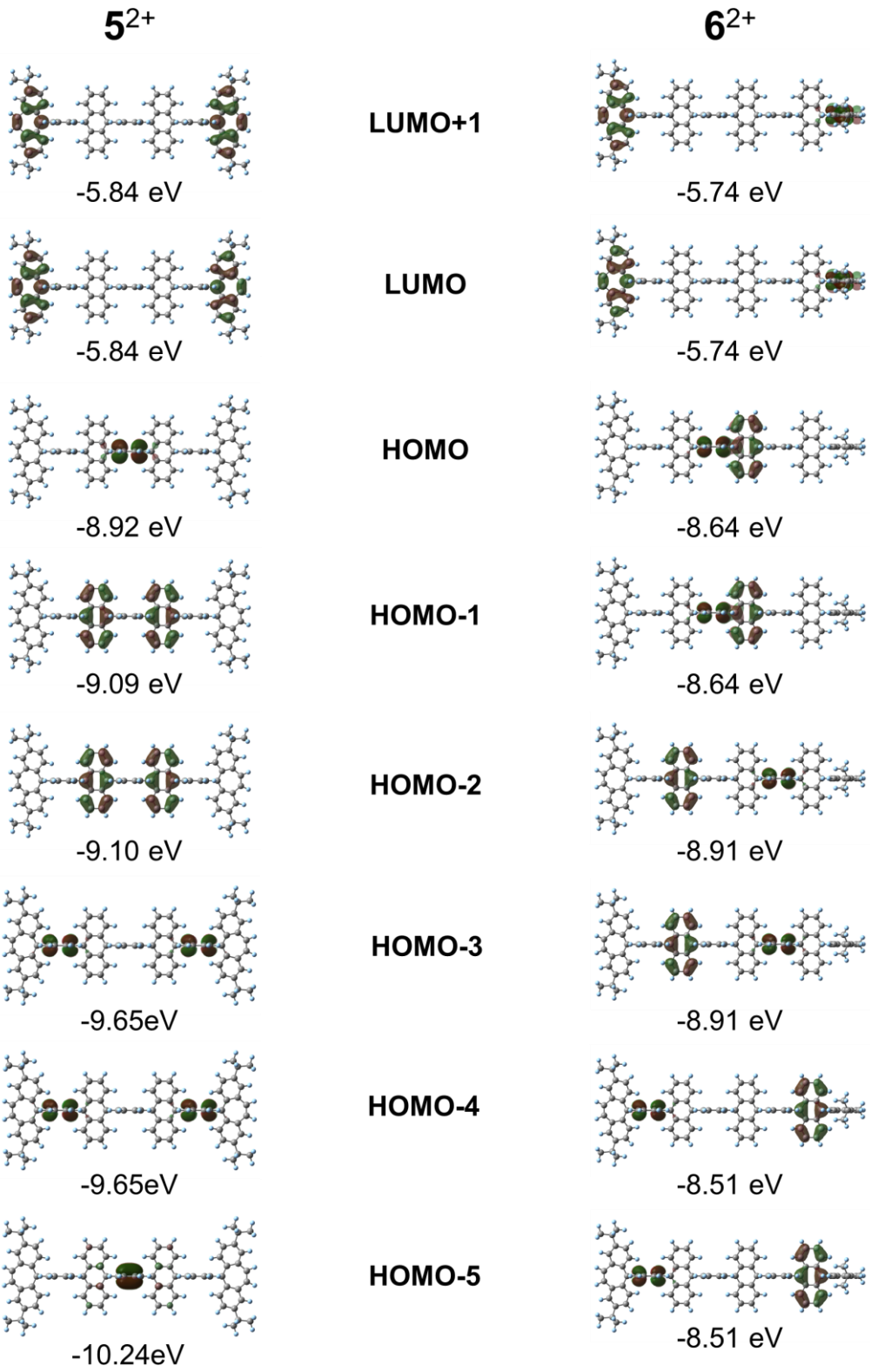

Figure 4-29. Molecular orbitals of dications $\mathbf{5}^{2+}$ and $\mathbf{6}^{2+}$ based on DFT calculations at the CAM-B3LYP/6-31G(d) level.

4-4-5. TD-DFT calculations of dications at the CAM-B3LYP/6-31G(d) level

1^{2+}
HOMO: 209, LUMO: 210
Excitation energies and oscillator strengths:

Excited State 1: Singlet-A 2.2003 eV 563.49 nm f=0.0000 <S**2>=0.000
209 -> 210 0.69772
This state for optimization and/or second-order correction.
Total Energy, E(TD-HF/TD-DFT) = -2320.59670294
Copying the excited state density for this state as the 1-particle RhoCI density.

Excited State 2: Singlet-A 2.2110 eV 560.77 nm f=0.0000 <S**2>=0.000
209 -> 211 0.69776

Excited State 3: Singlet-A 2.8027 eV 442.38 nm f=0.1520 <S**2>=0.000
207 -> 210 0.49095
208 -> 211 -0.49006

Excited State 4: Singlet-A 2.8226 eV 439.26 nm f=0.0000 <S**2>=0.000
207 -> 211 -0.49017
208 -> 210 0.49309

Excited State 5: Singlet-A 3.2720 eV 378.93 nm f=0.0000 <S**2>=0.000
204 -> 210 -0.31520
205 -> 211 0.42910
206 -> 210 -0.32643
207 -> 212 0.20948
208 -> 213 0.20994

Excited State 6: Singlet-A 3.2854 eV 377.38 nm f=0.2795 <S**2>=0.000
204 -> 211 -0.30598
205 -> 210 0.42387
206 -> 211 -0.32268
207 -> 213 -0.22550
208 -> 212 -0.22588

Excited State 7: Singlet-A 3.6675 eV 338.07 nm f=0.0000 <S**2>=0.000
203 -> 211 -0.13299
204 -> 210 -0.30511
206 -> 210 0.58087
207 -> 212 0.12906
208 -> 213 0.12954

Excited State 8: Singlet-A 3.6732 eV 337.54 nm f=0.0008 <S**2>=0.000
203 -> 210 -0.13548
204 -> 211 -0.30334
206 -> 211 0.58210
207 -> 213 -0.12791
208 -> 212 -0.12776

Excited State 9: Singlet-A 3.7284 eV 332.54 nm f=0.0017 <S**2>=0.000
206 -> 214 -0.11727
209 -> 212 0.68658

Excited State 10: Singlet-A 3.7426 eV 331.28 nm f=0.0000 <S**2>=0.000
209 -> 213 0.70220

2^{2+}
HOMO: 255, LUMO: 256
Excitation energies and oscillator strengths:

Excited State 1:	Singlet-A	1.9356 eV	640.55 nm	f=0.0000	<S**2>=0.000
254 -> 256	0.33917				
255 -> 256	0.59276				
255 -> 257	-0.11289				

This state for optimization and/or second-order correction.
Total Energy, E(TD-HF/TD-DFT) = -2858.64055102
Copying the excited state density for this state as the 1-particle RhoCI density.

Excited State 2:	Singlet-A	1.9356 eV	640.55 nm	f=0.0000	<S**2>=0.000
254 -> 256	0.13090				
254 -> 257	0.58905				
255 -> 257	-0.34558				
Excited State 3:	Singlet-A	2.8312 eV	437.92 nm	f=0.1826	<S**2>=0.000
252 -> 256	-0.48026				
253 -> 257	0.48033				
Excited State 4:	Singlet-A	2.8421 eV	436.25 nm	f=0.0000	<S**2>=0.000
252 -> 256	0.48038				
252 -> 257	-0.10266				
253 -> 256	0.10264				
253 -> 257	0.48031				
Excited State 5:	Singlet-A	2.9773 eV	416.43 nm	f=0.0000	<S**2>=0.000
254 -> 256	0.47257				
254 -> 257	0.15886				
255 -> 256	-0.15688				
255 -> 257	0.47479				
Excited State 6:	Singlet-A	2.9774 eV	416.42 nm	f=0.0000	<S**2>=0.000
254 -> 256	0.37393				
254 -> 257	-0.33195				
255 -> 256	-0.33289				
255 -> 257	-0.37111				
Excited State 7:	Singlet-A	3.2550 eV	380.90 nm	f=0.1130	<S**2>=0.000
247 -> 257	-0.16905				
248 -> 257	-0.28245				
249 -> 257	0.30745				
250 -> 257	0.34691				
251 -> 257	0.27979				
253 -> 258	0.17398				
253 -> 259	-0.17448				
Excited State 8:	Singlet-A	3.2550 eV	380.90 nm	f=0.1130	<S**2>=0.000
247 -> 256	0.16905				
248 -> 256	-0.28245				
249 -> 256	-0.30746				
250 -> 256	0.34691				
251 -> 256	-0.27979				
252 -> 258	-0.17457				
252 -> 259	-0.17390				
Excited State 9:	Singlet-A	3.4641 eV	357.92 nm	f=0.0006	<S**2>=0.000
254 -> 258	0.24740				
254 -> 259	0.24912				
255 -> 258	0.42999				
255 -> 259	0.42694				
Excited State 10:	Singlet-A	3.4641 eV	357.92 nm	f=0.0006	<S**2>=0.000
254 -> 258	0.42856				
254 -> 259	-0.42838				
255 -> 258	-0.24657				
255 -> 259	0.24995				

3^{2+}
HOMO: 301, LUMO: 302
Excitation energies and oscillator strengths:

Excited State	1:	Singlet-A	1.7740 eV	698.91 nm	f=0.0000	<S**2>=0.000
299 -> 302		0.27269				
299 -> 303		0.40962				
300 -> 302		0.40698				
300 -> 303		0.28044				

This state for optimization and/or second-order correction.
Total Energy, E(TD-HF/TD-DFT) = -3396.67334725
Copying the excited state density for this state as the 1-particle RhoCI density.

Excited State	2:	Singlet-A	1.7740 eV	698.91 nm	f=0.0000	<S**2>=0.000
299 -> 302		0.40984				
299 -> 303		-0.27290				
300 -> 302		-0.28023				
300 -> 303		0.40678				
Excited State	3:	Singlet-A	2.5340 eV	489.28 nm	f=0.0000	<S**2>=0.000
301 -> 302		0.70621				
Excited State	4:	Singlet-A	2.5342 eV	489.24 nm	f=0.0000	<S**2>=0.000
301 -> 303		0.70621				
Excited State	5:	Singlet-A	3.1886 eV	388.83 nm	f=0.0000	<S**2>=0.000
290 -> 303		-0.11509				
291 -> 302		0.15289				
292 -> 303		0.19101				
293 -> 302		-0.24936				
296 -> 303		0.41903				
297 -> 302		0.37069				
Excited State	6:	Singlet-A	3.1895 eV	388.73 nm	f=0.1179	<S**2>=0.000
290 -> 302		-0.11343				
291 -> 303		0.15130				
292 -> 302		0.18959				
293 -> 303		-0.24904				
296 -> 302		0.41999				
297 -> 303		0.37180				
Excited State	7:	Singlet-A	3.2013 eV	387.29 nm	f=0.0000	<S**2>=0.000
299 -> 302		0.36640				
299 -> 303		-0.34113				
300 -> 302		0.34586				
300 -> 303		-0.35989				
Excited State	8:	Singlet-A	3.2013 eV	387.29 nm	f=0.0000	<S**2>=0.000
299 -> 302		0.34131				
299 -> 303		0.36665				
300 -> 302		-0.35965				
300 -> 303		-0.34568				
Excited State	9:	Singlet-A	3.2984 eV	375.89 nm	f=0.0000	<S**2>=0.000
299 -> 305		-0.49327				
300 -> 304		0.49652				
Excited State	10:	Singlet-A	3.2986 eV	375.86 nm	f=0.0017	<S**2>=0.000
299 -> 304		-0.49324				
300 -> 305		0.49647				

4^{2+}
HOMO: 347, LUMO: 348
Excitation energies and oscillator strengths:

Excited State	1:	Singlet-A	1.6890 eV	734.09 nm	f=0.0000	<S**2>=0.000
345 -> 348		0.69727				

This state for optimization and/or second-order correction.
Total Energy, E(TD-HF/TD-DFT) = -3934.69978141
Copying the excited state density for this state as the 1-particle RhoCI density.

Excited State	2:	Singlet-A	1.6890 eV	734.09 nm	f=0.0000	<S**2>=0.000
344 -> 349		0.69727				
Excited State	3:	Singlet-A	2.2797 eV	543.87 nm	f=0.0000	<S**2>=0.000
346 -> 348		0.40193				
346 -> 349		0.15237				
347 -> 348		0.54831				
347 -> 349		-0.11542				
Excited State	4:	Singlet-A	2.2797 eV	543.87 nm	f=0.0000	<S**2>=0.000
346 -> 348		-0.11015				
346 -> 349		0.54939				
347 -> 348		-0.15622				
347 -> 349		-0.40045				
Excited State	5:	Singlet-A	2.6611 eV	465.91 nm	f=0.0000	<S**2>=0.000
346 -> 349		0.41603				
347 -> 349		0.56953				
Excited State	6:	Singlet-A	2.6611 eV	465.91 nm	f=0.0000	<S**2>=0.000
346 -> 348		0.56927				
347 -> 348		-0.41639				
Excited State	7:	Singlet-A	2.8552 eV	434.24 nm	f=0.2169	<S**2>=0.000
337 -> 349		-0.48920				
338 -> 348		0.48971				
Excited State	8:	Singlet-A	2.8594 eV	433.60 nm	f=0.0000	<S**2>=0.000
337 -> 349		0.49083				
338 -> 348		0.49030				
Excited State	9:	Singlet-A	3.1346 eV	395.53 nm	f=0.0378	<S**2>=0.000
334 -> 348		0.11682				
335 -> 348		-0.13296				
336 -> 348		0.17313				
338 -> 351		-0.11383				
339 -> 348		-0.37766				
340 -> 348		0.42624				
341 -> 348		-0.26253				
Excited State	10:	Singlet-A	3.1346 eV	395.53 nm	f=0.0378	<S**2>=0.000
334 -> 349		0.11682				
335 -> 349		0.13296				
336 -> 349		0.17313				
337 -> 350		0.11384				
339 -> 349		0.37767				
340 -> 349		0.42624				
341 -> 349		0.26252				

5^{2+}
HOMO: 393, LUMO: 394
Excitation energies and oscillator strengths:

Excited State	1:	Singlet-A	1.6378 eV	757.03 nm	f=0.0000	<S**2>=0.000
389 -> 394	-0.45580					
389 -> 395	-0.16879					
390 -> 394	0.47006					
390 -> 395	0.17052					

This state for optimization and/or second-order correction.
Total Energy, E(TD-HF/TD-DFT) = -4472.72264070
Copying the excited state density for this state as the 1-particle RhoCI density.

Excited State	2:	Singlet-A	1.6378 eV	757.03 nm	f=0.0000	<S**2>=0.000
389 -> 394	-0.17355					
389 -> 395	0.46894					
390 -> 394	-0.16567					
390 -> 395	0.45696					

Excited State	3:	Singlet-A	2.1383 eV	579.81 nm	f=0.0000	<S**2>=0.000
391 -> 394	0.46963					
391 -> 395	0.16205					
392 -> 394	0.46793					
392 -> 395	0.18159					

Excited State	4:	Singlet-A	2.1383 eV	579.81 nm	f=0.0000	<S**2>=0.000
391 -> 394	-0.16212					
391 -> 395	0.46981					
392 -> 394	0.18153					
392 -> 395	-0.46775					

Excited State	5:	Singlet-A	2.3468 eV	528.30 nm	f=0.0000	<S**2>=0.000
393 -> 394	0.70384					

Excited State	6:	Singlet-A	2.3468 eV	528.30 nm	f=0.0000	<S**2>=0.000
393 -> 395	0.70384					

Excited State	7:	Singlet-A	2.7064 eV	458.12 nm	f=0.0000	<S**2>=0.000
391 -> 394	-0.17502					
391 -> 395	0.47084					
392 -> 394	-0.16903					
392 -> 395	0.46801					

Excited State	8:	Singlet-A	2.7064 eV	458.12 nm	f=0.0000	<S**2>=0.000
391 -> 394	0.47102					
391 -> 395	0.17508					
392 -> 394	-0.46783					
392 -> 395	-0.16896					

Excited State	9:	Singlet-A	3.1587 eV	392.51 nm	f=0.0000	<S**2>=0.000
389 -> 396	0.36985					
389 -> 397	0.33160					
390 -> 396	0.36040					
390 -> 397	-0.34017					

Excited State	10:	Singlet-A	3.1587 eV	392.51 nm	f=0.0016	<S**2>=0.000
389 -> 396	0.34110					
389 -> 397	-0.35949					
390 -> 396	0.33063					
390 -> 397	0.37073					

6^{2+}
HOMO: 439, LUMO: 440
Excitation energies and oscillator strengths:

Excited State	1:	Singlet-B	1.5702 eV	789.61 nm	f=0.0000	<S**2>=0.000
434 -> 441		0.49311				
435 -> 440		0.49311				

This state for optimization and/or second-order correction.
Total Energy, E(TD-HF/TD-DFT) = -5010.73853593
Copying the excited state density for this state as the 1-particle RhoCI density.

Excited State	2:	Singlet-A	1.5702 eV	789.61 nm	f=0.0000	<S**2>=0.000
434 -> 440		0.49311				
435 -> 441		0.49311				
Excited State	3:	Singlet-B	2.0148 eV	615.36 nm	f=0.0000	<S**2>=0.000
436 -> 441		-0.49930				
437 -> 440		0.49930				
Excited State	4:	Singlet-A	2.0148 eV	615.36 nm	f=0.0000	<S**2>=0.000
436 -> 440		-0.49930				
437 -> 441		0.49930				
Excited State	5:	Singlet-A	2.1305 eV	581.95 nm	f=0.0000	<S**2>=0.000
438 -> 440		0.49984				
439 -> 441		0.49989				
Excited State	6:	Singlet-B	2.1305 eV	581.95 nm	f=0.0000	<S**2>=0.000
438 -> 441		0.49984				
439 -> 440		0.49989				
Excited State	7:	Singlet-A	2.3158 eV	535.40 nm	f=0.0000	<S**2>=0.000
438 -> 440		0.49991				
439 -> 441		-0.49986				
Excited State	8:	Singlet-B	2.3158 eV	535.40 nm	f=0.0000	<S**2>=0.000
438 -> 441		0.49991				
439 -> 440		-0.49986				
Excited State	9:	Singlet-A	2.6908 eV	460.78 nm	f=0.0000	<S**2>=0.000
436 -> 440		0.49998				
437 -> 441		0.49998				
Excited State	10:	Singlet-B	2.6908 eV	460.78 nm	f=0.0000	<S**2>=0.000
436 -> 441		0.49998				
437 -> 440		0.49998				

4-4-6. DFT calculations of neutral species at the (U)B3LYP/6-31G(d) level

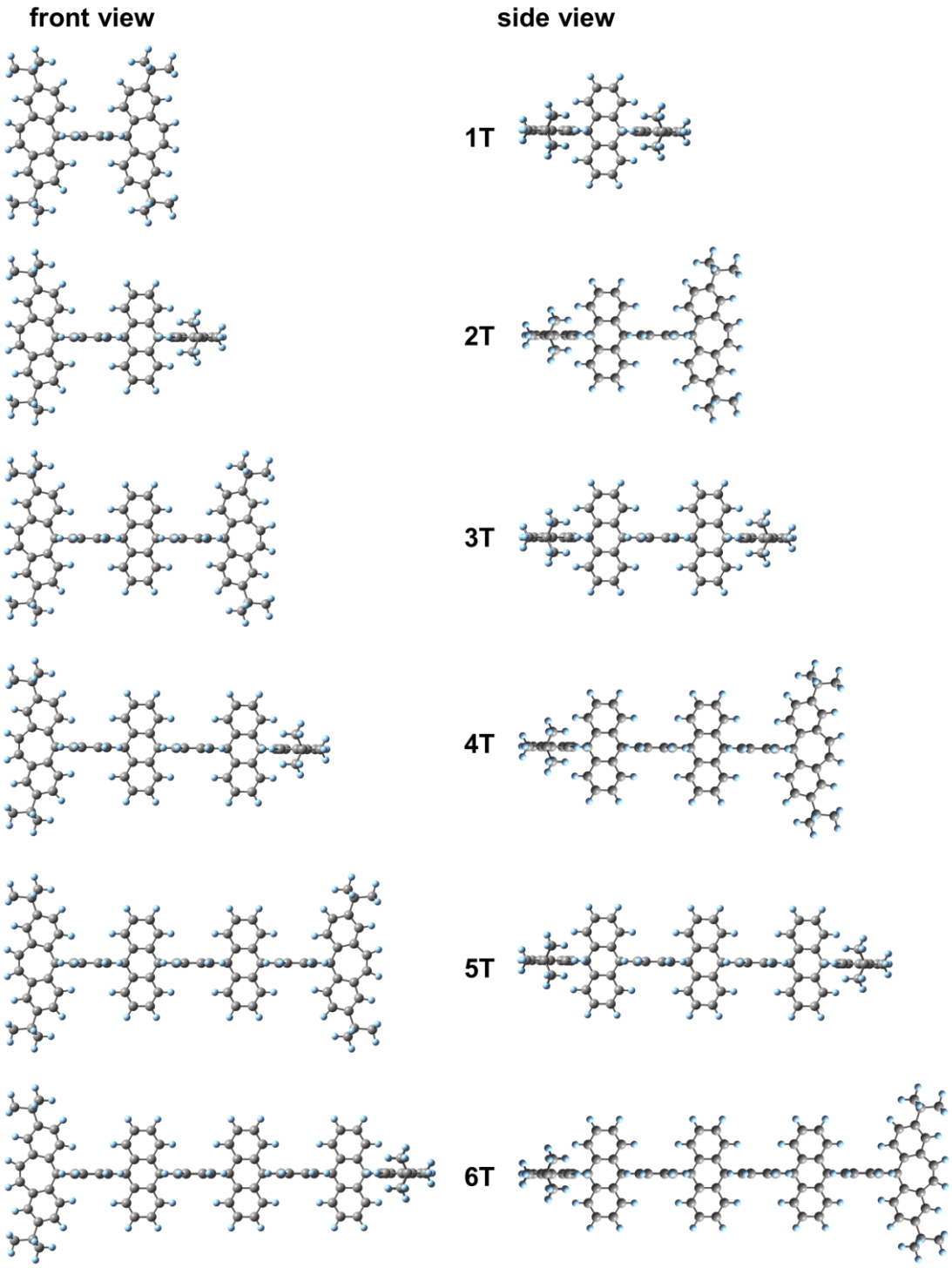

Figure 4-30. Optimized structures of biradicals **1T**-**6T** (triplet) based on DFT calculations at the UB3LYP/6-31G(d) level.

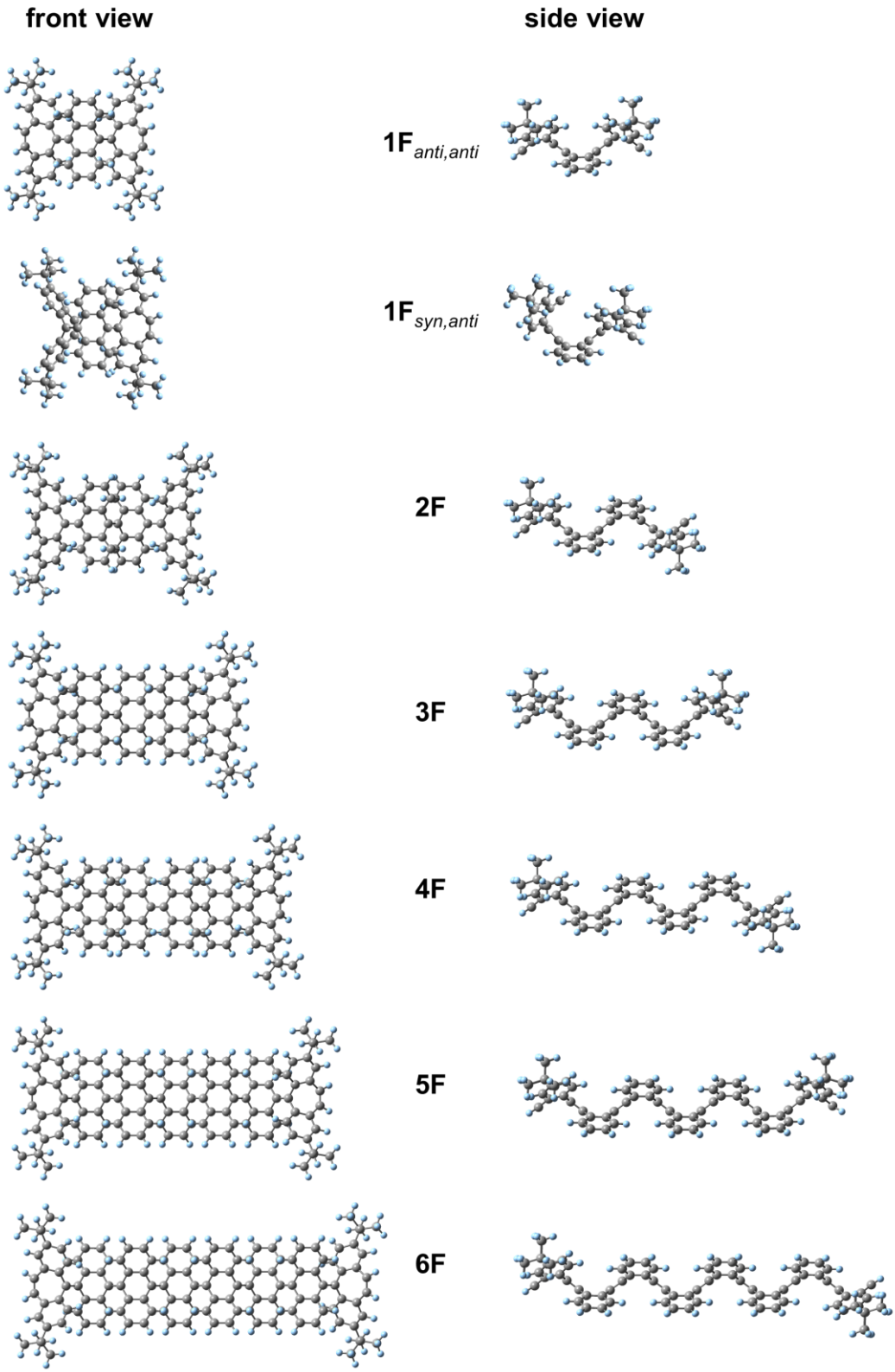

Figure 4-31. Optimized structures of closed-shell folded forms **1F**-**6F** based on DFT calculations at the B3LYP/6-31G(d) level.

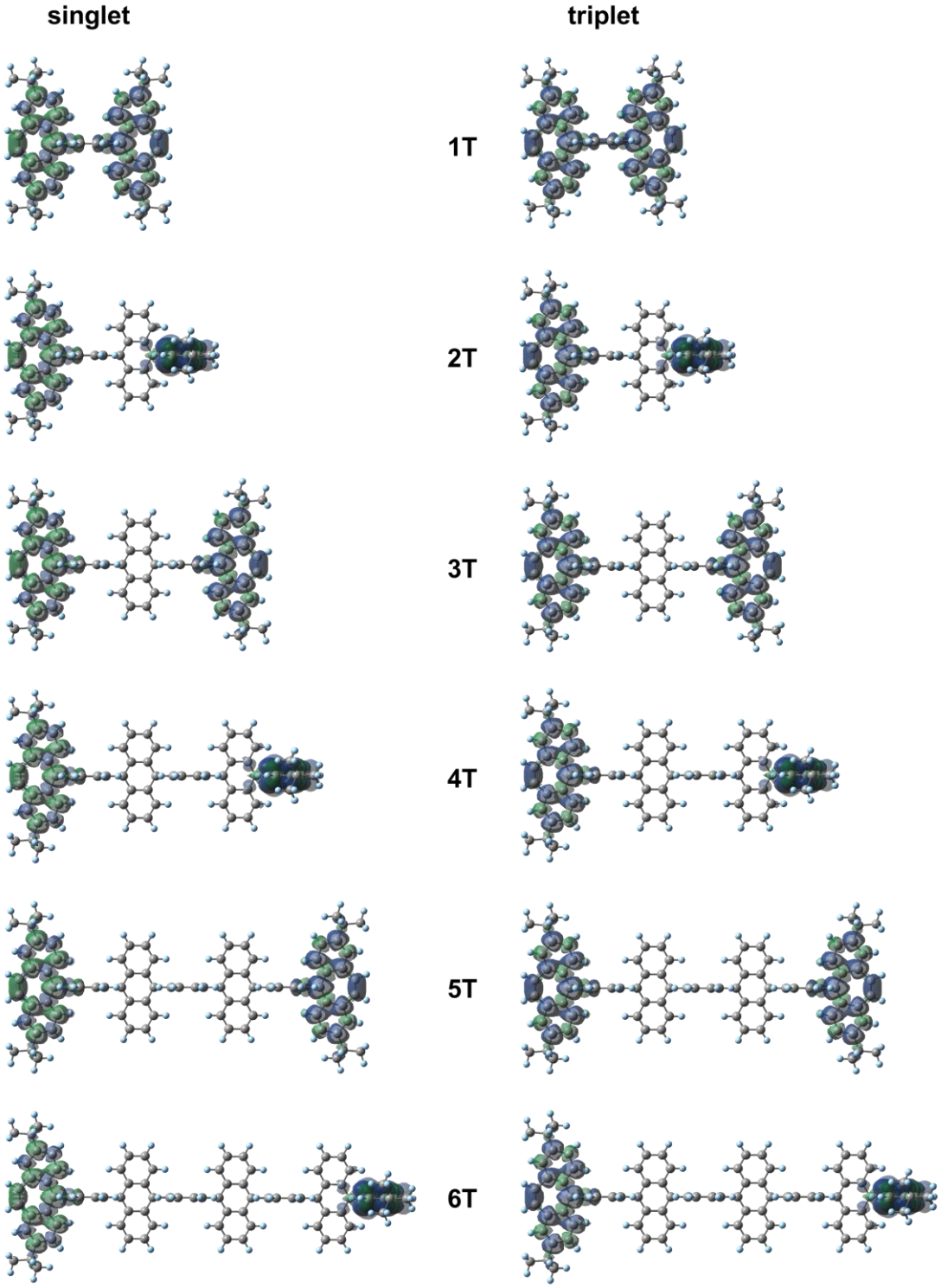

Figure 4-32. Spin density map of biradicals **1T-6T** based on DFT calculations at the UB3LYP/6-31G(d) level (left: singlet, right: triplet).

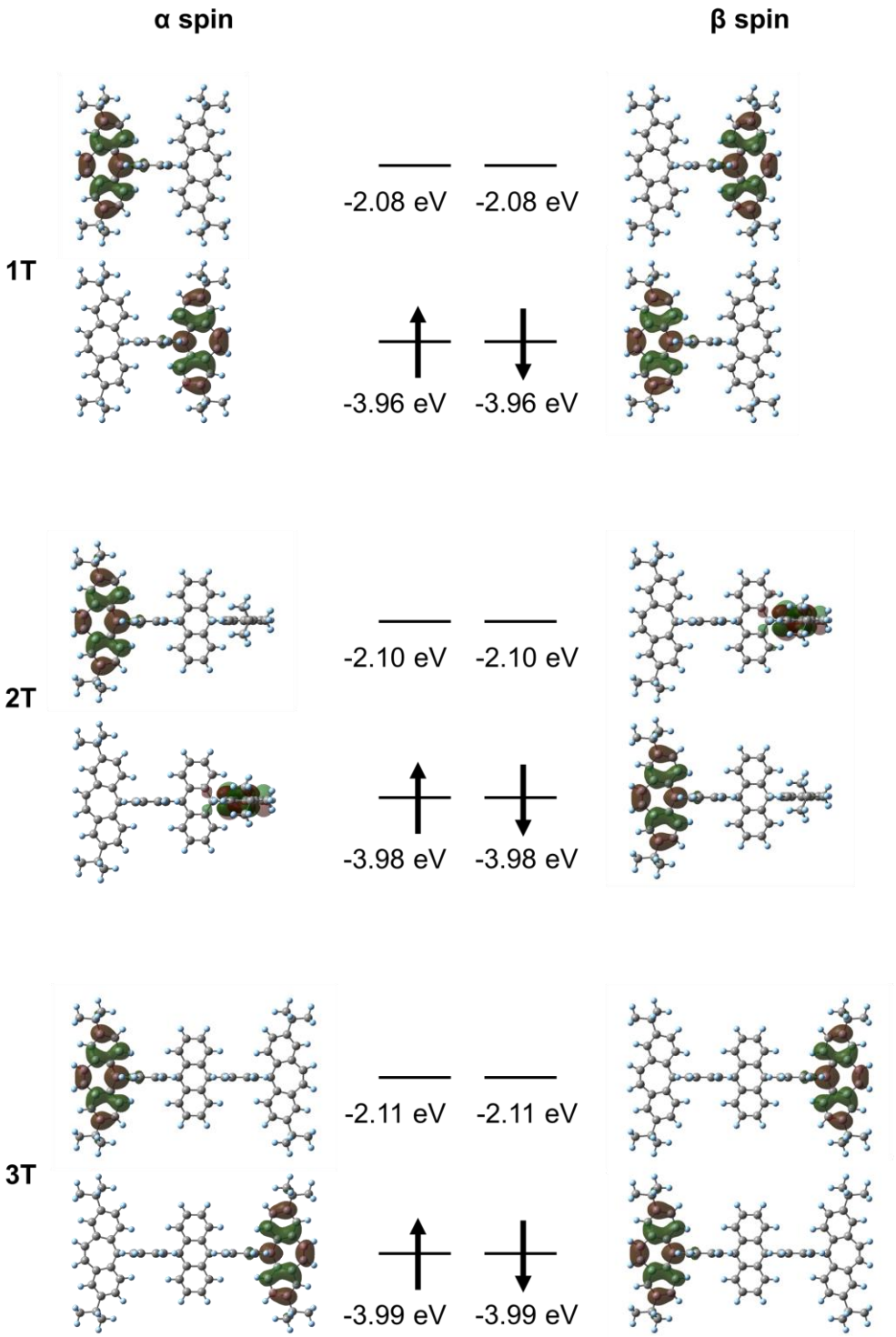

Figure 4-33. Molecular orbitals of singlet biradicals **1T**, **2T** and **3T** based on DFT calculations at the UB3LYP/6-31G(d) level.

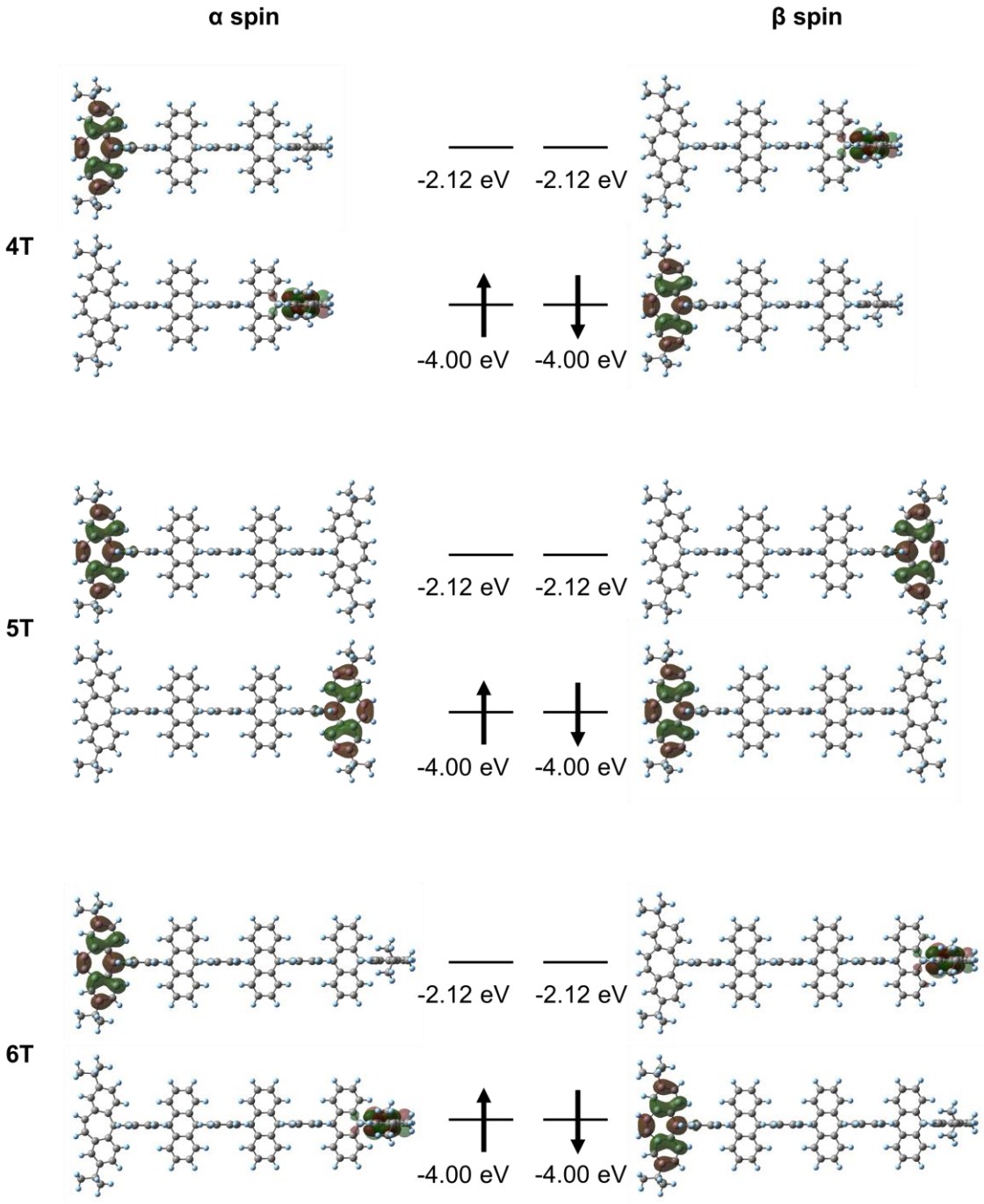

Figure 4-34. Molecular orbitals of singlet biradicals **4T**, **5T** and **6T** based on DFT calculations at the UB3LYP/6-31G(d) level.

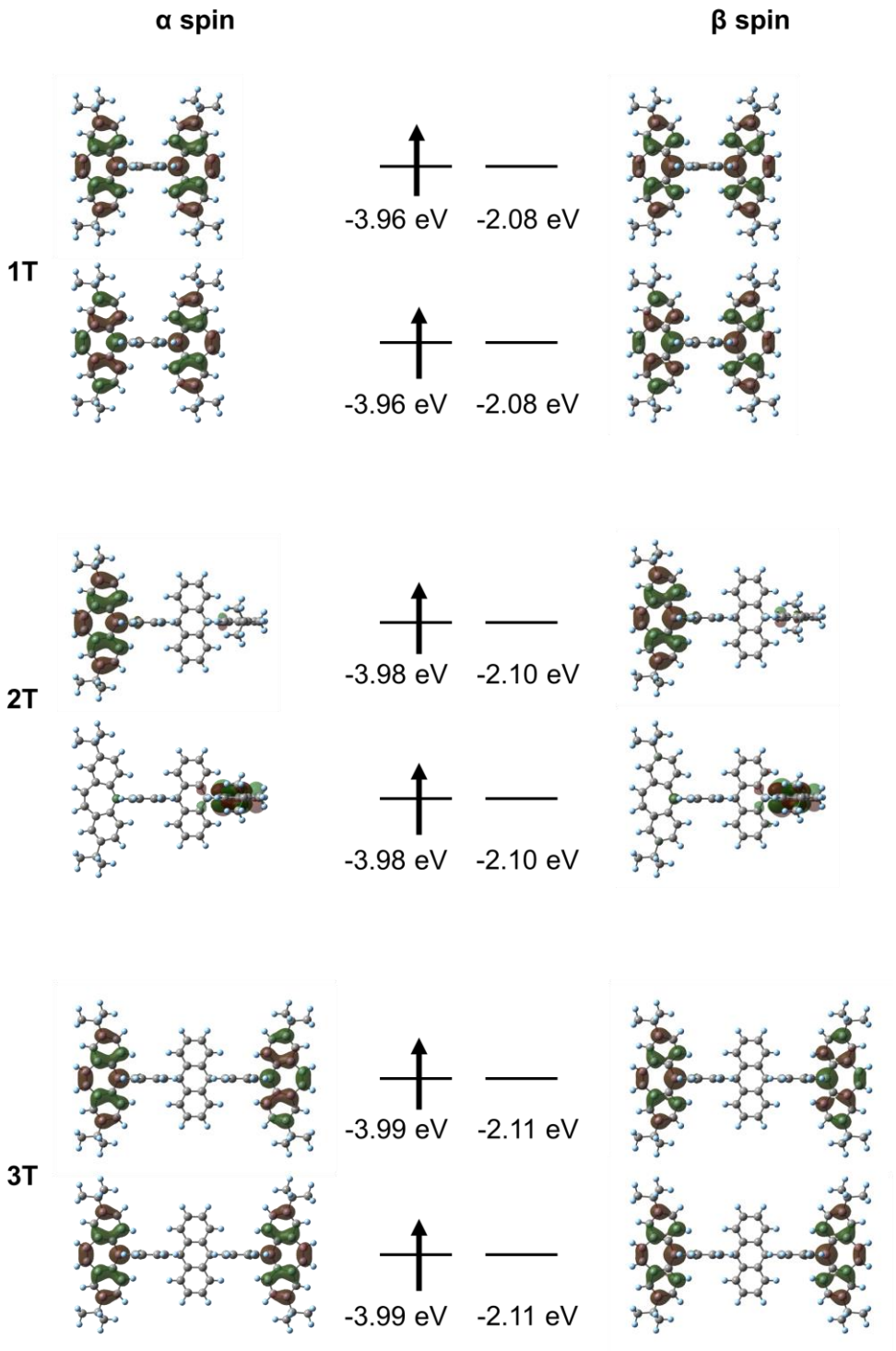

Figure 4-35. Molecular orbitals of triplet biradicals **1T**, **2T** and **3T** based on DFT calculations at the UB3LYP/6-31G(d) level.

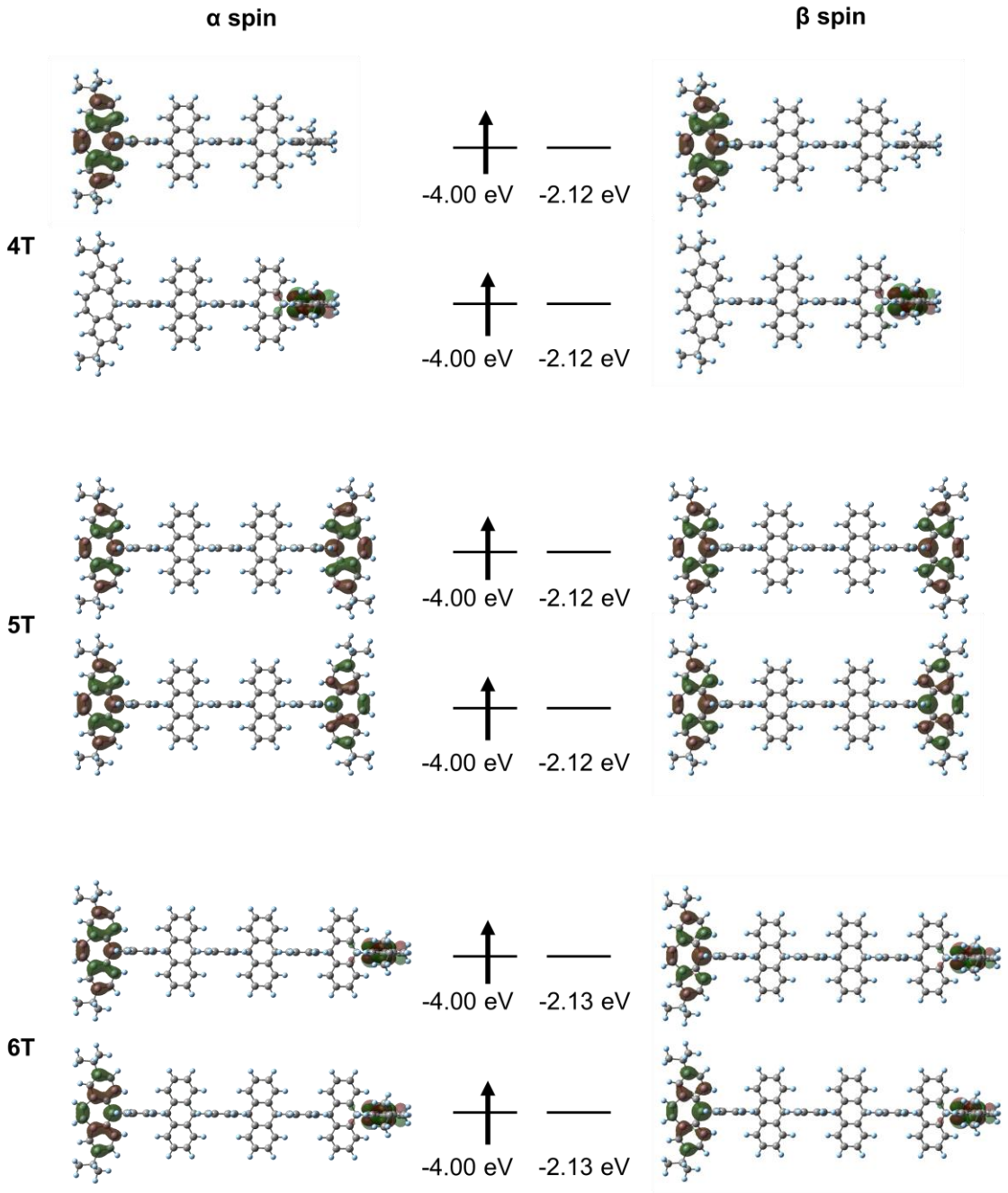

Figure 4-36. Molecular orbitals of triplet biradicals **4T**, **5T** and **6T** based on DFT calculations at the UB3LYP/6-31G(d) level.

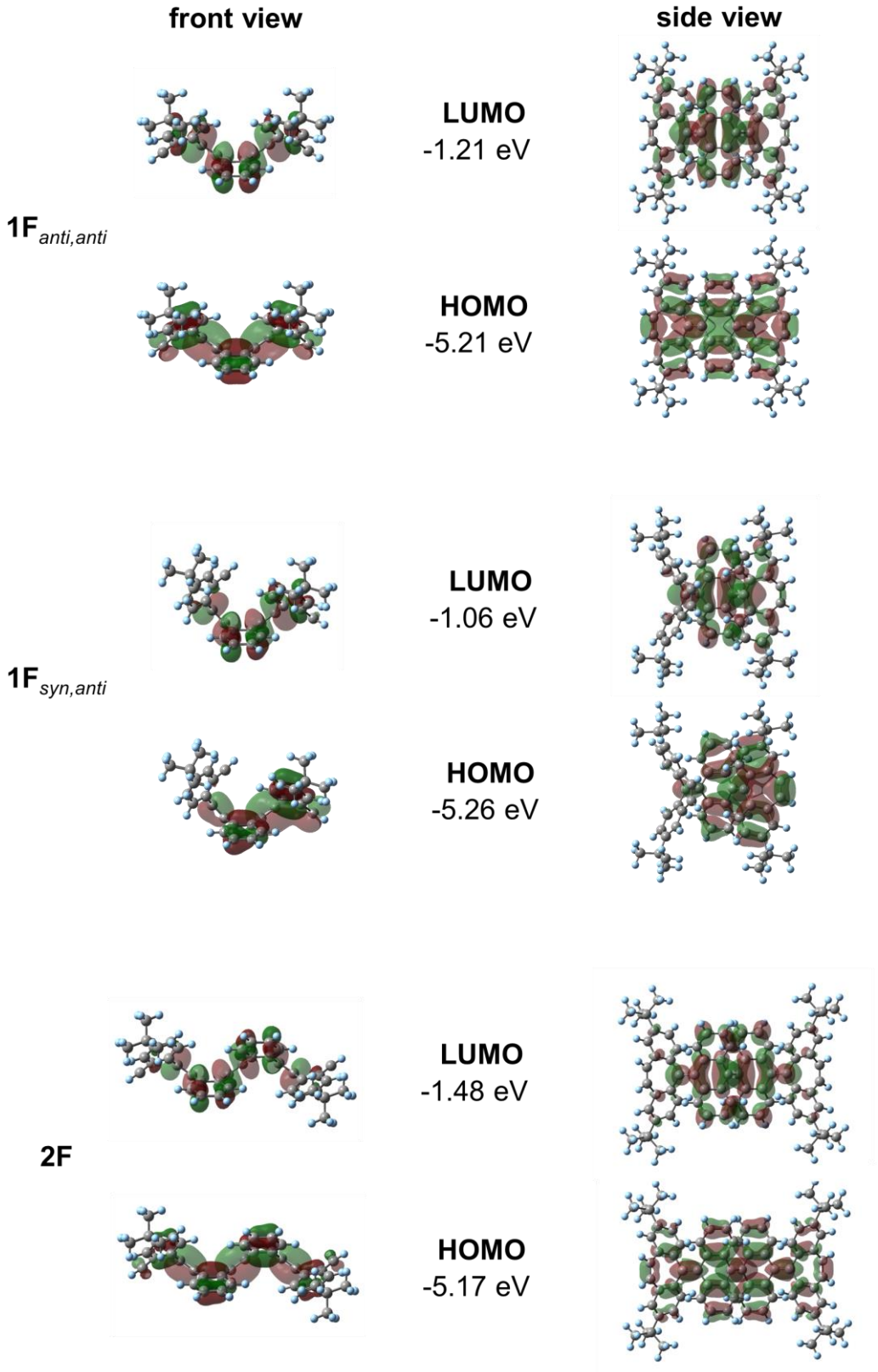

Figure 4-37. Molecular orbitals of closed-shell folded forms **1F**$_{anti,anti}$, **1F**$_{syn,anti}$ and **2F** based on DFT calculations at the B3LYP/6-31G(d) level.

4-5. References

(1) Martin, R. E.; Diederich, F. Linear Monodisperse π-Conjugated Oligomers: Model Compounds for Polymers and More. *Angew. Chem. Int. Ed.* **1999**, *38*, 1350–1377, DOI: 10.1002/(SICI)1521-3773(19990517)38:10<1350::AID-ANIE1350>3.0.CO;2-6.

(2) Yamaguchi, Y.; Takubo, M.; Ogawa, K.; Nakayama, K.; Koganezawa, T.; Katagiri, H. Terazulene Isomers: Polarity Change of OFETs through Molecular Orbital Distribution Contrast. *J. Am. Chem. Soc.* **2016**, *138*, 11335–11343, DOI: 10.1021/jacs.6b06877.

(3) Ivanov, M. V.; Thakur, K.; Boddeda, A.; Wang, D.; Rathore, R. Nodal Arrangement of HOMO Controls the Turning On/Off the Electronic Coupling in Isomeric Polypyrene Wires. *J. Phys. Chem. C* **2017**, *121*, 9202–9208, DOI: 10.1021/acs.jpcc.7b02264.

(4) Ivanov, M. V.; Wang, D.; Rathore, R. From Static to Dynamic: Electron Density of HOMO at Biaryl Linkage Controls the Mechanism of Hole Delocalization. *J. Am. Chem. Soc.* **2018**, *140*, 4765–4769, DOI: 10.1021/jacs.8b00466.

(5) Matsuno, T.; Ohtomo, Y.; Someya, M.; Isobe, H. Stereoselectivity in Spontaneous Assembly of Rolled Incommensurate Carbon Bilayers. *Nat. Commun.* **2021**, *12*, 1575, DOI: 10.1038/s41467-021-21889-8.

(6) Liess, P.; Hensel, V.; Schlüter, A.-D. Oligophenylene Rods: A Repetitive Approach. *Liebigs Ann.* **1996**, 1037–1040, DOI: 10.1002/jlac.199619960703.

(7) Lightowler, S.; Hird, M. Monodisperse Aromatic Oligomers of Defined Structure and Large Size through Selective and Sequential Suzuki Palladium-Catalyzed Cross-Coupling Reactions. *Chem. Mater.* **2005**, *17*, 5538–5549, DOI: 10.1021/cm0512068.

(8) Banerjee, M.; Shukla, R.; Rathore, R. Synthesis, Optical, and Electronic Properties of Soluble Poly-p-Phenylene Oligomers as Models for Molecular Wires. *J. Am. Chem. Soc.* **2009**, *131*, 1780–1786, DOI: 10.1021/ja805102d.

(9) Abdulkarim, A.; Hinkel, F.; Jänsch, D.; Freudenberg, J.; Golling, F. E.; Müllen, K. A New Solution to an Old Problem: Synthesis of Unsubstituted Poly(Para-Phenylene). *J. Am. Chem. Soc.* **2016**, *138*, 16208–16211, DOI: 10.1021/jacs.6b10254.

(10) Darzi, E. R.; Jasti, R. The Dynamic, Size-Dependent Properties of [5]–[12]Cycloparaphenylenes. *Chem. Soc. Rev.* **2015**, *44*, 6401–6410, DOI: 10.1039/C5CS00143A.

(11) Kayahara, E.; Kouyama, T.; Kato, T.; Yamago, S. Synthesis and Characterization of [n]CPP (n = 5, 6, 8, 10, and 12) Radical Cation and Dications: Size-Dependent Absorption, Spin, and Charge Delocalization. *J. Am. Chem. Soc.* **2016**, *138*, 338–344, DOI: 10.1021/jacs.5b10855.

(12) Segawa, Y.; Levine, D. R.; Itami, K. Topologically Unique Molecular Nanocarbons. *Acc. Chem. Res.* **2019**, *52*, 2760–2767, DOI: 10.1021/acs.accounts.9b00402.

(13) Li, Y.; Kono, H.; Maekawa, T.; Segawa, Y.; Yagi, A.; Itami, K. Chemical Synthesis of Carbon Nanorings and Nanobelts. *Acc. Mater. Res.* **2021**, *2*, 681–691, DOI:10.1021/accountsmr.1c00105.

(14) Ikemoto, K.; Akiyoshi, M.; Mio, T.; Nishioka, K.; Sato, S.; Isobe, H. Synthesis of a Negatively Curved Nanocarbon Molecule with an Octagonal Omphalos via Design‐of‐Experiments Optimizations Supplemented by Machine Learning. *Angew. Chem. Int. Ed.* **2022**, *61*, e202204035, DOI: 10.1002/anie.202204035.

(15) Ni, Y.; Gordillo-Gámez, F.; Peña Alvarez, M.; Nan, Z.; Li, Z.; Wu, S.; Han, Y.; Casado, J.; Wu, J. A Chichibabin's Hydrocarbon-Based Molecular Cage: The Impact of Structural Rigidity on Dynamics, Stability, and Electronic Properties. *J. Am. Chem. Soc.* **2020**, *142*, 12730–12742, DOI: 10.1021/jacs.0c04876.

(16) Tsubaki, K.; Miura, M.; Morikawa, H.; Tanaka, H.; Kawabata, T.; Furuta, T.; Tanaka, K.; Fuji, K. Synthesis of Optically Active Oligonaphthalenes via Second-Order

Asymmetric Transformation. *J. Am. Chem. Soc.* **2003**, *125*, 16200–16201, DOI: 10.1021/ja038910e.

(17) Tsubaki, K. Synthesis and Properties of the Chiral Oligonaphthalenes. *Org. Biomol. Chem.* **2007**, *5*, 2179, DOI: 10.1039/b703558f.

(18) Faggi, E.; Sebastián, R. M.; Pleixats, R.; Vallribera, A.; Shafir, A.; Rodríguez-Gimeno, A.; Ramírez de Arellano, C. Direct Assembly of Polyarenes via C−C Coupling Using PIFA/BF 3 ·Et 2 O. *J. Am. Chem. Soc.* **2010**, *132*, 17980–17982, DOI: 10.1021/ja107467c.

(19) Guo, W.; Faggi, E.; Sebastián, R. M.; Vallribera, A.; Pleixats, R.; Shafir, A. Direct Arylation of Oligonaphthalenes Using PIFA/BF 3 ·Et 2 O: From Double Arylation to Larger Oligoarene Products. *J. Org. Chem.* **2013**, *78*, 8169–8175, DOI: 10.1021/jo401001k.

(20) Takaishi, K.; Iwachido, K.; Takehana, R.; Uchiyama, M.; Ema, T. Evolving Fluorophores into Circularly Polarized Luminophores with a Chiral Naphthalene Tetramer: Proposal of Excimer Chirality Rule for Circularly Polarized Luminescence. *J. Am. Chem. Soc.* **2019**, *141*, 6185–6190, DOI: 10.1021/jacs.9b02582.

(21) Yagi, A.; Segawa, Y.; Itami, K. Synthesis and Properties of [9]Cyclo-1,4-Naphthylene: A π-Extended Carbon Nanoring. *J. Am. Chem. Soc.* **2012**, *134*, 2962–2965, DOI: 10.1021/ja300001g.

(22) Nojima, Y.; Hasegawa, M.; Hara, N.; Imai, Y.; Mazaki, Y. Stereogenic Cyclic Oligonaphthalenes Displaying Ring Size-Dependent Handedness of Circularly Polarized Luminescence (CPL). *Chem. Commun.* **2019**, *55*, 2749–2752, DOI: 10.1039/C8CC08929A.

(23) Matsuno, T.; Fukunaga, K.; Kobayashi, S.; Sarkar, P.; Sato, S.; Ikeda, T.; Isobe, H. Crystalline Naphthylene Macrocycles Capturing Gaseous Small Molecules in Chiral Nanopores. *Chem. Asian J.* **2020**, *15*, 3829–3835, DOI: 10.1002/asia.202000876.

(24) Collin, G.; Höke, H.; Talbiersky, J. Anthracene. In *Ullmann's Encyclopedia of Industrial Chemistry*; Wiley-VCH Verlag GmbH & Co. KGaA: Weinheim, Germany, 2006, DOI: 10.1002/14356007.a02_343.pub2.

(25) Huang, J.; Su, J.-H.; Tian, H. The Development of Anthracene Derivatives for Organic Light-Emitting Diodes. *J. Mater. Chem.* **2012**, *22*, 10977–10989, DOI: 10.1039/c2jm16855c.

(26) Chen, M.; Yan, L.; Zhao, Y.; Murtaza, I.; Meng, H.; Huang, W. Anthracene-Based Semiconductors for Organic Field-Effect Transistors. *J. Mater. Chem. C* **2018**, *6*, 7416–7444, DOI: 10.1039/C8TC01865K.

(27) Dumur, F. Recent Advances on Anthracene-Based Photoinitiators of Polymerization. *Eur. Polym. J.* **2022**, *169*, 111139, DOI: 10.1016/j.eurpolymj.2022.111139.

(28) Yoshizawa, M.; Klosterman, J. K. Molecular Architectures of Multi-Anthracene Assemblies. *Chem. Soc. Rev.* **2014**, *43*, 1885–1898, DOI: 10.1039/C3CS60315F.

(29) Toyota, S.; Tsurumaki, E. Exploration of Nano-Saturns: A Spectacular Sphere-Ring Supramolecular System. *Chem. Eur. J.* **2019**, *25*, 6878–6890, DOI: 10.1002/chem.201900039.

(30) Nishiuchi, T.; Kisaka, K.; Kubo, T. Synthesis of Anthracene‐Based Cyclic Π‐Clusters and Elucidation of Their Properties Originating from Congested Aromatic Planes. *Angew. Chem. Int. Ed.* **2021**, *60*, 5400–5406, DOI: 10.1002/anie.202013349.

(31) Weber, E.; Ahrendt, J.; Czugler, M.; Csöregh, I. Selective Inclusion and Separation of Isomeric and Homologous Hydrocarbons by Hydrocarbon Host Lattices. *Angew. Chem. Int. Ed. Engl.* **1986**, *25*, 746–748, DOI: 10.1002/anie.198607461.

(32) Bock, H.; John, A.; Christian, N.; Havlas, Z. Electron Transfer and Ion Pair Formation, 34 [1-3] Single Crystal Structure of the Solvent-Separated Ion Pair [9,9'-Bianthryl][Na(DME)3]. *Zeitschrift für Naturforsch. B* **1994**, *49*, 1339–1347.

(33) Kyzioł, J. B.; Zaleski, J. 9,9′-Bianthracenyl. *Acta Crystallogr. Sect. E Struct. Reports Online* **2007**, *63*, o1235–o1237, DOI: 10.1107/S160053680700339X.

(34) Manna, B.; Nandi, A.; Chandrakumar, K. R. S. Comparative Study of Exciton Dynamics in 9,9′-Bianthracene Nanoaggregates and Thin Films: Observation of Singlet–Singlet Annihilation-Mediated Triplet Exciton Formation. *J. Phys. Chem. C* **2022**, *126*, 10762–10771, DOI: 10.1021/acs.jpcc.2c03356.

(35) Wang, L.; Zhang, L.; Fang, Y.; Zhao, Y.; Tan, G.; Wang, X. Orthogonal Oriented Bisanthrancene - Bridged Bis(Triarylamine) Diradical Dications: Isolation, Characterizations and Crystal Structures. *Chem. Asian J.* **2019**, *14*, 1708–1711, DOI: 10.1002/asia.201801816.

(36) Pu, Y.-J.; Satake, R.; Koyama, Y.; Otomo, T.; Hayashi, R.; Haruta, N.; Katagiri, H.; Otsuki, D.; Kim, D.; Sato, T. Absence of Delayed Fluorescence and Triplet–Triplet Annihilation in Organic Light Emitting Diodes with Spatially Orthogonal Bianthracenes. *J. Mater. Chem. C* **2019**, *7*, 2541–2547, DOI: 10.1039/C8TC05817B.

(37) Jiménez, V. G.; Mayorga-Burrezo, P.; Blanco, V.; Lloveras, V.; Gómez-García, C. J.; Šolomek, T.; Cuerva, J. M.; Veciana, J.; Campaña, A. G. Dibenzocycloheptatriene as End-Group of Thiele and Tetrabenzo-Chichibabin Hydrocarbons. *Chem. Commun.* **2020**, *56*, 12813–12816, DOI: 10.1039/D0CC04489J.

(38) Mateo, L. M.; Sun, Q.; Liu, S.; Bergkamp, J. J.; Eimre, K.; Pignedoli, C. A.; Ruffieux, P.; Decurtins, S.; Bottari, G.; Fasel, R.; Torres, T. On - Surface Synthesis and Characterization of Triply Fused Porphyrin–Graphene Nanoribbon Hybrids. *Angew. Chem. Int. Ed.* **2020**, *59*, 1334–1339, DOI: 10.1002/anie.201913024.

(39) Okayasu, M.; Kikkawa, S.; Hikawa, H.; Azumaya, I. Co-Crystals of 9,9′-Bianthracene-10,10′-Dicarboxylic Acid with Linear Bidentate Basic Ligand Molecules: Synthesis, Crystal Structure, and Properties Based on the Layer Structure Exfoliated by Water. *CrystEngComm* **2020**, *22*, 497–505, DOI: 10.1039/C9CE01460H.

(40) Grabowski, Z. R.; Rotkiewicz, K.; Rettig, W. Structural Changes Accompanying Intramolecular Electron Transfer: Focus on Twisted Intramolecular Charge-Transfer States and Structures. *Chem. Rev.* **2003**, *103*, 3899–4032, DOI: 10.1021/cr9407451.

(41) Müllen, K.; Baumgarten, M.; Tyutyulkov, N.; Karabunarliev, S. A Class of Narrow-Band High-Spin Organic Polymers I. Polymers with Direct Exchange Interaction between Orthogonal π-Orbitals. *Synth. Met.* **1991**, *40*, 127–135, DOI: 10.1016/0379-6779(91)91495-V.

(42) Baumgarten, M.; Müller, U.; Bohnen, A.; Müllen, K. Oligo(9,10-Anthrylenes), Organic Compounds with Stable High-Spin States. *Angew. Chem. Int. Ed. Engl.* **1992**, *31* (4), 448–451, DOI: 10.1002/anie.199204481.

(43) Müller, U.; Adam, M.; Müllen, K. Synthesis and Characterization of Soluble Oligo(9,10 - anthrylene)S. *Chem. Ber.* **1994**, *127*, 437–444, DOI: 10.1002/cber.19941270221.

(44) Fritz, R.; Rettig, W.; Nishiyama, K.; Okada, T.; Müller, U.; Müllen, K. Excitonic and Charge Transfer States in Oligomeric 9,10-Anthrylene Chains. *J. Phys. Chem. A* **1997**, *101*, 2796–2802, DOI: 10.1021/jp9639814.

(45) Nishiyama, K.; Honda, T.; Reis, H.; Müller, U.; Müllen, K.; Baumann, W.; Okada, T. Electronic Structures of 9,10-Anthrylene Dimers and Trimers in Solution: Formation of Charge Separation States Depending on Alkyl Substituent Groups. *J. Phys. Chem. A* **1998**, *102*, 2934–2943, DOI: 10.1021/jp973251b.

(46) Mueller, U.; Baumgarten, M. Novel Oligo(9,10-Anthrylene)s: Models for Electron Transfer and High-Spin Formation. *J. Am. Chem. Soc.* **1995**, *117* (21), 5840–5850, DOI: 10.1021/ja00126a024.

(47) Adeloye, A. O.; Ajibade, P. A. Synthesis and Characterization of a Heteroleptic Ru(II) Complex of Phenanthroline Containing Oligo-Anthracenyl Carboxylic Acid Moieties. *Int. J. Mol. Sci.* **2010**, *11*, 3158–3176, DOI: 10.3390/ijms11093158.

(48) Adeloye, A. O.; Ajibade, P. A. Synthesis, Characterization and Preliminary Investigation of the Electro Redox Properties of Anthracenyl-Functionalized Terpyridyl Ligands. *Tetrahedron Lett.* **2011**, *52*, 274–277, DOI: 10.1016/j.tetlet.2010.11.022.

(49) Lim, Z.; Zheng, B.; Huang, K.-W.; Liu, Y.; Wu, J. Quinoidal Oligo(9,10-Anthryl)s with Chain-Length-Dependent Ground States: A Balance between Aromatic Stabilization and Steric Strain Release. *Chem. Eur. J.* **2015**, *21*, 18724–18729, DOI: 10.1002/chem.201503033.

(50) Hirao, Y.; Konishi, A.; Kubo, T. Anthroxyl-Based Biradical: Toward the Construction of Highly Stable Multi-Spin Systems. *Org. Chem. Front.* **2017**, *4*, 828–833, DOI: 10.1039/C7QO00130D.

(51) Sun, Q.; Yao, X.; Gröning, O.; Eimre, K.; Pignedoli, C. A.; Müllen, K.; Narita, A.; Fasel, R.; Ruffieux, P. Coupled Spin States in Armchair Graphene Nanoribbons with Asymmetric Zigzag Edge Extensions. *Nano Lett.* **2020**, *20*, 6429–6436, DOI: 10.1021/acs.nanolett.0c02077.

(52) Mishra, S.; Yao, X.; Chen, Q.; Eimre, K.; Gröning, O.; Ortiz, R.; Di Giovannantonio, M.; Sancho-García, J. C.; Fernández-Rossier, J.; Pignedoli, C. A.; Müllen, K.; Ruffieux, P.; Narita, A.; Fasel, R. Large Magnetic Exchange Coupling in Rhombus-Shaped Nanographenes with Zigzag Periphery. *Nat. Chem.* **2021**, *13*, 581–586, DOI: 10.1038/s41557-021-00678-2.

(53) Konishi, A.; Hirao, Y.; Nakano, M.; Shimizu, A.; Botek, E.; Champagne, B.; Shiomi, D.; Sato, K.; Takui, T.; Matsumoto, K.; Kurata, H.; Kubo, T. Synthesis and Characterization of Teranthene: A Singlet Biradical Polycyclic Aromatic Hydrocarbon Having Kekulé Structures. *J. Am. Chem. Soc.* **2010**, *132*, 11021–11023, DOI: 10.1021/ja1049737.

(54) Konishi, A.; Hirao, Y.; Kurata, H.; Kubo, T.; Nakano, M.; Kamada, K. Anthenes: Model Systems for Understanding the Edge State of Graphene Nanoribbons. *Pure Appl. Chem.* **2014**, *86*, 497–505, DOI: 10.1515/pac-2013-0811.

(55) Hayashi, H.; Yamaguchi, J.; Jippo, H.; Hayashi, R.; Aratani, N.; Ohfuchi, M.; Sato, S.; Yamada, H. Experimental and Theoretical Investigations of Surface-Assisted Graphene Nanoribbon Synthesis Featuring Carbon–Fluorine Bond Cleavage. *ACS Nano* **2017**, *11*, 6204–6210, DOI: 10.1021/acsnano.7b02316.

(56) Kolmer, M.; Steiner, A.-K.; Izydorczyk, I.; Ko, W.; Engelund, M.; Szymonski, M.; Li, A.-P.; Amsharov, K. Rational Synthesis of Atomically Precise Graphene Nanoribbons Directly on Metal Oxide Surfaces. *Science* **2020**, *369* (6503), 571–575, DOI: 10.1126/science.abb8880.

(57) Mallory, F. B.; Regan, C. K.; Bohen, J. M.; Mallory, C. W.; Bohen, A. A.; Carroll, P. J. Discovery of Deep-Seated Skeletal Rearrangements in the Photocyclizations of Some tert-Butyl-Substituted 1,2-Diarylethylenes. *J. Org. Chem.* **2015**, *80*, 8–17, DOI: 10.1021/jo501965y

(58) Raasch, M. S. Monothioanthraquinones. *J. Org. Chem.* **1979**, *44* (4), 632–633, DIO: 10.1021/jo01318a034.

(59) Ishigaki, Y.; Harimoto, T.; Sugawara, K.; Suzuki, T. Hysteretic Three-State Redox Interconversion among Zigzag Bisquinodimethanes with Non-Fused Benzene Rings and Twisted Tetra-/Dications with [5]/[3]Acenes Exhibiting Near-Infrared Absorptions. *J. Am. Chem. Soc.* **2021**, *143*, 3306–3311, DOI: 10.1021/jacs.1c00189.

(60) Krapp, A.; Bickelhaupt, F. M.; Frenking, G. Orbital Overlap and Chemical Bonding. *Chem. Eur. J.* **2006**, *12*, 9196–9216, DOI: 10.1002/chem.200600564.

(61) Murray, J. S.; Politzer, P. The Electrostatic Potential: An Overview. *WIREs Comput. Mol. Sci.* **2011**, *1*, 153–163, DOI:10.1002/wcms.19.

(62) Cai, J.; Ruffieux, P.; Jaafar, R.; Bieri, M.; Braun, T.; Blankenburg, S.; Muoth, M.; Seitsonen, A. P.; Saleh, M.; Feng, X.; Müllen, K.; Fasel, R. Atomically Precise Bottom-up Fabrication of Graphene Nanoribbons. *Nature* **2010**, *466*, 470–473, DOI: 10.1038/nature09211.

(63) Mishra, S.; Beyer, D.; Berger, R.; Liu, J.; Gröning, O.; Urgel, J. I.; Müllen, K.; Ruffieux, P.; Feng, X.; Fasel, R. Topological Defect-Induced Magnetism in a Nanographene. *J. Am. Chem. Soc.* **2020**, *142*, 1147–1152, DOI: 10.1021/jacs.9b09212.

(64) Shimajiri, T.; Suzuki, T.; Ishigaki, Y. Flexible C−C Bonds: Reversible Expansion, Contraction, Formation, and Scission of Extremely Elongated Single Bonds. *Angew. Chem. Int. Ed.* **2020**, *59*, 22252–22257, DOI: 10.1002/anie.202010615.

(65) Ishigaki, Y.; Hashimoto, T.; Sugawara, K.; Suzuki, S.; Suzuki, T. Switching of Redox Properties Triggered by a Thermal Equilibrium between Closed‐Shell Folded and Open‐Shell Twisted Species. *Angew. Chem. Int. Ed.* **2020**, *59*, 6581–6584, DOI: 10.1002/anie.201916089.

(66) Zeng, Z.; Sung, Y. M.; Bao, N.; Tan, D.; Lee, R.; Zafra, J. L.; Lee, B. S.; Ishida, M.; Ding, J.; López Navarrete, J. T.; Li, Y.; Zeng, W.; Kim, D.; Huang, K.-W.; Webster, R. D.; Casado, J.; Wu, J. Stable Tetrabenzo- Chichibabin's Hydrocarbons: Tunable Ground State and Unusual Transition between Their Closed-Shell and Open-Shell Resonance Forms. *J. Am. Chem. Soc.* **2012**, *134*, 14513–14525, DOI: 10.1021/ja3050579.

(67) Yin, X.; Low, J. Z.; Fallon, K. J.; Paley, D. W.; Campos, L. M. The Butterfly Effect in Bisfluorenylidene-Based Dihydroacenes: Aggregation Induced Emission and Spin Switching. *Chem. Sci.* **2019**, *10*, 10733–10739, DOI: 10.1039/C9SC04096J.

(68) Nishiuchi, T.; Ito, R.; Stratmann, E.; Kubo, T. Switchable Conformational Isomerization of an Overcrowded Tristricyclic Aromatic Ene. *J. Org. Chem.* **2020**, *85*, 179–186, DOI: 10.1021/acs.joc.9b02432.

(69) Wonink, M. B. S.; Corbet, B. P.; Kulago, A. A.; Boursalian, G. B.; de Bruin, B.; Otten, E.; Browne, W. R.; Feringa, B. L. Three-State Switching of an Anthracene Extended Bis-Thiaxanthylidene with a Highly Stable Diradical State. *J. Am. Chem. Soc.* **2021**, *143*, 18020–18028, DOI: 10.1021/jacs.1c05938.

(70) Li, K.; Xu, Z.; Xu, J.; Weng, T.; Chen, X.; Sato, S.; Wu, J.; Sun, Z. Overcrowded Ethylene-Bridged Nanohoop Dimers: Regioselective Synthesis, Multiconfigurational Electronic States, and Global Hückel/Möbius Aromaticity. *J. Am. Chem. Soc.* **2021**, *143*, 20419–20430, DOI: 10.1021/jacs.1c10170.

(71) Nishiuchi, T.; Aibara, S.; Sato, H.; Kubo, T. Synthesis of π-Extended Thiele's and Chichibabin's Hydrocarbons and Effect of the π-Congestion on Conformations and Electronic States. *J. Am. Chem. Soc.* **2022**, *144*, 7479–7488, DOI: 10.1021/jacs.2c02318.

(72) Suzuki, K.; Kobayashi, A.; Kaneko, S.; Takehira, K.; Yoshihara, T.; Ishida, H.; Shiina, Y.; Oishi, S.; Tobita, S. Reevaluation of Absolute Luminescence Quantum Yields of Standard Solutions Using a Spectrometer with an Integrating Sphere and a Back-Thinned CCD Detector. *Phys. Chem. Chem. Phys.* **2009**, *11* (42), 9850, DIO: 10.1039/b912178a.

(73) Frisch, M. J.; Trucks, G. W.; Schlegel, H. B.; Scuseria, G. E.; Robb, M. A.; Cheeseman, J. R.; Scalmani, G.; Barone, V.; Petersson, G. A.; Nakatsuji, H.; Li, X.; Caricato, M.; Marenich, A. V.; Bloino, J.; Janesko, B. G.; Gomperts, R.; Mennucci, B.; Hratchian, H. P.; Ortiz, J. V.; Izmaylov, A. F.; Sonnenberg, J. L.; Williams-Young, D.; Ding, F.; Lipparini, F.; Egidi, F.; Goings, J.; Peng, B.; Petrone, A.; Henderson, T.; Ranasinghe,

D.; Zakrzewski, V. G.; Gao, J.; Rega, N.; Zheng, G.; Liang, W.; Hada, M.; Ehara, M.; Toyota, K.; Fukuda, R.; Hasegawa, J.; Ishida, M.; Nakajima, T.; Honda, Y.; Kitao, O.; Nakai, H.; Vreven, T.; Throssell, K.; Montgomery, J. A. J.; Peralta, J. E.; Ogliaro, F.; Bearpark, M. J.; Heyd, J. J.; Brothers, E. N.; Kudin, K. N.; Staroverov, V. N.; Keith, T. A.; Kobayashi, R.; Normand, J.; Raghavachari, K.; Rendell, A. P.; Burant, J. C.; Iyengar, S. S.; Tomasi, J.; Cossi, M.; Millam, J. M.; Klene, M.; Adamo, C.; Cammi, R.; Ochterski, J. W.; Martin, R. L.; Morokuma, K.; Farkas, O.; Foresman, J. B.; Fox, D. J. *Gaussian 16, Revision B.01*; Gaussian, Inc., Wallingford CT, 2016.

(74) Dolomanov, O. V.; Bourhis, L. J.; Gildea, R. J.; Howard, J. A. K.; Puschmann, H. OLEX2 : A Complete Structure Solution, Refinement and Analysis Program. *J. Appl. Crystallogr.* **2009**, *42* (2), 339–341, DIO: 10.1107/S0021889808042726.

(75) Sheldrick, G. M. SHELXT – Integrated Space-Group and Crystal-Structure Determination. *Acta Crystallogr. Sect. A Found. Adv.* **2015**, *71* (1), 3–8, DIO: 10.1107/S2053273314026370.

(76) Sheldrick, G. M. Crystal Structure Refinement with SHELXL. *Acta Crystallogr. Sect. C Struct. Chem.* **2015**, *71* (1), 3–8, DIO: 10.1107/S2053229614024218.

(77) Ribar, P.; Šolomek, T.; Le Pleux, L.; Häussinger, D.; Prescimone, A.; Neuburger, M.; Juríček, M. Donor–Acceptor Molecular Triangles. *Synthesis (Stuttg).* **2017**, *49*, 899–909, DOI: 10.1055/s-0036-1588685.

Acknowledgements

This study was carried out under the direction of Associate Professor Dr. Yusuke Ishigaki (Department of Chemistry, Faculty of Science, Hokkaido University). The author would like to express his sincere gratitude to Associate Professor Dr. Yusuke Ishigaki for his consistent guidance, suggestion, valuable discussions, encouragement, and so much help through the course of his work. He taught the author the basics of the way to study.

The author would like to express the deepest appreciation to Professor Dr. Takanori Suzuki (Department of Chemistry, Faculty of Science, Hokkaido University) for his kind guidance, valuable discussion, encouragement, and so much help throughout the course of his work. The author has grown as a researcher under his guidance and is sincerely glad to be one of the members in his laboratory.

The author expresses deeply grateful to Assistant Professor Dr. Ryo Katoono (Department of Chemistry, Faculty of Science, Hokkaido University) for his helpful guidance, valuable discussion, encouragement and so much help throughout the course of this work.

The author would like to thank Professor Dr. Masaya Sawamura, Professor Dr. Takeshi Ohkuma and Professor Dr. Aiichiro Nagaki for their valuable suggestion and discussion.

The author would like to be really thankful to Dr. Wataru Nojo for his helpful guidance, valuable discussion, encouragement and so much help throughout the course of this work.

The author would like to give a special thanks to Assistant Professor Dr. Takuya Shimajiri (Department of Chemistry, Faculty of Science, Hokkaido University) for his helpful guidance, valuable discussion, encouragement and so much help throughout the course of this work.

The author expresses deeply grateful to Associate Professor Dr. Shuichi Suzuki (Graduate School of Engineering Science, Osaka University) for the measurements of electron spin resonance for the contents of Chapter 4.

The author is special grateful for Program for Leading Graduate Schools (Hokkaido University "Ambitious Leader's Program") from the Ministry of Education, Culture, Sports, Science, and Technology (MEXT), Japan for financial support and for giving him the opportunity to experience various valuable programs to develop the skills necessary for active on the global stage.

The author is really thankful to Dr. Eri and Mr. Yusuke Takada (GC-MS & NMR Laboratory, Graduate School of Agriculture, Hokkaido University) for the mass spectrometric analyses.

The author is deeply grateful to CNRS Research Director Dr. Maurice Médebielle and Assistant Professor Dr. Jérémy Merad (Institute for Molecular and Supramolecular Chemistry and Biochemistry (ICBMS), Université Claude Bernard Lyon 1) for their hospitable support, heartfelt guidance, valuable discussion, and so much encouragement during my stay in Lyon, France.

The author gives a special thanks to Mr. Keisuke Sugimoto, Dr. Sugawara, Mr. Hironori Aoki, Mr. Masataka Saito and other members in Suzuki Laboratory for their valuable discussion and giving his invaluable time.

The author is in acknowledgment of Research Fellowship of the Japan Society for the Promotion of Science (JSPS) for Young Scientists for Financial Support.

Finally, the author would like to express his deep and sincere gratitude to his family, Hiroko Hayashi, Akihiro Hayashi, Masayoshi Hayashi and Masako Hayashi for their continuous financial help and encouragement.

Yuki Hayashi

Graduate School of Chemical Science and Engineering
Hokkaido University
2023